



Emanuel Nery de Oliveira Quartin Costa

Mestre em Biologia Humana e Ambiente

Modulation of the haematopoietic stem cell niche by photo-triggerable nanoparticles

Dissertação para obtenção do Grau de Doutor em Bioengenharia

Orientador: Doutor Ricardo Neves, Investigador Auxiliar, Universidade de Coimbra

Co-orientador: Doutor Lino Ferreira, Investigador Coordenador, Universidade de Coimbra

Co-orientador: Doutor Manuel Luís Magalhães Nunes da Ponte, Professor Catedrático, Faculdade de Ciências e Tecnologia da Universidade Nova de Lisboa

Júri:

Presidente: Prof. Doutor Pedro Miguel Ribeiro Viana Baptista
Arguentes: Prof. Doutor João Pedro Taborda Barata
Prof. Doutor João Nuno Sereno Almeida Moreira

Vogais: Prof. Doutor Pedro Miguel Ribeiro Viana Baptista
Prof. Doutor Ricardo Neves Pires das Neves



Junho de 2018



Emanuel Nery de Oliveira Quartin Costa

Mestre em Biologia Humana e Ambiente

**Modulation of the haematopoietic
stem cell niche by photo-triggerable
nanoparticles**

Dissertação para obtenção do Grau de Doutor em
Bioengenharia

Orientador: Doutor Ricardo Neves, Investigador
Auxiliar, Universidade de Coimbra

Co-orientador: Doutor Lino Ferreira, Investigador
Coordenador, Universidade de Coimbra

Co-orientador: Doutor Manuel Luís Magalhães
Nunes da Ponte, Professor Catedrático, Faculdade de
Ciências e Tecnologia da Universidade Nova de
Lisboa



Junho de 2018

Direitos de Cópia • Copyright

Modulation of the haematopoietic stem cell niche by photo-triggerable nanoparticles. Copyright © Emanuel Nery de Oliveira Quartin Costa, Faculdade de Ciências e Tecnologia, Universidade Nova de Lisboa.

A Faculdade de Ciências e Tecnologia e a Universidade Nova de Lisboa têm o direito, perpétuo e sem limites geográficos, de arquivar e publicar esta dissertação através de exemplares impressos reproduzidos em papel ou de forma digital, ou por qualquer outro meio conhecido ou que venha a ser inventado, e de a divulgar através de repositórios científicos e de admitir a sua cópia e distribuição com objectivos educacionais ou de investigação, não comerciais, desde que seja dado crédito ao autor e editor.

The *Faculdade de Ciências e Tecnologia* and the *Universidade Nova de Lisboa* have the perpetual, and without geographical boundaries, right to archive and publish this dissertation through reproduced printed copies on paper or digital form, or by any other means known or hereafter to be invented, to disclose it through scientific repositories and to admit its copy and distribution with educational or research objectives, not commercial, as long as credit is given to the author and editor.

Acknowledgments

Gostaria de expressar o meu eterno agradecimento a tudo e a todos os acompanharam esta minha caminhada, que teria sido impossível sem todo o seu apoio direto ou indireto.

Primeiro que tudo agradecer ao MIT-Portugal por me ter proporcionado a oportunidade de realizar o doutoramento. Gostaria também de agradecer a todos os membros (alunos, professores e “staff”) do Programa Doutoral em Bioengenharia, sem os quais não teria começado em terminado esta jornada. Um especial agradecimento ao José Silva Lopes e à Fátima Lopes, por todo o vosso apoio, disponibilidade e preocupação em proporcionar a melhor experiência possível a todos os alunos do programa. Sem vocês, estávamos quase todos perdidos no meio da teia burocrática e organizacional inerentes ao bom funcionamento dum programa doutoral.

Aos meus orientadores, Ricardo Neves e Lino Ferreira, por me aceitarem e receberem no seu grupo de braços abertos e pelo seu acompanhamento ao longo de todo este percurso. Por todos os vossos ensinamentos e apoios, que me ajudaram a superar as dificuldades encontradas no decorrer deste trabalho, quer teóricas, praticas, emocionais ou pessoais. Obrigado por me terem dado espaço para errar e por apertarem comigo quando era preciso. Obrigado por todas as discussões e críticas construtivas dadas ao meu trabalho e evolução como futuro cientista. Obrigado, por me darem a oportunidade de explorar novos mundos e maneiras de fazer ciência. Obrigado pela vossa boa disposição e descontração, quer quando falávamos de trabalho ou de interesses comuns, excepto clubísticos!

Agradeço também ao Prof. Manuel Nunes da Ponte por toda a sua disponibilidade e apoio quando necessário.

I would like to thank to our collaborators for receiving me and for all the help during the development of my work during my visits to their labs.

To Dr. Dengli Hong and all his group in Shanghai Jiao Tong University, specially Dr. Yijun Cai, for receiving me and making all the efforts to proportionate the needed conditions to achieve our goals during my visit. Thank you very much for pleasant time in Shanghai, professionally and personally.

To Dr. Cristina Lo Celso, thank you to host me in your group at the last stage of my PhD work. Thank you for all the generosity, enthusiasm and guidance during my stay in London at the Imperial College. Your passion for science is truly inspiring and contagious. I would also like to thank to all the members of Bone Marrow Dynamics group, Myriam, Dina, Reema, Nicola and Sara for all your support. A special thanks to Delfim Duarte, Chiara Pirillo and Sara González Anton, for all the help, scientific discussions, to reach where my hands could not and on the top of all, thank you very much for all your help during the 405 marathons.

Quero deixar um enorme agradecimento a todos os membros do grupo de ETs, partilhar estes anos convosco foi um verdadeiro prazer. Obrigado por toda a paciência para as minhas dúvidas, mesmo quando eram meramente existenciais. Por toda a ajuda, pelos momentos de descontração e galhofa. Não vou referir todos os vossos nomes, pois corro o risco de me esquecer de algum, não por terem sido menos relevante neste meu percurso, mas sim porque são muitos, muitos bons colegas e especialmente amigos. Contudo não posso deixar de salientar o contributo de alguns membros, que foram como os meus orientadores no campo de batalha. Obrigado por todo o tempo que passamos juntos e por algum do que passámos a trabalho. Obrigado ao Carlos Boto por me ter introduzido ao grupo e ao seu trabalho, que serviu de base para o meu. Carlos obrigado por tudo, mesmo quando não era necessário! Adri e ao Vitó, os meus consultores e gurus da química, agradeço-vos por todo o conhecimento que bebi de vós, pela vossa paciência, disponibilidade e principalmente amizade. Á Sandra por todos os seus ensinamentos e generosidade de partilha tanto nas pequenas vitórias e principalmente nas grandes derrotas do quotidiano doutoral. Ao Zé Barnabé, que foi um grande colega em Portugal e um amigo

ainda melhor em Londres, fico-te a dever um fino de coca-cola. Por fim, ao Henrique por todos os conselhos e viagens, chegaste tarde neste percurso, mas cedo te mostraste um grande colega e amigo.

Sezin, thank you so much for everything, your enthusiasm and energy when comes to science is so inspiring. Thank you for all the laughs and all the scientific discussions.

Por fim, quero agradecer a toda a minha família e amigos, que sempre me apoiaram e ajudaram no que fosse preciso. Às famílias de ovelhas e outras de Evas, um enorme obrigado por me ajudarem a voltar a ligar à terra. À Sofia, por todo o apoio e amizade com quem tive o prazer de partilhar todo o meu percurso académico. À Maria, ao Xico, à Celeste e à Tatiana por estarem lá quando era preciso. À Raquel por toda a sua compreensão, apoio e ajuda, sem a qual esta tese provavelmente não existiria.

Aos meus avós, Avô Quim e Avô Fernando, por todo o conhecimento que me deram, livros sempre abertos, engendrados minuciosamente ao longo de décadas de muito trabalho e resiliência.

À minha mãe, Leonor, e ao meu pai João Carlos, que sempre acreditaram em mim e deram-me tudo o que (não) podiam para que fosse avante com as decisões pessoais, académicas e profissionais. Obrigado por alimentarem a minha constante e, assumo, muitas vezes esgotante questão “sabes porque?”. Obrigado por estimularem o meu gosto pela *experimentação*, fosse ela conjunta ou sorrateiramente singular.

Obrigado a todos os que fizeram parte desta aventura e peço desculpa se me esqueci de mencionar publicamente o meu agradecimento a algum de vós.

Support and financial acknowledgements

I wish to thank the MIT-Portugal PhD program and Centro de Neurociências e Biologia Celular for the scientific and technology conditions offered for the execution of this thesis. I also would like to thank the Shanghai Jiao Tong University and the Imperial College London for offering me conditions to pursue my PhD research abroad. I acknowledge the use of the Laboratório de Bio-imagem de Alta Resolução of the Faculty of Medicine of University of Coimbra. This work was funded by FEDER through the Programme COMPETE and by Portuguese funds through FCT (PTDC/CTM-NAN/120552/2010; UID/NEU/04539/2013; POCI-01- 0145-FEDER-016390:CANCEL STEM). The work was also funded by the European Community through the European Research Council (“Triggerable nanomaterials to modulate cell activity” - ERC; NanoTrigger Project, ERC-2012-StG_20111012).

I also would like to thank FCT for a PhD fellowship (SFRH/BD/90964/2012).

MIT Portugal



Imperial College
London

European Research Council
Established by the European Commission

FCT
Fundação para a Ciência e a Tecnologia
MINISTÉRIO DA CIÊNCIA, TECNOLOGIA E ENSINO SUPERIOR



GOVERNO DA REPÚBLICA
PORTUGUESA



UNIÃO EUROPEIA
Fundo Social Europeu

Publications and communications

Publications:

- Jiménez-Balsa A, Pinto S, **Quartin E**, Lino MM, Francisco F, and Ferreira L. "*Nanoparticles Conjugated with Photocleavable Linkers for the Intracellular Delivery of Biomolecules*". *Bioconjugate chemistry* 2018 29(5):1485-1489.
DOI: 10.1021/acs.bioconjchem.7b00820.
- Boto C.* & **Quartin E.***, Cai Y, Martín-Lorenzo A, Cenador M, Pinto S, Gupta R, Enver T, Sánchez-García I, Hong D, Neves R[#] and Ferreira L[#]. "*Prolonged intracellular accumulation of light-inducible nanoparticles in leukemia cells allows their remote activation*". *Nat. Commun.* 2017 8, 15204. DOI: 10.1038/ncomms15204. (*,[#] authors contributed equally to this work)
- Santos T, Ferreira R, **Quartin E**, Boto C, Saraiva C, Bragança J, Peça J, Rodrigues C, Ferreira L, Bernardino L. "*Blue light potentiates neurogenesis induced by retinoic acid-loaded responsive nanoparticles*". *Acta Biomaterialia* 2017 59:293-302.
DOI: 10.1016/j.actbio.2017.06.044
- **Quartin Costa E**, Boto C, Neves R, Cai Y, Hong D, Camarero IR, Gupta R, Enver T, Garcia IS and Ferreira L (2016). "*Light-activatable polymeric nanoparticles for intracellular delivery in cancer stem cells*". *Front. Bioeng. Biotechnol.* Conference Abstract: 10th World Biomaterials Congress. DOI: 10.3389/conf.FBIOE.2016.01.00695

Communications:

- "Prolonged intracellular accumulation of light-inducible nanoparticles in leukemia cells allows their remote activation". Poster presentation at 6th China-Europe Symposium on Biomaterials (CESB2017)
- "Prolonged intracellular accumulation of light-inducible nanoparticles in leukemia cells allows their remote activation". Oral presentation at 10th World Biomaterials Congress, WBC 2016 (Trainee Award).
- "Controlling the differentiation program of Cancer Stem Cells by photo-triggerable nanoparticles". Poster presentation at the 9th SPCE-TC International Meeting 2015.

Resumo

O nicho das células hematopoiéticas estaminais (CHE) na medula óssea (MO) é um microambiente protetor de difícil acesso, tornando-se difícil de modular no contexto de transplante de CHE e doenças hematopoiéticas. Nesta tese, desenvolvemos novas estratégias para ultrapassar estes obstáculos, utilizando uma combinação de ferramentas de nanomedicina com células, utilizadas como veículo. No contexto da leucemia, acredita-se que as células resistentes às terapias convencionais residam em nichos protetores. Aqui, descrevemos nanopartículas (NP) poliméricas induzíveis por luz que contêm ácido retinóico (RA). Estas NPs têm a capacidade de se acumular no citoplasma das células leucêmicas (CL) durante vários dias enquanto mantêm a capacidade de libertar grandes quantidade de RA, poucos minutos após exposição à luz azul / Ultravioleta. Quando comparadas com NPs não ativadas pela exposição à luz, RA⁺NPs reduzem mais eficientemente a clonogenicidade de CL da MO de pacientes com Leucemia mieloide aguda (LMA) e induzem a diferenciação de CL com sensibilidade ao RA reduzida. Adicionalmente, nós demonstramos *in vivo* que as CL transfectadas com RA⁺NPs fotossensíveis podem enxertar a MO na proximidade de outras CL, induzir a diferenciação após exposição à luz azul e libertar fatores parácrinos que modulam as células na proximidade das células utilizadas como veículo. Esta capacidade de modular remotamente o nicho leucêmico foi testada num modelo animal de LMA com sucesso. As RA⁺NPs induziram a diferenciação de LMA na linhagem monocítica / macrófágica no modelo animal em murinhos de LMA contendo o oncogene MLL-AF9. Além disso, demonstramos *in vitro* que as RA⁺NPs estimulam a ativação de macrófagos M1, com capacidades anti-tumorais. Esta indução de diferenciação em macrófagos *in vivo* parece ter efeito anti-leucêmico “sistêmico” dentro do nicho leucêmico da BM, pois observamos uma redução significativa de CL na MO de animais tratados com RA⁺NPs quando comparados com animais tratados com NPs vazias (RA⁻NPs). Por último, foram feitos estudos prospectivos tendo como objectivo o uso de CHes saudáveis como transportadoras de NP. Os nossos resultados mostraram que, apesar de serem um tipo celular mais sensível, as células UCB CD34⁺ podem ser carregadas com RA⁺NPs e, após a libertação de RA induzida pela luz, observamos um aumento de expressão de CD38. No contexto de utilização deste tipo de ferramentas na modulação do enxerto de CHE no contexto de transplante medular, fomos capazes de produzir HOXB4 funcional, um fator de transcrição fundamental para o normal funcionamento e expansão de CHE, através da indução dum estado de quiescência e paragens do ciclo celular em G0. Contudo a funcionalização de NP com este tipo de molécula constitui um desafio e poderá ser tema de trabalho futuro.

Palavras-chave: Nanopartículas, Administração direcionada de fármacos; Activação por luz; Leucemia Mieloide Aguda; células transportadoras

Abstract

The bone-marrow haematopoietic stem cell niche is a protective hard to reach microenvironment that is difficult to modulate in the context of HSC transplant and malignant haematopoietic disease. In this thesis we developed new strategies to tackle this by the use of a combination of nanomedicine tools and cell-mediated delivery systems. In the context of leukaemia, cells that are resistant to conventional therapies are thought to reside in protective niches. Here, we describe light-inducible polymeric retinoic acid (RA)-containing nanoparticles (NPs) with the capacity to accumulate in the cytoplasm of leukaemia cells for several days and release their RA payloads within a few minutes upon exposure to blue/UV light. Compared to NPs that are not activated by light exposure, these NPs more efficiently reduce the clonogenicity of bone marrow cancer cells from patients with AML and induce the differentiation of RA-low sensitive leukaemia cells. Importantly, we show that leukaemia cells transfected with light-inducible NPs containing RA can engraft into bone marrow *in vivo* in the proximity of other leukaemic cells, differentiate upon exposure to blue light and release paracrine factors that modulate nearby cells. This capacity of remotely modulating the leukaemic niche has been tested in an AML disease animal model with success. RA⁺NPs induced AML differentiation towards monocytic/macrophage lineage in the MLL-AF9 mouse model of AML. Also, we have shown *in vitro* that RA⁺NPs stimulate antitumoral M1 macrophage activation. This macrophage induced differentiation *in vivo* seems to have “systemic” anti-leukemic effect within the BM leukemic niche, as we observed a significant reduction of leukemic cells in the BM of animals treated with RA⁺NPs when compared with animals treated with empty NPs (RA⁻NPs). Finally, prospective studies on the use of healthy HSCs as carriers have shown that despite having a more sensitive behaviour UCB CD34⁺ cells can be loaded with RA⁺NP and after light-activated release of RA, induce CD38 expression and differentiate. Towards the use of this type of tools in the context of HSC transplant engraftment modulation we were able to produce functional HOXB4, a pivotal transcription factor for HSC potency, that was able to induce G0 quiescence, but NP-functionalization with this molecule remains a challenge and is the subject of future work.

Keywords: Nanoparticles; Targeted drug delivery; Light activation; Acute Myeloid Leukaemia; Carrier cells

Table of contents

CHAPTER 1 - Research Aim and Thesis Outline	7
CHAPTER 2 - State of the Art	11
2.1. Haematopoiesis	13
2.2. Adult BM niche	14
2.2.1. Endosteal niche.....	17
2.2.2. Perivascular niche.....	18
2.2.3. SNS and glia.....	20
2.2.4. Haematopoietic cell components of the niche	20
2.3. Haematological Malignancies	21
2.3.1. Initiation.....	22
2.3.2. Progression and expansion	23
2.3.3. AML	25
2.3.4. Traditional treatments.....	29
2.3.5. Differentiation therapy/APL.....	35
2.4. RA in the niche.....	36
2.5. Novel therapies.....	38
2.6. Nanomedicine.....	38
2.6.1. Proprieties.....	43
2.6.2. Composition	43
2.6.3. Drug delivery.....	44
2.6.4. Targeting the BM	48
2.6.5. Cells as carriers.....	50
CHAPTER 3 - Prolonged intracellular accumulation of light-inducible nanoparticles in leukaemia cells allows their remote activation	55
3.1. Abstract	57
3.2. Introduction	57
3.3. Results and discussion.....	58
3.4. Conclusions	81
3.5. Materials and Methods	82
CHAPTER 4 - Prospective studies on nanoformulations that are able to modulate healthy and leukemic niches	95

4.1. Abstract	97
4.2. Introduction	97
4.3. Results and discussion.....	99
4.4. Conclusions	116
4.5. Materials and Methods	117
CHAPTER 5 - General Conclusions and Future Work	121
CHAPTER 6 - References.....	125

List of figures

Figure 2.1 - Haematopoiesis.	14
Figure 2.2 - The adult bone marrow HSC niche.	15
Figure 2.3 - Two models of the interaction of leukemic cells and their microenvironment.....	22
Figure 2.4 - Haematopoietic stem cell transplantation strategies in AML	32
Figure 2.5 - Examples of organic and inorganic nanoparticles used in nanomedicine.....	44
Figure 2.6 - Types of targeting for NP delivery to tumour tissue	45
Figure 3.1 - Characterization of PEI derivatized with DMNC	59
Figure 3.2 - Properties and disassembly of light-triggerable NPs	60
Figure 3.3 - Release of RA from Light-triggerable RA+NPs.....	61
Figure 3.4 - Stability of RA+NPs suspended in water or cell culture media.	62
Figure 3.5 - Cytotoxicity of RA+NPs and light activation	63
Figure 3.6 - Cellular uptake and dilution of RA+NPs in human leukaemic cells.....	64
Figure 3.7 - Internalization mechanisms of RA+NPs in Zn-induced U937 cells	65
Figure 3.8 - Intracellular trafficking of FITC-labelled RA+NPs	66
Figure 3.9 - Effect of inhibition of P-gp in the accumulation of NPs.....	67
Figure 3.10 - Effect of RA+NPs on human leukaemia cells. Effect of RA+ NPs on human leukaemia cells.....	69
Figure 3.11- Differentiation profile of NB4 cells after treatment with soluble RA or RA+NPs	70
Figure 3.12 - Heat map of the differentiation pattern of NB4 cells after exposure to soluble RA or light-activatable RA+NPs.....	71
Figure 3.13 - Heat map of the differentiation pattern of Zn-induced U937 cells after exposure to soluble RA or light-activatable RA+NPs	72
Figure 3.14 - Genes modulated by RA during differentiation of NB4 cells as assessed by qRT-PCR analyses	73
Figure 3.15 - Effect of time in the activation of RA+NPs within the cells.....	74
Figure 3.16 - Effect of multiple light activation in the differentiation of Zn-induced U937-B412 cells	75
Figure 3.17 - Blue laser (405 nm) attenuation through murine skin or calvaria.....	76
Figure 3.18 - <i>In vivo</i> differentiation of NB4 cells exposed to light-activatable RA+NPs	77
Figure 3.19 - Leukaemia cells transfected with RA+NPs can home at leukaemia niches.....	78
Figure 3.20 - <i>In vivo</i> activation of leukaemic THP-1 differentiation program by light at the bone marrow	79
Figure 3.21 - Paracrine effect of cells treated with RA+NPs.	80
Figure 4.1 – <i>In vitro</i> Differentiation profile of MLL-AF9 YFP blast cells after treatment with soluble RA or RA+NPs.....	101
Figure 4.2 - <i>In vivo</i> activation of AML MLL-AF9 differentiation program by light at the bone marrow	103
Figure 4.3 - Cytotoxicity of RA+NPs and light activation at human AML CD34+ cell line (KG1a) and UCB CD34+.	105

Figure 4.4 - Cellular uptake and dilution of RA+NPs in human AML CD34+ cell line (KG1a) and UCB CD34+cells.....	107
Figure 4.5 - Differentiation profile of in human AML CD34+ cell line (KG1a) and UCB CD34+cells after treatment with soluble RA or RA+NPs.....	109
Figure 4.6 - Production and validation of biological activity of TAT-HoxB4	111
Figure 4.7 - TAT-HoxB4 Dosage effect in the cell cycle of human AML CD34+ cell line KG1a	113
Figure 4.8 - Genes modulated by HoxB4 during G0 induction in KG1a cells as assessed by qRT-PCR analyses.....	114
Figure 4.9 - HoxB4 ligation to light sensitive NP platforms	115

List of Tables

Table 2.1 - Soluble Factors in the Bone Marrow Niche Affecting Mammalian HSCs.	16
Table 2.2 - WHO classification AML subtypes ²¹⁴	27
Table 2.3 - Proposed Genomic Classification of AML ²²⁷	28
Table 2.4 – Therapeutic implication of current stratification of Molecular Genetic and Cytogenetic Alterations, according to ELN Recommendations*. Adapted from ²¹⁴	29
Table 2.5 - Successful Protocols for HSC Expansion Ex Vivo.	34
Table 2.6 - Current Approaches to Ex Vivo Manipulation of UCB Stem Cells in Clinical Trials.	35
Table 2.7 - Examples of clinical-stage nanomedicines for cancer therapy.....	40
Table 2.8 - Triggerable NPs examples.....	46
Table 2.9 - Rationales and applications of bone marrow-targeted delivery systems.....	49
Table 2.10 - Stem cells as a vehicle to transport nanoparticles (NPs): physical–chemical properties of NPs.....	51

List of abbreviations

- 99mTC - Technetium-99m
- ABX - ambraxane
- ADHs - alcohol dehydrogenases
- Adr β 2 - β 2 adrenergic receptor
- Adr β 3 - β 3-adrenergic receptor
- AF750 - alexafluor 750
- ALDHs - aldehyde dehydrogenases
- ALL - acute lymphocytic leukemia
- AML - acute myeloid leukaemia
- ANG1 - angiopoietin 1
- AnV/PI - Annexin V and PI staining
- ANXA2 - annexin 2
- APL - acute promyelocytic leukaemia
- ATO - arsenic trioxide
- ATP - Adenosine triphosphate
- ATRA - all-trans-retinoic acid
- AuNP - gold nanoparticle
- BCR - B-cell receptor
- bFGF - basic fibroblast growth factor
- BM - bone marrow
- BMP - bone morphogenetic protein
- BSA - bovine serum albumin
- CAR - chimeric antigenic receptor
- CAR cell - CXCL12-abundant reticular cell
- Cas9 – CRISPR associated protein 9
- CB - cord blood
- CBF-AML- core-binding factor AML
- CBFB - core-binding factor- β
- CCL3 - chemokine ligand 3
- CEBPA - CCAAT/ enhancer-binding protein- α
- CFU - colony-forming units
- CLL - chronic lymphocytic leukemia
- CLPs - common-lymphoid progenitors
- CLTC - clathrin heavy chain
- CME - clathrin-mediated endocytosis
- CML - chronic myeloid leukemia
- CMP - Common myeloid progenitors
- CO₂ - carbon dioxide
- COX2 - cyclooxygenase 2
- CR - complete remission
- CRABP - cellular retinoic acid-binding proteins
- CRBP I - cytosolic retinoid binding protein
- CRISPR - Clustered Regularly Interspaced Short Palindromic Repeats
- CRU - competitive repopulating unit
- CTC - circulation tumor cell.
- CXCL 4 - chemokine C-X-C motif ligand 4
- CXCL 12 - CXC-chemokine ligand 12

- DAMP - damage-associated molecular pattern
- DAPI - 4',6-diamidino-2-phenylindole
- DEACM - (7-diethylaminocoumarin-4-yl)methyl
- DMNC - 4,5-dimethoxy-2-nitrobenzyl chloroformate
- DMSO – Dimethyl sulfoxide
- DNA - deoxyribonucleic acid
- DOX - doxorubicin
- Dppa5 - developmental pluripotency associated 5
- DS - dextran sulfate
- EBM - Endothelial Growth Basal Medium
- EC - Endothelial cells
- EEA1 - Early Endosome Antigen 1
- EGFR - epidermal growth factor receptor
- EGM2 – Endothelial Growth Medium-2
- eIF5A - eukaryotic initiation factor 5A
- EMH - extramedullary haematopoiesis
- EMSA - electrophoretic mobility shift assay
- EPHA2 - ephrin type A receptor 2
- EPR - enhanced permeability and retention
- ER α - oestrogen receptor- α
- EVI-1 - ecotropic viral integration site 1
- FACs - Fluorescence activated cell sorting
- FBS - fetal bovine serum
- Fbxw7 - F-box and WD repeat domain containing 7, E3 ubiquitin protein ligase
- FDA - US Food and Drug Administration
- FFPE - formalin-fixed paraffin embedded tissues
- FGF1 - fibroblast growth factor 1
- FGF2 - fibroblast growth factor 2
- FGFR - FGF receptor
- FITC - Fluorescein isothiocyanate
- FLT3 - FMS-related tyrosine kinase 3
- FLT3-ID - FMS-like tyrosine kinase 3/internal tandem duplication
- FRET, fluorescence energy transfer
- FR- β - folate receptor- β
- FSC/SSC - Forward-scattered light / Side-scattered light
- G-CSF - granulocyte colony-stimulating factor
- GFP - green fluorescent protein
- GMPs - granulocyte-macrophage progenitors
- GVHD - Graft-versus-host disease
- H₂O - water
- HA – hydroxyapatite
- HCT-CI - Haematopoietic Cell Transplantation Co-morbidity Index
- HEPES - hydroxyethyl piperazineethanesulfonic acid
- HGF - hepatocyte growth factor
- HLA - Human leukocyte antigen
- HSCs - Haematopoietic stem cells
- HSCT - haematopoietic stem cell transplantations
- HUVECs – human vein umbilical endothelial cells
- ICP-MS - inductively coupled plasma mass spectrometry
- IDH - isocitrate dehydrogenase

- IDH1 - isocitrate dehydrogenase 1
- IFN- γ - interferon
- IGF1 - insulin-like growth factor 1
- IGF1R - IGF1 receptor
- IGF2 - insulin-like growth factor 2
- IL-1 α - interleukin-1 α
- IL-3 - interleukin 3
- IL-6 - interleukin-6
- IMDM - Iscove's Modified Dulbecco's Medium
- ISH - in situ hybridization
- ITD - internal tandem duplication
- IT-HSC - intermediate-term haematopoietic stem cells
- JAK2 - Janus kinase 2
- KCl - Potassium chlorate
- Kcps - kilo counts per second
- KSP - kinesin spindle protein (also known as KIF11)
- LDLR - low-density lipoprotein receptor
- LepR- leptin receptor
- lncRNA - long non-coding RNA
- LNP - lipid NP
- LSCs - leukaemia Stem Cells
- LSK - lineage-SCA1+KIT+
- LT - long-term
- LTC-IC - long-term culture-initiating cell
- LT-HSC - long-term haematopoietic stem cells
- M.F.I - mean fluorescence intensity
- MAFIA - macrophage-Fas-induced apoptosis transgenic
- mCRPC - metastatic castration resistant prostate cancer
- MDS - myelodysplastic syndrome
- MEPs - megakaryocyte/erythroid progenitors
- MIP-1 α - macrophage inflammatory protein-1 α
- miR - microRNA
- MKL1 - megakaryoblastic leukaemia (translocation) 1
- MKs - megakaryocytes
- MLL - myeloid/lymphoid or mixed-lineage leukaemia (also known as KMT2A)
- MLL-AF9 YFP cells
- MLLT3 - MLL translocated to 3
- MNPs - magnetic nanoparticles
- MPB - mobilized peripheral blood
- MPL - myeloproliferative leukaemia protein
- MPN - myeloproliferative neoplasm phenotype
- MPS - mononuclear phagocyte system
- MPS - myeloproliferative syndrome
- MRD - minimal residual disease
- MRI - magnetic resonance imaging
- MS-5 - murine MS-5 stromal cell line
- MSC - mesenchymal stem cell
- MSN - mesoporous silica NP
- mTOR - mammalian target of rapamycin
- MUC1 - membrane bound mucin 1

- MYH11 - myosin heavy chain 11 smooth muscle
- NA- not applicable
- nab - nanoparticle albumin bound
- NaCl - Sodium chloride
- NC – nanocrystal
- NIR - near infrared regions
- NK - normal karyotype
- NMR - Nuclear magnetic resonance
- NP – nanoparticles
- NPM1 - nucleophosmin
- NPY - neuropeptide Y
- NSCLC - non small cell lung cancer
- NSCs - neural stem cells
- NSG - Nod-Scid-gamma
- NUP214 - nucleoporin 214kDa
- OBC - osteoblastic lineage cells
- OPN - osteopontin
- P - pellets
- PB - peripheral blood
- PBS - Phosphate-buffered saline
- PcG - Polycomb group family
- PCL - photocleavable linker
- PCS - photon correlation spectroscopy
- PDGF- β - platelet-derived growth factor- β
- PDMS - poly(dimethylsiloxane)
- PdPc(OBu)₈ - 1,4,8,11,15,18,22,25-octabutoxyphthalocyaninato-palladium-(II)
- PEComa - perivascular epithelioid cell tumours
- PEG - poly(ethylene glycol)
- PEI - poly(ethyleneimine)
- Pen-Strep - Penicillin Streptomycin
- P-gp - P-glycoprotein
- pI - isoelectric point
- PLGA - poly(lactic acid-co-glycolic acid)
- PLK1 - polo like kinase 1
- PMF - primary myelofibrosis
- PML - promyelocytic leukaemia
- PNIPAM - poly(N-isopropylacrylamide)
- polyArg - peptide sequence with nine arginines;
- Prx-1 - paired related homeobox-1
- PSMA - prostate specific membrane antigen
- PTC - Pseudotumour cerebri
- PTK7 - protein tyrosine kinase 7
- PTX - paclitaxel
- QD - quantum dot
- q-RT-PCR – quantitative Reverse transcription polymerase chain reaction
- RA - retinoic acid
- RAREs - retinoic acid response elements
- RARs - retinoic acid receptors
- RAR α or RARA - retinoic receptor α
- Rary - retinoic acid receptor γ

- Rb - retinoblastoma
- RBC - red blood cells
- RBM15 - RNA-binding motif protein 15
- RES - reticulo-endothelial system
- RNAi - RNA interference
- ROBO4 - roundabout guidance receptor 4
- ROS - reactive oxygen species
- RPMI-1640 - Roswell Park Memorial Institute medium-1640
- RPN1 - ribophorin I
- RUNX1 - Runt-related transcription factor 1
- RUNX1T1 - RUNX1 translocated to 1
- RXR - retinoid X receptor
- s.e.m. - standard error of mean
- SBDS - Schwachman-Bodian-Diamond syndrome
- SCA1 - spinocerebellar ataxia type 1 protein
- SCF - stem-cell factor
- SDS-PAGE - sodium dodecyl sulfate-polyacrylamide gel electrophoresis
- SERS - surface-enhanced Raman scattering
- Shh - Sonic hedgeho
- shRNA - short hairpin RNA
- siRNA - small interfering RNA
- SMA - smooth muscle actin
- SMANCS - poly(styrene co maleic acid) conjugated neocarzinostatin
- SN - supernatants
- SNS - sympathetic nervous system
- SP - side population
- SR-1 - StemRegenin1
- SSC - skeletal stem cell
- ssDNA - single-stranded DNA
- STR-HSCs - short-term repopulating haematopoietic stem cells
- TET2 - tet methylcyto-sine dioxygenase 2
- TfR - transferrin receptor
- TFs - transcription factors
- TGFβ1 - transforming growth factor β1
- THPO - thrombopoietin
- TIE2 - tyrosine kinase with Ig and EGF homology domains 2
- TLR - Toll-like receptor
- TNC - total nucleated cells
- TNF - tumour necrosis factor
- TNF- β - transforming growth factor-β
- TNFα- Tumour necrosis factor alpha
- TPO - thrombopoietin
- TRITC – Tetramethylrhodamine
- TRM - treatment related mortality
- TSP1 - thrombospondin-1
- UCB - umbilical cord blood
- UCBT - umbilical cord blood transplants
- USPIO - ultra-small paramagnetic iron oxide
- UV - Ultraviolet light
- VE-cadherin - vascular endothelial-cadherin

- VEGF-A - vascular endothelial growth factor A
- VEGFR2 - vascular endothelial growth factor receptor-2
- WBC - white blood cells
- WHO - World Health Organization
- Wnt - wingless-type
- WT1 - Wilms tumour 1
- XIAP - X-linked inhibitor of apoptosis protein
- β -ER - β -estradiol

CHAPTER 1 - Research Aim and Thesis Outline

Research aim and thesis outline

Nanomedicine has gained enormous focus on the last decade with nanoplatforms presenting themselves as an attractive strategy to improve old and open new venues of cancer therapy. However, most of these advancements have been made only in solid tumours and not in leukaemia and other “liquid tumours”. Despite all advances, approximately 25% of APL patients receiving RA will develop serious complications, such as “differentiation syndrome”¹. Hence, there is a need for more effective formulations to deliver RA into leukaemia cells while preventing RA side effects. In addition, leukaemia cells resistant to conventional therapies reside in microenvironmental niches in the bone marrow that are difficult to access by therapeutic interventions². New strategies are required to address these problems. With this work, we explore the potential of using stem cells as carriers for targeted delivery of photo-triggerable NPs not only to modulate the diseased HSC BM niche in AML but also healthy HSC BM niches.

This PhD thesis is divided in five chapters: **Chapter 1** provides a general overview of the present work, providing information about the problem, motivations and contribution to the state of art. **Chapter 2** reviews the state of the art on the bone marrow microenvironment during healthy and malignant haematopoiesis along with a description on the latest advances in nanomedicine and targeted drug delivery in leukaemia. In **Chapter 3** and **4** there is a description of all the results obtained during the development of a novel photo-triggerable nanoformulation, the pivotal element in our controlled drug delivery system, in which cells are used as carriers of photo-triggerable RA⁺NPs, allowing precise control of timing, duration and magnitude targeted drug delivery system. In **Chapter 3**, initial work on NP formulation and *in vitro* testing was developed by Dr. Carlos Boto, which I followed and continued with *in vitro* and *in vivo* experiments. In this chapter, we were able to demonstrate that RA⁺NPs can reduce the clonogenicity of bone marrow tumour cells from patients with acute myeloid leukaemia bone marrow and induce the differentiation of RA-low sensitive leukaemia cells expressing the chimeric promyelocytic leukaemia zinc finger/RAR α fusion protein. RA released from light-activated NPs was superior at inducing leukaemia cell differentiation compared to soluble RA and RA released from NPs by passive diffusion. Further, we demonstrate the importance of temporal activation of the nanoformulation during the intracellular trafficking to maximize RA effect and show *in vivo* that leukemic cells loaded with NPs kept their natural tropism to leukaemic BM niches and that NPs can be light-activated to release RA, thereby allowing greater spatio-temporal control of drug delivery. In **Chapter 4**, we continue to explore the applicability of our drug delivery system. In this chapter, we show that RA⁺NPs have a paracrine effect *in vivo* within the BM leukaemic niche upon NP activation. We were able to decrease total disease burden in RA⁺NPs mice, which could be explained by the differentiation of RA⁺NPs carriers cells in macrophages, confirmed *in vitro* and *in vivo*, along with the observed activation in pro-inflammatory and anti-tumoral M1 macrophages observed *in vitro*. We also tested NP loading and activation in human CD34⁺ and the use of a nanoformulation for the transport of a transcription factor involved in the HSC self-renewal and expansion. Finally, in **Chapter 5** we summarize the main findings, general conclusions and future directions opened by this work.

In **Chapter 6** we list all the references used in this work.

.

CHAPTER 2 - State of the Art

2.1. Haematopoiesis

Every day, thousands of blood cells and immune cells are produced in our body by a continuous hierarchical process called haematopoiesis. On top of this hierarchy are haematopoietic stem cells (HSCs). This immature cell type can be functionally defined by the capacity for self-renewal and differentiation into multipotent progenitors. These progenitors will in turn become progressively more restricted to committed precursors until they give origin to the different types of mature blood cells (**Figure 2.1**).

The origin of the concept of an immature cell common to all blood lineages goes back to the early 20th century^{3,4}, but it was only in the 1960s, with the work of James Till and Ernest McCulloch⁵, that this concept was first demonstrated. They were able to rescue lethally irradiated mice with a transplant of a donor bone marrow (BM), which reconstituted the recipient BM. Later, in 1978, Schofield⁶ proposed that HSCs reside in a specialized tissue microenvironment “niche”, where HSCs could be protected and regulated. Since then, extensive studies have been made to identify the cellular components of this niche, as well as the autocrine, endocrine and paracrine signals and cell-to-cell interactions that are essential for the correct regulation of haematopoiesis.

Most studies on this subject have been carried out using mouse models, which are considered comparable to humans in terms of haematopoiesis; despite presenting some differences, mostly in terms of location⁷. After birth, most HSCs are almost exclusively found in the BM. In response to acute stress, however, haematopoiesis can take place in extramedullary tissues. Similarly, during development, HSCs reside in the foetal liver and spleen⁸.

Due to their high heterogeneity, the classification and isolation of HSC subpopulations has been a challenge. Although it is still not clear whether HSCs can be naturally divided into subpopulations or if they represent a continuum of states of the same population, the most widely accepted model for haematopoiesis categorizes HSCs and progenitor cells based on their self-renewal capacities^{9,10}, life span¹¹⁻¹³ and differentiation capabilities¹⁴.

Based on transplantation experiments, HSCs can be divided in 3 subpopulations: long-term (LT-HSC), intermediate-term (IT-HSC), and short-term repopulating HSCs (ST-HSC)¹⁵. This division is based on distinct capabilities of HSCs to engraft, repopulate, and maintain multilineage haematopoiesis in irradiated recipients¹⁶. LT-HSCs self-renewal capacity assures the maintenance of a pool of clonal haematopoietic progenitor cells and haematopoiesis sustainability throughout an individual's life-span. They are less frequent, mostly found in quiescent state and can be isolated by the CD150 marker^{17,18}. The IT-LSC represents an intermediate population with six to eight months of reconstitution potential before their clones become exhausted and can be isolated from both LT and ST-HSC fractions using the integrin $\alpha 2$ (CD49b) marker¹⁹. By contrast, ST-HSCs have a limited self-renewal capacity (up to two months) and are found mostly in the peripheral blood where they contribute to the pool of progenitor cells which will reconstitute the myeloid and lymphoid compartments. Common myeloid progenitors (CMP) are the source of megakaryocyte/erythroid progenitors (MEPs) and granulocyte-macrophage progenitors (GMPs). GMPs give rise to the committed precursors of mast cells, eosinophils, neutrophils, and macrophages, whereas common-lymphoid progenitors (CLPs) are the source of committed precursors of B and T lymphocytes¹³. The contribution of HSC to lymphoid and myeloid lineages is still not clear and seems to be biased by the diversity of the BM niches they occupy²⁰⁻²². This supports the

hypothesis that there is not a unique BM niche, but rather a variety of “microniches”, that at the same time create and are created by chemotactic gradients and different cell populations. Each of these microniches induces different responses in HSCs such as homing, mobilization, quiescence, self-renewal, or lineage commitment.

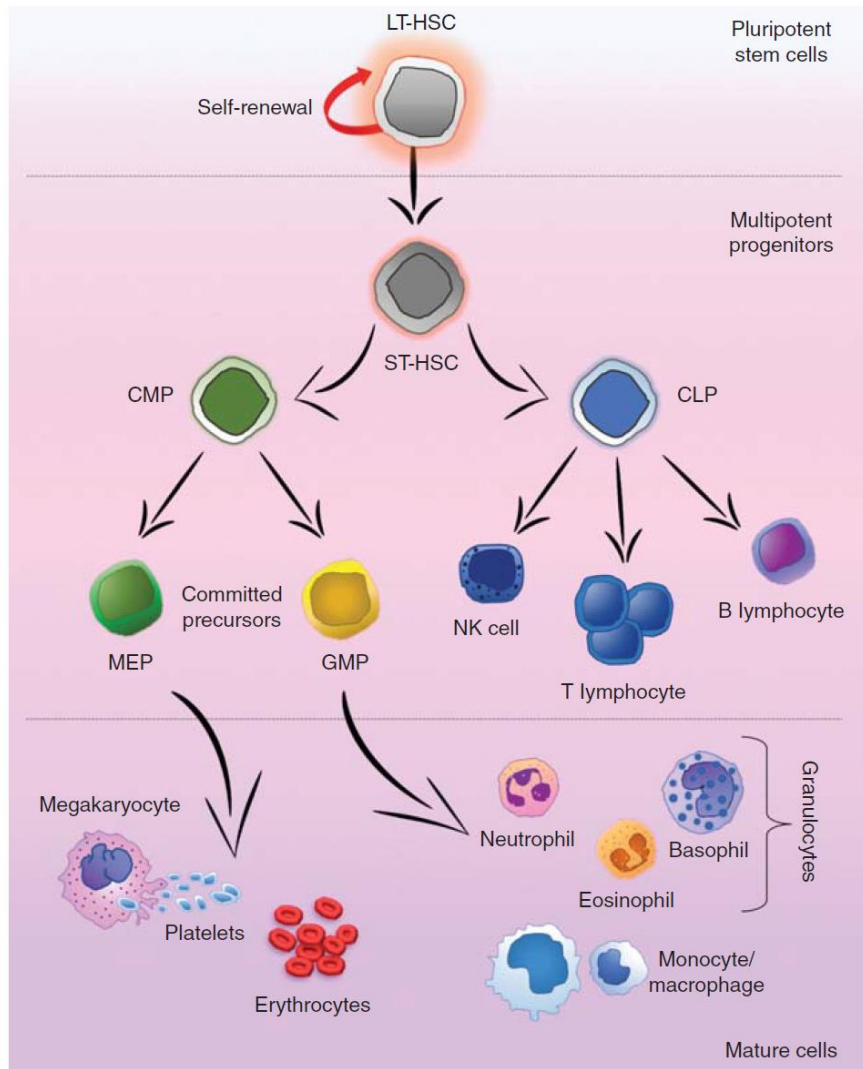


Figure 2.1 - Haematopoiesis. The long-term reconstitution potential of the pluripotent long-term haematopoietic stem cells (LT-HSCs), can further differentiate toward the multipotent short-term (ST)-HSCs in the BM. Subsequent differentiation gives rise to either the common-lymphoid progenitors (CLPs), able to generate the complete lymphoid lineage (natural killer [NK] cells as well as B and T lymphocytes) or the common-myeloid progenitors (CMPs), which are able to differentiate into the myeloid lineage. Following these committed progenitors, both megakaryocyte/erythroid progenitors (MEPs) and granulocyte-macrophage progenitors (GMPs) are able to form all mature myeloid lineage cells in the BM. Figure and legend adapted from ²³.

2.2. Adult BM niche

In mice, haematopoiesis is supported by all bones, but in humans it is only supported by axial skeleton such as the skull, sternum, ribs, spine, sacrum, and pelvis^{24,25}. HSCs, along with other haematopoietic cells, blood vessels and neurons form the soft tissue of the bone, which is distributed by

the interconnecting bone rods and trabeculae, which in turn is covered by a cellular layer called endosteum. Recent extensive studies have uncovered that many cell types in the BM participate in niche activities to support HSC function. Although more than one HSC niche has been defined in the bone marrow, all have the commonality to maintain the unique features of HSCs over time. The bone marrow is a cellularly diverse and dynamic structure that includes HSCs, stromal cells, vascular cells, osteolineage cells, neuronal cells, and the extracellular matrix in which these cells reside. HSC niches are formed from these elements and function to regulate haematopoiesis and maintain HSC quiescence (**Figure 2.2**) either by direct contact or by the production of niche factors that regulate HSCs and other cells populations of the niche (**Table 2.1**).

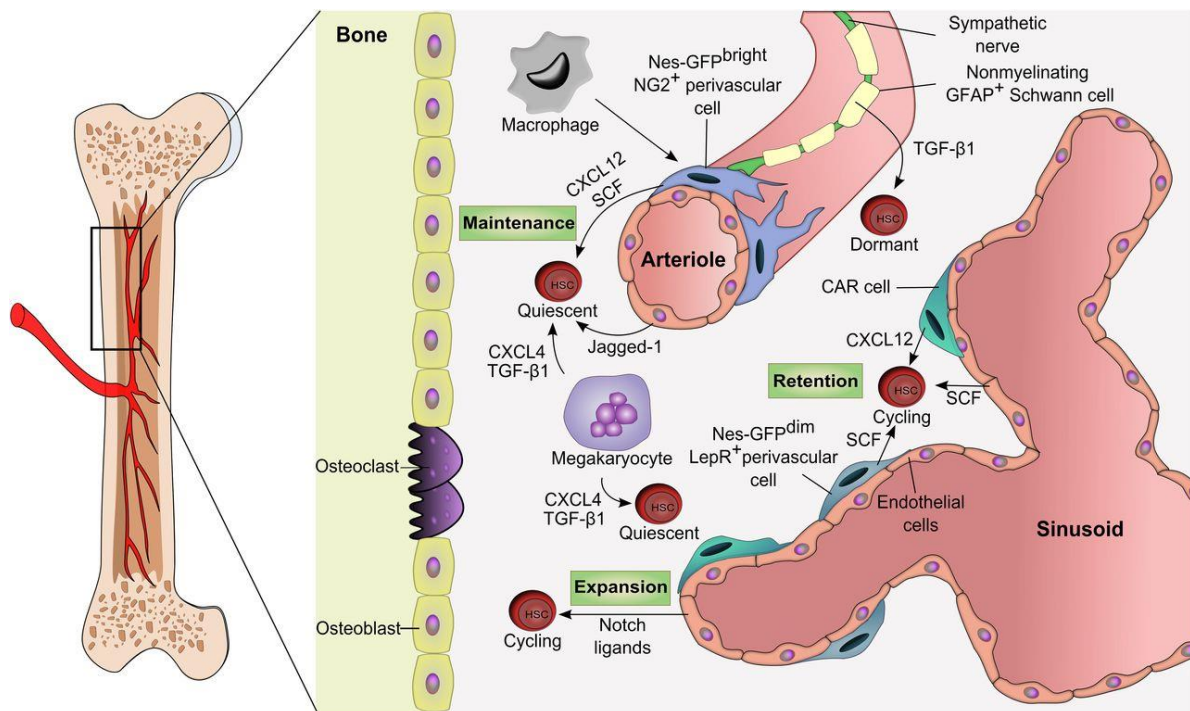


Figure 2.2 - The adult bone marrow HSC niche. The vasculature has emerged as a key structure for the maintenance of HSCs in the bone marrow. Dormant HSCs are found around arterioles where factors such as CXCL12 and SCF secreted by perivascular, endothelial, Schwann, and sympathetic neuronal cells promote their maintenance. Less quiescent or activated HSCs are located near sinusoidal niches which are likely diverse in their influence for self-renewal, proliferation, and differentiation. Haematopoietic cells such as macrophages or megakaryocytes are examples of HSC-derived progeny that can feed back to the niche to influence HSC migration or proliferation. GFAP, glial fibrillary acidic protein; TGF-β1, transforming growth factor beta-1. Figure and legend adapted from ²⁶.

Table 2.1 - Soluble Factors in the Bone Marrow Niche Affecting Mammalian HSCs.

Factor	Source	Receptor	Responding cell type or types	Effect on niche or hematopoiesis
Angiogenin ²⁷	Mesenchymal stromal cells and hematopoietic cells	Secreted RNase that changes RNA processing in a cell-type-specific manner	HSCs, LSK cells and myeloid progenitors	Promotes quiescence in HSCs and the proliferation of myeloid progenitors
Angiopoietin 1 ²⁸	HSCs, KIT+ cells and LEPR+ cells	TIE2	Endothelial cells	Promotes the regeneration of patent blood vessels after vascular injury
Angiopoietin-like protein 3 ²⁹	Sinusoidal endothelial cells and liver cells	Unknown	HSCs	Promotes the maintenance of HSCs and some types of restricted hematopoietic progenitor
BMPs ³⁰⁻³²	Osteoblasts, endothelial cells and megakaryocytes	Complexes of BMP type I and type II receptors	HSCs	Canonical signaling does not affect HSC maintenance or haematopoiesis; BMP4 is required for normal niche function
CXCL 4 ³³	Megakaryocytes	Unknown	HSCs	Inhibits self-renewal and induces quiescence
CXCL 12 ^{34,35}	Osteoblasts, endothelial cells, CAR cells, MSCs, LepR+ perivascular cells	CXCR4	HSCs and lymphoid progenitors	Positive regulator of self-renewal, retention and function
FGF1 ^{36,37}	Megakaryocytes	FGFR1	HSCs and megakaryocytes	Promotes the regeneration of HSCs and megakaryocytes after myeloablation
FGF2 ³⁸	Bone marrow stromal cells	Multiple FGFRs are present on HSCs	HSCs	Promotes the proliferation of HSCs and stromal cells after myeloablation
G-CSF ^{39,40}	Monocytes and macrophages, bone marrow stromal cell populations	G-CSF receptor	Stromal cells and myeloid progenitors	Mobilizes HSCs and increases myelopoiesis
IL-6 ^{41,42}	T cells and macrophages	IL-6 receptor	HSCs and restricted progenitors	Promotes HSC self-renewal and regulates the function of restricted progenitors
IGF1 ^{43,44}	Liver and osteoblasts	IGF1R	HSCs, myeloid progenitors and pro-B cells	Reduced plasma IGF1 levels promote increased HSC self-renewal and increase the frequency of myeloid progenitors
Leptin ^{45,46}	Adipocytes	LEPR	LEPR+/CAR perivascular stromal cells	Causes LEPR+ cells to form adipocytes at the expense of bone

Notch ligands ^{47,48}	Bone marrow stromal cells, endothelial cells and osteoblasts	Notch receptors, particularly Notch 2	HSCs, progenitors and endothelial cells	Notch 2 promotes HSC regeneration after myeloablation
Osteopontin ⁴⁹	Osteoblasts	Integrins and CD44	HSCs	Negatively regulates HSC frequency
Oestrogen ⁵⁰	Ovary	ER α	HSCs as well as other hematopoietic cells	Promotes HSC self-renewal and EMH
Pleiotrophin ⁵¹	Endothelial cells and LEPR+ perivascular stromal cells	Inhibits protein tyrosine phosphatase receptor- ζ	HSCs	Knockout mice have a reduced HSC frequency and show impaired recovery after irradiation
SCF ^{52,53}	Osteoblasts, endothelial cells, MSCs, nestin+ MSCs	c-KIT receptor (CD117)	HSCs	Induces HSC maintenance and self renewal
SLIT ligands ⁵⁴⁻⁵⁶	SLIT2 and SLIT3 are produced by perivascular stromal cells	ROBO4	HSCs and sinusoidal endothelial cells	Has cell-autonomous and non-cell-autonomous effects on HSC engraftment and mobilization
TGF β ^{36,57}	Multiple cells including megakaryocytes; other cells such as Schwann cells regulate TGF β activation	Multiple type I and type II TGF β receptors	HSCs and other cell types	Promotes HSC quiescence and self-renewal
Thrombopoietin ⁵⁸⁻⁶⁵	Highest production in the liver and kidney, but the source of the thrombopoietin that acts on HSCs is not known	MPL	HSCs and megakaryocytes	Required for the postnatal maintenance of HSCs, and for megakaryocyte and platelet production
WNT ligands ⁶⁶⁻⁶⁸	Bone marrow stromal cells and lymphoid cells	Frizzled receptors	HSCs and lymphoid progenitors	Canonical WNT signaling through β -catenin and γ -catenin is dispensable for adult HSC maintenance and for hematopoiesis

FGFR - FGF receptor; IL-6, interleukin-6; LSK, lineage-SCA1+KIT+; ROBO4, roundabout guidance receptor 4; SCA1, spinocerebellar ataxia type 1 protein; TIE2, tyrosine kinase with Ig and EGF homology domains 2. CAR cell, CXCL12-abundant reticular cell; EMH, extramedullary haematopoiesis; ER α , oestrogen receptor- α ; IGF1, insulin-like growth factor 1; IGF1R, IGF1 receptor; MPL, myeloproliferative leukaemia protein; SSC, skeletal stem cell.

Endosteal niche

The formation and regulation of bone matrix is mediated by the opposing actions of the osteoblasts and osteoclasts (cellular components of the endosteum), contributing to the structural foundations for the development of the soft tissue. Together, these osteolineage cells create the “endosteal niche”, the preferential site for homing of transplanted HSCs⁶⁹⁻⁷². Furthermore, HSCs isolated from this region tend to be more primitive, with higher proliferation rate and long term reconstitution potential^{73,74}. After birth, the development of the haematopoietic systems is closely related with bone formation^{75,76}. Osteolineage

cells are probably the most studied haematopoietic niche component, with osteoblasts being initially identified as key regulators of haematopoiesis by *in vitro* studies showing they can promote the expansion of haematopoietic progenitor cells in culture⁷⁵⁻⁷⁹. In the beginning of this century, two independent studies have shown the first *in vivo* evidence that osteoblasts regulate the self-renewal and expansion of HSCs^{53,80}. The increased osteoblast proliferation achieved either by using an osteolineage-specific activator of parathyroid hormone (PTH), or conditional deletion of bone morphogenetic protein (BMP) receptor type IA was correlated with an increase of HSCs numbers. Osteoblasts are also contributing for the pool of cytokines and growth factors involved in the regulation of HSC homing, mobilization, and quiescence, such as: CXC-chemokine ligand 12 (CXCL12), which controls HSC homing, retention and repopulation⁸¹; stem-cell factor (SCF), a key component in HSCs maintenance, although mainly secreted by perivascular cells, is also produced by osteoblasts⁵²; osteopontin (OPN), a component of the glycoprotein matrix responsible for the retention, migration, proliferation and differentiation of HSCs at the endosteal surface^{49,82,83}; granulocyte colony-stimulating factor (G-CSF), important in myelo-differentiation of HSCs^{75,84}; annexin 2 (ANXA2), involved in the control of HSCs homing and engraftment⁸⁵; angiopoietin 1 (ANG1) produced by osteoblast, induces HSC quiescence and adhesion by interaction with TIE2^{86,87}; or thrombopoietin (TPO), involved in the regulation of LT-HSCs quiescence⁶⁰.

Despite these evidences, more recent studies have questioned the importance of osteolineage cells in haematopoiesis regulation, mainly in HSCs steady-state maintenance. For example, specific deletion of CXCL12, SCF or N-cadherin of osteolineage cells did not seem to influence the HSCs number in the BM^{34,52,88}. Also, HSC expansion promoted by osteoblasts through parathyroid hormone (PTH) administration is due to increased Jagged-1 expression in osteoblasts and consequent activation of Notch-1 signalling pathway in HSCs⁸⁹⁻⁹¹. However, inhibition or conditional deletion of receptors of canonical Notch-1 pathway in HSCs did not affect their maintenance in the BM⁹². Additionally, imaging studies have shown no association between phenotypic HSCs and osteoblasts^{93,94}. Nevertheless, these observations are not necessarily contradictory but rather be an evidence of different regulation mechanism dependent on the differentiation state of osteolineage cells. Immature osteoblasts are more associated with the regulation of primitive HSCs, whereas mature osteoblasts and osteocytes are more connected to the regulation and mobilization of haematopoietic progenitor cells. For instances, in osteoblast-ablated mice, LT-HSCs show reduced long-term engraftment and self-renewal capacity as well as loss of quiescence⁹⁵. On the other hand, it seems that osteopontin, mainly produced by mature osteoblasts and osteocytes, negatively regulates the HSC pool⁴⁹. Also, a decrease in osteoblast number, similar to what happens during haematopoietic aging, promotes myeloid expansion at the expense of lymphoid and erythroid expansion and may predispose the BM to the development of acute myeloid leukaemia (AML)⁹⁶.

Perivascular niche

The continuous production of blood cells is a metabolic demanding process that depends on a distribution system for gas exchange, nutrient supply, waste removal and to facilitate the trafficking of haematopoietic cells between the BM and the rest of the organism. This is why the niche is in close proximity to blood vessels which are extremely relevant in the maintenance and proliferation of HSCs¹⁷ (**Figure 2.2**). The blood vessels entry point in the compact BM is made through the bone canal by

arteries that branch first into small arterioles and then to venous sinusoids near the endosteum surface. Venous sinusoids are composed of ECs, separated by basal lamina from discontinuous pericytes, which allow mobilization of mature blood and HSCs⁹⁷.

Despite of first experimental evidence that pointed the endosteal area as the main HSC-supporting niche⁶⁹, further studies gave indication that endogenous HSCs were more closely related with sinusoids¹⁷, with the majority of quiescent HSCs occupying the perivascular niche⁹⁸⁻¹⁰⁰. Also, perivascular cells have a major contribution for the pool of niche factors^{101,102}. Endothelial cells (EC) are one of the components of the perivascular niche and regulate HSC by the secretion of angiocrine factors such as CXCL12, vascular endothelial growth factor A (VEGF-A), fibroblast growth factor 2 (FGF2), ANG1 and thrombospondin-1 (TSP1)¹⁰³⁻¹⁰⁵. EC isolated from the BM have shown to promote proliferation and differentiation of human HSC *in vitro*¹⁰⁶. Neutralization of vascular endothelial growth factor receptor-2 (VEGFR2) and vascular endothelial-cadherin (VE-cadherin) reduced the supportive function of ECs to LT-HSCs⁴⁷. Although ECs have reduced expression of CXCL12 and SCF, the conditional deletion of these niche factors has shown a reduction in HSC number in the bone marrow^{52,88}. Deletion or blockage of E-selectin, an adhesion molecule expressed only by bone marrow ECs, increases HSC quiescence and survival¹⁰⁷. The activity of HSCs is also regulated by direct cell-to-cell contact through Notch signalling⁴⁷. Besides ECs, the perivascular niche is also composed by stromal cells of mesenchymal origin. The best characterized are the CXCL12-abundant reticular (CAR) cells¹⁰⁸. These cells are mainly found around sinusoids and create a homogeneous tangled network throughout the BM³⁵. CAR cells express high levels of *Cxcl12* and *Scf* genes, for example CAR cells express *Cxcl12* levels about 100-fold and 1000-fold higher than ECs and osteoblasts, respectively⁵². Most of CAR cells also express the receptor for leptin (LepR), a hormone secreted by adipocytes^{46,52,98}. Indeed, conditional deletion of *Cxcl12* from LepR-cre-marked cells promoted the mobilization of HSC from the BM to the peripheral blood and spleen but HSC numbers in the BM remained unaltered⁸⁸. On the other hand, conditional deletion of *Scf* on these cells, depleted HSCs in the BM, indicating that CXCL12 and SCF produced in LepR cells are critical for the mobilization and maintenance, respectively, of HSC in the BM⁵². Other markers have been identified to characterize the perivascular stromal cells, including the transcription factor *Osx*, paired related homeobox-1 (*Prx-1*)^{34,88} and neural/glial antigen 2-Cre-marked cells (NG2)¹⁰⁹, expressed exclusively in cells marked with green fluorescent protein (GFP) under regulation of the Nestin promoter (Nes-GFP+). However, these markers are mostly overlapping with CAR LepR+ cells in respect to location and *Cxcl12* and *Scf* expression levels^{93,101}.

More recently it has been proposed that there are two anatomically and functionally distinct perivascular niches, the peri-arteriole and peri-sinusoidal. This is supported by the evidence that LT-HSCs seem to be more closely located to the arterioles rather than venous sinusoids^{93,97,98,110}. Also, some heterogeneity can be observed in EC and stromal cells. EC expressing higher levels of CD31 and endomucin found in the end terminal arterioles also express higher levels of SCF when compared to EC associated with sinusoids^{97,110,111}. Similarly, stromal cells expressing *Nes*-GFP can be divided in two populations regarding the GFP expression. Similarly, stromal cells expressing *Nes*-GFP can be divided in two populations regarding the GFP expression: *Nes*-GFP_{dim} stromal cells which are closely associated with perisinusoidal cells and overlap with LepR+ and CAR cell; and *Nes*-GFP_{bright} stromal cells found close to arterioles⁵². Furthermore, the lower permeability of arterioles promotes a more hypoxic microenvironment, protecting HSC from reactive oxygen species concentration (ROS), preventing their

differentiation¹¹². On the contrary, venous sinusoids are covered by fenestrated basal lamina making them more permeable and exposed to the blood stream, increasing ROS concentration, promoting HSC differentiation.

SNS and glia

The bone marrow is highly innervated by myelinated and non-myelinated nerve fibres and associated Schwann cells^{113, 114}. Although most nerve fibres are found near the arterioles rather than sinusoids^{93,97} and have no direct contact with HSCs⁹⁸, the sympathetic nervous system (SNS) has an important role in the regulation of haematopoiesis. SNS controls the circadian mobilization of HSC to the BM by catecholamine signalling, which are delivered to the BM niche through the blood circulation or by secretion from the nerve endings acting in a paracrine mode¹¹⁵. Catecholamines acts on the $\beta 3$ adrenaline receptor of Nes-GFP+, suppressing their niche function by regulation of CXCL12 expression¹¹⁶. SNS is also related to HSC mobilization controlled by granulocyte colony-stimulating factor (G-CSF)^{113,117,118}. Non-myelinating Schwann cells produce numerous niche factors and promote HSC quiescence by activation of transforming growth factor- β (TGF- β)^{57,119}.

Haematopoietic cell components of the niche

Megakaryocyte

More recent findings have identified HSC directly adjacent to megakaryocytes (MKs)³³, which are found in close proximity to sinusoidal endothelium, with extensions of cytoplasmic protrusions into the sinusoids to produce platelets¹²⁰. MK regulate haematopoiesis in steady-state haematopoiesis^{33, 121} and under stress³⁶. Under homeostatic conditions MK regulate HSCs quiescence by the production of multiple cytokines (e.g., TPO, TGF β , and CXCL4)^{119,121,122}. Conditional ablation of MKs *in vivo* led to loss of quiescence in HSCs and consequently increased HSC frequency and proliferation^{36,123}. This effect could be reverted by the administration of transforming growth factor $\beta 1$ (TGF $\beta 1$, encoded by *Tgfb1*)³⁶ or the chemokine C-X-C motif ligand 4 (CXCL4, also known as platelet factor 4, PF4)¹²³. Accordingly, *Cxcl4* and *Tgfb1* knock-out mice have both shown increased HSC proliferation^{33,36}. Under stress conditions, after BM radioablation, endogenous MK are recruited to the endosteum by thrombopoietin (TPO) signalling¹²⁴. There, MKs promote HSCs engraftment and BM reconstitution by synthesizing MK-derived mesenchymal growth factors, such as fibroblast growth factor 1 (FGF1)^{36,37} and platelet-derived growth factor- β (PDGF- β), which stimulates osteoblast expansion¹²⁴.

Macrophages

Macrophages have been identified as an important BM niche player. They can be found near the endosteal osteoblasts and actively participate in bone mineralization¹²⁵⁻¹²⁷. Moreover, conditional deletion of macrophages by using macrophage-Fas-induced apoptosis transgenic (MAFIA) mice or administrating clodronate-loaded liposomes in wild-type mice led to HSC mobilization from the BM and reduction of endosteal osteoblasts. The same phenotype could be observed in G-CSF-induced HSC mobilization, where a reduction of macrophages and bone loss was detected^{40,128}.

Macrophages, more specifically CD169+ macrophages, regulate HSC maintenance in the BM endosteal niche by promotion of CXCL12 expression in Nes-GFP⁺ stromal cells¹²⁹ through secretion of oncostatin M¹³⁰. The ligand for VCAM-1, integrin VLA-4 which is expressed by macrophages, also regulates HSC maintenance in the BM and spleen¹³¹⁻¹³³. More specifically, in the spleen, silencing or conditional deletion of VCAM-1 in CD169+ macrophages promoted HSCs retention in the spleen¹³⁴. It has also been proposed that macrophages mediate BM HSCs mobilization after phagocytosis of aged neutrophils¹³⁵. A rare subset of macrophages, identified by expression of smooth muscle actin (SMA), were found close to HSC of the BM¹³⁶. They promote HSC expansion after irradiation by cyclooxygenase 2 (COX2)-mediated expression of prostaglandin E2, associated with decreased ROS levels in HSCs¹²⁸. Prostaglandin E2 increases CXCL12 expression in Nes-GFP+ stromal cells¹³⁶ and CXCR4 expression on HSCs¹³⁷. Macrophages also contribute to steady-state and stress-induced erythropoiesis. Reduction of BM erythroblasts is observed after specific depletion of CD169+ macrophages in mice. This depletion also led to myeloablation, decreased erythropoietic recovery followed by acute blood loss, myeloablation¹³⁸. In contrast, in JAK2(V617F)-driven mouse model of polycythemia vera, characterized by elevated erythropoiesis, macrophage depletion normalized the erythroid compartment.¹³⁹

Macrophages are also key regulators of the neuroprotective effect of neuropeptide Y, which regulates homeostasis in tissue expressing Y receptors¹⁴⁰⁻¹⁴². Moreover, neuropeptide Y (NPY) deficient mice showed impaired HSC survival and BM regeneration, which could be rescued by pharmacological elevation of NPY¹⁴³.

Neutrophils

Neutrophils are the most abundant subpopulation of leukocytes, are highly migratory cells and are sensitive to tissue damage or infection¹⁴⁴. Neutrophil expansion in the BM is induced by G-CSF¹⁴⁵ and may lead to mesenchymal stem cell (MSC) and osteoblast apoptosis and consequent reduction of several cytokines and receptors essential for HSC maintenance in the BM¹⁴⁶. *In vitro* experiments have shown that neutrophils synthesize serine proteases, which are capable of cleaving CXCL12¹⁴⁷ CXCR4¹⁴⁸, VCAM-1¹⁴⁹, c-Kit¹⁵⁰ and SCF¹⁵¹. However, serine proteases might not be essential *in vivo*, as no alteration of G-CSF-induced mobilization was observed *in vivo* in mice without these proteases¹⁵². Furthermore, HSC mobilization is not directly proportional to neutrophil numbers in the BM⁴⁰. Under homeostatic conditions, BM neutrophils seem to shadow HSC circulation regulated by the circadian rhythm. Aged neutrophils show higher tropism to the BM by low CD62L and high CXCR4 expression levels. Clearance of aged neutrophils is done by CD169+ macrophages which inhibit CXCL12 production by Nes-GFP⁺ stromal cells, promoting HSC mobilization from the BM¹³⁵.

2.3. Haematological Malignancies

Haematopoiesis balance can be deregulated in response to stress, like infection and wounding, by induction of HSC. These return to a quiescent state when the stress is over or the injury is healed¹⁵³. However, disruption of homeostasis can lead to haematological malignancies, and ultimately to

leukaemia (**Figure 2.3**), which is sustained by leukaemia stem cells (LSC), which share many biological features with HSC¹⁵⁴.

Emerging evidence shows that alterations of the complex and dynamic signalling network regulated by cells of the BM niche are critical in the initiation, maintenance and outcome of myeloid and lymphoid disorders. These alterations can be driven by genetic mutations in stromal cells of the BM and/or promoted by malignant cells, which hijack BM niche supportive function, promoting a leukaemic niche at the expense of HSC¹⁵⁵⁻¹⁶². Although most research has been done in leukaemic settings, these mechanisms can also be observed in multiple myeloma patients¹⁶³.

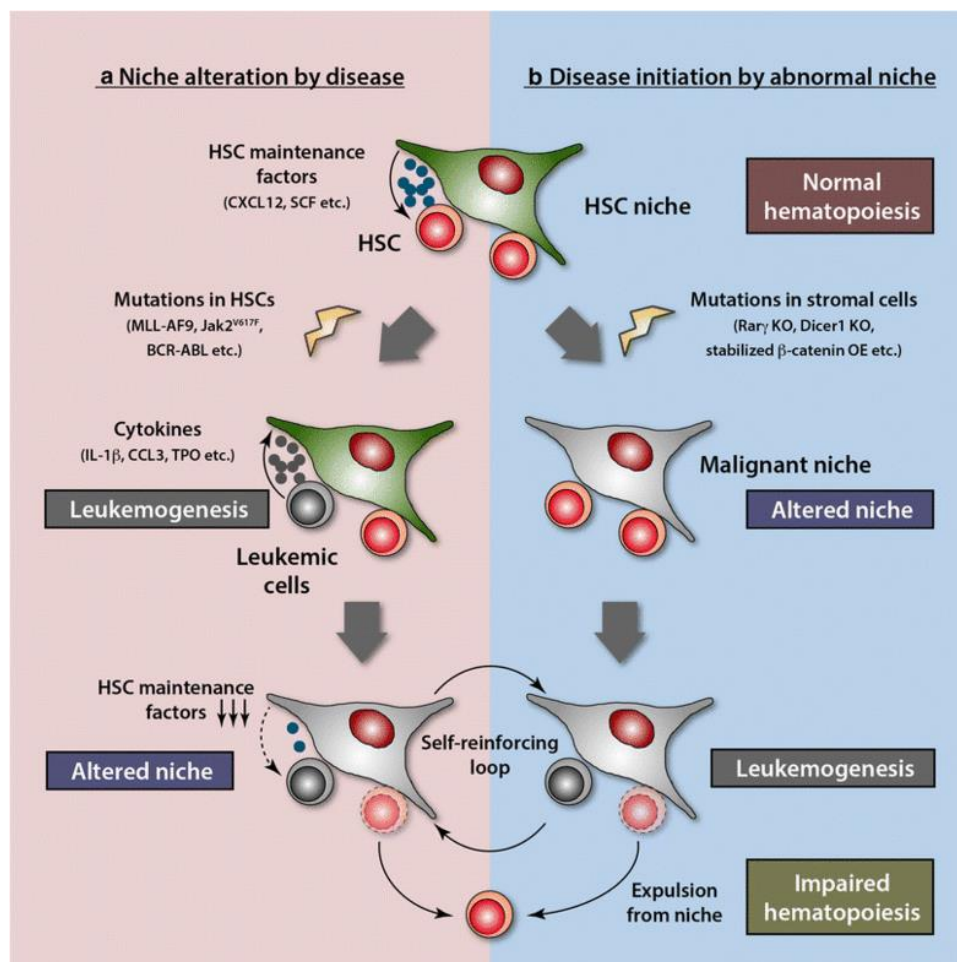


Figure 2.3 - Two models of the interaction of leukemic cells and their microenvironment. While leukemic cells can induce changes in HSC niche (**a**), abnormalities in bone marrow microenvironment have a potential to initiate hematological malignancies (**b**). It is of note that these two models are not mutually exclusive. They can form a self-reinforcing loop, contributing to the disease progression. *KO* knockout, *OE* overexpression. Figure and legend adapted from¹⁶⁴.

2.3.1. Initiation

The first cue for a disease-initiation in the niche was given by the observation of donor-derived leukaemia in patients receiving allogeneic stem cell transplantations¹⁵⁸. This concept gained support by

the experimental observation of myeloproliferative neoplasm phenotype (MPN) induced by genetic deletion of retinoblastoma (Rb) or retinoic acid receptor γ (RAR γ) in mice. Furthermore, only transplantation of healthy HSCs to mutant mice and not transplantation of mutant HSC to wild-type mice, lead to MPN-like disease^{155,156}. Development of MPN was also observed in mice with impaired Notch signalling in nonhaematopoietic cells¹⁶⁵ and more recently in genetically altered Nes⁺ stromal cells¹⁶⁰.

Alterations at the endosteal niche, more specifically, mutations in osteoblastic lineage cells (OBC) have been implicated in the development of myelodysplasia (MDS)¹⁶² and AML disease¹⁵⁹. Inactivation of Dicer1 in OBC promotes aberrant gene expression and led to MDS in mice. For example, a downregulation of *slds*, the gene mutated in Schwachman-Bodian-Diamond syndrome (SBDS)¹⁶² was observed when Dicer1 was inactivated. In a subsequent study, *slds* deletion in stromal cells promoted an inflammatory response which increased oxidative stress and DNA-damage response in HSC. This effect was driven by the activation of Toll-like receptor (TLR) signalling in HSC, by stromal secretion of endogenous damage-associated molecular pattern (DAMP) molecules S100A8/9. Interestingly, AML development risk in MDS patients can be predicted by the expression levels of S100A8/9¹⁶⁶

Deregulation of Notch pathway was also shown to promote MDS development which rapidly evolves to AML. A mutation in mice OBC led to overexpression of Jagged-1, a Notch ligand, followed by Notch signalling activation in HSC and β -catenin accumulation. This pathway triggered recurrent chromosomal aberrations and somatic mutations promoting clonal expansion^{91,159}. Notably, stromal cells isolated from MDS/AML patients have also shown increased Jagged1-expression together with downregulation of key molecules in HSC regulation. MSC derived from MDS patients show decreased osteogenic differentiation and impaired support of healthy CD34⁺ in long-term culture-initiating cell assays. These observations were correlated with hypermethylation patterns in these MSC¹⁶¹.

2.3.2. Progression and expansion

The impaired haematopoietic function and decreased HSC numbers observed in patients with haematological malignancies suggests that HSCs are being expelled from their niche by LSC. This action takes possession of the niche for leukaemogenesis. Alongside with this concept, morphological and functional changes in the BM microenvironments were also reported in patients with different haematological malignancies, such as primary myelofibrosis (PMF), myelodysplastic syndrome (MDS), and different kinds of leukaemia¹⁵⁷. Recent advances in murine mouse models of haematopoietic malignancies have helped to gain further insight in the mechanism of BM niche remodelling by myelodysplastic cells. More specifically, LSCs can remodel osteoblastic, neural, and endothelial BM microenvironments, by deregulated production of a variety of signals, including proinflammatory and angiogenic chemokines and cytokines, such as CXCL12, VEGF, tumour necrosis factor (TNF)- α , IL-1, IL-6, and IL-8¹⁶⁶⁻¹⁶⁸.

Aberrant endosteal niche

Besides all the HSC-intrinsic transformation steps that need to occur in AML there are extrinsic niche-specific factors that are fundamental for disease development. The characterization of the impact

that the disease has in the niche, and *vice-versa*, is very important. Clinical reports of osteopenia and osteoporosis in MDS and AML patients has been attributed to the observation of reduced numbers of osteoblasts in newly diagnosed AML patients. Decreased levels of cell cycle related genes and CXCL12 was also observed in BM plasma of AML patients, but MSC isolated from the same patients had increased levels of Jagged-1 and CXCL12 that favour leukaemogenesis^{169,170}. Furthermore, better prognosis after chemotherapy was correlated with an increase in osteoblast activity and bone mass¹⁷¹⁻¹⁷³. Accordingly, in AML and ALL mouse models deletion of OBC led to a reduction of bone mineral density accompanied by an increase in bone remodelling osteoclasts. This alteration of the endosteum niche seems to favour leukaemia progression and reduce HSC maintenance¹⁷⁴⁻¹⁷⁶.

The role of osteoblast microenvironment in leukaemia was further elucidated by stimulated normal haematopoiesis, delayed disease engraftment, reduced tumour burden, and prolonged survival, after pharmacological induced maintenance of osteoblast number⁹⁶. In a more recent study, the establishment of a human AML xenotransplant model in Nod-Scid-gamma (NSG) mice allowed to observe that patient-derived MSC can grow and differentiate effectively at the NSG-mice BM cavity, recapitulating the leukaemic-supportive function and LSC increased engraftment promoted by the formation of functional vascularized ossicles¹⁷⁷.

Similar to AML, in pediatric ALL patients, it was also observed a decrease in CXCL12 in the BM and peripheral blood plasma when compared with samples of healthy donors¹⁷⁸. This observation was reinforced using osteoblastic T cell ALL mouse models, where a decrease in OBC numbers was accompanied by a reduced CXCL12 expression. This could be reversed by administration of Notch inhibitors¹⁷⁶, in accordance with the observation of decreased CXCL12 in Notch-induced T cell ALL mouse model¹⁷⁹.

Furthermore, with the help of intravital imaging at the calvaria BM, was also possible to observe that Nalm-6 ALL transplanted cells can compete with haematopoietic progenitor stem cells for perivascular niches and are able to disrupt normal HSC regulation by the upregulation of SCF and downregulation of CXCL12 recruitment CD34⁺ HSC to leukaemic niches and impaired CD34⁺ mobilization in response to G-CSF¹⁸⁰.

An opposite effect at the endosteal niche has been observed in BCR/ABL transgenic chronic myeloid leukemia (CML) mice. In this model, transplantation of BCR/ABL mutant cells into wild-type mice promoted the expansion of OBCs in the BM. This effect was mediated by direct contact of leukaemic cells with MSC and increased secretion of inflammatory cytokines and chemokines, including macrophage inflammatory protein-1 α (MIP-1 α), chemokine ligand 3 (CCL3), TPO, interleukin-1 α (IL-1 α), IL-1 β , tumour necrosis factor- α (TNF- α), IL-6, and G-CSF. This proinflammatory environment compromised HSC support function of OCB, with loss of LT-HSC at the BM and establishment of leukaemia supportive microenvironment^{181,182}.

Perivascular niche

Malignant cells have also been shown to manipulate the perivascular niche in ALL and AML. Increased expression levels of VEGF and basic fibroblast growth factor (bFGF) are found in BM plasma of ALL patients. Also, evidence of neoangiogenesis was observed in immunocompromised mice when transplanted with cells from primary ALL patients¹⁸³. Cells isolated from AML patients were shown to

induce EC proliferation when co-cultured with human lung or dermal microvascular ECs, this was associated with increased levels of pro-angiogenic CXCL8, and decreased levels of anti-angiogenic factors CXCL9, CXCL10, and CXCL11¹⁸⁴. In AML models, leukaemia cells can modulate ECs by upregulation of c-FOS and senescence-related genes, including interferon signalling and COL3A1¹⁸⁵. Interestingly, the perivascular niche seems to act as a protective AML niche, as leukaemic cells adjacent to vessels become more quiescent and resistant to chemotherapy¹⁸⁶. Accordingly, pharmacological degradation of EC adhesion molecules, reduced AML chemoresistance¹⁸⁷.

Neuropathy induced by malignant cells alters the BM Niche

The SNS niche was also shown to be disrupted in a murine MPN model generated by Janus kinase 2 (JAK2) mutation. In this model, damage of sympathetic nerve fibres and death of Schwann cells was induced by IL-1 β produced in mutant cells, which lead to a reduction of Nes⁺MSCs and followed by decreased CXCL12 levels. Recovery of Nes⁺MSCs and reduction of leukaemia burden at the BM could be achieved by treatment with β 3-adrenergic receptors (Adr β 3) agonist¹⁸⁸. Similar results were obtained in a MLL-AF9 AML model, where SNS niche disruption led to a decrease of Adr β 3 expression and HSC maintenance factors, such as CXCL12, SCF, ANG1, and VCAM1 followed by expansion of MSC primed for osteoblastic differentiation. This effect could be mediated by β 2 adrenergic receptor (Adr β 2) as increased number of LSC were observed at the BM when using Adr β 2 antagonist but not (Adr β 3)¹⁷⁵.

Exosomes

The observation of high numbers of microvesicles in leukaemic areas of ALL, CLL, AML and CLL patients, associated with detection of VEGF, bFGF, hepatocyte growth factor (HGF), and TNF- α in the plasma and urine of patients, indicates that exosomes might be instrumental during BM niche modulation by haematological malignancies^{189,190}. Moreover, *in vitro* studies have shown examples of leukaemia-secreted exosomes in CML, AML cells lines and primary AML samples¹⁹¹. These exosomes, enriched in unique RNA and microRNA, can be up taken by BM stromal cells, which leads to direct and indirect effects on HSC. Exosomes isolated from AML cells induced downregulation of CXCL12 and SCF in stromal cells as well as downregulation of CXCR4 and c-kit in HSCs^{191,192}. In CML, exosomes induce IL-8 production in stromal cells, a CML survival factor and also carried miR126, which targets HSC niche factors CXCL12 and VCAM1^{193,194}. ECs and MSCs can be reprogrammed to leukaemia supporting cells by CLL-derived exosomes. Leukaemia cell proliferation and angiogenesis was promoted by secretion of cytokines from these cells and was observed *ex vivo* after CLL-exosome uptake¹⁹⁵. Exosomes released from BM MSC collected from MDS patients can modulate *in vitro* CD34⁺ cells expression of MDM2 and TP53 genes by transferring miR-10a and miR-15a, suggesting that intercellular communication between malignant BM niche and HSC can also be mediated by exosomes¹⁹⁶.

2.3.3. AML

AML is a malignant blood disorder characterized by rapid abnormal proliferation and differentiation of HSCs, resulting in the accumulation of immature myeloid precursors (myeloblasts) in the BM and peripheral blood (PB). This uncontrolled expansion of malignant haematopoietic precursor cells at the

expense of normal haematopoietic cells results in the exhaustion of the BM. AML it's the most common type of acute leukaemia in adults¹⁹⁷, with an incidence of 3 to 5 cases per 100.000 in patients with less than 65 years old and in patients older than 65. After an increased incidence observed in the last quarter of the 20th century, AML incidence started to stabilize in this century¹⁹⁸. To this contributed the advancement of diagnostic and treatment procedures, which led to an improvement in the disease outcome, mostly in young patients. With a median age at diagnosis of approximately 70 years¹⁹⁹, AML has the worst prognosis within all types of leukaemia, especially in elder patients²⁰⁰, with a recovery rate of 35% to 40% in patients younger than 65 years old and only 5% to 15% in patients older than 65 years old, within the first year of the diagnosis^{198,201-203}.

In most of the cases, AML appears as a *de novo* malignancy in previously healthy individual or as therapy-related AML, as a consequence to previous treatments by exposure to DNA-damaging and cytotoxic agents (for example, ionizing radiation, alkylating agents or topoisomerase II inhibitors)^{204,205}. Although no strong evidence of familiar predisposition to AML has been reported, except relatives of young patients, there is an increased risk for haematological malignancies and solid tumours among relatives of AML patients²⁰⁶. Also, there is predisposition of AML development in individuals with inherit disorders, such as Down syndrome, Fanconi anemia, Bloom syndrome, ataxia-telangiectasia, Diamond–Blackfan anemia, Schwachman–Diamond syndrome and severe congenital neutropenia (also called Kostmann syndrome) (for a review see REF²⁰⁷).

The clinical diagnosis of acute leukaemia is established by the presence of 20% or more blasts in the BM or PB²⁰². Furthermore, AML and its subtypes are distinguished from other leukaemias by immunophenotyping, cytogenetic and molecular characterization of the myeloblasts. The cytogenetic heterogeneity in AML has been known for more than 30 years, with about half of all AMLs having structural cytogenetic changes visible at the karyotype level, with translocations and chromosomal gains or losses²⁰⁸⁻²¹⁰. For example, the chromosomal translocations such as t(8:21) in core-binding factor AML (CBF-AML) or t(15:17) in acute promyelocytic leukaemia (APL) result in the formation of chimeric proteins (RUNX1-RUNX1T1 and PML-RARA, respectively), which alter the normal maturation process of myeloid precursor cells.

However, advancements of the past decade have uncovered an enormous molecular heterogeneity of the disease. In fact, genetic mutations can be found in more than 97% of the cases, independently of the presence of large chromosomal changes^{211,212}. In 2016 a report from World Health Organization (WHO), classified AML based in genetic criteria along with morphological, immunophenotyping and clinical presentation to define five major disease entities(**Table 2.2**): AML with recurrent genetic abnormalities, AML with myelodysplasia-related features; therapy-related AML; AML not otherwise specified; myeloid sarcoma; and myeloid proliferation related to Down syndrome²¹³. The recognition of different combinations and accumulations of genetic abnormalities in AML, allowed better prognosis definition and adjustment of treatments to the specific AML subtype^{211,214}

Table 2.2 - WHO classification AML subtypes ²¹⁵.

WHO classification of AML subtypes
AML with recurrent genetic abnormalities
• AML with t(8;21)(q22;q22); RUNX1–RUNX1T1
• AML with inv(16)(p13.1q22) or t(16;16)(p13.1;q22); CBFβ–MYH11
• APL with t(15;17)(q22;q12); PML–RARA
• AML with t(9;11)(p21.3;q23.3); <i>MLLT3-KMT2A</i>
• AML with t(9;11)(p22;q23); <i>MLLT3-MLL</i>
• AML with t(6;9)(p23;q34); DEK–NUP214
• AML with inv(3)(q21q26.2) or t(3;3)(q21;q26.2); RPN1–EVI1
• AML with inv(3)(q21.3q26.2) or t(3;3)(q21.3;q26.2); <i>GATA2, MECOM</i>
• AML (megakaryoblastic) with t(1;22)(p13;q13); RBM15–MKL1
• Provisional entity: AML with mutated NPM1
• Provisional entity: AML with mutated CEBPA
• Provisional entity: AML with BCR-ABL1
• Provisional entity: AML with mutated RUNX1
AML with myelodysplasia-related changes*
Therapy-related myeloid neoplasms
AML not otherwise specified
• AML with minimal differentiation
• AML without maturation
• AML with maturation
• Acute myelomonocytic leukaemia
• Acute monoblastic and monocytic leukaemia
• Acute erythroid leukaemia
• Acute megakaryoblastic leukaemia
• Acute basophilic leukaemia
• Acute panmyelosis with myelofibrosis
Myeloid sarcomas
Myeloid proliferations related to Down syndrome
• Transient abnormal myelopoiesis
• Myeloid leukaemia associated with Down syndrome
Blastic plasmacytoid dendritic cell neoplasms

CBFB, core-binding factor-β; CEBPA, CCAAT/ enhancer-binding protein-α; MKL1, megakaryoblastic leukaemia (translocation) 1; MLL, myeloid/lymphoid or mixed-lineage leukaemia (also known as KMT2A); MLLT3, MLL translocated to 3; MYH11, myosin heavy chain 11 smooth muscle; NPM1, nucleophosmin; NUP214, nucleoporin 214kDa; PML, promyelocytic leukaemia; RBM15, RNA-binding motif protein 15; RPN1, ribophorin I; RUNX1, Runt-related transcription factor 1; RUNX1T1, RUNX1 translocated to 1. *Includes specific recurrent chromosomal abnormalities.

Classification/Genetics

Observations in animal models that more than one cooperating mutations is necessary to develop AML led to the concept of a two-hit model of leukaemogenesis ²¹⁶⁻²¹⁸. According to this model, these mutations can be categorized in three functional groups: Class I, mutations which activates cell signalling pathways involved in the regulation of cell proliferation and survival; Class II, mutation in genes encoding transcription factors which regulate cell differentiation and self-renewal; and Class III, mutations in epigenetic modifiers which regulate the expression of several genes with effect on both cellular differentiation and proliferation. Impairment of normal haematopoiesis and consequent leukaemia development requires the conjugation of class I mutations with class II and/or III^{219,220}. However, data from genome sequencing revealed a large number of functional categories, also including

cohesin complex and spliceosome mutation ²¹¹ (Table 2.3). The combination of mutations is highly variable, but some combinations can be specific, as for example, acquired mutation in GATA-binding protein 2 (*GATA2*) are always paired with mutations in CCAAT/enhancer-binding protein- α (*CEBPA*) suggesting that they are cooperative ²²¹. Other combinations appear to be mutually exclusive, for example, the coincidence of the FMS-related tyrosine kinase 3 (*FLT3*) and *RAS* or of isocitrate dehydrogenase (*IDH*), tet methylcytosine dioxygenase 2 (*TET2*) and Wilms tumour 1 (*WT1*) mutations is uncommon, suggesting they are functionally related²¹¹. Somatic mutations in genes involved in epigenetic regulation, including genes involved in the regulation of DNA methylation and post-translational histone modifications, such as *DNMT3A*, *TET2*, *WT1*, *IDH1* and *IDH2*. These recurrent mutations are found in preleukaemic HSC, which are capable of multilineage differentiation and confer these cells a higher resistance to chemotherapy and increased probability of relapse during remission ²²²⁻²²⁴. Recent studies show that these kinds of mutations increase with age in clonal haematopoiesis and are associated with higher risk of haematological malignancies and death²²⁵⁻²²⁷.

Table 2.3 - Proposed Genomic Classification of AML ²²⁸ .

Genomic Subgroup	Frequency in the Study Cohort (N = 1540) no. of patients (%)	Most Frequently Mutated Genes* gene (%)
AML with <i>NPM1</i> mutation	418 (27)	<i>NPM1</i> (100), <i>DNMT3A</i> (54), <i>FLT3ITD</i> (39), <i>NRAS</i> (19), <i>TET2</i> (16), <i>PTPN11</i> (15)
AML with mutated chromatin, RNA-splicing genes, or both [†]	275 (18)	<i>RUNX1</i> (39), <i>MLLPTD</i> (25), <i>SRSF2</i> (22), <i>DNMT3A</i> (20), <i>ASXLI</i> (17), <i>STAG2</i> (16), <i>NRAS</i> (16), <i>TET2</i> (15), <i>FLT3ITD</i> (15)
AML with <i>TP53</i> mutations, chromosomal aneuploidy, or both [‡]	199 (13)	Complex karyotype (68), -5/5q (47), -7/7q (44), <i>TP53</i> (44), -17/17p (31), -12/12p (17), +8/8q (16)
AML with <i>inv(16)(p13.1;q22)</i> or <i>t(16;16)(p13.1;q22)</i> ; <i>CBFB-MYH11</i>	81 (5)	<i>inv(16)</i> (100), <i>NRAS</i> (53), +8/8q (16), +22 (16), <i>KIT</i> (15), <i>FLT3TKD</i> (15)
AML with biallelic <i>CEBPA</i> mutations	66 (4)	<i>CEBPA</i> biallelic (100), <i>NRAS</i> (30), <i>WT1</i> (21), <i>GATA2</i> (20)
AML with <i>t(15;17)(q22;q12)</i> ; <i>PML-RARA</i>	60 (4)	<i>t(15;17)</i> (100), <i>FLT3ITD</i> (35), <i>WT1</i> (17)
AML with <i>t(8;21)(q22;q22)</i> ; <i>RUNX1-RUNX1T1</i>	60 (4)	<i>t(8;21)</i> (100), <i>KIT</i> (38), -Y (33), -9q (18)
AML with <i>MLL</i> fusion genes; <i>t(x;11)(x;q23)</i> [§]	44 (3)	<i>t(x;11q23)</i> (100), <i>NRAS</i> (23)
AML with <i>inv(3)(q21q26.2)</i> or <i>t(3;3)(q21;q26.2)</i> ; <i>GATA2</i> , <i>MECOM(EVII)</i>	20 (1)	<i>inv(3)</i> (100), -7 (85), <i>KRAS</i> (30), <i>NRAS</i> (30), <i>PTPN11</i> (30), <i>ETV6</i> (15), <i>PHF6</i> (15), <i>SF3B1</i> (15)
AML with <i>IDH2R172</i> mutations and no other class-defining lesions	18 (1)	<i>IDH2R172</i> (100), <i>DNMT3A</i> (67), +8/8q (17)
AML with <i>t(6;9)(p23;q34)</i> ; <i>DEK-NUP214</i>	15 (1)	<i>t(6;9)</i> (100), <i>FLT3ITD</i> (80), <i>KRAS</i> (20)
AML with driver mutations but no detected class-defining lesions	166 (11)	<i>FLT3ITD</i> (39), <i>DNMT3A</i> (16)
AML with no detected driver mutations	62 (4)	
AML meeting criteria for ≥ 2 genomic subgroups	56 (4)	

* Genes with a frequency of 15% or higher are shown in descending order of frequency. Key contributing genes in each class are shown in boldface type.

† Classification in this subgroup requires one or more driver mutations in *RUNX1*, *ASXL1*, *BCOR*, *STAG2*, *EZH2*, *SRSF2*, *SF3B1*, *U2AF1*, *ZRSR2*, or *MLLPTD*. In the presence of other class-defining lesions — namely, *inv(16)*, *t(15;17)*, *t(8;21)*, *t(6;9)*, *MLL* fusion genes, or complex karyotype or driver mutations in *TP53*, *NPM1*, or *CEBPA* biallelic — two or more chromatin-spliceosome mutations are required.

‡ Classification in this subgroup requires *TP53* mutation, complex karyotype, or in the absence of other class-defining lesions, one or more of the following: *-7/7q*, *-5/5q*, *-4/4q*, *-9q*, *-12/12p*, *-17/-17p*, *-18/18q*, *-20/20q*, *+11/11q*, *+13*, *+21*, or *+22*.

§ Multiple fusion partners for *MLL* were found, with the clinical implications depending on the specific fusion partner.

2.3.4. Traditional treatments

If eligible for intensive treatment, according to a modification of the widely used European LeukaemiaNet guidelines, newly diagnosed AML patients are divided in four risk groups based on the cytogenetic and molecular abnormalities. This classification has prognostic and recommended treatment indications, as well as recommendation to use or not allogeneic HSCT after first complete remission (CR) (Table 2.4).

Table 2.4 – Therapeutic implication of current stratification of Molecular Genetic and Cytogenetic Alterations, according to ELN Recommendations*. Adapted from ²¹⁵.

Risk Profile	Subsets	Induction therapy	Consensus regarding allogeneic HSCT after first CR	Risk of relapse with or without HSCT	Comments
Favorable	<i>t(8;21)(q22;q22)</i> ; <i>RUNX1-RUNX1T1</i> <i>inv(16)(p13.1q22)</i> or <i>t(16;16)(p13.1;q22)</i> ; <i>CBFB-MYH11</i> Mutated <i>NPM1</i> without <i>FLT3</i> -ITD (normal karyotype) Biallelic mutated <i>CEBPA</i> (normal karyotype)	Standard induction# or FLAG-Ida+	Not recommended	<ul style="list-style-type: none"> • 40–50% without • 15–20% with 	Consider HSCT if: Risk of TRM with HSCT is <10% (HCT-CI:0); MRD is present after two courses of chemotherapy
Intermediate I†	Mutated <i>NPM1</i> and <i>FLT3</i> -ITD (normal karyotype) Wild-type <i>NPM1</i> and <i>FLT3</i> -ITD (normal karyotype) Wild-type <i>NPM1</i> without <i>FLT3</i> -ITD (normal karyotype)	Standard induction# or FLAG-Ida+	Usually recommended	50–70% without 20–30% with	Consider no HSCT if the risk of TRM with HSCT is >30% (HCT-CI: >4)
Intermediate II	<i>t(9;11)(p22;q23)</i> ; <i>MLL3-KMT2A</i> Cytogenetic abnormalities not classified as favorable or adverse‡	Standard induction# or FLAG-Ida+	Strongly recommended	70–80% without 30–40% with	As in intermediate I
Adverse	<i>inv(3)(q21q26.2)</i> or <i>t(3;3)(q21;q26.2)</i> ; <i>GATA2-MECOM (EVII)</i> <i>t(6;9)(p23;q34)</i> ; <i>DEK-NUP214</i> <i>t(v;11)(v;q23)</i> ; <i>KMT2A</i> rearranged <i>-5</i> or <i>del(5q)</i> ; <i>-7</i> ; <i>abnl(17p)</i> ; complex karyotype§	FLAG-Ida+ or clinical trial	Strongly recommended	90–100% without 40–50% with	CR rate is <50% with standard Induction and -5/del5q.-7/del7q or complex 7 Consider no HSCT if the risk of TRM is >40% (HCT-CI>7)

* Three changes were made to the original recommendations reported by ²²⁹ First, cases of AML with mutated *CEBPA* are now restricted to cases with biallelic *CEBPA* mutations.⁴ Second, the molecular designation of *inv(3)(q21q26.2)* or *t(3;3)(q21;q26.2)* has been changed to *GATA2-MECOM (EVII)*.³ Finally, for *MLL*, the official gene symbol *KMT2A* (lysine [K]-specific methyltransferase 2A) has been adopted.

† This category includes all cases of AML with a normal karyotype except for those included in the favourable subgroup; most of these cases are associated with a poor prognosis, but they should be reported separately because of the potential different response to treatment.

‡ Adequate numbers of most abnormalities have not been studied to draw firm conclusions regarding their prognostic significance.

§ A complex karyotype is defined as three or more chromosomal abnormalities in the absence of one of the World Health Organization–designated recurring translocations or inversions — t(8;21), inv(16) or t(16;16), t(9;11), t(v;11) (v;q23), t(6;9), and inv(3)/t(3;3). About two thirds of patients with AML with a complex karyotype have a mutation of *TP53*, a deletion of *TP53*, or both. *TP53* alterations in AML rarely occur outside a complex karyotype.

#Standard induction therapy consists of an anthracycline for 3 days combined with cytarabine for 7–10 days.

+ FLAG-Ida consists of high-dose cytarabine, idarubicin, fludarabine and granulocyte colony-stimulating factor.

HCT-CI, Haematopoietic Cell Transplantation Co-morbidity Index; ITD, internal tandem duplication; MRD, minimal residual disease; NK, normal karyotype

Traditional treatment of AML is normally divided in induction, consolidation and maintenance phases. Eligible patients will first undergo induction therapy (cytotoxic chemotherapy) until they achieve CR, however, minimal residual disease often persists, and a relapse is highly likely to occur after induction phase is completed, so a round of consolidation therapy is usual applied after induction. Except for the cases when HSCT is used, consolidation therapy is usually in a similar or slightly lower intensity than induction therapy. During maintenance therapy, doses of the cytotoxic agents are normally lower than the previous phases. Usually it is applied only: after 3-4 cycles of induction and consolidation therapy in patients aged 60 or less, and after 2-3 cycles in older patients²⁰². The dose intensity of the cytotoxic therapy is also defined taking in account the efficacy/adverse effects ratio, which is strongly related with patient age.

The typical induction therapy consists of 7 to 10 days of continuous infusion of cytarabine (also known as ARA-C), combined with 3 days of an anthracycline and is generally offered to patients with a favorable to intermediate prognosis and a low risk of treatment related mortality (TRM)²³⁰. Standard induction doses consist of 100-200 mg/m² of cytarabine daily infusion, although higher doses have shown higher efficacy, this came with increased toxicity to the patients, thus only used in refractory disease²³⁰⁻²³². In leukaemia treatment, more specifically in AML, daunorubicin (60-90 mg/m²) or idarubicin (12 mg/m²) are the commonly used anthracyclines, both with similar CR and survival rates^{230,233,234}. Higher doses of daunorubicin can be beneficial in patients with DNMT3A and KMT2A mutations, which represents a poor prognostic marker²¹². Typically, in patients younger than 65 years old, induction therapy has a CR rate between 60-80%²³⁵, but 25% to 50% of the patients still present persistent cytological evidence of the disease after one cycle of induction therapy and require reinduction²³⁶. In these cases, treatment options include a second cycle of cytarabine combined with an anthracycline, higher doses of cytarabine alone or patients can also be administrated with a combination of fludarabine, cytarabine (ARA-C) and G-CSF (FLAG) and in some cases with the addition of idarubicin (FLAG-IDA), although it did not increase CR rate, it increased remission duration^{230,237-239}. Patients older than 65 are more likely to present more adverse cytogenetic-risk profiles, are less likely to respond to chemotherapy (up to 40%-60% CR rates) and often more susceptible to treatment related toxicities. Despite the significantly worse prognosis, induction therapy still shows better survival rates when compares to supportive care and palliative chemotherapy and should be pursued when possible²³². Taking in account the low success rate of conventional therapy in older patients, they are usually considered good candidates for investigational therapies.

Other cytotoxic agents have been studied as an alternative to traditional induction regimes. For example, the use of hypomethylating agents, traditionally used in the treatment of myelodysplastic syndrome (MDS), as recently arise as a potential candidate for the treatment of older patients as well as patients with adverse cytogenetic-risk profile or MDR-AML²⁴⁰. Also, the addition to induction therapy of Gemtuzumab ozogamicin, a humanized anti-CD33 monoclonal antibody (present in AML blast) combined with the cytotoxic agent calicheamicin, have shown to reduce the risk of relapse and improved survival in patients with favorable and intermediate risk profiles^{241,242}. Although Gentumuzab ozogamicin is no longer available in USA and Europe, analogues of it are in clinical trials. More recently, a large randomized international study suggested that the addition of Midostaurin (a multikinase inhibitor) to induction and consolidation therapy and its use as a single agent during maintenance improved overall and event-free percentages²⁴³.

While in remission, patients should be offered consolidation therapy to eliminate residual disease and reduce the risk of relapse. The standard consolidation therapy includes conventional chemotherapy and allogeneic haematopoietic stem cell transplantation (allo-HSCT) alone or most commonly in combination. The choice between them is based mainly on the leukaemic genetic risk profile and on the risk of death weighed against the likelihood of treatment failure or relapse^{202,244-246}. In patients with favorable prognosis, chemotherapy is normally the first choice as HSCT shows no benefit in these patients when compared with chemotherapy in patients with a favourable cytogenetic-risk profile^{247,248}. Consolidation chemotherapy protocols consist of an intermediate dose of cytarabine (2-4 cycles of six doses at 2–3 g/m²) which has been shown to be as efficient as high dose cytarabine or multi-agent protocols and have cure rates around 60%-70%^{231,237,249}. In patients with intermediate or high-risk profile, allo-HSCT remains the most effective long-term therapy for AML. However, several patients never become eligible for transplant given co-morbidities, failure to achieve CR or lack of suitable donor²⁵⁰⁻²⁵². Autologous HSCT normally does not improve the outcome, but it can be considered as an alternative consolidation therapy for selected patients²⁵³.

Haematopoietic stem cell transplantation

The potentially lethal levels of chemotherapy during induction phase may compromise the function of normal haematopoiesis. Post-remission allogeneic HSCT provides an important rescue tactic for the replenishment of normal haematopoiesis and also to trigger an immunological antileukaemic response, the graft-versus-leukaemia effect^{245,254} (**Figure 2.4**).

Before transplantation, immunosuppressive conditioning is necessary to permit the engraftment. Chemoradiotherapy is often chosen because of its immunosuppression plus anti-leukaemic effect. However, HSCT is not risk-free (e.g. Graft-versus-host disease – GVHD) and the choice of whether to perform HSCT or not after remission is dependent on balancing the reduction in relapse rate against the procedure related mortality and morbidity, being HSCT normally reserved for intermediate and adverse-risk AML patients who otherwise are unlikely to achieve an extended complete remission^{244,246,247,255-259}.

The discovery of Human leukocyte antigen (HLA) system of MHC class I and II receptors, which engage T-cell antigen receptors, allowed to find histocompatible matching donors and recipients and open the doors to implement HSCT as a therapy^{260,261}. The most common sources of HSC for transplant are the BM and mobilized PB. Their use was initially restricted to HLA-matched siblings but since the late 1980's, HLA-matched unrelated donors have been used with similar outcomes.

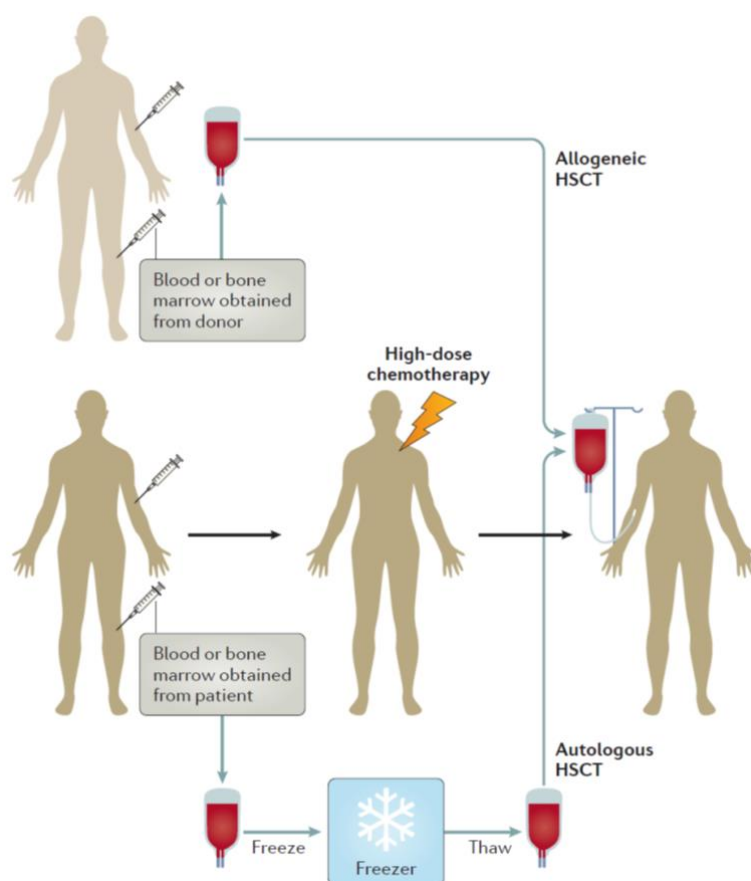


Figure 2.4 - Haematopoietic stem cell transplantation strategies in AML. Allogeneic HSCT refers to the option in which a human leukocyte antigen-matched sibling or an unrelated adult donor voluntarily donates either bone marrow or peripheral blood stem cells to be infused in a recipient, who received prior conditioning with cytotoxic and immunosuppressive therapy to allow engraftment and prevent host-versus-graft and graft-versus-host reactions. Autologous HSCT refers to the option in which the stem cells from the patient are harvested and frozen to be thawed and re-infused after high-dose cytotoxic therapy to enable haematopoietic recovery. Figure and legend adapted from²¹⁵.

However, these donors are not identified as often as necessary, especially for patients from minority ethnic backgrounds^{262,263}. As an alternative approach for patients lacking an HLA-matching donor, conditioning and immunosuppressive regimes have been applied to allow haploidentical HSCT with reduced GVHD, but these regimes can increase the probability of opportunistic infections and relapse²⁶⁴. Also, closely matched umbilical cord blood (UCB) units have been shown to be a good alternative source of HSCs^{265,266}. However, the HSC number in a single UCB unit is insufficient for HSCT in adults²⁶⁷. The HSC number is crucial for the time required for engraftment and patient survival²⁶⁷⁻²⁶⁹. Due to lack of sufficient HLA-matched donors and HSC number from common sources, specially UCB²⁷⁰, still present serious limitations to HSCT eligibility in cancer or other haematological disorders treatment.

Despite the low HSC numbers in UCB²⁶⁷ and delayed engraftment when compared to BM or PB, the ease of collection and banking, plus the possibility to perform UCB transplants (UCBT) in mismatched donors²⁷¹ lead to an increased interest in finding strategies to enable UCBT to more patients. To achieve this, most studies have aimed to increase HSC number by *ex-vivo* expansion using molecular

factors. But other efforts have also been made to improve UCBT, such as: HSC harvesting and purification methods^{272,273}; HSC survivability²⁷⁴; HSC homing to the BM and engraftment²⁷⁵.

To be able to achieve HSC expansion, symmetrical self-renewal divisions over unlimited differentiation are required. The balance in HSC self-renewal is modulated by cell-intrinsic factors (i.e. transcription factors, epigenetic modifiers and cell cycle regulators) or by extrinsic factors produced by both local niche and systemic environment.

HSC expansion - Intrinsic Factors, e.g. HOXB4

One of the first molecules to be described as able to expand HSC was HoxB4, a member of the Antp homeobox family, transcription factors with specific DNA-binding domains²⁷⁶. The ectopic expression of Hoxb4 led to a 40-1000-fold expansion of HSC *in vitro* and *in vivo*²⁷⁷⁻²⁷⁹. Furthermore, HSC expansion could also be achieved by extrinsic delivery of the recombinant fusion protein TAT-HOXB4, however the levels of expansion were much lower when compared with the ectopic protein expression²⁸⁰. The study of other transcription factors involved in haematopoiesis regulation allowed to identify other possible candidates to use in HSC expansion, such as other members of the HoxA and HoxB clusters (e.g. HoxA4, HoxA9, HoxB6)²⁸¹⁻²⁸⁴ Gata2²⁸⁵ and Gfi1²⁸⁶. Ectopic expression of chromatin-associated factors has also shown to improve HSC expansion, specially proteins members of the Polycomb group family (PcG), such as Ezh2 and Bmi1, which modulate HSC activity either by preventing stem cell expansion or by increasing HSC self-renewal²⁸⁷⁻²⁸⁹. Despite the high levels of HSC expansion achieved with ectopic expression, the introduction of genetic material is undesired in clinical protocol²⁹⁰ and the use of recombinant proteins is often limited by their stability in culture²⁸⁰. Therefore, transient activation of self-renewal by extrinsic factors or molecules that regulate the activity of intrinsic factors can be a good alternative.

Extrinsic factors, e.g. cytokines and small molecules

The first attempts to expand HSCs *ex-vivo* were made using combinations of haematopoietic cytokines identified to be produced *in vivo* by the HSC microenvironment, such as SCF, TPO, Flt3L, IL-6, IL-3, G-CSF^{291,292}. However, the efficiency of these cytokines in HSC expansion remains controversial, as they often do not achieve the desired expansion and usually leads to HSC differentiation and/or exhaustion^{277,293-295}. Nonetheless, a mix of SCF and Flt3L with IL-11 (mouse) or TPO (human) become the core cocktail of cytokines routinely used *in vitro* for haematopoietic stem and progenitor cell culture, supporting their survival, proliferation and maintenance in culture and is often complemented with other cytokines and other small molecules (**Table 2.5**)^{291,296,297}.

Table 2.5 - Successful Protocols for HSC Expansion Ex Vivo.

Factors	Cells tested	Species	Supplement	Culture period	Assay	Fold expansion
Cytokines²⁹¹	CB CD34+38-	H	SCF, Flt3L, G-CSF, IL-3, IL-6	4 days	CFU and CRU (HSC frequency)	15-fold CFU; fourfold chimera
Cytokines²⁹²	CB CD34+38-	H	Flt-3, SCF, IL- 3, IL-6, and G- CSF	5–8 days	CFU, LTC-IC, CRU (HSC frequency)	100-fold CFU; fourfold LTC-IC; twofold CRU
Angiopoietin²⁹⁸	SP CD45+ Sca-1+	M	SCF, THPO, FGF-1, IGF-2	10 days	CRU (HSC frequency)	24–30-fold
Pleiotrophin²⁹⁹	CD34- LSK, CB CD34+ 38-	M and H	SCF, Flt3L, THPO	7 days	CRU frequency/LT engraftment	Fourfold CRU; 10-fold chimera
HOXB4³⁰⁰	CB CD34+	H	Co-culture on MS-5 mouse stromal cells	4–5 weeks	LTC-IC assay, reconstitution analysis	20-fold LTC-ICs; 2.5-fold long- term repopulation
Fbxw7³⁰¹	LSK	M	SCF, THPO	10 days	Competitive reconstitution analysis	>Twofold long- term repopulation
Dppa5³⁰²	CD34-48- LSK	M	SCF, THPO	14 days	Competitive reconstitution analysis	6–10-fold
PDH inhibitor (1- aminoethylphosphinic acid, 1-AA)³⁰³	CD34-Flts- LSK	M	SF-O3 medium 1.0% BSA, serum-free, SCF, THPO	2–4 weeks	CFU/competitive reconstitution analysis	Twofold CFUs; fivefold LT repopulation
Mitochondrial phosphatase Ptpmt1 inhibitor, alexidine dihydrochloride (AD)³⁰⁴	LSK and in vivo treatment CD34+ 38-	M H	SCF, THPO, Flk-3	7 days	CFU and LT chimera 34+38_ number/CFU	Twofold CFUs; 3–5-fold LT repopulation Twofold number; twofold CFUs
GSK-3b inhibitor, CHIR99021^{305,306}	LSK and CB CD34+ LSK Flk-	M and H M	With rapamycin in cytokine-free X-VIVO medium SCF, THPO, and insulin	7 days 14 days	HSC frequency/LT engraftment Competitive reconstitution analysis	10–20-fold HSC number; 2–5-fold LT repopulation 100-fold number; 2–10-fold LT repopulation
SR-1³⁰⁷	CD34+ MPB UBC	H	SCF, Flt3L, THPO, IL-6	7–21 days	Number/CFU/ competitive reconstitution analysis	65-fold CFUs; 17-fold enhanced chimera
UM171³⁰⁸	CD34+ MPB UBC	H	SCF, Flt3L, THPO	7–21 days	Number/CFU/ competitive reconstitution analysis	>100-fold LT- HSC; 35-fold enhanced chimera

CB, cord blood; CRU, competitive repopulating unit; Dppa5, developmental pluripotency associated 5; Fbxw7, F-box and WD repeat domain containing 7, E3 ubiquitin protein ligase; IGF-2, insulin-like growth factor 2; IL-3, interleukin 3; LT, long-term; MPB, mobilized peripheral blood; MS-5, murine MS-5 stromal cell line; SP, side population; SR-1, StemRegenin1; THPO, thrombopoietin; TFs, transcription factors.

Further studies were made in developmentally conserved signalling pathways with critical roles during ontogeny and fetal haematopoiesis, such as, wingless-type (Wnt)³⁰⁹, Notch (Jagged/Delta)³¹⁰, Sonic hedgehog (Shh)/BMP³¹¹, FGF³¹², IGF and Angptls^{298,313}, pleiotrophin²⁹⁹, and the TGFβ/smud4

signalling pathway. Adult HSCs have been shown to express receptors that can activate all these pathways, indicating that these pathways could be used for extrinsically control HSC fate in culture. More recently, powered by emergence of computational methods, small molecules have emerged as valuable tools for regulation stem cell fate, as they present several advantages such as easier manipulation, typically rapid and reversible effects, various and unlimited concentrations and structures, and rapid phenotype-based high-throughput screening and many of these factors are currently being used in clinical trials for UCB expansion and transplantation (Table 2.6)^{295,314-316}.

Table 2.6 - Current Approaches to Ex Vivo Manipulation of UCB Stem Cells in Clinical Trials.

Ex Vivo Treatment	Biologic Rationale	Ex Vivo Expansion	Ex Vivo Processing	Median Days to Myeloid Engraftment	Long-term Engraftment by Treated UCB	Immune Reconstitution
Tetraethylene pentamine (SCF, FLT-3L, TPO, IL-6)³¹⁷	copper chelation blocks HSC differentiation	TNC +++, CD34 +, CFUs ++	21 days	granulocytes: 30; platelets: 48	not evaluated	not evaluated
Notch ligand Delta 1 (fibronectin, SCT, FLT-3L, TPO, IL-6, IL-3)³¹⁸	provides HSC proliferative signal	TNC +++, CD34 +	16 days	granulocytes: 13; platelets: 38	<5%	not evaluated
Mesenchymal stromal cells (SCF, FLT3L, TPO, G-CSF)³¹⁹	MSCs provide signals for HSC expansion	TNC +, CD34 ++, CFUs ++	14 days	granulocytes: 15; platelets: 42	<10%	not evaluated
16,16-dimethyl prostaglandin E2³²⁰	facilitates HSC homing, proliferation, and self-renewal	N/A	2 hr	granulocytes: 18; platelets: 43	83%	delayed
Nicotinamide (SCF, FLT-3L, TPO, IL-6)³²¹	inhibits HSC differentiation; facilitates HSC homing	TNC +++, CD34 ++	21 days	granulocytes: 13; platelets: 33	60%–80%	not evaluated
Fucosylation³²²	facilitates HSC homing	N/A	30 min	granulocytes: 17; platelets: 35	50%	not evaluated
StemRegenin-1 (SCF, FLT-3L, TPO, IL-6)³²³	SR-1 inhibition of aryl hydrocarbon receptor blocks HSC differentiation	TNC +++, CD34 +, CFUs ++	15 days	granulocytes: 15; platelets: 49	65%	delayed

TNC, total nucleated cells; N/A, not applicable.

2.3.5. Differentiation therapy/APL

The notion that acute leukaemias arise not only from the uncontrolled proliferation but also halted differentiation of haematopoietic stem or progenitor cells has encouraged the pursue of treatments which stimulate the terminal differentiation and subsequent proliferation arrest of malignant leukaemic cells. A successful example of this is the differentiation therapy applied to patients with APL, a subtype of

AML. APL characterized by a balanced reciprocal translocation between chromosomes 15 and 17 leading to the fusion of promyelocytic (PML) gene with the retinoic receptor α (RAR α). This results in a PML-RARA fusion protein with oncogenic potential, has this protein is responsible for arresting the differentiation of myeloid precursors in promyelocytes and is able to induce leukaemia in animal models^{324,325}.

What was once a rapidly onset fatal disease, characterized by a harmful coagulopathy which could result in life threatening hemorrhages and more rarely thrombosis, became highly curable disease with the introduction of differentiation therapy, which increased the median of survival from 1 week to a stable CR (<90% rate) over 5 years^{324,326}. The first agent used in differentiation therapy was all-trans-retinoic acid (ATRA) and later arsenic trioxide (ATO). These drugs are able to degrade the PML-RARA oncoprotein and induce the terminal differentiation of leukaemic promyelocytes in APL^{327,328}. Although ATRA was initially used as a single agent in induction therapy with CR rates of up to 80%, the long-term results were not satisfactory as a high relapse rate was observed, especially in high risk profile patients³²⁹⁻³³¹. Currently, ATO plus ATRA without chemotherapy is offered as standard induction and consolidation therapy for low risk patients (white blood cells (WBC) count <10,000/ μ L)³³². For patients with higher risk profile, although more data is still needed, standard treatment consists of ATO plus ATRA with the addition of an anthracycline (reviewed in³³³).

Despite the success of the differentiation therapy in APL treatment, some complication can still occur in the first weeks of ATRA and/or ATO administration. The most common is the differentiation syndrome (DS-previously known as “retinoic acid syndrome”), with an incidence of 25-30%, DS is characterized by the increased differentiation of WBC and capillary leakage³³⁴. Prophylactic steroids can be administered to prevent DS, especially in high-risk patients (WBC count >10,000/ μ L)³³⁵. Hepatic toxicity and cardiac arrhythmia are also common in protocol where ATO is administered alone or in combination with ATRA. In more rare cases (3% incidence), *Pseudotumour cerebri* (PTC) can be observed in patients, mostly in children and adolescents^{332,336}.

2.4. RA in the niche

The success of differentiation therapy raised the interest on the role of ATRA signalling pathways in normal and malignant haematopoiesis and possible use of ATRA in other AML subtypes. In fact, preclinical studies have gathered evidence that specific molecular abnormalities can increase ATRA sensitivity in non-APL AML patients' cells. More specifically, in AML with: a FMS-like tyrosine kinase 3/internal tandem duplication (FLT3-ID)³³⁷; mutant nucleophosmin gene (NPM1)³³⁸⁻³⁴⁰; mutant isocitrate dehydrogenase 1 (IDH1)³⁴¹; overexpression of ecotropic viral integration site 1 (EVI-1)³⁴²; and in MLL-positive AML^{343,344}.

ATRA is a member of retinoids, a class of signalling molecules and active metabolites of Vitamin A (retinol), which are essential for normal embryonic development in vertebrates and modulation of multiple biological processes, such as haematopoiesis, vision, reproduction, immune function and cell growth and communication³⁴⁵⁻³⁵⁰.

Dietary vitamin A can be obtained from plant sources (as provitamin A carotenoids, mostly β -carotene) and animal sources as retinyl esters. Retinols are oxidized in the body first by alcohol

dehydrogenases (ADHs) into retinaldehyde (crucial for vision) and then by aldehyde dehydrogenases (ALDHs) into ATRA³⁵¹. After being synthesized, ATRA is transported within the cells by CRABP (cytoplasmic retinoic acid binding protein^{352,353} and CRBP II (cytosolic retinoid binding protein), which can signal ATRA for degradation mediated by the bone marrow stroma's expressed cytochrome P450 retinoid-inactivating enzyme, CYP26^{354,355} or transport it to the nucleus. Within the nucleus, ATRA acts as a ligand for two families of nuclear hormone receptors, preferentially to the retinoic acid receptors (RAR), specific to the retinoid signalling pathway, and retinoid X receptor (RXR), which has higher affinity to 9-cis-RA than to ATRA and, can heterodimerize with other members of the nuclear hormone receptors³⁵⁶, such as vitamin D and thyroid hormone receptors³⁵⁷.

Retinoid acid receptors are composed by three subtypes (α , β and γ), each subtype with at least 2 different isoforms created by alternative splicing^{358,359}. All are structurally similar and differ mainly on the tissue and development expression (for example, RAR γ is expressed at higher levels in skin and RAR α in haematopoietic cells)³⁶⁰. RARs can act as transcriptional modulators by forming homodimers or, mainly, heterodimers with RXR, which bind to specific retinoic acid response elements (RAREs) present in the promoter region of RA signalling target genes³⁵⁶. In the absence of ligands, RAR-RXR heterodimers repress transcription by forming complexes with nuclear receptor co-repressors with histone deacetylase activity, which promote chromatin condensation and subsequent transcriptional repression³⁶⁰⁻³⁶³. When ATRA (or other retinoids) interact with RARs, promotes a conformational exchange and silencing of the co-repressor complex and allows for the recruitment of transcriptional co-activators, including histone acetyltransferases, which leads to transcriptional activation of retinoid target genes by chromatin decondensation^{360,363}.

Despite of the key role of RA signalling during vertebrate's development and in the early embryonic haematopoiesis being well documented^{346,348,364-366}, the role of ATRA in regulation of adult haematopoiesis, more specifically in haematopoietic stem and progenitor cell biology remains controversial.

Some studies have reported increased proliferation of human haematopoietic progenitor cells³⁶⁷⁻³⁶⁹, while others report an inhibitory effect on both proliferation and differentiation of human and murine haematopoietic progenitor cells, upon ATRA treatment³⁷⁰⁻³⁷⁴. Furthermore, murine models have shown that HSC expansion can be achieved either by activation of the RA pathway³⁷⁵ or its inhibition via retroviral-mediated expression of dominant negative RAR α ³⁷⁶. These contradictory effects of ATRA may be due to combination of the following: cells targeted by ATRA³⁷⁷, differential expression and activity of RARs^{329,378,379} and metabolic state in such cells³⁸⁰, and regulation of intrinsic RA concentration by the microenvironment^{355,381}.

While initial studies were done using either mice fed with a Vitamin A deficient diet³⁸² with a pan-RAR-antagonist³⁸³, the emergence of RAR knockout murine models and specific agonists and antagonist for the different RAR subtypes, allowed a better understanding of RA signalling in haematopoiesis. Purton *et al* demonstrated that ATRA has a pleiotropic effect on murine haematopoiesis by showing that ATRA is a potent inducer of terminal differentiation in normal promyelocytes (linage negative, ckit positive, sca-1 negative LKS⁻ cells) but has the opposite effect in more primitive HSC (LSK⁺) cells³⁷⁷. Furthermore, it was observed that expression of RARs is not the same in purified populations of murine haematopoietic cells. The more primitive population of HSC (LSK⁺) express RAR α 1, RAR α 2, RAR β 2, RAR γ 1, and RAR γ 2³⁸⁴. Due to this, most studies have focused on the role of RAR α and RAR γ in RA

signalling during haematopoiesis. The strongest evidence for the involvement of RARs in haematopoiesis has come from the knowledge gained with APL, demonstrating the importance of RAR α in myelopoiesis^{385,386}. Activation or overexpression of RAR α shows an increase in granulocytes expression^{379,384}. Surprisingly, RAR α knock-out mice, despite the early lethality, show no defects in myelopoiesis^{387,388}. Also, overexpression or activation of RAR γ promotes the self-renewal and expansion of HSC^{379,384}. On the other hand, mice deficient for RAR γ are anemic³⁸⁹, show reduced HSCs numbers with significantly increased granulocyte/macrophage progenitors and develop a microenvironment induced myeloproliferative syndrome (MPS)^{155,384}. Interestingly, transplantation studies indicate that this disorder is likely mediated through a defect in the microenvironment that supports HSC activity rather than an autonomous defect in the HSCs themselves. Collectively, these studies indicate a key role of RAR γ signalling in the homeostasis of the haematopoietic in response to RA.

Retinoic acid is also a well-known modulator of the cell cycle, causing an accumulation of cells in G0/G1 phase and a decrease in the S phase population³⁹⁰. Accordingly, ATRA treatment *in vitro* has also been shown to promote cell-cycle arrest in G0/G1 phase in HSC^{371,377}. In a more recent study, it was shown *in vitro* and *in vivo* that ATRA and Vitamin A are responsible to maintain primitive HSC in a dormant state and protecting them from entering in cell-cycle under stress conditions. This reduced metabolic state of HSCs promoted their maintenance in long-term self-renewal and low proliferation and was associated with decreased *Cdk6* levels, expression of transcription factors essential for HSC maintenance, such as *Hoxb4*, reduced ROS generation and low *c-myc* levels³⁸⁰

2.5. Novel therapies

The deeper understanding of the molecular, epigenetic and metabolic abnormalities responsible for the development of haematopoietic malignancies and their resistance to conventional therapy, allied with the development of new molecular and nanotechnology tools, allowed the development of new strategies to treat leukaemia. More recent studies try to target directly LSC, by: using antibody based therapy specific for LSC cell surface markers; engineering chimeric antigenic receptor(CAR) T/NK cells; using nanoplateforms for accurate delivery of anti-leukaemic compounds; or more recently, direct genetic correction of molecular abnormalities, made possible with the discovery of CRISP-CAS9 molecular tool. Targeting of LSC can be indirect, by disrupting the metabolic environment that favours LSC expansion and resistance (e.g. hypoxia); or epigenetic manipulation of the malignant niche

2.6. Nanomedicine

Since 1980s, with the first FDA of a nanoparticle (NP) formulation, for cancer treatment³⁹¹, nanotechnologies gained increased interest from the scientific and medical community. Nanomedicine is defined as the use of nanotechnology, materials with size ranging from 1 to 100 nm in health and medicine, although of nano-sized materials with several hundred nanometres can be considered as long they have a relevant biological effect³⁹². These nanocarriers have unique

characteristics that allows its use for the improvement of drug delivery, diagnosis and imaging, synthetic vaccine development and miniature medical devices³⁹³⁻³⁹⁸. Current problems in cancer treatment³⁹⁹ (e.g. low specificity, rapid drug clearance, biodegradation and limited targeting) could be potentially addressed by the use of NP platforms. Their nanoscale size, high surface-to-volume ratios, favourable drug release profiles, and targeting modifications, can allow them to better reach target tumour tissue and release drugs in a stable, controlled manner³⁹². Furthermore, NPs are able to incorporate multiple features allowing to have diagnostic, tracking, targeting and drug delivery all combined in a single nanoformulation. Currently, a wide variety of NP platforms (e.g. lipo-based, polymer-based, inorganic, viral and drug conjugates) are being investigated for cancer diagnosis and treatment, with several of them already approved for clinical use (**Table 2.7**).

Table 2.7 - Examples of clinical-stage nanomedicines for cancer therapy.

Therapy modality	Generic name and/or proprietary name	Nanotechnology platform	Active pharmaceutical ingredients	Cancer type	Status
Chemotherapy: non-targeted delivery	Liposomal doxorubicin (Doxil) ⁴⁰⁰	Pegylated liposome	Doxorubicin	HIV-related Kaposi sarcoma, ovarian cancer, and multiple myeloma	Approved by FDA (1995) EMA (1996)
	Liposomal daunorubicin (DaunoXome) ⁴⁰⁰	Liposome (non-PEGylated)	Daunorubicin	HIV-related Kaposi sarcoma	Approved by FDA (1996)
	Liposomal vincristine (Marqibo) ⁴⁰⁰	Liposome(non-PEGylated)	Vincristine sulfate	Philadelphia chromosome negative acute lymphoblastic leukaemia	Approved by FDA (2012)
	Liposomal irinotecan (Onivyde or MM-398) ⁴⁰¹⁻⁴⁰⁴	Pegylated liposome	Irinotecan	Post-gemcitabine metastatic pancreatic cancer (2nd line) Small cell lung cancer, metastatic pancreatic adenocarcinoma, pediatric solid tumors	Approved by FDA (2015) Phase I, II, III (2017)
	Liposomal doxorubicin (Myocet) ⁴⁰⁰	Liposome	Doxorubicin	Metastatic breast cancer	Approved in Europe EMA (2000) and Canada
	Mifamurtide (Mepact) ⁴⁰⁰	Liposome (non-PEGylated)	Muramyl tripeptide phosphatidyl-ethanolamine	Nonmetastatic, resectable osteosarcoma	Approved in Europe EMA (2009)
	Nab-paclitaxel (Abraxane) ^{400,405}	Albumin NP	Paclitaxel	Metastatic Breast, advanced non-small-cell lung and metastatic pancreatic cancer	Approved by FDA(2005) and by EMA (2008)
	SMANCS ⁴⁰⁰	Polymer protein conjugate	Styrene maleic anhydride Neocarzinostatin (SMANCS)	Liver and renal cancer	Approved in Japan (1994)
	Polymeric micelle paclitaxel (Genexol-PM) ^{400,406-408}	PEG-PLA Polymeric micelle	Paclitaxel	Breast cancer and NSCLC Lung cancer, Ovarian cancer Gynecologic cancer, hepatocellular carcinoma, advanced breast cancer, non-small cell lung cancer	Approved in South Korea (2007) Phase I/II 2016*

	Liposomal cisplatin (Lipoplatin) ⁴⁰⁹	Pegylated liposome	Cisplatin	NSCLC	Phase III
	NK-105 ⁴¹⁰	Polymeric micelle	Paclitaxel	Metastatic or recurrent breast cancer	Phase III
	Liposomal paclitaxel (EndoTAG-1) ⁴¹¹⁻⁴¹⁴	Liposome	Paclitaxel	Pancreatic cancer, liver metastases and HER2 negative and triple-negative breast cancer	Phase II
	Nab-rapamycin (ABI-009) ^{415,416}	Albumin NP	Rapamycin	Advanced malignant PEComa and advanced cancer with mTOR mutations	Phase II
	CRLX 101 ⁴¹⁷⁻⁴¹⁹	Polymeric NP	Camptothecin	NSCLC, metastatic renal cell carcinoma and recurrent ovarian, tubal or peritoneal cancer rectal, fallopian tube, lung (small cell and non-small cell) primary peritoneal, stomach, gastroesophageal, and esophageal cancers	Phase I/II (2016)
Chemotherapy: targeted delivery	MM-302 ⁴²⁰	HER2 targeting liposome	Doxorubicin	HER2-positive breast cancer	Phase II/III
	BIND-014 ^{421,422}	PSMA-targeting polymeric NP	Docetaxel	NSCLC and mCRPC	Phase II
	MBP-426 ⁴²³	TfR targeting liposome	Oxaliplatin	Gastric, oesophageal and gastro-oesophageal adenocarcinoma	Phase I/II
	Anti EGFR immunoliposomes loaded with doxorubicin ^{424,425}	EGFR targeting liposome	Doxorubicin	Solid tumours, Breast cancer	Phase I/II (2016)
Chemotherapy: stimuli-responsive delivery	ThermoDox ⁴²⁶	Liposome	Doxorubicin	Hepatocellular carcinoma	Phase III
Chemotherapy: combinatorial delivery	Liposomal cytarabine–daunorubicin (CPX-351 or Vyxeos) ⁴²⁷	Liposome	Cytarabine and daunorubicin (5:1)	High-risk acute myeloid leukaemia	Phase I (2014) Phase III
	CPX-1 ⁴²⁸	Liposome	Irinotecan and floxuridine (1:1)	Advanced colorectal cancer	Phase II
Hyperthermia	NanoTherm ⁴⁰⁰	Iron oxide NP	NA	Thermal ablation glioblastoma	Approved in Europe EMA (2010)
	AuroLase ^{429,430}	Silica core with a gold nanoshell	NA	Prostate, head and neck cancer, and primary and metastatic lung tumours	Pilot study Phase I 2016
Radiotherapy	NBTXR3 ⁴³¹	Hafnium oxide NP	NA	Adult soft tissue sarcoma	Phase II/III

Gene or RNAi therapy	SGT53 ^{432,433}	TfR targeting liposome	Plasmid encoding normal human wild-type p53 DNA	Recurrent glioblastoma and metastatic pancreatic cancer	Phase II
	PNT2258 ⁴³⁴	Liposome	DNA oligonucleotide against BCL-2	Relapsed or refractory non-Hodgkin lymphoma and diffuse large B-cell lymphoma	Phase II
	SNS01-T ⁴³⁵	Polyethylenimine NP	siRNA against eIF5A and plasmid expressing eIF5A K50R	Relapsed or refractory B cell malignancies	Phase I/II
	Atu027 ⁴³⁶	Liposome	siRNA against protein kinase N3	Advanced or metastatic pancreatic cancer	Phase I/II
	TKM-080301 ⁴³⁷	Lipid NP	siRNA against PLK1	Neuroendocrine tumours, adrenocortical carcinoma and advanced hepatocellular carcinoma	Phase I/II
	DCR MYC ⁴³⁸	Lipid NP	Dicer-substrate siRNA against MYC	Hepatocellular carcinoma	Phase I/II
	MRX34 ⁴³⁹	Liposome	miR 34 mimic	Primary liver cancer, solid tumours and haematological malignancies	Phase I
	CALAA-01 ⁴⁴⁰	TfR targeting polymeric NP	siRNA against ribonucleotide reductase M2	Solid tumours	Phase I
	ALN-VSP02 ^{441,442}	Lipid NP	siRNAs against KSP and VEGFA	Solid tumours	Phase I
	siRNA EPHA2 DOPC ⁴⁴³	Liposome	siRNA against EPHA2	Advanced cancers	Phase I
	pbi shRNA STMN1 LP ⁴⁴⁴	Lipid NP	shRNA against stathmin 1	Advanced and/or metastatic cancer	Phase I
Immunotherapy	Tecemotide ⁴⁴⁵	Liposome	MUC1 antigen	NSCLC	Phase III
	dHER2 + AS15 ⁴⁴⁶	Liposome	Recombinant HER2 (dHER2) antigen and AS15 adjuvant	Metastatic breast cancer	Phase I/II
	DPX-0907 ⁴⁴⁷	Liposome	Multi-tumour associated antigens	HLA-A2-positive advanced stage ovarian, breast and prostate cancer	Phase I
	Lipovaxin-MM ⁴⁴⁸	Liposome	Melanoma antigens	Malignant melanoma	Phase I
	JVRS 100 ⁴⁴⁹	Lipid NP	Plasmid DNA	Relapsed or refractory leukaemia	Phase I
	CYT 6091 ⁴⁵⁰	Colloidal gold NP	TNF	Advanced solid tumours	Phase I

EGFR, epidermal growth factor receptor; eIF5A, eukaryotic initiation factor 5A; EPHA2, ephrin type A receptor 2; FDA, US Food and Drug Administration; KSP, kinesin spindle protein (also known as KIF11); mCRPC, metastatic castration resistant prostate cancer; miR, microRNA; mTOR, mammalian target of rapamycin; MUC1, membrane bound mucin 1; NA, not applicable; nab, nanoparticle albumin bound; NSCLC, non small cell lung cancer; PEComa, perivascular epithelioid cell tumours; PEG, poly(ethylene glycol); PLK1, polo like kinase 1; PSMA, prostate specific membrane antigen; RNAi, RNA interference; shRNA, short hairpin RNA; SMANCS, poly(styrene-co maleic acid) conjugated neocarzinostatin; TfR, transferrin receptor

2.6.1. Proprieties

Depending on their material composition, size, shape, surface charge and chemistry, NPs offer a wide variety of physico-chemical and biological proprieties which can be tailor made to treat specific tumours. Size is important for travel the bloodstream and to bypass biological barriers (e.g. blood brain barrier) to reach the desired location and cellular uptake. While smaller particles are more easily internalized by cells and able to accumulate more easily in the leaky blood vessels of tumours, known as the enhanced permeability and retention (EPR) effect, they can also extravasate to normal tissue. On the other hand, bigger NPs are less likely to accumulate in normal tissue, but their bloodstream distribution is highly variable. Thus, optimization of particle size can be important to improve specific uptake in tumour tissue⁴⁵¹. The shape of NPs can influence fluid dynamics and cellular uptake, with spherical nanocarriers being the most common used shape, as their synthesis and testing is less challenging than non-spherical varieties⁴⁵². The charge of NPs is also important for their stability, distribution and cellular uptake. Positively charged particles were shown to target tumour vessels more efficiently⁴⁵³. Also, positively charged NPs are more likely to interact with the negatively charged lipids of cellular membranes and, when inside of endosomes, to disrupt them by activating the proton pumps and increase the osmotic pressure inside the endosome, culminating in the swelling/bursting of the endosome, thus avoiding lysosomal degradations of the drug, also called the “proton-sponge effect”⁴⁵⁴.

2.6.2. Composition

Both organic and inorganic materials have been used in the synthesis of NPs (**Figure 2.5**), both with pros and cons. In general, organic NPs have better drug loading capacity and biocompatibility and have been the most explored nanocarriers for cancer treatment, including: dendrimers, which are highly branched, allowing the delivery of cargo and produced by controlled polymerization with a maximum of 10 nm of size; lipid-based NPs, such as liposomes and micelles that may carry a hydrophobic cargo and typically have 50–100 nm of size; polymeric NPs, produced in a size range from 10 to 400 nm from synthetic, natural, hydrolytically, or enzymatically degradable polymers onto which a cytotoxic drug can be covalently attached, dissolved, encapsulated, or entrapped; and more recently, natural NPs, such as exosomes, have also been used⁴⁵⁵⁻⁴⁵⁸. On the other hand, inorganic NPs offer advantages in terms of chemical proprieties (e.g. conjugation) and *in vivo* quantification. These nanomaterials include carbon-based NPs (e.g. carbon nanotubes, graphene) which feature unique electrical proprieties, quantum dots (QDs), which have been mainly explored for optical imaging since they show narrow and tuneable emission spectra, and metal NPs (e.g. gold, silver and iron oxide), which are easy to synthesize and functionalize. Gold NPs (AuNPs) have been used for drug and gene delivery, thermal ablation, radiotherapy augmentation and also diagnostics, due to their high sensitivity. Iron oxide NPs, beside the possibility for surface functionalization, they feature unique magnetic proprieties, which can be used as contrast agent for magnetic resonance imaging (MRI), hyperthermia and drug delivery.

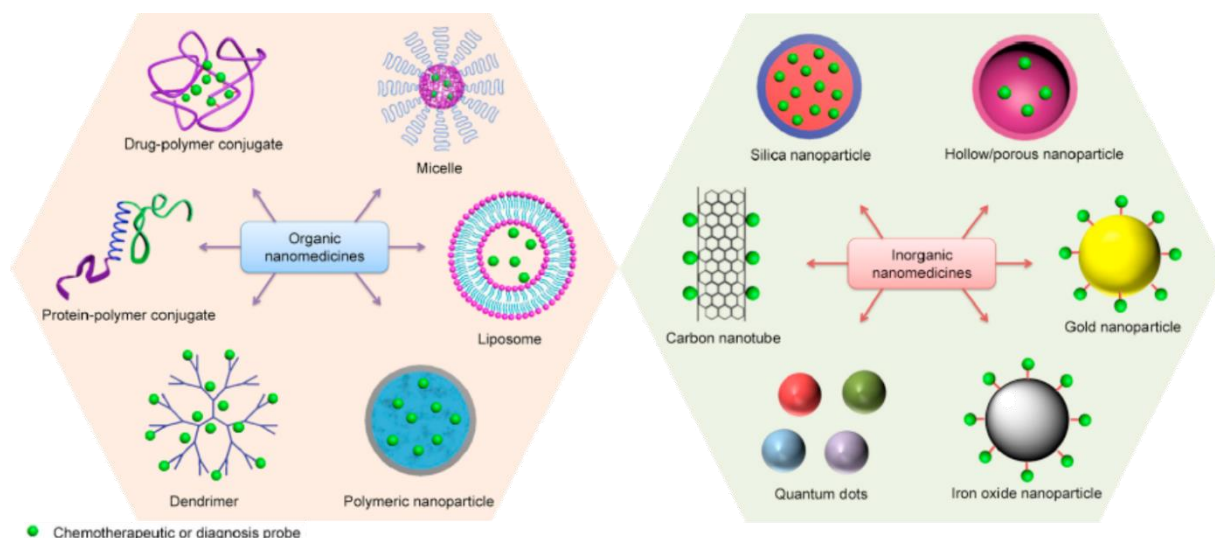


Figure 2.5 - Examples of organic and inorganic nanoparticles used in nanomedicine. Figure adapted from⁴⁵⁹

2.6.3. Drug delivery

The use of nanocarriers for drug delivery offers several advantages to conventional drug administration routes, such as increased drug stability and bioavailability, increased specificity and decrease of possible side effects. In turn, these advantages can translate to an increased success of the clinical application of many molecules, such as small molecules, proteins and nucleic acids used in gene therapy (e.g. siRNA, miRNA, lncRNA; CRISP-CAS9 system).

The first generation of NP was mostly aimed to increase the stability of hydrophobic drugs, which can be rapidly eliminated from the bloodstream. The use of hydrophilic NPs to encapsulate hydrophobic drugs may improve their solubility, increasing their bioavailability *in vivo* and thus a more effective delivery can be achieved using NP, without the need to increase the concentrations of the drug administered and consequent increased toxicity^{392,399,451,460}. Furthermore, many biomolecules have negative charge (e.g. nucleic acids) at physiological pH, which may represent a limitation in their use for intracellular delivery, as negatively charged molecules are less likely to be internalized by cells⁴⁶¹. Coating NPs with poly(ethylene glycol) (PEG), a hydrophilic and non-ionic polymer, was shown to increase NP solubility and stability⁴⁵¹ without disrupting the function of charged molecules⁴⁶². Masking hydrophobicity of NPs and carried molecules, prolongs their circulation in the blood and subsequently the likelihood of reaching their target, as it decreases the activity of the reticulo-endothelial system (RES), also known as the mononuclear phagocyte system (MPS)⁴⁶³. MPS recognizes hydrophobic materials as foreign and initiate a local inflammation response, increasing NP clearance from the blood stream⁴⁶⁴.

Most nanocarriers are administered systemically, so its important make sure NPs reach their target efficiently without accumulating in other tissues and only release their cargo when they reach the tumour microenvironment. Therefore, efforts have been made by researchers to increase the control of NP targeting and drug release beyond the more simplistic passive targeting and drug release (**Figure 2.6**). Drug delivery systems can rely on intrinsic and biological proprieties (e.g. pH, enzymes, redox gradient or EPR) to passively reach and release the cargo to target environment⁴⁶⁵. However, passive

targeting does not eliminate the potential for accumulation of NPs in tissues with fenestrated blood vessels, such as the liver and spleen³⁹². Furthermore, the environment of the disease site can be highly heterogeneous, differing between patients, which makes difficult to control and predict the NP pharmacokinetics⁴⁶⁶⁻⁴⁶⁹. Modifications of the NP surface with ligands allows a more precise, active targeting. These ligands have high specificity to receptors and other specific ligands expressed at the surface of tumour cells⁴⁷⁰. Such ligands include transferrin, folic acid, enzymes, engineered antibodies, and macromolecules like proteins and carbohydrates^{392,451}. However, these systems still lack control of the dose of drug release.

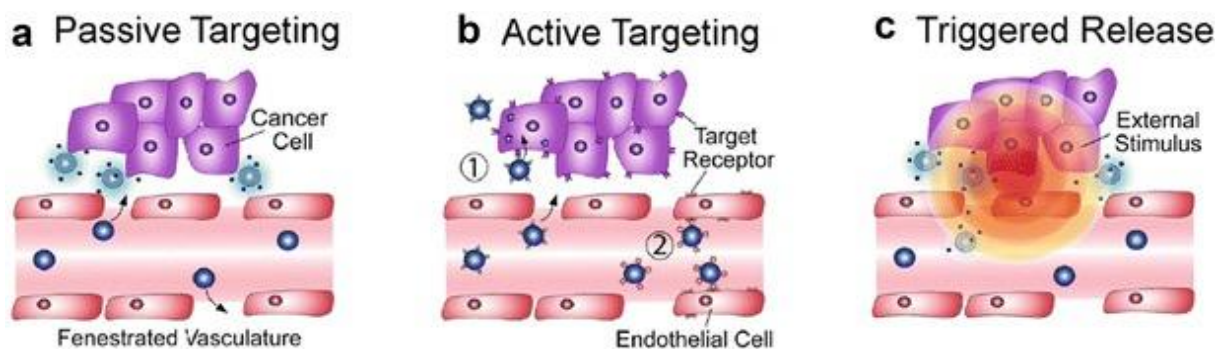


Figure 2.6 - Types of targeting for NP delivery to tumour tissue. (A) Passive targeting relies on the leaky vasculature that is exhibited by tumours, allowing NPs to travel through the fenestrations and reach tumours. (B) Active targeting can be used when NPs have ligands on their surface that can recognize and bind receptors that are overexpressed on tumour cells. (C) Triggered release allows NPs to congregate if exposed to an external stimulus such as a magnetic field or light. Figure and legend adapted from ⁴⁷¹.

Triggerable nanoformulation

Actively triggered systems are probably the most useful regarding the improvement of the therapeutic effect of drug delivery nanotechnology, as it allows a more precise control of targeting without the need of specific ligands (i.e. application of stimulus at desired area/tissue), time of drug release (spatio-temporal control) and/or dose. Triggered drug delivery events can be achieved with several external stimuli such as: ultrasound, magnetic, thermic, chemical, electric or light (**Table 2.8**).

Light can penetrate the human body ~1mm with 440nm wavelength, up to more than 4mm with wavelengths above 650nm^{472,473}, and offers some advantages relatively to other stimuli, such as: possibility of activating multiple drug systems using specific wavelengths; step-wise drug release from a single nanoformulation, using ligands responsive to different wavelengths; more precise targeting drug release at specific areas with a resolution determined by laser spot; and a light-trigger is user friendly, since the operator can easily change parameters such as intensity and wavelength of light^{474,475}.

Table 2.8 - Triggerable NPs examples.

Stimulus	Mechanism (effector molecule or material, if applicable)	Drug delivery systems (main parameter or trigger in parentheses)
Light	Photocleavage reactions (molecules with photolabile groups, such as <i>o</i> -nitrobenzyl or coumarin-4-yl-methyl groups)	Coumarin-functionalized nanoparticles (420 or 800 nm light) ⁴⁷⁶
	Photoisomerization (azobenzenes and spiropyrans)	Spiropyran-functionalized nanoparticles (365 nm light) ⁴⁷⁷
	Upconversion (for example, photosensitizers and annihilators for triplet–triplet annihilation)	DEACM-caged micelles (530 nm light) ⁴⁷⁸
	Photodynamic reaction (photosensitizers, for example, PdPc(OBu) ₈)	Photosensitizer-loaded liposomes (730 nm light) ⁴⁷⁹
	Photothermal effect (plasmonic nanoparticles, such as gold nanoparticles)	Gold nanorods attached to liposomes (808 nm light) ⁴⁸⁰
Gold nanocages (790 nm light) ⁴⁸¹		
Magnetic field	Heating (magnetic nanoparticles, such as nanoparticles of magnetite, maghemite and ferrites)	PNIPAM-based nanogels (alternating magnetic field of 220–260 kHz) ⁴⁸²
		Hydrogels composed of MNPs and thermoresponsive microgels (200 kHz magnetic field) ⁴⁸³
	Mechanical deformation (MNPs)	Liposomes attached to chains of MNPs (10 kHz magnetic field) ⁴⁸⁴
	Magnetic guidance (MNPs)	PLGA-based nanoparticles loaded with paclitaxel and superparamagnetic iron oxides (static magnetic field) ⁴⁸⁵
Ultrasound	Cavitation	Microbubble–liposome complexes (pulsed ultrasound with an amplitude of 1.9 MPa) ⁴⁸⁶
		Liposomes (continuous-wave ultrasound with intensity >100 mW cm ⁻²) ⁴⁸⁷
	Phase transition	Phase-transition droplets (high-intensity focused ultrasound with an amplitude of 11 MPa) ⁴⁸⁸
	Heating	Liposomes (pulsed high-intensity (1,300 W cm ⁻²) focused ultrasound) ⁴⁸⁹
Electric field	Electrokinetic flow	Polyelectrolyte hydrogels (constant 1.0 mA current for 1–10 min) ⁴⁹⁰
	Redox reaction	Conductive polymers (3 V potential for 150 s) ⁴⁹¹
	Redox reaction and electrokinetic flow	Conductive polymer nanoparticles embedded in hydrogel (–1.5 V and 0.5 V potentials) ⁴⁹²
Chemical	Binding interaction	Hydrogel containing ssDNA ⁴⁹³
		Aptamer-functionalized hydrogels (complementary nucleic acid sequences) ⁴⁹⁴
	Chemical ligation	Hydrogels containing antibiotic-binding units (novobiocin) ⁴⁹⁵
		Antibody–drug conjugates (tetrazine) ⁴⁹⁶

DEACM, (7-diethylaminocoumarin-4-yl)methyl; MNPs, magnetic nanoparticles; PdPc(OBu)₈, 1,4,8,11,15,18,22,25-octabutoxyphthalocyaninato-palladium(II); PLGA, poly(lactic acid-co-glycolic acid); PNIPAM, poly(*N*-isopropylacrylamide); ssDNA, single-stranded DNA.

Light-triggered drug delivery systems

Absorbed light can induce chemical changes in administered or endogenous compounds such as: photochemical reactions (i.e. photocleavage or photoswitching, or by generation of reactive oxygen species in photodynamic therapy); emission of light (e.g. fluorescence); or the transfer of energy to other forms (e.g. heat or acoustic waves)⁴⁹⁷. Most common wavelengths of light used in light triggered systems are within the ultraviolet (UV) and near infrared regions (NIR) of the light spectrum. NIR radiation can penetrate deeper in the body^{498,499} and has been used in the clinic for more than 30 years. Therefore, NIR exposure safe limits have already been established^{500,501}. Despite being a safer type of irradiation, NIR low-energy radiation has reduced capacity to break chemical bonds (e.g. between a drug and its carrier)⁴⁹⁸, limiting its application as a trigger in light-sensitive nanoformulations. On the other hand, UV light is a high-radiation energy, able to break chemical bonds but it has a lower penetration capacity in biological tissues⁴⁷³ and prolonged exposure of cells and tissues to UV light may induce deleterious effects (e.g. DNA damage and ROS production)^{502,503}. Nevertheless, short exposure to UV light has been used in the clinic to treat various diseases (e.g. skin disorders and ocular conditions)⁵⁰⁴ and its limited body penetration can be circumvented through the use of optical fibre and endoscopic apparatus^{498,505,506}. Also, it should be considered that in cancer therapy, more harmful forms of radiation are used (i.e. radiotherapy).

The wavelength of the light determines its uses in photo-triggered nanoformulations. Higher energy lights (e.g. UV) have sufficient energy to cleave chemical compounds (i.e. photolabile or photocaging groups) such as *o*-nitrobenzyl, coumarin-4-yl-methyl, *p*-hydroxyphenacyl and 7-nitroindoline derivatives⁵⁰⁷. Photocleavage can be used to drive destabilization of hydrophobic/hydrophilic balance of NPs and consequent release of its cargo⁵⁰⁸, release drugs by cleaving the link between drug and NP⁵⁰⁹ or by removing protective moieties from ligands at NP surface, allowing their binding to cells⁵¹⁰. UV light can also be used to induce reversible photoisomerization of photochromic groups such as azobenzenes and spiropyrans. When a photochromic group is embedded in a nanoformulation, photoisomeration can induce changes in the geometry, polarity or hydrophobicity of the groups can lead to reorganization or disassembly of the NPs, followed by drug release^{477,511}.

NIR-triggered nanoformulations rely on photochemical reactions such as upconversion and plasmonic effect. Upconversion has been explored to take advantage of the deep tissue penetration of NIR with the high energy of UV, by combining the energy of multiple NIR photons to achieve a higher energy state or to create a single UV photon. This can be achieved by a two-photon absorption process, in which chemical groups that are normally sensitive to UV light, such as *o*-nitrobenzyl and coumarin derivatives, simultaneously absorb two photons of NIR light to achieve a chemical reaction⁵⁰⁷. Another way to achieve upconversion is by using higher energy states rather than higher photon energy. For example, polymeric micellar nanoparticles were designed with a photosensitizer in their cores that, when irradiated with green light, transfers its energy to annihilator molecules, which then undergo triplet-triplet annihilation upconversion. The upconverted energy can then be transferred by Förster resonant energy transfer (FRET) to cleave and release a hydrophobic photocleavable group, reactivating the activity of a cell-binding peptide^{478,512}.

Nobel metal NPs (e.g. AuNPs) can respond to NIR by producing heat (i.e. photothermal effect). Under NIR irradiation, the free electrons in metal NPs collectively oscillate in phase with the electric field of the incident radiation, a phenomenon known as surface plasmon resonance (SPR). The SPR

spectrum is dependent on the geometry of the nanostructures, as explained by the Mie-Gans theory^{513,514} and allows plasmonic NPs to efficiently convert photon energy to heat, increasing the temperature in their immediate vicinity, leading to drug release events⁵¹⁵. For example, the heat produced can induce the release of oligonucleotides from the NP by dehybridization⁵¹⁶, by triggering drug-release from nanoformulation composed of thermally responsive polymers, such as Poly(*N*-isopropylacrylamide) (PNIPAM)^{517,518}, or by using the heat produced by gold nanorods to destabilize the liposomal lipid bilayers present in lipidic NPs (LNPs), with a consequent phase transition and drug release^{480,519}.

2.6.4. Targeting the BM

When drug administration is systemic, drug availability is often quite low at the BM, due to rapid metabolism and clearance. Most injected drugs are either cleared by the body's metabolic and excretory system or accumulate in other highly perfused organs before reaching the BM. Thus, drugs are always administered in high doses and/or frequency to achieve the therapeutic effect at the BM, which can lead to unwanted systemic side effects⁵²⁰. Although the combination of leaky vasculature with poor lymphatic drainage has shown to promote accumulation of NPs due to EPR, little is known about EPR at the BM compartment⁵²¹. Moreover, the existence of fenestrae (size between 85 nm and 150 nm) at the endothelium of BM vascular sinusoids can represent a limitation to NPs sized over 150 nm⁵²². However, several studies have demonstrated that the BM is the main organ for the specific uptake of bioparticles (i.e. senescent cells, lipoproteins and nuclei from erythroid precursor cells) by the MPS⁵²³⁻⁵²⁶, suggesting that phagocytic activity in the bone marrow can be potentially used for NP drug delivery. In fact, early formulation studies using liposome-based drug delivery systems have demonstrated that negatively charged LNPs accumulate more in the BM, with increased BM macrophage uptake⁵²⁷⁻⁵³¹. Selective uptake of LNPs by macrophages seems to occur through the scavenger receptor on BM's macrophages, as polyanions such as dextran sulphate and polyinosinic acid have been reported as ligands for this receptor^{532,533}.

To overcome the problem of low accumulation at the BM, some nanotechnologies have been developed for leukaemia treatment and BM targeting⁵³⁴, with some of them already in clinical trials (**Table 2.9**).

In this case, NPs have been conjugated with specific ligands (e.g. CD45, CD20, CD19, E-E-selectin)^{535,536}, or have been activated by intrinsic or extrinsic cues at the BM leukaemic niche⁵³⁷⁻⁵⁴⁰.

Table 2.9 - Rationales and applications of bone marrow-targeted delivery systems.

Carrier type	Targeting	Drug	Application
liposome ^{541,542}	anionic low-cholesterol liposome promotes accumulation in BM	cytarabine: daunorubicin	increase drug accumulation in leukemia cells inside BM and enhance efficacy in AML mice
liposome ⁵⁴³	folate binds to FR- β	doxorubicin	folate-modified liposomes increase median survival times of AML mice
SLN ⁵⁴⁴	n.a.	ATRA	<i>In vitro</i> acute leukemia (HL60, Jurkat and THP1 cell lines)
LNP ⁵⁴⁵	n.a.	<i>Mcl1</i> siRNA	<i>In vitro</i> mantle cell lymphoma [JeKo-1 (normal) and MAVER-1 (aggressive) cell lines]
LNP ⁵⁴⁶	CD45.2 antibody	AntagomiR-126	<i>In vitro/in vivo</i> AML (human primary cells; murine model)
lipid nanocapsule ⁵⁴⁶	Healthy primary T-cells (live vector)	Topoisomerase I poison SN-38	<i>In vivo</i> lymphoma (murine model)
micellar NPs protected by porous silicon (pSi) coating ⁵³⁶	E-selectin thioaptamer (ESTA) (bone marrow-directed aptamer)	Parthenolide (PTL)	<i>In vivo</i> AML (patient-derived murine xenografts)
Nanopolymer ⁵³⁵	CD19 antibody	DOX	<i>In vitro/in vivo</i> ALL (REH and RS4; 11 cell lines: human-derived murine xenografts)
MSN (pH-controlled delivery) ⁵⁴⁷	Rituximab (CD20 antibody)	DOX and rituximab	<i>In vitro/in vivo</i> B-cell lymphoma (Raji and Daudi cell lines; murine model)
PEG-PLGA nanoparticle ⁵⁴⁸	alendronate-HA binding in bone matrix	bortezomib	pretreatment inhibits myeloma growth better than free drug in myeloma mice model
PEG-PLA micelle ⁵⁴⁹	alendronate-HA binding in bone matrix	ponatinib, SAR302503	extend survival time of BaF3/T315I cells inoculated CML mice

porous silicon particle ⁵⁵⁰	E-selectin specific thioaptamer	parthenolide	impairment of LSCs in AML secondary transplantation mice
nanostructured lipid carrier ⁵⁵¹	dual targeting via alendronate-HA and folate-FR- β bindings	mitoxantrone	deliver drugs to LSCs in bone marrow for refractory leukemia therapy
QD-CdTe ⁵⁵²	n.a.	Wogonin	<i>In vitro/in vivo</i> multidrug-resistant leukemia (K562-A02 cell line; leukemia-bearing mice)
MNP-Fe₃O₄ ⁵⁵³	n.a.	Wogonin	<i>In vitro</i> multidrug-resistant leukemia (K562-A02 cell line)
MNP-Fe₃O₄ ⁵⁵⁴	n.a.	Cytarabine	<i>In vitro</i> acute leukemia (HL60 and KG1 cell lines) Burkitt's lymphoma (Raji cell line)
AuNP or AuNP controlled drug release via presence of BIRC5 mRNA ⁵⁵⁵	BIRC5 dsDNA oligonucleotide	Dasatinib	<i>In vitro/in vivo</i> CML (K562 cell line; K562-derived murine xenografts)
AuNP ^{556,557}	n.a.	Lestaurtinibmidostaurin sorafenib quizartinib (FLT3 inhibitors)	<i>In vitro</i> AML (THP1 and OCI-AML3 cell lines)
AuNP ⁵⁵⁹	Folic acid	Fludarabine phosphate	<i>In vitro</i> AML (KG1 cell line)
AuNP ⁵⁵⁸	n.a.	BCR-ABL1 ssDNA oligonucleotide (e14a2)	<i>In vitro</i> CML (K562 cell line)
AgNP ⁵⁵⁹	Rituximab (detection of CD20)	Rituximab	<i>In vitro</i> Burkitt's lymphoma (Daudi and Raji cell lines)
DNPs ⁵⁶⁰	Idiotypic-peptide specific BCR	BCL2 siRNA	<i>In vitro</i> lymphoma (murine A20 cell line)
NP-albumin-bound PTX ⁵⁶¹	Rituximab (CD20 antibody)	PTX and rituximab	<i>In vitro/in vivo</i> B-cell lymphoma (Daudi cells; human B-cell lymphoma murine model)

HA, hydroxyapatite; FR- β , folate receptor- β ; AuNP, gold nanoparticle; CLL, chronic lymphocytic leukemia; PTK7, protein tyrosine kinase 7; FRET, fluorescence energy transfer; QD, quantum dot; SERS, surface-enhanced Raman scattering; ISH, in situ hybridization; FFPE, formalin-fixed paraffin embedded tissues; XIAP, X-linked inhibitor of apoptosis protein; CTC, circulation tumor cell; AF750, alexafluor 750; CML, chronic myeloid leukemia; DOX, doxorubicin; polyArg, peptide sequence with nine arginines; PTX, paclitaxel; BCR, B-cell receptor; LNP, lipid NP; MSN, mesoporous silica NP; ABX, ambraxane.

2.6.5. Cells as carriers

Despite the huge advances in the development of nanoformulations, their therapeutic efficiency is restricted by inefficient avoidance of MPS or targeting. As an alternative strategy, cell-mediated drug

delivery strategies have been explored. This concept emerged from a pioneering study in the 1970s that successfully encapsulated β -glucosidase and β -galactosidase into red blood cells (RBCs) for the treatment of Gaucher's disease⁵⁶². Since then, RBCs, leukocytes and stem cells (**Table 2.10**), have been studied in cell-mediated drug delivery due to their long circulation, specific tropism to diseased tissue and ability to cross biological barriers, such as blood brain barrier⁵⁶³. In fact, leukocytes and stem cells are already used for tumour immunotherapy and tissue regeneration in clinical trials⁵⁶⁴⁻⁵⁶⁷.

Table 2.10 - Stem cells as a vehicle to transport nanoparticles (NPs): physical–chemical properties of NPs.

Formulation	Drug (conc.)	NP size (nm)	NP zeta (mV)	Intracellular retention of NPs (days)	NP degradation	Response to remote trigger	Stem cells as transporter
Phototriggerable polyplex NPs ⁴⁰⁰	Retinoic acid (150 μ g per mg of NPs)	160	+22	Up to 6 days	Yes	Yes	LSCs
Poly(lactic acid) (PLA) NPs and lipid nanocapsules (LNCs) ⁵⁶⁸	Coumarin	136 (PLA) 88 (LNC)	-2.1 (PLA) -3.7 (LNC)	Up to 7 days	Yes	No	MSCs
Assembly of superparamagnetic NPs with biodegradable polymers ⁵⁶⁹	Paclitaxel	110	-	-	-	Yes	ADSCs
Porous hollow silica NPs ⁵⁷⁰	Purpurin18	150–200	-	Up to 5 days	-	Yes	MSCs
Mesoporous silica NPs ⁵⁷¹	Doxorubicin	190	+23.3	Up to 5 days	-	No	MSCs
pH-sensitive NPs ⁵⁷²	Docetaxel	100	-	Conjugation to the cell membrane (up to 7 days)	-	-	NSCs
Ultrasound-responsive copolymer covalently grafted to mesoporous silica NPs ⁵⁷³	Doxorubicin	~150	+23	Up to 6 days	-	Yes	MSCs
Poly(lactic-coglycolic acid) NPs ⁵⁷⁴	Doxorubicin	150	-37	Up to 1 day	-	No	MSCs
Gold nanorods conjugated with CXCR4 antibody ⁵⁷⁵	No	~50:10	-	Up to 3 days	No	Yes	iPSCs

NSCs, neural stem cells; HSCs, hematopoietic stem cells; MSCs, mesenchymal stem cells.

Red Blood Cells

RBC are natural carriers of oxygen and nutrients to all parts of the body and are the most readily available and abundant cells. Besides their high number, they also possess other attractive characteristics to increase the efficiency of drug delivery such as long-life span and widespread circulation; they protect encapsulated drugs, thus can be used as drug reservoir for a sustained drug release in the blood; and they are completely biodegradable, non-toxic and show very low to no immunogenic response⁵⁷⁶. RBCs can be loaded with NPs by hypotonic dialysis, an encapsulation process involving reversible hypotonic swelling of the RBCs, which transiently opens pores in the membrane allowing drugs or NPs to diffuse into the cells and when changed back to an isotonic medium, pores are sealed and the cargo entrapped^{577,578}. However, this process can induce structural and chemical changes on RBCs, affecting their normal function and can be recognized by MPS^{579,580}. More recently, a novel encapsulation process was developed to overcome these obstacles. By conjugating the drug with a cell penetrating peptide via disulphide linkage, RBCs could be loaded without affecting their natural structure and functionality. Once inside RBCs, the cell penetrating peptide is detached from the drug by degradation of the disulphide bond, due to the presence of high levels of cytoplasmic glutathione found in RBCs⁵⁸¹. This technique was successfully applied to target acute lymphoblastic leukaemia (ALL) and increase L-asparaginase half-life in mouse models⁵⁸².

Leukocytes

Leukocytes are a more attractive cell type than RBCs to be used as NP carriers. They can be used as drug depots for a sustained and prolonged drug release, with the added advantage of their natural ability to home into inflammation tissues^{563,583,584}. The process of inflammation triggers the mobilization of leukocytes from the BM or its vicinity into blood circulation, with a specific migration to diseased sites. This migration is mediated by the overexpression of cell adhesion molecules on the surface of the EC layer, which facilitates the initial process of leukocyte rolling, attachment to endothelial layer and transmigration to the inflammation site^{585,586}. This process was first explored by producing microspheres with leukocyte adhesion ligands attached to their surface. The microspheres successfully mimicked the leukocyte migration behaviour into inflammation sites⁵⁸⁷⁻⁵⁸⁹. Later, leukocytes were directly used as carriers in Parkinson's disease model. Bone marrow derived macrophages were able to carry and cross blood brain barriers to deliver catalase NPs, with increased accumulation in the brain⁵⁶³.

The inflammatory response has been shown to play an important role in all stages of tumour development^{583,590}, with evidence showing that tumour cells produce high levels of chemoattractants, which can recruit a large number of leukocytes, mainly T-cells and macrophages^{591,592}. In one study, drug loaded NPs were attached to the surface of T-cells and promoted tumour reduction and prolonged survival of mice when compared with free NP administration⁵⁹³. In another study, monocytes were used as NP carriers for co-delivery of echogenic polymer/C5F12 bubbles and doxorubicin-loaded polymer vesicles towards hypoxia regions of malignant tumours⁵⁹⁴.

Stem cells

Over the last decade, stem cells have emerged as a promising therapeutic option for a wide range of diseases. As leukocytes, stem cells exhibit an intrinsic tropism to injury, inflammation and tumour sites⁵⁹⁵⁻⁵⁹⁸, with other additional advantages comparing to other cell types, as stem cells can secrete trophic factors promote the recovery of the damaged tissue and potentially differentiate to a wide variety of functional cells and consequently help in the repopulation of their target site. Moreover, MSCs and HSCs have high bioavailability and can be harvested readily from bone marrow of healthy unaffected individuals or isolated from UCB units⁵⁹⁹⁻⁶⁰⁴. MSCs have been used as NP carriers to target brain tumours^{568,605} and in regenerative medicine, for example in the treatment of ischemic hindlimbs, where MSC loaded with NPs conjugated with VEGF were able to promote vascularization and tissue regeneration⁶⁰⁶, MSCs have also been used as carriers for anti-cancer therapy. In one study, MSC transfected with liposomes containing a constructed vector, were able to inhibit tumour growth by way of lymphoma cell apoptosis induction through the bystander effect when co-cultured with Raju cells^{604,607}.

HSCs are also good candidates to target NPs to the HSC niche at the bone marrow in regenerative medicine and to treat haematological malignancies. NPs can modulate HSC paracrine activity and their engraftment in the BM. For example, protamine-sulfate coated PLGA NPs encapsulating an MRI agent have the capacity to downregulate the immune response of HSCs, by decreased expression of proinflammatory cytokines (e.g. interferon (IFN)- γ , IL-8, macrophage inflammatory protein (MIP)-1 and TNF- α)⁶⁰⁸. In another study, HSCs were chemically decorated with NPs containing Wnt activator, enabling continuous pseudo autocrine stimulation of the transplanted HSCs, which translated into a 6-fold increase in HSC engraftment, without affecting their multilineage differentiation potential⁵⁹³. NPs can also be used to target HSCs into the BM niche or to recruit other cells to the niche. For example, PLGA NPs were surface modified with bisphosphonate to provide them with a bone-binding capacity⁵⁴⁸. The bisphosphonates are calcium-ion-chelating molecules that, after systemic administration, deposit in bone tissue, particularly at the sites of high bone remodelling. In another study, CXCL12 loaded chitosan NPs were able to induce BM MSCs migration *in vitro*⁶⁰⁹.

**CHAPTER 3 - Prolonged intracellular
accumulation of light-inducible nanoparticles in
leukaemia cells allows their remote activation**

3.1. Abstract

Leukaemia cells that are resistant to conventional therapies are thought to reside in protective niches. Here, we describe light-inducible polymeric retinoic acid (RA)-containing nanoparticles (NPs) with the capacity to accumulate in the cytoplasm of leukaemia cells for several days and release their RA payloads within a few minutes upon exposure to blue/UV light. Compared to NPs that are not activated by light exposure, these NPs more efficiently reduce the clonogenicity of bone marrow cancer cells from patients with AML and induce the differentiation of RA-low sensitive leukaemia cells. Importantly, we show that leukaemia cells transfected with light-inducible NPs containing RA can engraft into bone marrow *in vivo* in the proximity of other leukaemic cells, differentiate upon exposure to blue light and release paracrine factors that modulate nearby cells. The NPs described here offer a promising strategy for controlling distant cell populations and remotely modulating leukaemic niche.

3.2. Introduction

The differentiation of leukaemia cells is a therapeutic strategy often used in the clinic to eradicate blood cancers. The concentration of the agent used for inducing leukaemia cell differentiation and the spatio-temporal control of its application are important variables for the success of this therapeutic approach⁶¹⁰. Induction of leukaemia cell differentiation by RA is a therapeutic strategy that has been used with great success in the treatment of APL^{611,612}. RA activates nuclear RA receptors (RARs) that induce cell growth arrest and differentiation⁶¹³. Despite its clear therapeutic efficacy, approximately 25% of patients receiving RA will develop serious complications, such as “differentiation syndrome”¹. Hence, there is a need for more effective formulations to deliver RA into leukaemia cells while preventing RA side effects. In addition, leukaemia cells resistant to conventional therapies reside in microenvironmental niches in the bone marrow that are difficult to access by therapeutic interventions². New strategies are required to address these problems.

NPs that disassemble in response to light⁶¹⁴⁻⁶¹⁶ offer a promising approach for reducing the side effects of conventional therapies and increasing access of therapeutic agents to the target cells. Recently, light-inducible NPs have been reported to target solid tumours due to their specific accumulation in tumour vasculature after intravenous injection⁶¹⁷. However, such an approach is not applicable to leukaemia. The hypotheses of the present work are: (i) light-inducible NPs containing RA may be a more effective strategy for differentiating leukaemia cells because they release high and more effective concentrations of RA in a short period of time (within minutes) after NP disassembly, and (ii) light-inducible NPs containing RA accumulated in the cytoplasm of leukaemia cells may offer a unique opportunity to remotely differentiate these cells in leukaemic niches in the bone marrow, which in turn may interfere with the differentiation profile of leukaemia cells in a paracrine manner.

Here, we describe light-inducible polymeric NPs containing RA that effectively disassemble within cells after light activation. These NPs accumulate in the cytoplasm of leukaemia cells for more than 6 days. They are internalized primarily through a clathrin-mediated mechanism and at minor extent by macropinocytosis. They escape in few hours the endolysosomal compartment and accumulate in cell cytoplasm. We show that these NPs are more efficient and quicker at inducing transcription from the RARE-luciferase locus than RA in solution. We further show that these NPs can be activated to release

RA *in vivo* in a highly controlled manner. Finally, we demonstrate that leukaemia cells transfected with these cells can home in the bone marrow in the same niche as other leukaemia cells, differentiate after blue laser activation and modulate the activity/phenotype of the resident leukaemia cells.

3.3. Results and discussion

3.3.1 Nanoparticle preparations and in vitro photo-disassembly

To prepare light-inducible polymeric NPs, poly(ethyleneimine) (PEI) was initially derivatized with 4,5-dimethoxy-2-nitrobenzyl chloroformate (DMNC), a light-sensitive photochrome (**Figure 3.A**). PEI was selected as the initial NP block because it facilitates the cellular internalization of NPs and their subsequent escape from endosomes^{618,619}, while DMNC was selected because it responds rapidly to light (**Figure 3.B**) and its degradation products are relatively non-cytotoxic⁶²⁰. PEI-DMNC was then added to dextran sulphate (DS) to form NPs by electrostatic (PEI:DS) and hydrophobic (DMNC:DMNC) interactions. To stabilize the NP formulation, zinc sulfate was added^{619,621}. NPs with an average diameter of 108.1 ± 9.9 nm and a zeta potential of 27.4 ± 1.6 mV were obtained (**Figure 3.2 A and B**). To demonstrate that the NP formulation could be photo-disassembled, a suspension of NPs was exposed to UV light for up to 10 min. The number of NPs (as assessed by Kcps) decreased to below half of the initial number after 1 min of UV exposure, confirming NP disassembly (**Figure 3.2B**). The disassembly was likely due to a change in the NP's hydrophilic/hydrophobic balance after DMNC photo-cleavage. Importantly, a conventional blue laser (405 nm, 80 mW) (**Figure 3.2D**) or a blue confocal laser (405 nm, 30 mW) (**Figure 3.2E**) can replace the UV light to induce the photo-disassembly of NPs. The response of the NPs to a blue laser was mediated by DMNC coupled to PEI, as NPs without DMNC did not respond to the laser (**Figure 3.2B**).

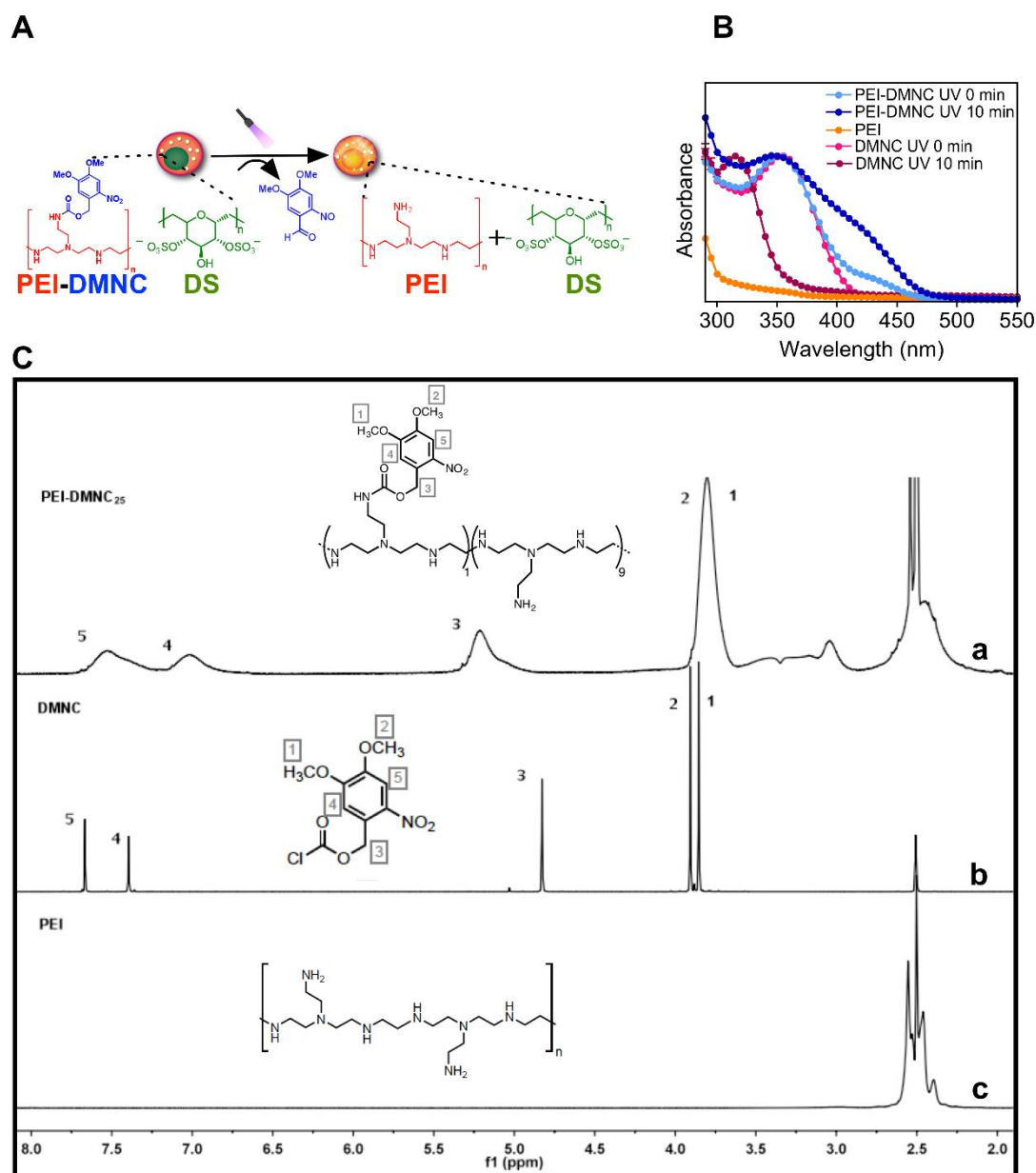


Figure 3.1 - Characterization of PEI derivatized with DMNC. (A) Schematic representation for the photo-disassembly of RA+NPs. (B) Effect of UV light (365nm, 100Watts) in the absorbance properties of PEI-DMNC (1mg/mL in DMSO), PEI (1mg/mL in DMSO) and DMNC (250 μ g/mL in DMSO). The experimental degree of substitution of PEI-DMNC was 10% as determined by spectrophotometry, using a calibration curve of DMNC and by (C) ^1H NMR spectra in DMSO- D_6 of (a) PEI-DMNC conjugate, (b) DMNC and (c) PEI. For DMNC, the absorption maximum at 355nm reverted back to baseline levels after 10 min of UV exposure, indicating the photo-cleavage of DMNC and a new absorption peak was observed at 320nm, due to the formation of 4,5-dimethoxy-2-nitrobenzyl alcohol. For PEI-DMNC, there was a decrease in intensity of the 355nm peak and a concomitant increase in the 320nm peak; however, our results suggest that not all the attached DMNC molecules were photo-cleaved.

We further evaluated the feasibility of triggering intracellular NP disassembly. For that purpose, human vein umbilical endothelial cells (HUVECs) were transfected with quantum dots 525-labelled NPs for 4 h (**Figure 3.2E and F**), and a small region of the cell housing NPs was excited by a blue laser (405 nm) under a confocal microscope. Under these conditions, NP fluorescence increases compared to a reference region not excited with UV light. This increase is due to NP disassembly and a resultant

decrease in the quenching of the quantum dots immobilized in the NPs. Overall, our results show that we can disassemble NPs by light, either *in vitro* or within cells.

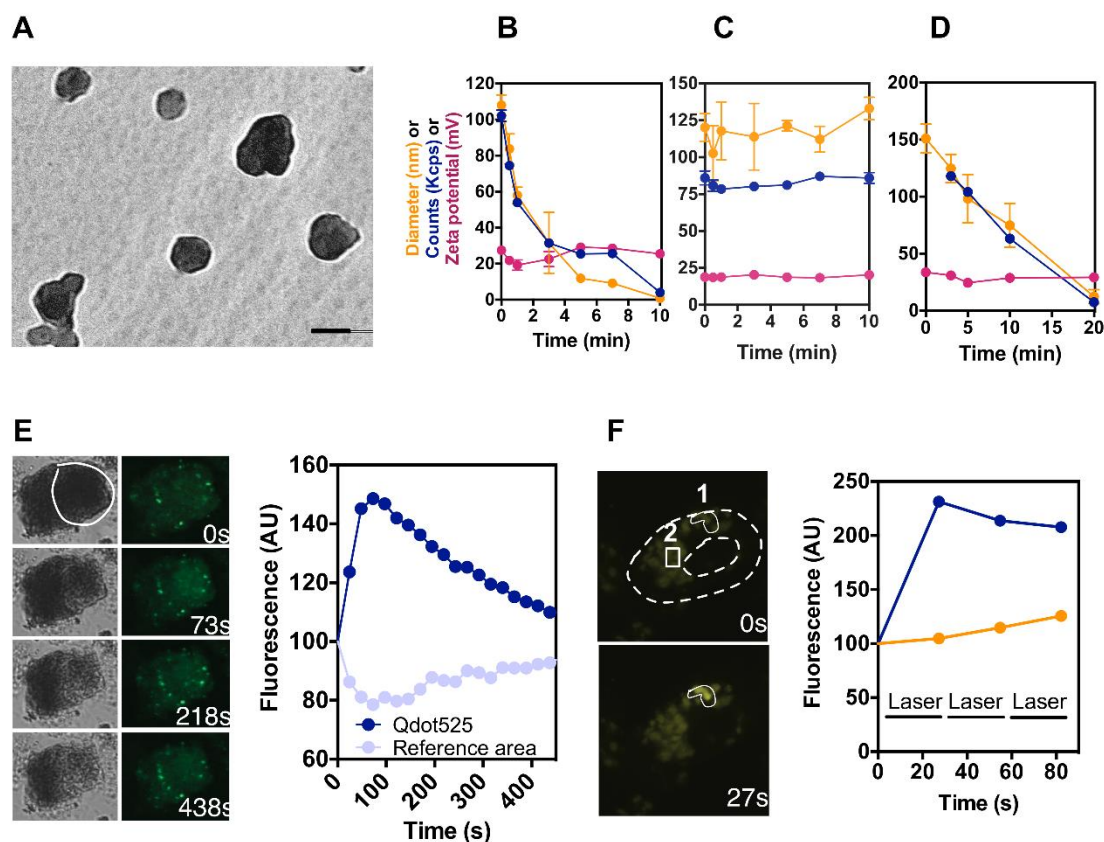


Figure 3.2 - Properties and disassembly of light-triggerable NPs. (A) TEM of the light-triggerable NPs. Bar represents 100 nm. (B, C, D) Size, zeta potential and number of NPs (Kcps) of an aqueous suspension of NPs. (B) UV light (365nm, 100W) activation of NPs exposed up to 10 min. (C, D) Blue laser (405 nm, 80 mW) activation of NPs with (D) and without (C) DMNC photochrom, exposed up to 20 min. A suspension of NPs (100 μ L, 100 μ g, in water) was exposed to a UV (up to 10 min) or a blue laser (up to 20 min). Then, the NP suspension was diluted up to 50 μ g/mL in water and the size, zeta potential and number of NPs (Kcps) in the suspension was evaluated by dynamic light scattering. Results are expressed as mean \pm s.e.m (n = 5). (E and F) Confocal images showing light-disassembly of quantum dots 525 (Qdot525)-labeled NPs. (E) A section of a NP aggregate (area delimited in the figure) was bleached continuously by a laser at 405 nm as confocal images were collected every 20 s. The images show the disassembly of the bleached area of the NP aggregate. Fluorescence intensity of the area bleached by the laser and reference area (i.e. not activated by the laser) overtime. Our results show that fluorescence intensity increases after light exposure due to the disassembly of the NP and the decrease in the quenching of Qdot fluorescence after NP disassembly. (F) Confocal imaging of HUVECs after exposure for 4 h to QDot525-labelled NPs. A small section of the cell (region 1, created by a mask) was then exposed to blue light laser cycles (405 nm) in a Zeiss confocal microscope and the intensity of fluorescence at 525 nm monitored. In parallel, the fluorescence of another section of the cell (region 2) not excited with the laser was monitored as a control. Our results show that the fluorescence intensity in region 2 maintains overtime while in region 1 the intensity increases. Blue dots and line presents the blue light laser-exposed area of Qdot525-labelled NPs; orange dots and line presents the control unexposed area of Qdot525-labelled NPs. Dashed areas show cell membrane and nucleus.

3.3.2. Loading and controlled release of Retinoic acid.

To evaluate the light-inducible polymeric NPs as a method for the controlled release of RA, a solution of RA with PEI-DMNC was assembled with DS in aqueous solution to form NPs (RA⁺NPs). Under these conditions, the carboxyl groups of RA tend to form electrostatic interactions with the amine groups of PEI¹⁴. The resultant NP formulation contained approximately 150 µg of RA per mg of NP, an average diameter of 160 nm and a zeta potential of 22 mV. The release profile of the NP formulation containing [3H]RA was monitored by scintillation after NP exposure to UV light or a blue laser for up to 10 min (**Figure 3.3A**). Up to 50 ng of RA was released per µg of NP after 10 min of activation. In the absence of light, up to 10 ng of RA was released per µg of NP after 8 days (**Figure 3.3B**).

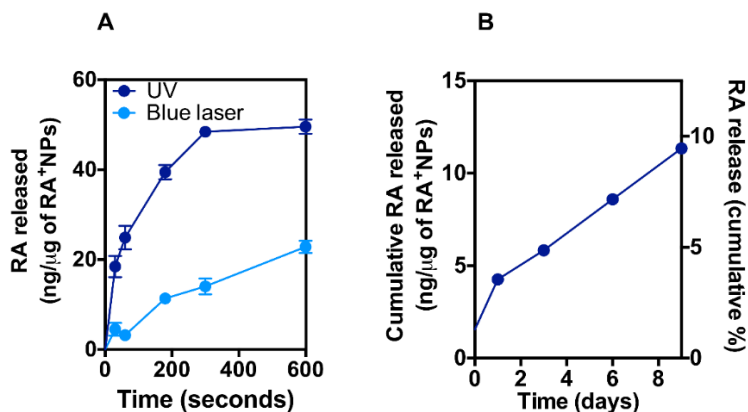


Figure 3.3 - Release of RA from Light-triggerable RA+NPs. (A) Release of [3H]-RA from an aqueous suspension of RA+NPs after exposure to UV or a blue laser. (B) Passive release of RA from RA+NPs without light activation. In (A) the NPs were prepared using [3H]-RA, diluted to 10 µg/mL NP suspension and then exposed to UV or blue laser up to 10 min. The released RA was measured in the supernatant by scintillations counts, after centrifugation (14000g, 3 min) of the of RA+NPs. In (B) RA+NPs (2.5 mg) were placed in PBS (0.5 mL) and incubated under mild agitation at 37 °C. At specific intervals of time, the nanoparticle suspension was centrifuged (at 14.000 g for 3min) and 0.4 mL of the release medium removed and replaced by a new one. The reserved supernatant was stored at 4°C until the RA content in release samples was assessed by spectrophotometry at 350 nm. Concentrations of RA were determined by comparison to a standard curve. Results are expressed as mean±s.e.m (n=3).

3.3.3. Cytotoxicity of nanoparticles and light activation in leukaemic and non-leukaemic human cells

Next, we asked whether leukaemia cells could uptake light-inducible NPs. According to our dynamic light scattering studies, RA⁺NPs are positively charged when resuspended in different culture media and relatively stable for at least 24 h (**Figure 3.4**).

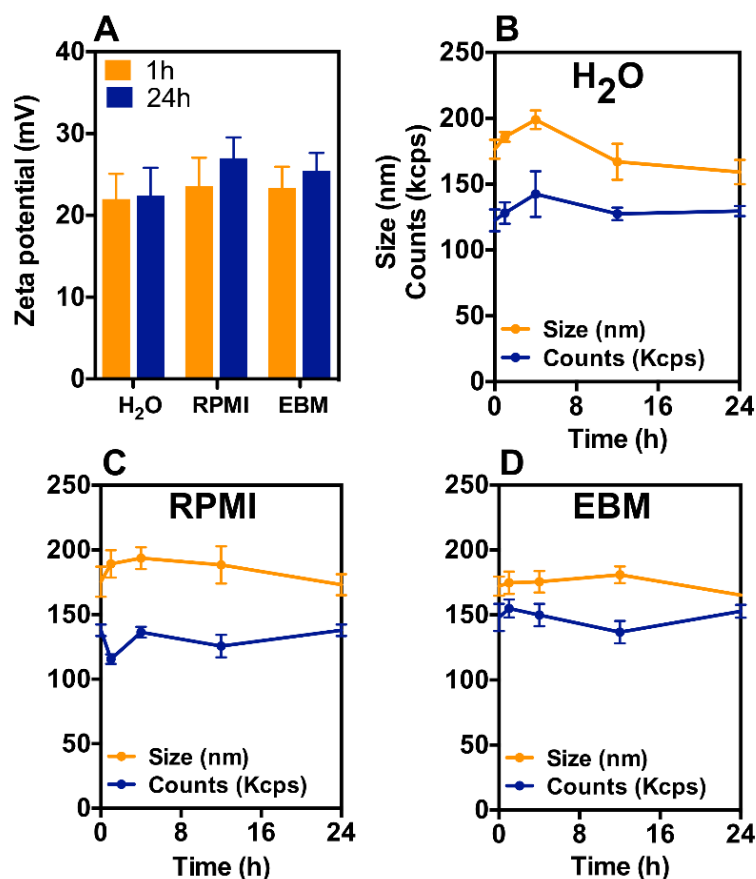


Figure 3.4 - Stability of RA+NPs suspended in water or cell culture media. (A) Zeta potential of RA+NPs suspended in water, serum-free RPMI (medium used for leukaemia cells) or EBM medium (medium used for HUVECs). It should be noted that the transfection of the cells with RA+NPs was always performed in serum-free media. Diameter (nm) and counts (Kcps) of RA+NPs suspended in water (B), RPMI medium (C) or EBM medium (D). A suspension of RA+NPs (2 mL, 25 μ g/mL) was prepared and diameter, counts and zeta potential determined by dynamic light scattering method (DLS) using a Zeta Plus Analyzer (Brookhaven). Results are expressed as mean \pm s.e.m (n = 3).

RA⁺NPs had no substantial effect on cell metabolism, as evaluated by an ATP assay for concentrations up to 20 μ g/mL in human leukaemic cell lines (Figure 3.5A) and in case of non-leukaemic cells no cytotoxicity was observed for NP concentrations up to 10 μ g/mL (Figure 3.5B), also confirmed by AnnexinV/PI assay (Figure 3.5C). For ATP and AnnexinV/PI assays Human bone marrow APL NB4 cells, human myelomonoblastic U937 cells (expressing a chimeric PLZF/RAR α fusion protein^{622,623} and showing impaired sensitivity to RA^{624,625}, HUVECs and human dermal fibroblasts were exposed to NPs for 4 h, washed to remove excess NPs not taken up by the cells, either exposed or not to UV light for 10 min, and finally cultured for an additional 20 h. Because the activation of RA⁺NPs by UV or blue light can induce double-stranded DNA breaks, we used HUVECs to evaluate the effect of this radiation on the phosphorylation of histone H2A (γ H2AX), an early biomarker of DNA damage⁶²⁶. Our results indicate that neither UV nor blue light exposure for 10 min had a significant impact on DNA damage (Figure 3.5D and E).

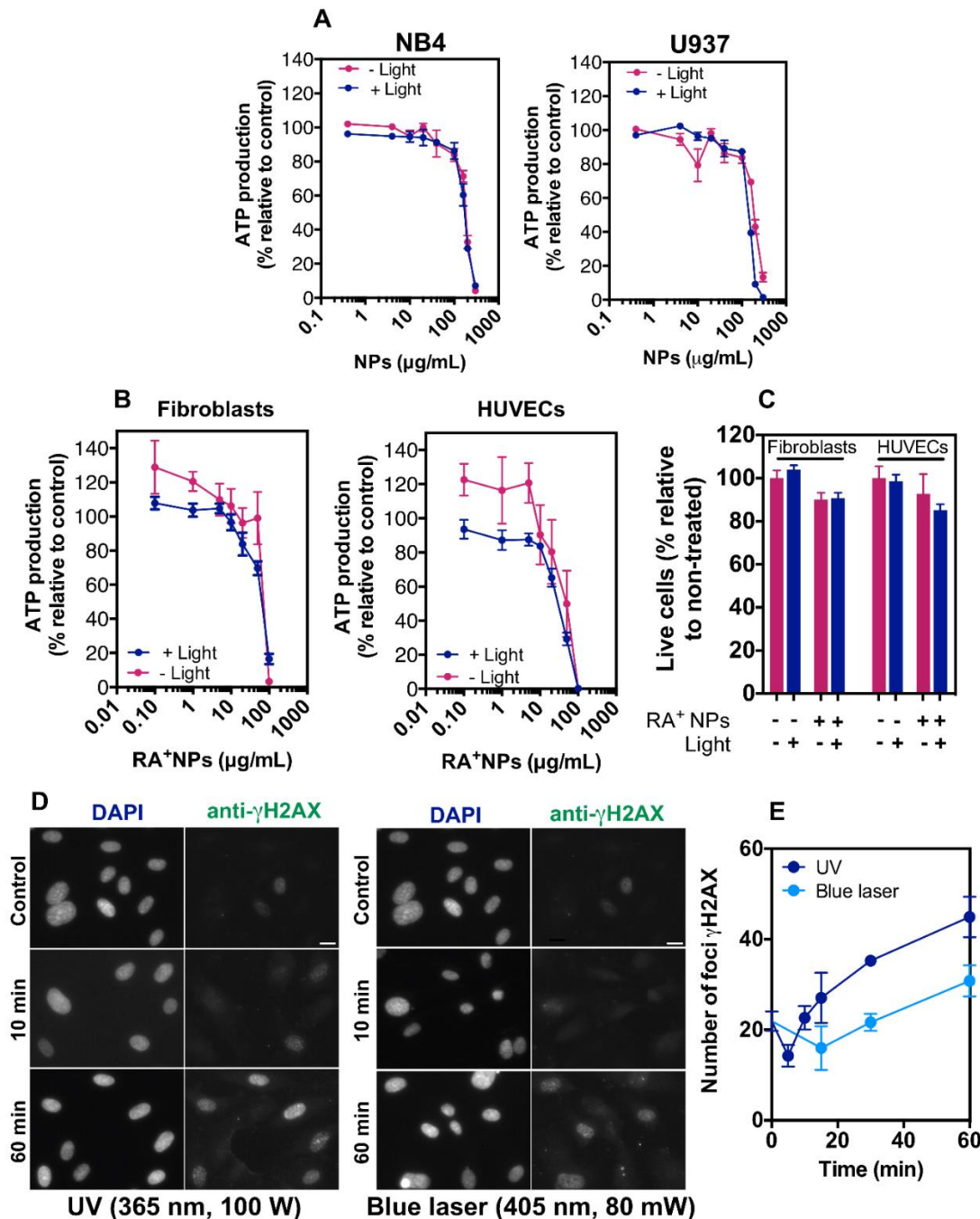


Figure 3.5 - Cytotoxicity of RA+NPs and light activation. (A) Cytotoxicity of RA+NPs against human leukaemic cell lines NB4 and U937 cells. Cells were cultured in medium supplemented with light-sensitive RA+NPs for 4 h, washed, exposed or not to a UV light for 10 min, and then cultured for 20 h. Cell cytotoxicity was evaluated by an ATP kit. (B, C) Cytotoxicity of RA+NPs against HUVECs or human dermal fibroblasts. Cells were cultured in medium supplemented with light-sensitive RA+NPs for 4 h, washed, exposed or not to a UV light for 5 min, and then cultured for 20 h. Cell cytotoxicity was evaluated by an ATP kit (B) or Annexin V/PI staining (C) followed by flow cytometry analyses. In this case, the concentration of RA+NPs was 10 $\mu\text{g/mL}$. Live cells were negative for Annexin V and PI staining. In A, B and C results are expressed as mean \pm s.e.m (n = 3). (D) HUVECs were exposure to 10 min or 60 min of UV light (left panel) or blue light (right panel) and allowed to recover for 6 h. Cells were then fixed and stained to identify γH2AX -containing foci, as biomarker for nuclear sites of DNA damage in affected cells. Bar corresponds to 10 μM . (E) Time-dependent increase of γH2AX after UV light (365 nm, 100 W) or blue light (405 nm, 80 mW) irradiation. Quantitative analysis of foci intensity were quantified using ImageJ software and normalized to the control condition. Results are expressed as Mean \pm SEM. The calculations were performed in 5 different images for a total of ca. 250 cells (ca. 50 cells per image).

3.3.4. Characterization of the internalization kinetics and pathways of RA+NPs

The intracellular accumulation of RA⁺NPs was monitored by flow cytometry and inductively coupled plasma mass spectrometry (ICP-MS) (Figure 3.6). Our results show that NP internalization peaked at 6 h (Figure 3.6A and B) and the intracellular concentration was dependent on the initial NP loading (Figure 3.6C). No significant differences were observed in the internalization profiles between cells. Importantly, 60-100% of the leukaemia cells retained NPs in culture for at least six days, as confirmed by flow cytometry (Figure 3.6D and E). This corresponded to the retention of 25-50% of the initial mass of the NPs during 8-10 cell doublings, as obtained by ICP-MS analyses (Figure 3.6F). Altogether, NPs were efficiently internalized by human leukaemia cells and accumulated intracellularly for several days.

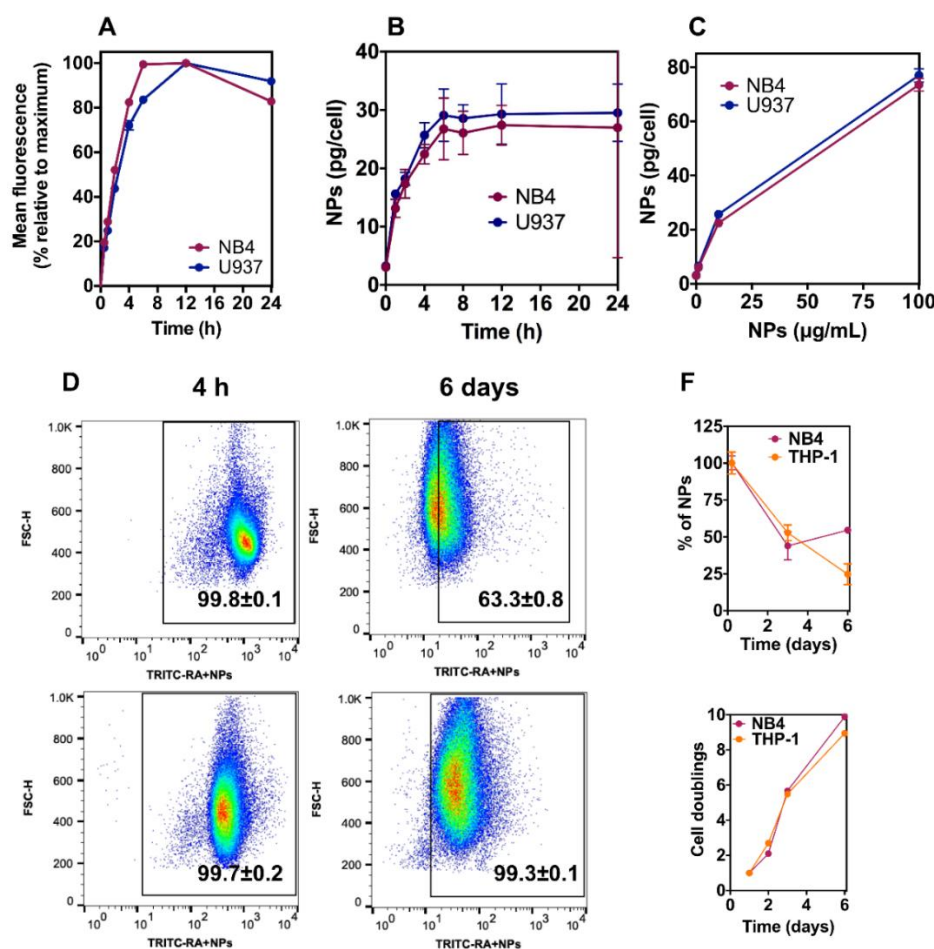


Figure 3.6 - Cellular uptake and dilution of RA+NPs in human leukaemic cells. (A) Uptake of TRITC-labeled RA+NPs (10 µg/mL) in leukaemia cell lines (NB4 and U937) as determined by FACS. Cells were cultured in medium supplemented with NPs for the time defined in the graph, washed and characterized by flow cytometry. The results are expressed as mean±s.e.m (n = 3). (B-C) Quantification of RA+NP internalization in leukaemia cell lines as determined by ICP-MS analysis (Zn quantification). Cells were incubated with 10 µg/mL NPs (B and C) or 100 µg/mL NPs (C) up to 24 h. After each incubation period, the cells were extensively washed with PBS followed by the addition of an aqueous solution of nitric acid (1 mL, 69% (v/v)). The concentration of intracellular levels of Zn was quantified by ICP-MS. The concentration was normalized per cell. The estimation of NPs was done based on standard solutions. The results are expressed as mean±s.e.m (n=3). (D, E) Dilution of TRITC labeled RA+NPs with cell culture. NB4 (D) and THP-1 (E), were transfected with RA+NPs in serum-free media for 4h, washed with PBS to remove non-internalized RA+NPs and cultured in complete media for additional 4h, 3 days and 6 days. After each incubation time cells were washed, counted (to monitor cell doublings) and NP dilution evaluated by flow cytometry (D, E) and by ICP-MS (F). The results are expressed as mean±s.e.m (n=3).

To identify the pathways of RA⁺NP internalization, U937 cells were incubated in the presence of endocytosis chemical inhibitors at non-cytotoxic concentrations. Fluorescent-labelled RA⁺NPs were then added, and the internalization monitored by flow cytometry. Whenever possible, molecules that enter by a specific internalization pathway were used as positive controls to show the efficacy of our inhibitors (**Figure 3.7A**). Dynasore treatment (clathrin-mediated endocytosis (CME) inhibitor) reduced the uptake of RA⁺NPs by 90% compared to control cells (**Figure 3.7B**). To further confirm the endocytosis mechanisms involved in RA⁺NP internalization, U937 cells were transfected with siRNAs to downregulate key components of different endocytosis pathways (**Figure 3.7C**). We observed a ~60% and ~70% reduction in NP uptake upon downregulation of clathrin heavy chain (CLTC), and low-density lipoprotein receptor (LDLR), respectively, confirming a role for CME. The knockdown of macropinocytosis regulators Rac1 and CTBP1 led to a ~40% and ~50% decrease in RA⁺NPs uptake, respectively, suggesting that macropinocytosis was also involved in RA⁺NP internalization (**Figure 3.7C**).

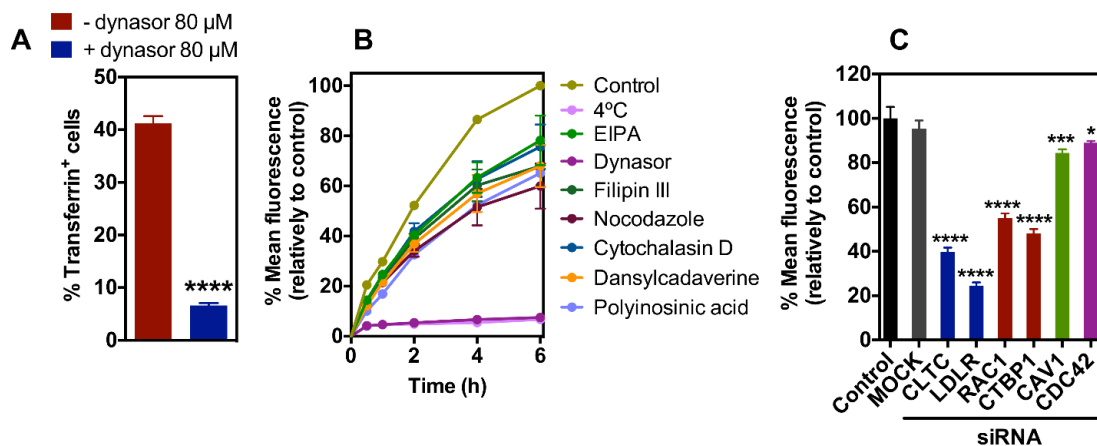


Figure 3.7 - Internalization mechanisms of RA⁺NPs in Zn-induced U937 cells. (A) Transport of FITC-labeled transferrin (1 μg/mL) known to selectively enter cells via clathrin-mediated endocytosis. Dynasore at concentration of 80 μM inhibits the internalization of transferrin in U937 cells. Cells were exposed to culture medium with and without dynasore for 30min, exposed to FITC-labeled transferrin for 3 min, at 4 °C, and finally characterized by FACS. Results are expressed as mean±s.e.m (n = 3). Statistical analyses were performed by an unpaired t-test. **** Denotes statistical significance (P<0.0001). (B) Uptake of TRITC-labeled RA⁺NPs by U937 cells in the presence of several endocytosis inhibitors. Filipin III inhibits cholesterol dependent internalization mechanisms, ethylisopropylamiloride (EIPA) inhibits macropinocytosis, nocodazole inhibits microtubule dependent pathways, cytochalasin D inhibits all pathways dependent on actin (including macropinocytosis), dansylcadaverine and dynasore inhibits clathrin-mediated endocytosis and polyinosinic acid inhibits scavenger receptors. Results are expressed as mean±s.e.m (n = 3). (C) Uptake of TRITC-labelled RA⁺NPs after silencing of key regulators on endocytosis by transfection of siRNAs in U937 cells. Results are expressed as mean±s.e.m (n = 3). Statistical analyses were performed between control and the remain experimental groups using one-way ANOVA followed by a Newman-Keuls post-test. *P<0.05, ***P<0.001, ****P<0.0001.

3.3.5. Intracellular trafficking and endolysosomal escape of NPs

To elucidate the intracellular trafficking of our NPs, we used adherent cells (HUVECs) to allow for this characterization by confocal microscopy. The intracellular trafficking of our NPs was assessed first by performing a LysoTracker staining to see the general distribution of FITC-labelled RA⁺NPs in the endolysosomal system. During the first few hours, there was an increase in the intracellular signal of

FITC-labelled RA⁺NPs and a clear drop in the intensity of LysoTracker, suggesting an increase in the pH of the endolysosomal vesicles by the presence of intracellular PEI (a strong base), as well as possible vesicle disruption, as the FITC-labelled NP signal was increased in the cytoplasm (**Figure 3.8A**). At later time points (12 h) of incubation with FITC-labelled NPs, the intensity of LysoTracker reached control levels, suggesting that the endolysosomal system regained its normal characteristics. Our results further show that most of the NPs (~80% of NP fluorescence) escape endolysosomes within a few hours (**Figure 3.8B**). At 6 h, most of the FITC-labelled NPs were distributed throughout the cytoplasm (~80% of the fluorescence) (**Figure 3.8B**), and those that accumulated in the endolysosomal compartment were located in vesicles positive for Rab5 (early/late endosomes) and Rab7 (endosome/lysosomes) (**Figure 3.8C and D**). This is consistent with a rapid escape of the NPs from endosomes after uptake by the cell, likely due to their buffering capacity which gives rise to osmotic swelling and endosome rupture⁶¹⁹.

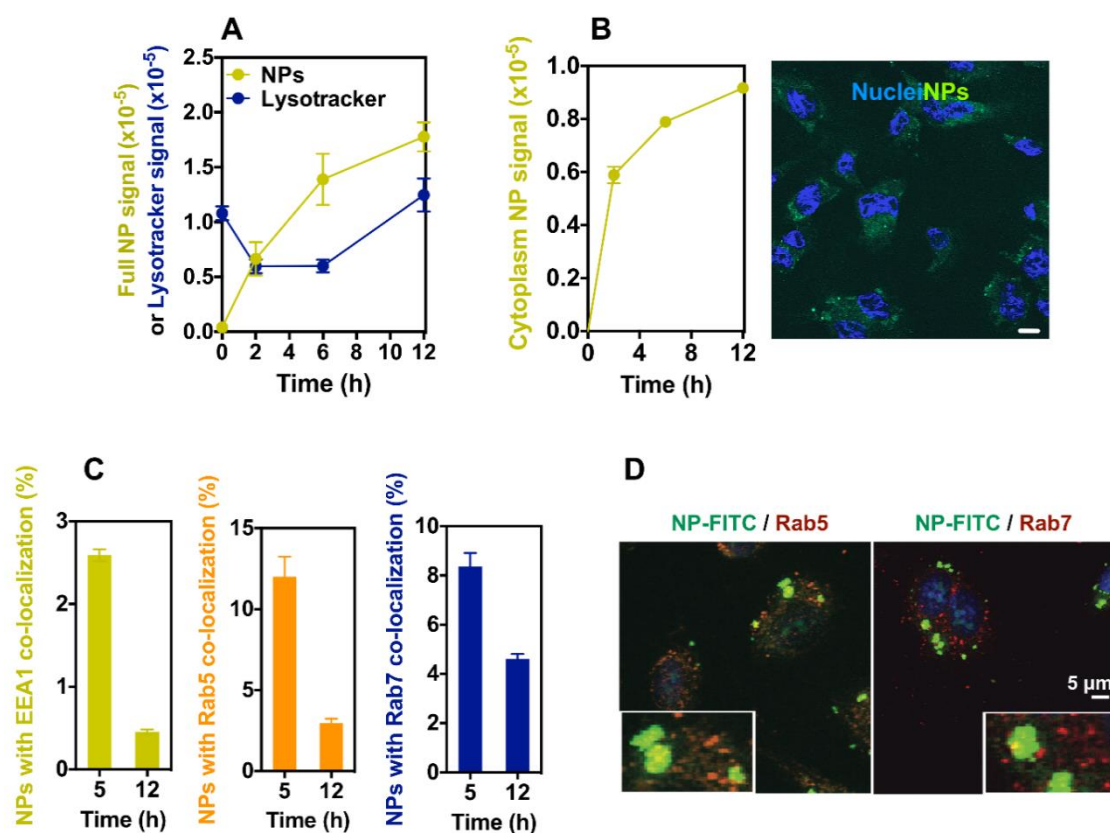


Figure 3.8 - Intracellular trafficking of FITC-labelled RA+NPs. (A) HUVECs were incubated with FITC-labelled RA+NPs (1 μg/mL) for 4h, washed extensively, cultured in EGM-2 cultured in normal conditions for 1, 2 or 8 additional hour/s, respectively, and stained with LysoTracker DND-99 before cell fixation to monitor the NPs trafficking through the endolysosomal compartment overtime. (B) Fluorescence of NPs in the cytoplasm measured by confocal microscopy. Scale bar represents 10 μm. Results are expressed as mean ± s.e.m (n = 5). (C, D) Early endosome were stained with EEA1 antibody, early/late endosomes were stained with Rab5 antibody and late endosome/lysosomes were stained with Rab7 antibody. (C) Quantification of FITC-labelled RA+NPs co-localized with EEA1, Rab5 and Rab7. Results are expressed as mean ± s.e.m (n = 70-100 cells). At 5 h, there is a clear accumulation of FITC-labeled NPs within vesicles that are mostly Rab5 and/or Rab7 positive with very low EEA1 co-localization. The high co-localization with Rab5 and the size of the vesicles containing NPs (see D) suggests that macropinocytosis is also an entrance route for these NPs. (D) Representative images of the intracellular distribution of FITC-labelled RA+NPs at time 5 h in relation to early/late endosomes stained with Rab5 antibodies (left image), and late endosome/lysosome stained with Rab7 antibody (right image).

Next, we asked whether RA⁺NPs would be effluxed by leukaemia cells overtime. It is known that tumour cells express high levels of P-glycoprotein (P-gp), a membrane transporter that is responsible for the efflux of drugs⁶²⁷ and NPs⁶²⁸. Therefore, we used flow cytometry to study the effects of the P-gp antagonist, verapamil⁶²⁸, on the intracellular accumulation of RA⁺NPs in Zn-induced U937-B412 cells expressing P-gp (**Figure 3.9A**). Our results show that the intracellular accumulation of RA⁺NPs in U937 slightly decreases from 4 h to 12 h (**Figure 3.9B**), in contrast to the control, ultra-small paramagnetic iron oxide (USPIO). The intracellular accumulation of USPIO was highly dependent on the inhibition of P-gp (**Figure 3.9C**). Overall, our results indicate that RA⁺NP endocytosis takes place primarily through a clathrin-mediated mechanism and at minor extent by macropinocytosis. It is likely that both endocytic pathways are interconnected, as has been demonstrated recently for lipid NPs^{21,22}. Our results further show that the internalization of RA⁺NPs occurs quickly, and within the first 2 h, a significant percentage of NPs tend to escape the endolysosomal compartment, while the ones that do not escape accumulate in early/late endosomes.

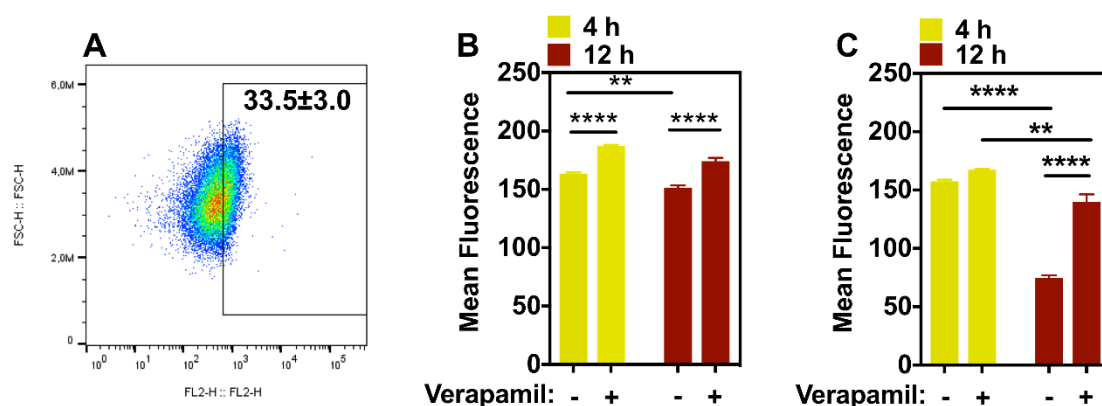


Figure 3.9 - Effect of inhibition of P-gp in the accumulation of NPs. Expression of P-gp in Zn-induced U937 cells as evaluated by flow cytometry. (A) Representative flow cytometry gating strategy of TRITC positive cells. Percentage of positive cells was calculated based in the isotype control. (B) TRITC-labeled RA⁺NPs (10 µg/mL) or (C) TRITC-labeled USPIO NPs (100 µg/mL) intracellular accumulation in Zn-induced U937 cells in the presence of the P-gp antagonist verapamil. Cells were exposed to culture medium with verapamil, TRITC-labeled NPs for 4 h, cultured for additional 8 h and finally characterized by flow cytometry. In A, B and C, results are expressed as Mean ± SEM, n=3. Statistical analyses were performed using a One-Way Anova followed by a Newman-Keuls posttest. *P<0.05, ** P<0.01, *** P<0.001, **** P<0.0001.

3.3.6. Differentiation of leukaemic cells by photo-release of RA from NPs

Previously, liposomes⁶²⁹ and block copolymer NPs⁶³⁰ have been used for the release of RA in myeloid leukaemia cell lines. However, no significant differences were observed between liposome/NP formulations and soluble RA in their capacity to induce leukaemia cell differentiation. Therefore, we evaluated the capacity of light-inducible RA⁺NPs to prompt the differentiation of human CD34⁺ primary leukaemia cells isolated from the bone marrow aspirates of AML patients, taken at diagnosis. We evaluated their clonogenic potentials in short term (blast colony-forming units, CFU) and long term (long-term culture-initiating cell, LTC-IC) assays following treatment with RA or RA⁺NPs (**Figure 3.10A**). Our results indicate that light-inducible RA⁺NPs were more effective than soluble RA at decreasing the number of CFUs (**Figure 3.10B**). Our results further indicate that RA⁺NPs activated by

CHAPTER 3 - Prolonged intracellular accumulation of light-inducible nanoparticles in leukaemia cells allows their remote activation

light are more effective in decreasing the number of CFUs (**Figure 3.10C**) and LTC-ICs (**Figure 3.10D**) than non-activated RA⁺NPs. We extended the previous studies to different leukaemia cell lines, including U937, NB4 and THP-1 (**Figure 3.10E, G and K**).

The differentiation process was monitored by the expression of myeloid maturation marker CD11b, a protein involved in the regulation of leukocyte adhesion and migration. For equivalent concentrations of RA, U937 (**Figure 3.10E**) or NB4 (**Figure 3.10G**) cells treated with RA⁺NPs more readily differentiated into myeloid cells than cells treated with soluble RA, likely due to the higher efficiency of the NPs to deliver RA intracellularly (**Figure 3.10J**). The differences in the intracellular accumulation of RA are likely explained by the differences in RA uptake mechanism. The RA is a hydrophobic small molecule with limited water solubility (63 mg/L⁶³¹) and thus *in vivo*, it is transported by proteins called cellular retinoic acid-binding proteins (CRABP) both in extracellular and intracellular compartments⁶³². The expression of CRABP is relatively low in undifferentiated leukaemic cells⁶³³ and thus the transport of soluble RA to inside of the cell might be limited. In contrast, the transport of RA⁺NPs occurs by endocytosis which might facilitate the intracellular accumulation of RA.

U937 (**Figure 3.10F**), NB4 (**Figure 3.10H**) or THP-1 (**Figure 3.10K**) cells treated with light-activated RA⁺NPs showed a higher capacity for myelocytic differentiation than cells treated with non-activated RA⁺NPs. In the case of NB4 cells, RA released from light-inducible RA⁺NPs promoted a higher percentage of cells expressing CD13^{high}CD11b⁺ and CD13^{low}CD11b⁺ (**Figure 3.11A and B**) than soluble RA.

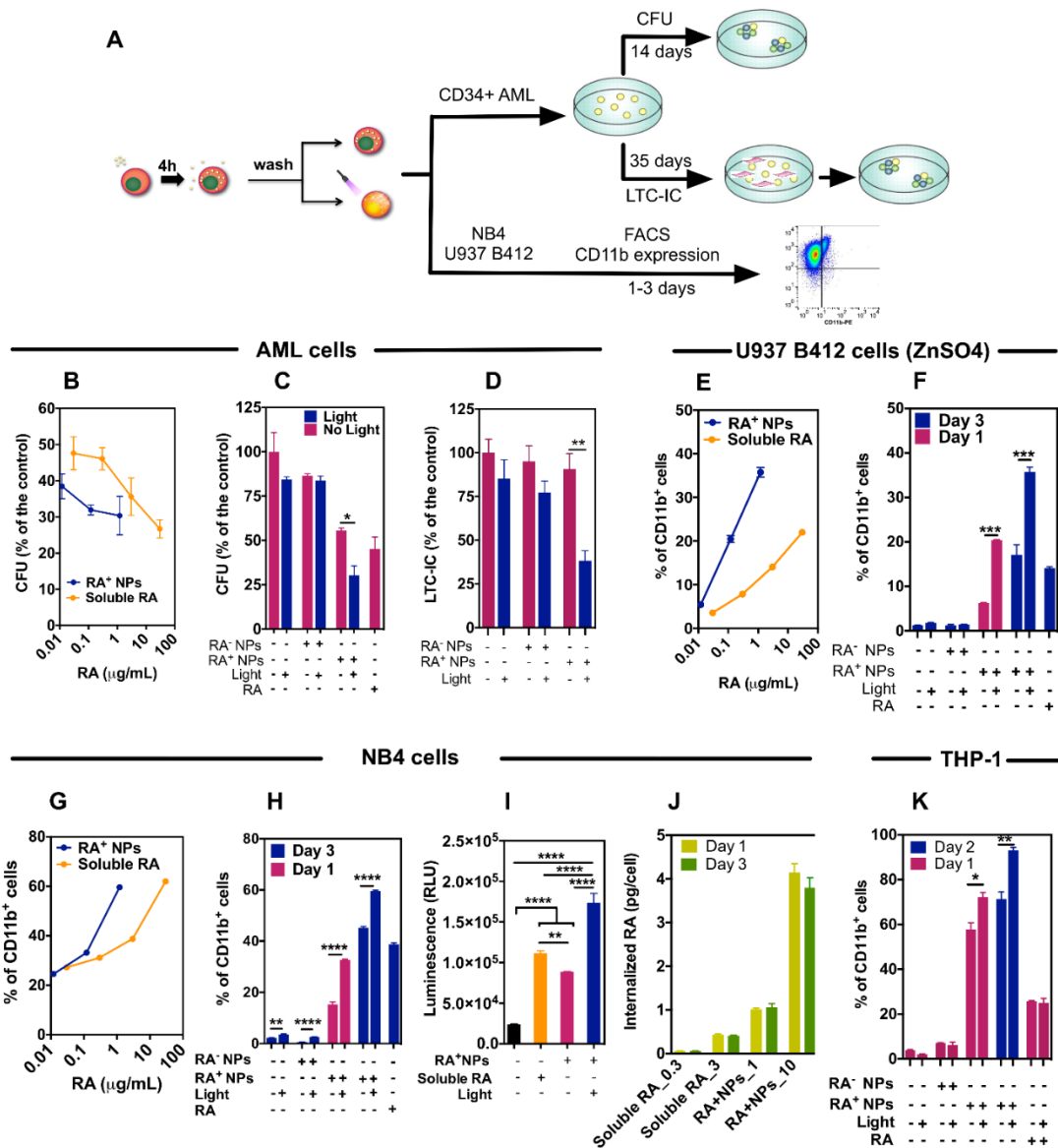


Figure 3.10 - Effect of RA+NPs on human leukaemia cells. Effect of RA+ NPs on human leukaemia cells. (A) Schematic representation of the methodology used. (B) Differentiation of CD34⁺ AML cells isolated from the bone marrow aspirates of patients with AML cultured with light-activated RA⁺NPs or soluble RA. (C, D) Differentiation of CD34⁺ AML cells with RA+NPs (10 μg/mL) or blank (RA-NPs) NPs (10 μg/mL, exposed or not to UV light), by a CFU (C) or LTC-IC (D) assays. Results are expressed as a mean percentage of control plates containing only AML cells. (E, F) Myelocytic differentiation of human Zn-induced U937-B412 cells cultured with light-activated NPs or soluble RA at day 3 (E) or cultured with RA⁺NPs with or without light activation (F). (G, H) Myelocytic differentiation of human NB4 cells cultured with light-activated NPs or soluble RA at day 3 (G) or cultured with RA⁺NPs with or without light activation for 1 or 3 days (H). (I) Intracellular release of RA as evaluated by a RARE luciferase cell line. NB4-RARE cells were cultured with soluble RA (3 μg of RA per ml) for the entire duration of the experiment, or light-activatable RA⁺NPs (5 μg/mL; 0.6 μg of RA per mL). Cells were exposed to NPs for 1 h, washed with PBS and resuspended in cell media. Some samples were exposed to UV light for 5 min. The cells were then cultured for 24 h before luciferase luminescence reading. (J) [³H]-RA uptake by NB4 cells. NB4 cells were cultured with soluble [³H]-RA (0.3 and 3 μg/mL) for the entire duration of the experiment, or light-activatable [³H]-RA⁺NPs (1 and 10 μg/mL) for 4 h and then the cells were washed and cultured in cell medium for additional 20/68 h before scintillation counting. (K) Myelocytic differentiation of human THP-1 cells. THP-1 cells were cultured with soluble RA (3 μg of RA per mL) in culture medium for the entire duration of the experiment, or light-activatable RA+NPs (10 μg of NPs/mL, i.e., 1.2 μg of RA per mL), or light-activatable NPs without RA (10 μg of NPs/mL). From B to K, results are expressed as mean±s.e.m. (n=3). In C, D, F, H, K, statistical analyses were performed by an unpaired t-test while in I were performed by one-way ANOVA followed by a Newman-Keuls post-test. *P<0.05, **P<0.01, ***P<0.001 and ****P<0.0001.

NB4 cells differentiated by light-inducible RA⁺NPs have a different morphology from undifferentiated cells, showing polylobular nuclei, decreased nuclear:cytoplasmic ratios and decreased cytoplasm staining, as characterized by a May-Grunwald Giemsa staining (**Figure 3.11C**).

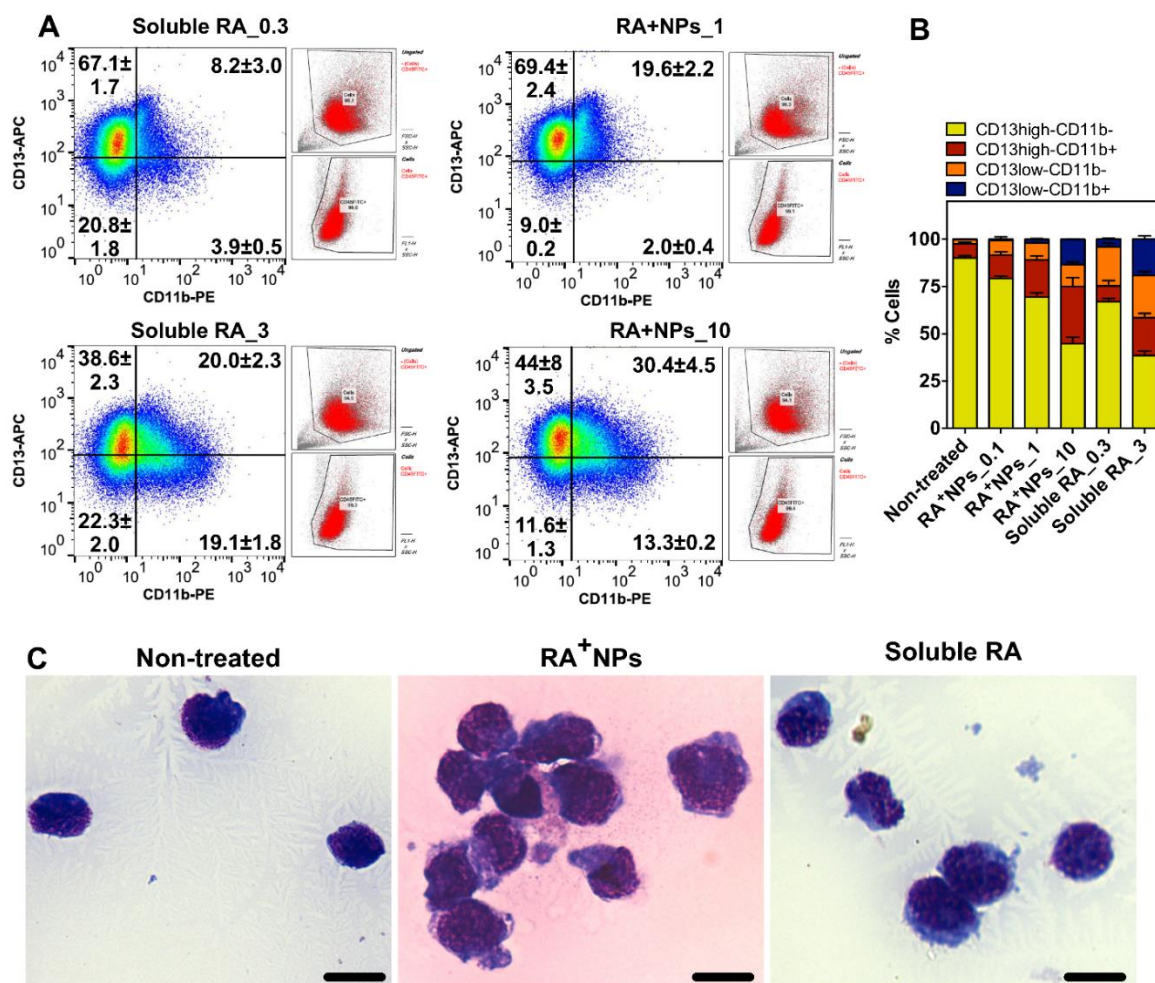


Figure 3.11- Differentiation profile of NB4 cells after treatment with soluble RA or RA+NPs. NB4 cells were incubated in serum-free RPMI-1640 with RA+NPs (1 or 10 $\mu\text{g/mL}$; RA+NPs_1 and RA+NPs_10, respectively) for 4 h. Then, cells were washed three times with PBS to remove NPs not internalized, activated by UV light (365nm, 100W) during 5 min, and cultured in complete medium for additional 3 days. Alternatively, NB4 cells were cultured in complete medium for 3 days having soluble RA (0.3 or 3 $\mu\text{g/mL}$; RA_0.3 and RA_3, respectively). (A) Flow cytometry analysis of differentiated NB4 cells cultured for 3 days. Cells were initially gated in an FSC/SSC plot (in red; attached to the scatter plot) and then gated for the expression of CD45 (in red; attached to the scatter plot). Percentages of positive cells were calculated based in the isotype controls and are shown in each scatter plot. Results are expressed as mean \pm s.e.m. (n=3). (B) Percentages of CD13^{high}CD11b⁻ CD13^{high}CD11b⁺, CD13^{low}CD11b⁻ and CD13^{low}CD11b⁺ in NB4 cells differentiated for 72 h. Results are expressed as mean \pm s.e.m. (n=3). (C) Representative May-Grunwald Giemsa stains of NB4 cells cultured for 72 h after exposure to RA+NPs (10 $\mu\text{g/mL}$; therefore 1.2 $\mu\text{g/mL}$ of RA) or soluble RA (3 $\mu\text{g/mL}$). Bar corresponds to 20 μm .

The efficiency of the RA⁺NPs in delivering RA inside NB4 cells and inducing a RA-dependent signalling pathway was also confirmed using a NB4-RARE reporter cell line. The RA-dependent induction of a RARE element driving the transcription of the firefly luciferase gene was used to evaluate the kinetics of RA-induction using RA⁺NPs or RA in solution. Our results showed that RA⁺NPs were

able to induce high levels of luciferase activity shortly after light activation (**Figure 3.10J**). RA⁺NPs were more efficient and quicker at inducing transcription from the RARE-luciferase locus than RA in solution.

3.3.7. Transcriptional regulation of retinoic acid during differentiation

Next, we monitored the effects of soluble RA and RA released from RA⁺NPs in the transcriptional regulation of 96 genes involved in the differentiation program of NB4 and U937 cells^{634,635} (**Figure 3.12** and **Figure 3.13**). In the case of NB4 cells, CD52, CDKN1A (also known as the p21 gene) and TNF α are recognized as direct targets of RA⁶³⁴; CD52 and CDKN1A are upregulated and TNF α is downregulated in response to RA. Our results show that the upregulation of CDKN1A and CD52 mRNA transcripts was significantly higher in cells treated with RA⁺NPs compared to those treated with soluble RA for 8 h and 24-48 h, respectively (**Figure 3.14**).

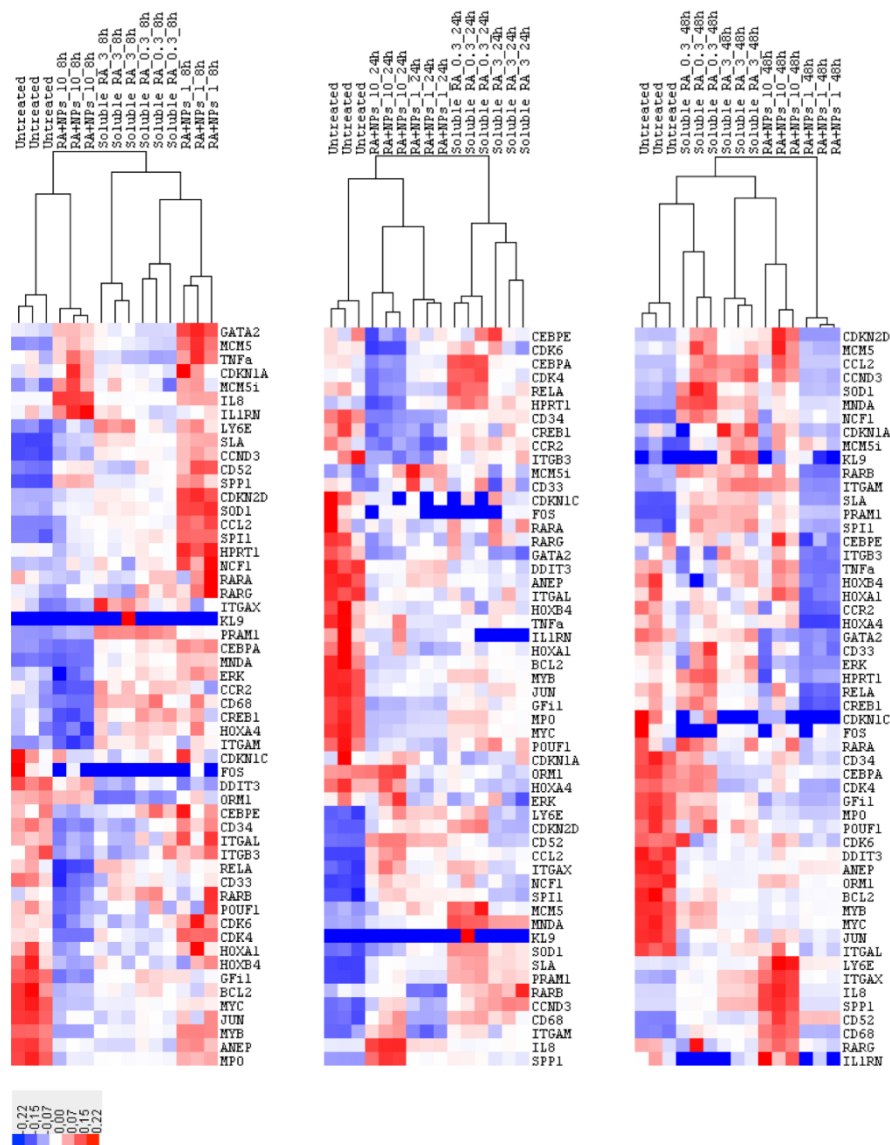


Figure 3.12 - Heat map of the differentiation pattern of NB4 cells after exposure to soluble RA or light-activatable RA+NPs. Cells were treated with RA+NPs (1 or 10 $\mu\text{g/mL}$) for 4 h, washed, activated with UV light (365 nm, 100 W) for 5 min, and then cultured for up to 48 h. In case of cells treated with soluble RA (0.3 or 3

On the other hand, the downregulation of $TNF\alpha$ occurred more slowly in cells treated with RA^+NPs than in those treated with soluble RA. Other RA-responsive genes were also evaluated by qRT-PCR^{634,636}. The number of mRNA transcripts for IL-8 and Ly6E genes was higher in cells treated with RA^+NPs than in those treated with soluble RA for 8-24 h and 24-48 h, respectively. In addition, the number of mRNA transcripts for CCR2 and $CEBP\alpha$ genes were lower in cells treated with RA^+NPs than in those treated with soluble RA for 8-48 h and 8 h, respectively. Importantly, no significant variation in mRNA transcripts for $RAR\alpha$, $RAR\beta$ and $RAR\gamma$ (Figure 3.12 and Figure 3.14) was found between all experimental groups. Therefore, our results suggest that the differentiation profile induced by RA^+NPs is similar to that observed for soluble RA; however, the magnitude of the effect in the initial stages (up to 24 h) is higher in cells treated with RA^+NPs .

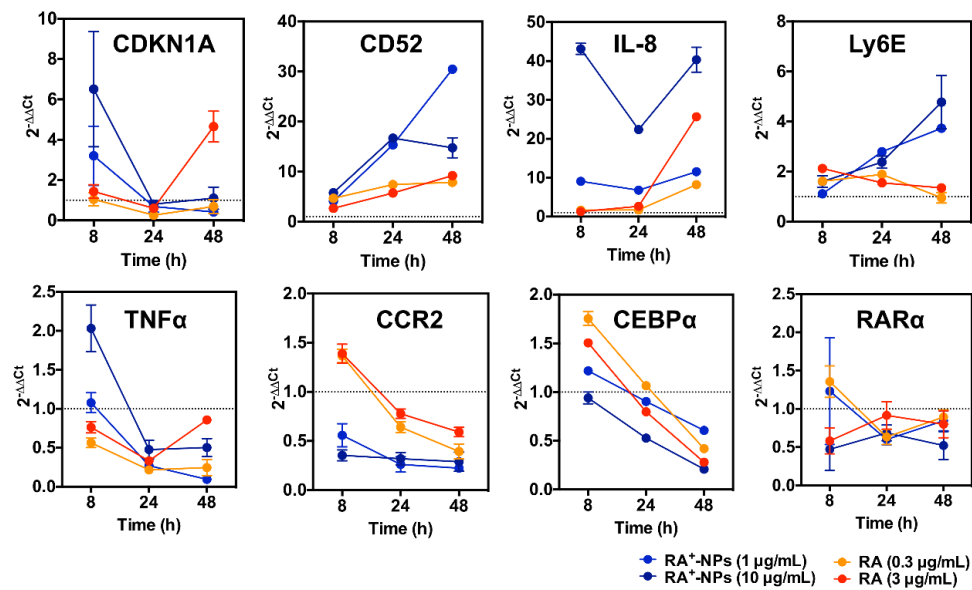


Figure 3.14 - Genes modulated by RA during differentiation of NB4 cells as assessed by qRT-PCR analyses. Results are expressed as mean \pm s.e.m (n=3). In each run, the expression of each gene was normalized by GAPDH gene. Gene expression in each experimental group was normalized by the corresponding gene expression observed in nontreated NB4 cells.

3.3.8. Effect of time and irradiation rounds on RA^+NPs induced differentiation

Recent studies report that lipid-based NPs are able to release siRNA cargo in the cytosol only during a limited window of time, when the NPs reside in a specific compartment that shares early and late endosomal characteristics^{637,638}. Therefore, we evaluated the impact of temporal activation of RA^+NPs on the differentiation of NB4 and U937 cells. The effect of the intracellular release of RA was evaluated in terms of cell differentiation into the myeloid lineage (expression of CD11b at day 3) (Figure 3.15A).

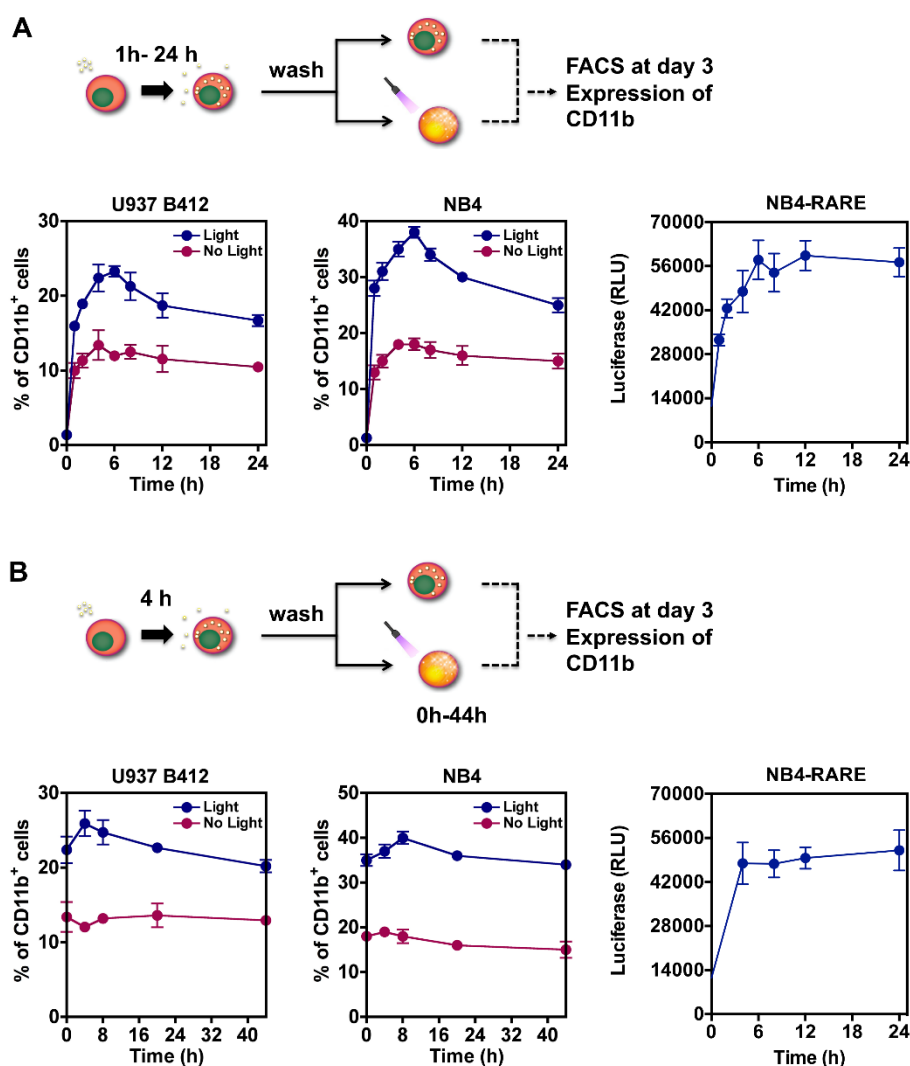


Figure 3.15 - Effect of time in the activation of RA+NPs within the cells. (A) Zn-induced U937-B412, NB4 or NB4-RARE-luciferase reporter cells were cultured with RA+NPs (1 $\mu\text{g}/\text{mL}$) for variable period of times (1 up to 24 h), washed with PBS, resuspended in cell culture media, exposed to UV light (365 nm, 100 Watts) for 5 min, and cultured for 12 h (luciferase measurements) or 72 h (flow cytometry analyses). Results are expressed as mean \pm s.e.m (n = 3). (B) Zn-induced U937-B412, NB4 or NB4-RARE-luciferase reporter cells were cultured with RA+NPs (1 $\mu\text{g}/\text{mL}$) for 4 h, washed with PBS, resuspended in cell culture media, exposed to UV light for 5 min at variable periods of time (0 up to 44 h), and cultured for 12 h (luciferase measurements) or 72 h (flow cytometry analyses). Results are expressed as mean \pm s.e.m (n = 3). In NB4-RARE, the activation of RA-dependent signalling pathway was measured by luminescence while in U937 B412 and NB4, cell differentiation was evaluated by the expression of CD11b by flow cytometry.

Cells that were incubated with RA⁺NPs for 4 to 8 h and subsequently activated by light showed the highest differentiation into the myeloid lineage. Interestingly, cells incubated with RA⁺NPs for 1 h showed an already high level of differentiation, indicating that NP uptake is rapid, and their endosomal escape is efficient. Then, we asked whether cells exposed for the same time (4 h) to NPs but activated at different times (up to 44 h) during the intracellular trafficking of RA⁺NPs would have differences in their differentiation pattern (**Figure 3.15B**). Our results show that even after 44 h following NP internalization, the NPs can be activated and the resultant delivery of RA in the cytosol can be relatively efficient. Similar results were obtained when the effect of temporal intracellular RA release was

evaluated by the induction of the NB4-RARE reporter cell line (**Figure 3.15B**). Overall, these results show that the NPs can be accumulated in the intracellular environment and activated after a few days, without losing their capacity to promote cell differentiation. Importantly, a single activation procedure seems to be sufficient to activate RA release from the NPs because no significant increase in efficiency was observed when multiple rounds of light activation were performed (**Figure 3.16**).

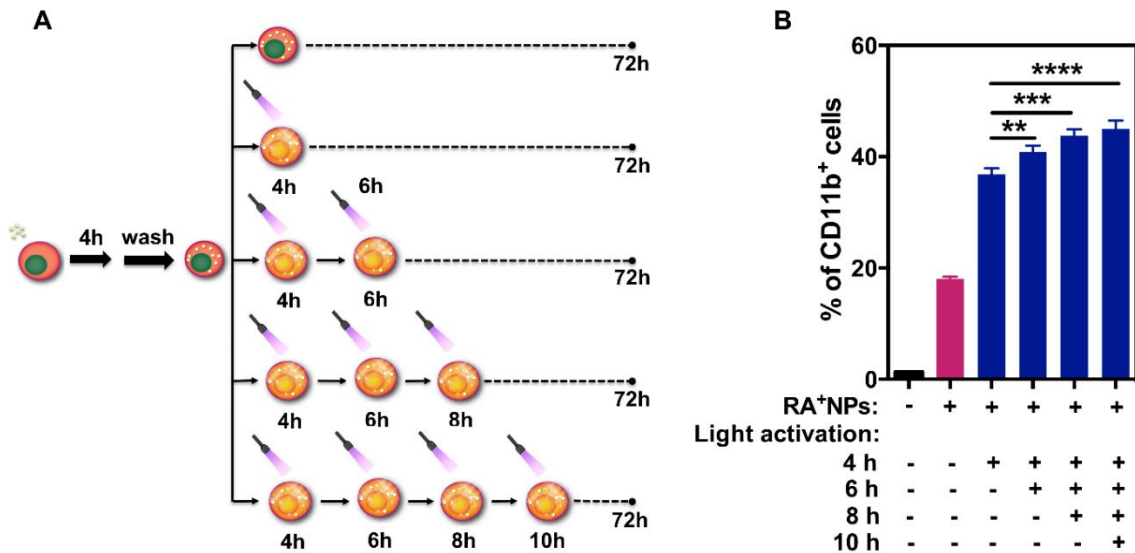


Figure 3.16 - Effect of multiple light activation in the differentiation of Zn-induced U937-B412 cells. (A) Schematic representation of the methodology. Cells were cultured with RA+NPs (10 $\mu\text{g}/\text{mL}$) for 4 h, washed with PBS, resuspended in cell culture media, exposed to multiple 5 min-cycles of UV light (365 nm, 100 Watts) during the 72 h of culture. (B) Myelocytic differentiation at 72 h, as assessed by the expression of CD11b (by flow cytometry), of human leukaemia Zn-induced U923-B412 cells. Results are expressed as mean \pm s.e.m (n = 3). Statistical analyses were performed using a One-Way Anova followed by a Newman-Keuls post-test. *P<0.05 and **P<0.01.

3.3.9. In vivo differentiation of NB4 cells transfected with RA+NPs

Next, we evaluated if RA⁺ NPs can function *in vivo*. We investigated whether leukaemic cells loaded with RA⁺NPs could be activated *in vivo* after subcutaneous transplantation. We selected a Matrigel plug subcutaneous model because we know what the attenuation of the blue laser through the murine skin is (**Figure 3.17A**) and we could easily remove the cells from the Matrigel plug and evaluate their differentiation by flow cytometry. Initially we evaluated whether the *in vivo* environment could interfere with the differentiation program of leukaemic cells after *ex vivo* activation.

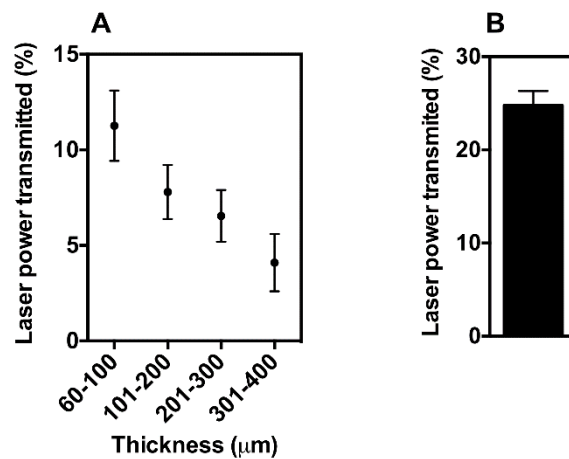


Figure 3.17 - Blue laser (405 nm) attenuation through murine skin or calvaria. NOD/SCID mice were euthanized followed by hair shaving and removal of dorsal and ventral skin as well as calvaria bone. Both tissues were kept in cold PBS until further analyses. For the laser attenuation studies, 2 cm x 2 cm skin or 0.5 cm x 0.5 cm calvaria were placed in a plastic petri dish on top of a thermal power sensor (Thorlabs, s310c). Both tissues were then irradiated with a 405 nm laser at 80 mW during 1 min. Laser attenuation values were calculated by normalizing against laser power values obtained with the empty petri dish. The thickness of the skin and bone was measured by a caliper. (A) Blue laser attenuation as a function of skin thickness. Results are expressed as mean±s.e.m (n = 2-6 per each thickness interval). (B) Blue laser attenuation in calvaria bone (≈ 260 μM). Laser attenuation in calvaria bone is lower than the skin likely due to the high transparency of the bone. Results are expressed as mean±s.e.m (n = 4).

Human NB4 cells were cultured with RA⁺NPs for 4 h, washed and activated *ex vivo* by exposure to a 405 nm blue laser (80 mW) for 5 min, embedded in Matrigel and then injected into a cylindrical poly(dimethylsiloxane) (PDMS) construct that was previously implanted subcutaneously in NOD/SCID recipients (Figure 3.18A). The PDMS cylinder was used to restrict cell position inside the animal. After five days, human cells were isolated from the implants and CD11b expression measured by flow cytometry (Figure 3.18B).

Consistent with our *in vitro* data, CD11b expression was statistically higher in NB4 cells treated *ex vivo* with light-activated RA⁺ NPs than in cells treated with RA⁺ NPs without light activation (Figure 3.18B). The experiment was repeated with *in vivo* activation. One day after implantation, the recipients were exposed to a 405 nm blue optical fibre for 5 min at the implant site (Figure 3.18C). After three days, the recipients were sacrificed, the human cells were isolated and CD11b expression was assessed. CD11b expression was higher in NB4 cells from mice that had been exposed to the blue laser, demonstrating that internalized RA⁺ NPs can be activated to release RA *in vivo* in a highly controlled manner (Figure 3.18C).

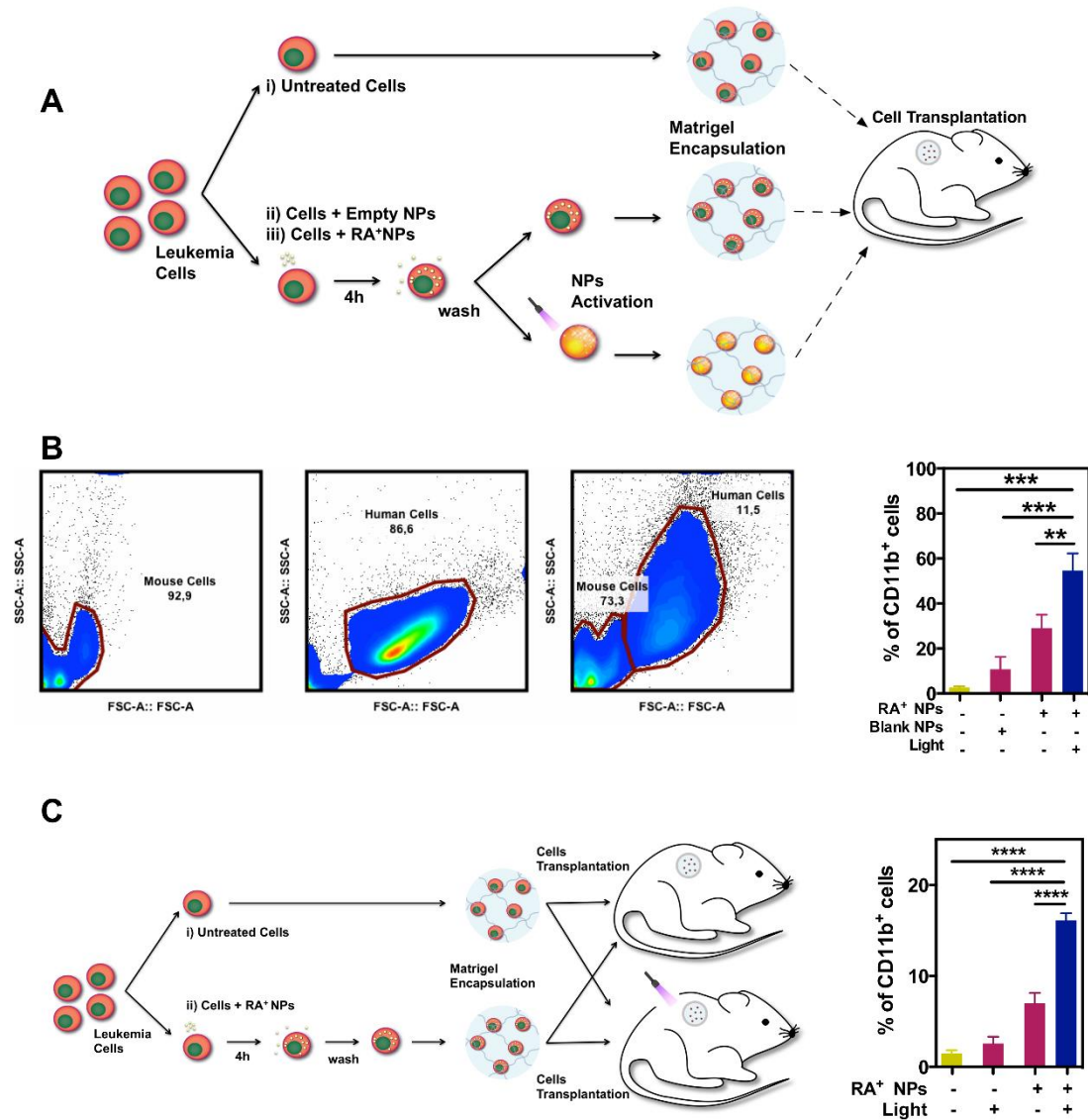


Figure 3.18 - In vivo differentiation of NB4 cells exposed to light-activatable RA+NPs. (A) Schematic representation of the in vivo experimental set up. Cells were treated with blank or RA+NPs (both at 10 $\mu\text{g/mL}$) for 4 h, washed and then activated or not with a blue optical fibre (405 nm, 80mW) for 5 min. Cells were then resuspended in a 1:1 (v/v) Matrigel solution and subcutaneously injected in a PDMS cylinder construct implanted in the dorsal region of mice. After 5 days, cells were removed from the construct and characterized by flow cytometry, for CD11b expression. (B) Representative flow cytometry plots for mice recipient cells (left), human leukaemia NB4 cells (middle) and a mixture of mice recipient cells with human leukaemia NB4 cells (right) and percentage of CD11b⁺ cells in human leukaemia NB4 cells collected 5 days after subcutaneous injection. (C) Schematic representation of the in vivo experimental set up. Cells were treated with RA+NPs (10 $\mu\text{g/mL}$) for 4 h, washed and then encapsulated in a 1:1 (v/v) Matrigel solution and subcutaneously injected in a PDMS cylinder construct implanted in the dorsal region of mice. After 24 h, some experimental groups were activated *in vivo* with a blue optical fibre for 5 min. Plot shows the percentage of CD11b⁺ cells in human leukaemia NB4 cells collected 3 days after the in vivo activation. In B, C, results are expressed as mean \pm s.e.m. (n=3–4). Statistical analyses were performed by one-way Anova followed by a Newman–Keuls post-test. **P<0.01, ***P<0.001, ****P<0.0001.

3.3.10. Bone marrow homing and engraftment of THP1 treated with RA+NPs

Leukaemia cells that resist therapy reside in microenvironmental niches in the bone marrow that are difficult to reach by conventional therapy². Therefore, we investigated whether leukaemia cells transfected with RA⁺NPs could engraft into the bone marrow and localize at nearby resident leukaemia cells. For this purpose, we transplanted leukaemia cells into immunodeficient CB17-Prkdcscid/J (NOD/SCID) mice treated with anti-CD122 to deplete innate immune cells (NS122). Green fluorescent protein (GFP)-labelled THP-1 cells, a human APL cell line (NB4 cells were unable to engraft), were injected into sub-lethally irradiated mice in the tail vein, followed by the injection of THP-1 cells transfected with RA⁺NPs after 24 h (**Figure 3.19A**). After 1-2 days, animals were sacrificed and the cells in the animal's calvaria (cranium) were characterized by *ex vivo* imaging (**Figure 3.19B**). Both cells (GFP-labelled and NP-labelled THP-1 cells) could engraft in the bone marrow of the animals and were detected after one or two days. Therefore, NP-labelled THP-1 cells (delivery cells) could enter the same niche as the GFP-labelled cells (target cells).

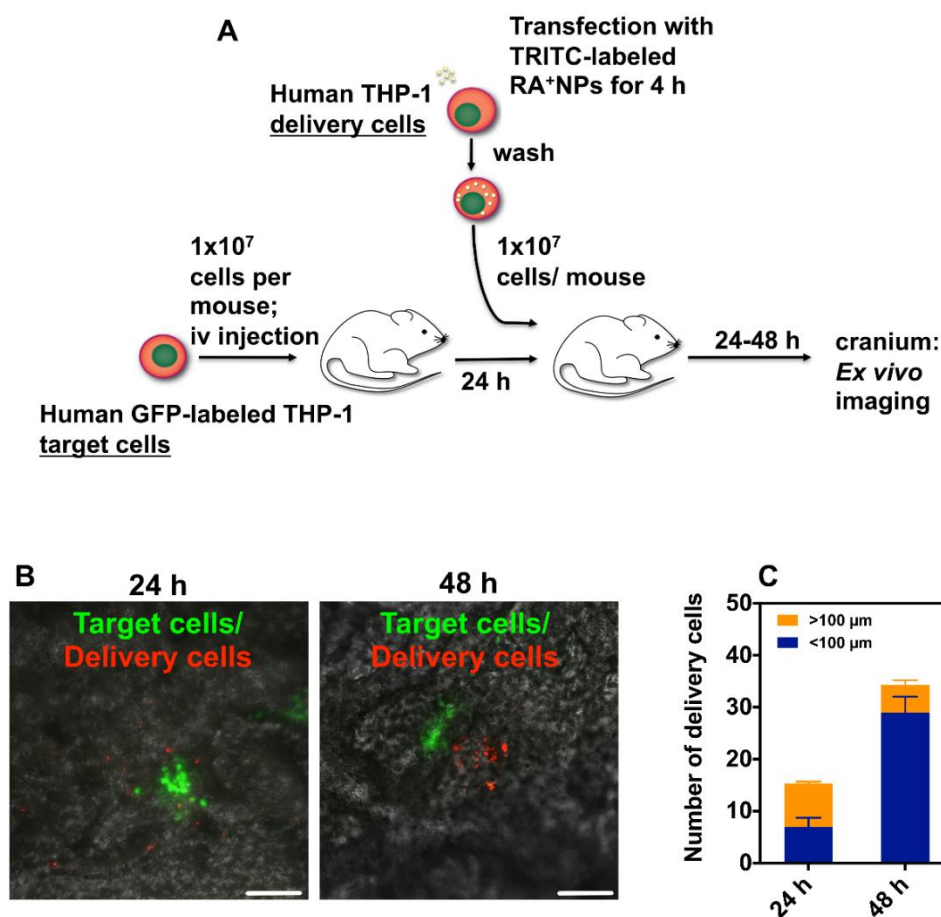


Figure 3.19 - Leukaemia cells transfected with RA+NPs can home at leukaemia niches. (A) Schematic representation of the protocol. Human GFP-labelled THP-1 cells were employed as the target cells and human THP-1 cells without GFP label were employed as delivery cells. On day 0, the target cells were injected into the NOD/SCID mice by intravenous injection through the tail vein. On day 1, the delivery cells loaded with RA⁺NPs were injected intravenously through the tail vein. After 24 (n=3) or 48 h (n=3) of the delivery cell injection, the mice were euthanized, the craniums collected and examined with a confocal microscope. (B) Both target and delivery cells were observed in mice craniums at 24 and 48 h. Bar scale means 100 μm. (C) Delivery cells close (<100 μm) or distant (>100 μm) to target cells were quantified. According to our results, the delivery cells can enter into the same niche as the target cells. Results are expressed as mean±s.e.m. (n=3).

3.3.11. Modulation of cell differentiation at the bone marrow niche

Next, we investigated whether we could differentiate the NP-labelled human THP-1 cells (delivery cells) at the bone marrow niche (more specifically at the calvaria), and whether they could modulate nearby cells (Figure 3.20A).

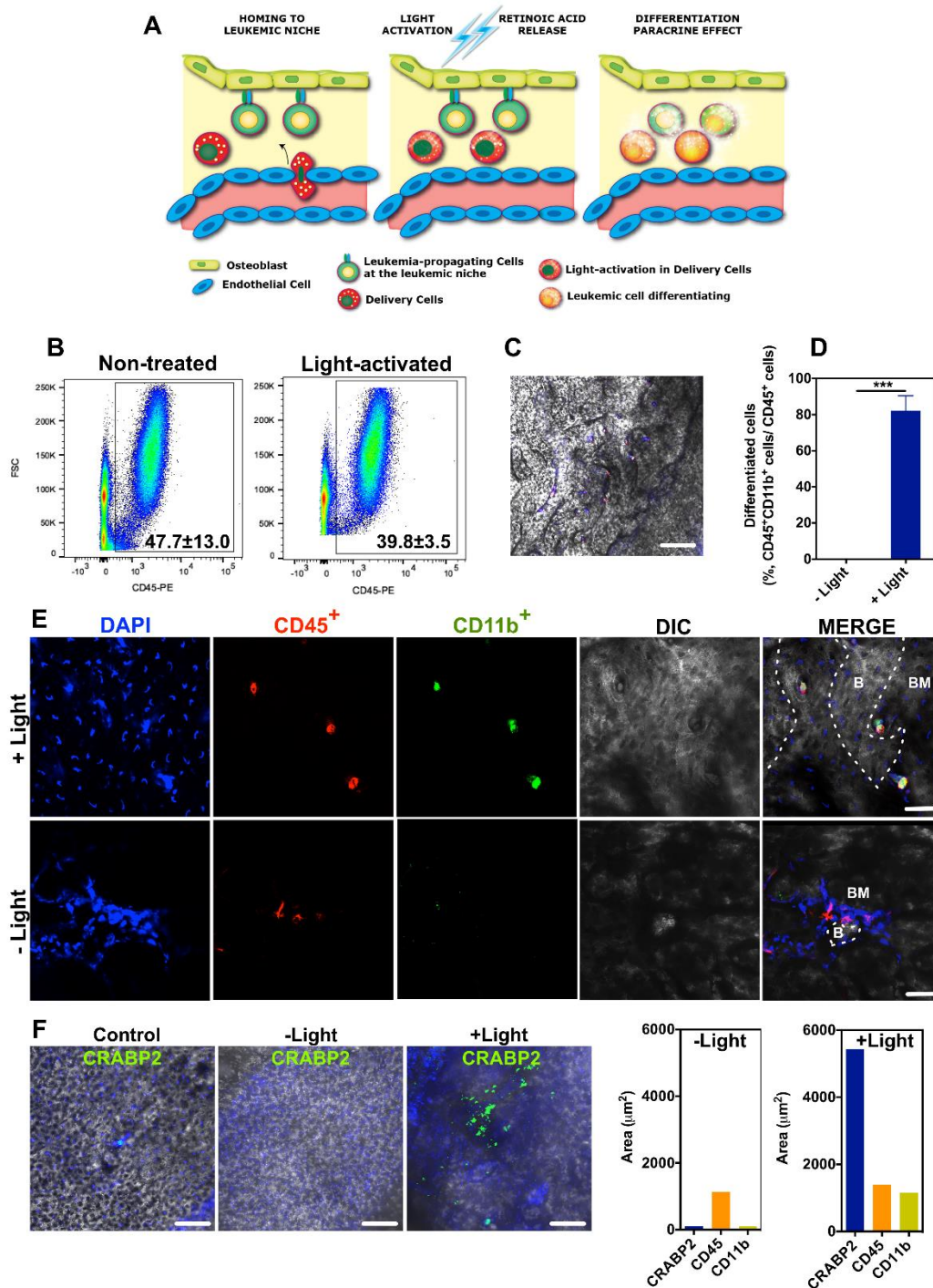


Figure 3.20 - In vivo activation of leukaemic THP-1 differentiation program by light at the bone marrow. (A) Schematic representation for the activation of human THP-1 cells transfected with RA⁺NPs in the bone marrow niche leading to the modulation of leukaemia cells. (B) Percentage of human CD45⁺ cells in the long bones as evaluated by flow cytometry. NOD/SCID mice were injected intravenously with THP-1 cells transfected with RA⁺NPs through the tail vein. After 6 days, animals (n=6) were either irradiated by a blue laser (5 min, 405 nm, 80mW) or not in the calvaria (n=6). Three days after irradiation, mice were killed and the long bones were collected. Cells in the long bones were characterized by flow cytometry for the expression of human CD45 epitope.

The engraftment of THP-1 cells was slightly higher in the non-treated than light-activated animals, but not statistically different. Percentages of positive cells were calculated based in the isotype controls and are shown in each scatter plot. Results are mean±s.e.m. (n=3). (C-E) Differentiation of human CD45⁺ cells into CD11b⁺ cells, as evaluated by immunofluorescence, in the calvaria of animals irradiated or not with a blue laser. B, bone; BM, bone marrow. In D, results are mean±s.e.m. (n=3). ***P<0.001. (F) Expression of CRABP2 in cells of calvaria of animals irradiated or not with a blue laser. Scale in, C, E, F means 200, 50 and 100 µm.

Blue laser attenuation studies in the calvaria bone using a photometer showed an attenuation of ≈ 75% (Figure 3.17B). Human THP-1 cells transfected with RA⁺NPs were injected intravenously into CB17-Prkdcscid/J (NOD/SCID) mice, and six days after injection, the cranium was exposed to a blue laser for 5 min. Seventy-two hours after blue laser irradiation, the engraftment of human CD45⁺ cells in the long bones of non-irradiated and blue laser-irradiated mice was 47.7 ± 13.0 and 39.8 ± 3.5%, respectively (Figure 3.20B). No statistical difference was found for the engraftment in both groups. *Ex vivo* staining of mice calvaria showed that human CD45⁺ cells in the non-irradiated mice did not express CD11b, while ~80% of the human CD45⁺ cells in blue-irradiated mice expressed CD11b (Figure 3.20C-E). In addition, cells surrounding CD45⁺CD11b⁺ cells in irradiated mice expressed CRABP, a RA protein transporter, while negligible levels of CRABP were found in non-irradiated mice (Figure 3.20F). Therefore, THP-1 cells differentiated by a blue laser had the capacity to modulate the cells in the vicinity. This is likely due to RA secreted (including exosomes containing RA) by the THP-1 cells, as observed *in vitro* using the NB4 cell line (Figure 3.21). Overall, our results show that leukaemia cells transfected with RA⁺NPs could (i) engraft into the bone marrow and localize near to resident leukaemia cells, (ii) differentiate after blue laser activation and (iii) modulate the activity/phenotype of the resident leukaemia cells. It is possible that the cells that reach the bone marrow are the ones that are less affected by the passive diffusion of RA (i.e., RA release without light activation) within the cells. Therefore, the cells that engraft are likely the ones that have less leaky RA⁺NPs and thus are undifferentiated leukaemic cells (CD11b^{negative} phenotype).

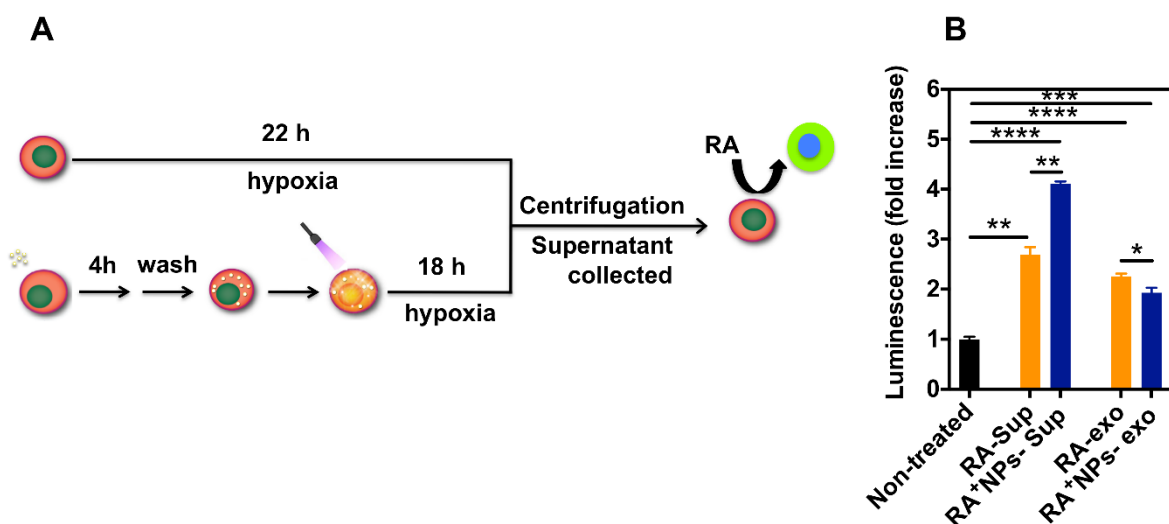


Figure 3.21 - Paracrine effect of cells treated with RA+NPs. (A) Schematic representation of the assay. NB4 cells (3,000,000/mL) were grown in RPMI supplemented with 10% (v/v) FBS, penicillin and streptomycin. Cells were treated with RA⁺NPs (10 µg/mL) for 4 h, washed with PBS to remove the NPs that were not internalized, activated by a blue laser for 5min, and then cultured for 18 h under hypoxia conditions (0.5% O₂) in exosome-depleted medium. A separate group of cells was treated with RA (3 µg/mL) for 22 h in hypoxia conditions (0.5%

O₂) in exosome-depleted medium. Then, in both groups, cells were centrifuged at 10.000g (4°C; 30 min) and part of the supernatant (named in the plot as "Sup") added to NB4 RARE cells (100,000/mL; 1 mL of the Sup). Alternatively, in both groups, cells were centrifuged in multiple steps (please see methods) to remove exosomes (named in the plot as "exo") and added to NB4 RARE cells (100,000/mL; 5 µg/mL de exosomes per mL of media) plated in a 24 well plate. After 24 h, the luciferase assay was performed according to instructions of the luciferase kit (britelite™). **(B)** Activation of NB4 RARE reporter cell line with the factors secreted by the NB4 cells for 22 h cultured with soluble RA or RA+NPs. Results are expressed as mean±s.e.m (n = 3). Statistical analyses were performed using a One-Way Anova followed by a Newman-Keuls post-test. * P<0.05, ** P<0.01, *** P<0.001 and ****P<0.0001.

3.4. Conclusions

In conclusion, we have developed a light-inducible polymeric NP for the spatio-temporal release of RA within leukaemia cells. We showed the efficiency of RA release both *in vitro* and *in vivo*. The efficiency is due to a combination of several factors, including (i) high concentration of intracellular RA, (ii) high endolysosomal escape (80% of the NPs escape the endolysosomal compartment in the first 5 h), (iii) prolonged intracellular accumulation of the NPs (more than six days in leukaemia cells) and (iv) rapid disassembly of the NPs once activated by UV or blue light (within minutes). We further showed that cells transfected with light-inducible NPs can be activated after six days while maintaining the same inductive properties. This gives an opportunity to use cells for activation at specific sites in the human body and differentiate cells in their proximity. Although the present study uses a RA delivery system as a proof of concept, a similar approach could be implemented for other drugs relevant to therapeutic or regenerative medicine.

The present research reports a blue laser/UV-inducible NP. The platform was designed for initial proof of concept regarding the modulation of leukaemic cell niches in the bone marrow. Recent studies have explored UV/blue laser approaches to trigger *in vivo* the presentation of bioligands with spatial temporal control to regulate cell adhesion, inflammation, and vascularization of biomaterials⁶³⁹ and to detect protease activity at sites of disease⁶⁴⁰. However, the *in vivo* applications of this light trigger are limited, as the optical properties of biological tissue cause attenuation and scattering of light rays, reducing their penetration depth. The recent advances in developing NPs activated by near-infrared light⁶⁴¹ may provide a better option for enhancing light penetration in tissues. For example, up-conversion nanocrystals that convert near infrared light into visible light (blue light) may be an interesting possibility for the photo-cleavage of linkers to which RA is chemically bound⁶⁴².

We have used leukaemic cells as a programmable delivery system that recognizes the leukaemic niches and modulate them after light activation. The aim of the study was to show the feasibility in remotely induce the differentiation of leukaemic cells in the bone marrow and not to demonstrate the exhaustion of cancer cells, as this will be difficult using the blue laser activation process. The concept here is different from previous studies that have used therapeutic NPs coated with aptamers to direct them to the bone marrow⁵⁵⁰. Although the results achieved are interesting, the side effects of the systemic administration of the NPs containing a powerful anti-leukaemic agent remain to be determined. In the present study we have used cancer biology to fight cancer. We have used leukaemia cells loaded with a clinical-approved AML differentiating agent able to home to leukaemic niches in the bone marrow. Although not explored in the current study, normal haematopoietic stem cells may also be used as a

CHAPTER 3 - Prolonged intracellular accumulation of light-inducible nanoparticles in leukaemia cells allows their remote activation

nanoparticle carrier as they are able to home to leukaemic niches¹⁸⁰, which we explore in the next chapter.

3.5. Materials and Methods

Preparation and characterization of PEI conjugated with DMNC. DMNC (48.5 mg, Sigma) was slowly added to a solution of PEI in DMSO (2 mL containing 50 mg/mL PEI, Sigma) containing triethylamine (24.5 L, Sigma), and the reaction flask cooled to 0 °C by immersion on ice. Then, the reaction was allowed to proceed for 24 h at 25 °C with stirring. At the end, the PEI-DMNC conjugate was purified by dialysis (Spectra/Por[®] 1 Regenerated Cellulose dialysis membrane, MWCO 6000-8000 Da, Spectrum) against DMSO overnight at room temperature. Reaction yields above 54 % were obtained. For NMR characterization, PEI-DMNC (in DMSO) was precipitated in water, washed, freeze-dried, and then dissolved (10 mg/mL) in DMSO-d₆ and ¹H NMR spectra were acquired using a Bruker Avance III 400 MHz spectrometer.

Preparation of NPs. Non-activatable NPs were prepared by the electrostatic interaction of PEI (polycation) with dextran sulfate (DS, polyanion) in water, at room temperature, as previously described by us⁶¹⁹. Briefly, an aqueous DS solution (1 mL, 10 mg/mL) was added drop-by-drop to an aqueous solution of PEI (5 mL, 10 mg/mL) and stirred for 5 min. Then, an aqueous solution of ZnSO₄ (0.6 mL; 1 M) was added and stirred for 30 min. The NP suspension was then dialyzed (Spectra/Por[®] 1 regenerated cellulose dialysis membrane, MWCO 6000-8000 Da, Spectrum) for 24 h, in the dark, against an aqueous solution of mannitol (5 %, w/v), lyophilized for 1 day and stored at 4 °C before use.

Light-activatable NPs were prepared by adding a PEI-DMNC solution (66.7 μL, 150 mg/mL, in DMSO) to an aqueous solution of DS (5 mL, 0.4 mg/mL) and stirred for 5 min. Then, an aqueous solution of ZnSO₄ (120 μL, 1 M) was added and stirred for 30 min. The NP suspension was then dialyzed (Spectra/Por[®] 1 Regenerated Cellulose dialysis membrane, MWCO 6000-8000 Da, Spectrum) for 24 h, in the dark, against an aqueous solution of mannitol (5 %, w/v), lyophilized for 1 day and stored at 4 °C before use. In some cases, PEI-DMNC was labelled with Qdot525. For that purpose, an aqueous solution of 1-ethyl-3-(3-dimethylaminopropyl)carbodiimide hydrochloride (EDC; 500 μL of EDC (10 mg/mL, aqueous solution at pH 6.0)) was added to a suspension of Qdots525 (0.16 mmoles, in 310 μL of PBS). After 5 min, PEI-DMNC solution (200 μL, 25 mg/mL in DMSO) was added to the previous solution and allowed to react for 1 h, in the absence of light, at room temperature.

For the preparation of RA-containing NPs (RA⁺NPs), a RA solution (24 μL, 50 mg/mL, in DMSO) was added to a solution of PEI-DMNC (66.7 μL, 150 mg/mL in DMSO) and maintained at room temperature for 30 min, under stirring. The solution was then carefully added to an aqueous solution of DS (5 mL, 0.4 mg/mL) and stirred for 5 min. The NPs in suspension were treated with an aqueous solution of ZnSO₄ (120 μL; 1 M) for 30 min. RA that was not encapsulated in the NPs was removed by centrifugation (12,000 g for 3 min). The NP suspension was then dialyzed (Spectra/Por[®] 1 Regenerated Cellulose dialysis membrane, MWCO 6000-8000 Da, Spectrum) for 24 h, in the dark, against an aqueous solution of mannitol (5%, w/v), lyophilized for 1 day and stored at 4 °C before use.

For the preparation of fluorescently labelled NPs, NPs (2 mg) were resuspended in 0.1 M carbonate/bicarbonate buffer (1 mL, pH 8.3) followed by the addition of FITC or TRITC (5 μ L in DMSO, 3-fold molar excess). The NP suspension was stirred for 1 h in the absence of light and then dialyzed (Spectra/Por[®] 1 regenerated cellulose dialysis membrane, MWCO 6000-8000 Da, Spectrum) for 24 h against an aqueous solution of mannitol (5 %, w/v), lyophilized, and stored at 4 °C before use.

Characterization of the NPs. The diameter of the NPs was measured by photon correlation spectroscopy (PCS) using quasi-elastic light scattering equipment (Zeta-Pals[™] Zeta Potential Analyzer, Brookhaven Instruments Corp., Holtsville, NY) and ZetaPlus[™] Particle Sizing Software (version 4.03). To measure NP diameter, the NP suspension (2 mL, 50 μ g/mL in water for molecular biology) was added to a cuvette and allowed to stabilize for 10 min. The sample was then vortexed for 5 s and subjected to NP size analysis in the ZetaPlus[™] for 3 min (3 times; all data were recorded at 90°). After each reading the cuvette was again vortexed for 5 s and exposed to UV light (365 nm) or blue light (405 nm) for a certain period of time (see above). The values of NP diameter and NP counts were recorded. The average diameters described in this work are number-weighted average diameters. The zeta potential of NPs was determined in a 1 mM KCl pH 6 solution, at 25 °C (2 mL, 50 μ g/mL). All data were recorded with at least 5 runs (in triplicate) with a relative residual value (measure of data fit quality) of 0.03. The diameter of NPs was also confirmed on a FEI-Tecnaï G2 Spirit Bio Twin at 100 kV. NP suspensions (in H₂O) were placed on a 200-mesh copper grid coated with a carbon support film (Taab Labs Ltd.) and dried overnight.

Release of RA from RA⁺NPs. [³H]RA solution in DMSO was used for the preparation of NPs, using a 1:20 ratio of labelled to unlabelled RA (1 nCi/ μ g RA). The initial RA cargo in the NPs was quantified using 2/3 of the original NP suspension (1 mg/ml). To quantify the controlled release of the RA, a suspension of [³H]RA-NPs (10 μ g/mL) was prepared and irradiated with UV light (365 nm) or blue light (405 nm). For each time point (0s, 30s, 60s, 180s, 300s, 600s) the NP suspension was centrifuged at 14.000g for 3 min, the supernatant collected and mixed with liquid scintillation fluid (1 mL; Packard Ultima Gold) and the scintillations counted in a TriCarb 2900 TR Scintillation analyser (Perkin Elmer).

Cell culture. HUVECs (Lonza) were cultured in EGM-2 medium (Lonza) in a CO₂ incubator at 37 °C, 5% CO₂ in a humidified atmosphere, with media changes performed every other day. Cells were passaged every 2-5 days and used for experiments between passage 4 and 6. Human bone marrow acute promyelocytic leukaemia NB4 cells, kindly provided by Dr. Arthur Zelent (Institute of Cancer Research, Royal Cancer Hospital), were cultured in RPMI-1640 (Gibco) supplemented with 10 % fetal bovine serum (Gibco) and 100 U/mL PenStrep (Lonza). Human myelomonoblastic cell lines U937-MT and U937-B412, kindly provided by Dr. Estelle Duprez (Centre de Recherche en Cancérologie de Marseille, France), were maintained at exponential growth in RPMI-1640 medium supplemented with 10% fetal bovine serum and 100 U/mL of PenStrep. For PLZF/RARA induction cells were stimulated with 0.1 mM ZnSO₄ for at least 24 h. Human acute monocytic leukaemia cell line THP-1 (DSMZ no. ACC16) was cultured in RPMI-1640 media supplemented with HEPES (10 mM), sodium pyruvate (1.0 mM) and 2-mercaptoethanol (0.05 mM).

NP cytotoxicity studies. NPs were suspended in a solution of milli-Q water with PenStrep (5 $\mu\text{L}/\text{mL}$ of 10000 U/mL stock solution, Lonza) and Fungizone (2.5 $\mu\text{g}/\text{mL}$, Sigma-Aldrich) for 30 min, centrifuged (14,000 g for 10 min), and finally resuspended in serum free cell culture medium. K562, NB4 and U937 cells (0.1×10^6 cells/condition) were incubated in serum free RPMI-1640 for 4 h in a 96-well plate containing variable amounts of PEI-DMNC:DS NPs. Once the incubations were terminated the cells were washed gently with medium to remove NP excess, and half of the samples were exposed to UV light (365 nm, 100 Watts) for 10 min. The cells were then cultured for 20 h in 100 μL of complete medium (RPMI-1640 medium supplemented with 10 % fetal bovine serum and 100 U/mL PenStrep). A CellTiter-Glo[®] luminescent cell viability assay (ATP, Promega, USA) was performed according to the recommendations of the vendor.

Assessment of histone γH2AX phosphorylation (DNA damage) induced by UV light or blue light irradiation. HUVEC cells (passage 4) were cultured on 1% gelatin-coated slides until subconfluency in EGM-2, followed by exposure to UV light (365 nm, 100 Watts) or blue light (405 nm, 80 mW) up to 60 min. Control conditions did not receive any light radiation. Following treatment, the medium was replaced by fresh medium and the cells were incubated for additional 6 h on normal culture conditions. The cells were then fixed with 4% paraformaldehyde (Electron Microscopy Sciences) for 10 min at room temperature and then washed with PBS. The cells were then permeabilized with 1 % (v/v) Triton-X, blocked with PBS + 2 % BSA and stained for 1 h with anti-human primary γH2AX antibody (clone: N1-431, BD Biosciences). Detection was done with secondary antibody anti-mouse Cy3 conjugate (Jackson ImmunoResearch). Cell nuclei were stained with 4',6-diamidino-2-phenylindole (DAPI) (Sigma), and the slides were mounted with mounting medium (Dako) and examined with a Zeiss inverted fluorescence microscope. Quantitative analysis of foci intensity were quantified using ImageJ software and normalized to the control condition. The calculations were performed in 5 different images for a total of ca. 250 cells (ca. 50 cells per image).

NP internalization studies. NP internalization was monitored by inductive coupled plasma mass spectrometry (ICP-MS). In this case, the intracellular levels of Zn were measured before and after cell exposure to NPs. NB4 and U937 cells (0.1×10^6 cells/well) were plated in 24 well plates and incubated in serum free RPMI-1640 from 1 to 24 h with variable amounts of PEI-DMNC:DS NPs. After incubations, NPs that were not internalized by the cells were washed (three times with PBS) and the cells were centrifuged; followed by the addition of an aqueous solution of nitric acid (1 mL, 69 % (v/v)). The samples were analysed by ICP-MS for the concentration of intracellular levels of Zn. The concentration of Zn was normalized per cell. The estimation of NPs was done based on controlled standard solutions.

Mechanism of NP uptake. U937 cells were cultured on 24 well plates (1×10^5 cells/well) and inhibited by one of the following chemicals during 30 min before adding a suspension of TRITC-labelled NPs (5 $\mu\text{g}/\text{mL}$): EIPA (50 μM), dynasor (80 μM), dansylcadaverine (100 μM), cytochalasin D (10 μM), nocodazole (50 μM), filipin III (100 μM) and polyinosinic acid (100 $\mu\text{g}/\text{mL}$). The inhibitor concentrations were based in values reported in literature and further validated by us to have no cytotoxic effect over the period of the assay (6 h), as confirmed by ATP assay. The incubation of the cells with

NPs for different times was performed in the presence of the inhibitor. As controls, we used cells without NPs and cells incubated with NPs without inhibitor. At the end of each time point, cells were centrifuged at 1300 rpm, 20 °C for 5 min with PBS, washed one time with cold trypan blue solution (200 µL; 600 µg/mL), re-washed 3 times with cold PBS and then resuspended in PBS containing 2.5 % FBS (500 µL) for flow cytometry analysis. A total of 10,000 events were obtained per measurement. To validate the inhibitory activity of dynasor we performed uptake studies of FITC-labelled transferrin, known to selectively enter cells via clathrin-mediated endocytosis. Briefly, U937 cells were cultured on 24 well plates (1×10^5 cells/well) and treated or not with dynasor (80 µM, 30 min pre-incubation), followed by addition of 1 µg/mL FITC-labelled transferrin (Life Technologies). The transferrin was allowed to bind for 3 min at 4 °C. Cells were then evaluated as before.

The NP uptake mechanism was also studied on U937 cells by silencing specific proteins of clathrin-mediated endocytosis (CLTC and LDLR), caveolin-mediated endocytosis (CAV1), GEEC-CCLIC pathways (CDC42) and macropinocytosis (RAC1 and CTBP1) by siRNA (Thermo Fisher). Transfection was performed in a 24 well plate with 0.5×10^5 cells in antibiotic-free complete medium with 100 nM siRNA and 1.5 µL of Lipofectamine RNAiMAX (Life Technologies) transfection reagent for 24 h. After this initial period, the transfection medium was replaced by complete medium and the cells incubated for another 48 h. Then, cells were cultured with TRITC-labelled NPs (5 µg/mL) for 6 h. Once the incubations were terminated, the cells were centrifuged at 1300 rpm, 20 °C for 5 min, with PBS, washed one time with cold trypan blue solution (200 µL; 600 µg/mL), re-washed 3 times with cold PBS and then resuspended in PBS containing 2.5 % FBS (500 µL) for flow cytometry analysis. Non-transfected cells or cells transfected with lipofectamine but without siRNAs (MOCK) were used as controls. In all flow cytometry analysis, a total of 10,000 events were recorded per run. All conditions were performed in triplicate.

Intracellular trafficking analyses of NPs. HUVEC cells (passage 4) were cultured on 1 % gelatin-coated slides until subconfluency in EGM-2. The cells were then incubated with FITC-labelled NPs (1 µg/mL) for 1 or 4 h, washed extensively, exposed or not to UV light (365 nm, 100 Watts) and cultured in normal conditions for up to 12 h. For LysoTracker staining, at time points 2, 6 and 12 h, the cells were incubated with LysoTracker Red DND-99 (50 nM, Invitrogen). After 30 min of incubation, the coverslips were washed extensively with PBS, followed by cell fixation with paraformaldehyde (4%, Electron Microscopy Sciences) for 10 min at room temperature and then washed with PBS. Cell nuclei were stained with 4',6-diamidino-2-phenylindole (DAPI) (Sigma), and the slides were mounted with mounting medium (Dako) and examined with a Zeiss LSM 50 confocal microscope.

Co-localization analysis was performed by culturing HUVEC cells (passage 4) on 1 % gelatin-coated slides until subconfluency in EGM-2. Cells were treated with 1 µg/mL FITC-labelled NPs for 1 or 4 hours, washed extensively and cultured in normal conditions for 1 or 1/8 additional hour/s, respectively. Then the cells were fixed with 4 % paraformaldehyde (Electron Microscopy Sciences) for 10 min at room temperature, blocked with 2 % (w/v) BSA, and when necessary, permeabilized with 0.5 % (v/v) Triton-X. Cells were then stained for 1 h with anti-human primary antibodies against EEA1 (clone: C45B10, Cell Signalling), rabankyrin-5 (Rab 5, ANKFY1 (D-15), Santa Cruz Biotechnology), or rabankyrin-7 (Rab 7, clone: D95F2, Cell Signalling). In each immunofluorescence experiment, an isotype-matched IgG control was used. Binding of primary antibodies to specific cells was detected with

CHAPTER 3 - Prolonged intracellular accumulation of light-inducible nanoparticles in leukaemia cells allows their remote activation

anti-rabbit or anti-goat IgG Cy3 conjugate (Jackson ImmunoResearch). Cell nuclei were stained with 4',6-diamidino-2-phenylindole (DAPI) (Sigma), and the slides were mounted with mounting medium (Dako) and examined with a Zeiss LSM 50 confocal microscope. Co-localization analysis was done in ImageJ through assessment of the percentage of overlapping objects. Two objects are considered to be co-localizing when their intensity profile is overlapping more than 40 %. For this analysis the number (percentage of FITC-labeled NPs foci that are positive for EEA-1/Rab-5/Rab-7) and the intensity volume (percentage of FITC-labeled NPs in the EEA-1/Rab-5/Rab-7-positive compartments) were used. This approach was found to be more adequate than classical co-localization tools in ImageJ or other softwares that measure pixel co-occurrence and correlation analyses, because it allowed us to (i) discriminate between background and vesicle/NP-foci fluorescence and (ii) interpret the results in terms of percentage of NP-foci that are localized to vesicles in another channel of interest.

NP dilution during cell proliferation. NP dilution with cell growth was monitored over 6 days by inductive coupled plasma mass spectrometry (ICP-MS) by the quantification of intracellular levels of Zn. NB4 and THP-1 cells (0.5×10^6 cells/mL) were plated in 6 well plates and incubated in serum free RPMI-1640 with 20 μ g/mL of RA⁺NPs. After 4 h incubation, NPs that were not internalized by the cells were washed three times with PBS and the cells were left to grow at 0.2×10^6 cells/mL in complete medium for additional 4 h, 3 days and 6 days, maintaining always an exponential growth. After each incubation, cells were counted, collected by centrifugation and resuspended in nitric acid (1 mL, 69 % (v/v) for ICP analysis. The concentration of Zn was normalized per cell. The estimation of NPs was done based on Zn quantification in 20 μ g of NPs. In some experiments, cells were transfected with RA⁺NPs labelled with TRITC, and their fluorescence monitored by flow cytometry overtime, to evaluate NPs distribution within the cells.

Exocytosis analyses of NPs. To determine exocytose of NPs, NP uptake assays were performed in the presence of P-gp antagonist verapamil or the endosome disruption agent chloroquine. U937 cells were cultured on 24 well plates (1×10^5 cells/well) and chloroquine (100 μ M, no pre-incubation) and verapamil (100 μ M, 60 min pre-incubation) conditions were tested. The chemical agents concentrations were based on values reported in the literature and further validated by us to have no cytotoxic effect over the period of the assay (12 h). After the pre-incubation with the chemical agents, TRITC-labelled PEI-DMNC:DS NPs (10 μ g/mL) or TRITC-labelled poly-L-lysine USPIO NPs (100 μ g/mL) were added to the cells, maintaining the chemical agents concentration. As controls we used cells incubated without NPs and cells incubated with NPs without chemical agents. At the end of each experiment, the cells were centrifuged at 1300 rpm, 20 °C for 5 min with PBS, washed one time with cold trypan blue solution (200 μ L; 600 μ g/mL), re-washed 3 times with cold PBS and then resuspended in PBS containing 2.5 % FBS (500 μ L) for flow cytometry analysis. A total of 10,000 events were recorded per measurement, and all conditions were performed in triplicate.

[³H]RA internalization studies. [11, 12-³H(N)]-Retinoic acid, 50.4 Ci/mmol, was purchased from Perkin Elmer. [³H]RA solution for cell culture assays was prepared on the day of experiments by dissolving [³H]RA in DMSO with unlabelled RA in a 1:1000 ratio to a final concentration of 10 μ M of RA. [³H]RA solution in DMSO for the preparation of NPs was prepared on the day of experiments using

a 1:4000 ratio of labelled to unlabelled RA. Experiments were initiated by the adding the [³H]RA solution (1 μM and 10 μM; representing less than 1% in volume of the total cell culture medium) or [³H]RA-NP suspension (1 μg/mL and 10 μg/mL) to cultures (60,000 cells/condition, 24-well plate, 1 mL) of NB4 or U937 cells. In case of soluble RA, cells (NB4 or U937; 60,000 cells/condition, 24-well plate) were cultured with medium containing [³H]RA (1 μM and 10 μM; 1 mL of medium) for 24 or 72 h, washed with PBS (2 times), harvested, lysed with lysis buffer (100 μL) and kept on ice until scintillation counting procedure. In case of RA-containing NPs, cells (same conditions as for soluble RA) were cultured with [³H]RA-NPs (1 μg/mL and 10 μg/mL) for 4 h, washed with PBS and cultured for additional 20 or 68 h in the respective culture medium. Cells were then collected to eppendorfs, washed with PBS, centrifuged (1500 rpm, 5 min), lysed with lysis buffer (see above) and kept on ice until scintillation counting procedure. The lysed samples (100 μL) were mixed with liquid scintillation fluid (1 mL; Packard Ultima Gold) and the scintillations counted in a TriCarb 2900 TR Scintillation analyser (Perkin Elmer).

Time-activation of NPs within cells. NB4 and Zn-induced U937-B412 cells (6.0×10^4 cells/condition) were plated in 24-well plates and transfected with RA⁺ NPs (1 μg/mL) for different time periods (1, 2, 4, 6, 8, 12 and 24 h). The cells were then washed by centrifugation (1300 rpm, 5 min) to remove non-internalized NPs, and immediately exposed to UV light (365 nm, 100 Watts, 5 min). In a second experimental setup, NB4 and Zn-induced U937-B412 cells (6.0×10^4 cells/condition) were plated in 24-well plates and transfected with RA⁺ NPs (1 μg/mL) for 4 h. The cells were then washed by centrifugation (1300 rpm, 5 min) to remove non-internalized NPs, cultured in normal conditions and exposed to UV light (365 nm, 100 Watts, 5 min) at different time points (0, 4, 8, 20 and 44 h). The effect of the intracellular release of RA was evaluated in terms of differentiation of the cells into the myeloid lineage (as assessed by the expression of CD11b) at day 3, as assessed by flow cytometry. All conditions were performed in triplicate.

NB4-RARE cells (2.5×10^4 cells/condition) were plated in v-shaped 96-well plates and transfected with RA⁺ NPs (1 μg/mL) for different time points (1, 2, 4, 6, 8, 12 and 24 h). The cells were then washed by centrifugation (1300 rpm, 5 min) to remove non-internalized NPs, and immediately exposed to UV light (365 nm, 100 Watts, 5 min). For the second experimental setup, NB4-RARE cells (2.5×10^4 cells/condition) were plated in v-shaped 96-well plates and transfected with RA⁺ NPs (1 μg/mL) for 4 h. The cells were then washed by centrifugation (1300 rpm, 5 min) to remove non-internalized NPs, cultured in normal conditions and exposed to UV light (365 nm, 100 Watts, 5 min) at different time points (0, 4, 8, 20 and 44 h). The cells were then cultured for 12 hours after each condition light activation in RPMI-1640 medium supplemented with 10 % fetal bovine serum and 100 U/mL PenStrep. After these procedures luciferase luminescence was quantified as described above for the luciferase assays. All conditions were performed in triplicate.

Multiple activation of NPs within cells. Myelocytic differentiation of Zn-induced U937 cells was assessed by the quantification of CD11b expression by flow cytometry. U937-B412 cells (6.0×10^4 cells/condition) were cultured with ZnSO₄ (0.1 mM) in culture medium up to 24 h prior to experiment to induce the expression of promyelocytic leukaemia zinc finger/RARα (PLZF/RARα). Then cells were

CHAPTER 3 - Prolonged intracellular accumulation of light-inducible nanoparticles in leukaemia cells allows their remote activation

transfected with RA⁺ NPs (1 µg/mL) for 4 h, washed, placed in normal culture medium and then differentially activated by UV light (365 nm, 100 Watts, 5 min). Cells without light activation were used as control. The following conditions were tested: i) single light activation at 4 h; ii) light activations at 4 h and 6 h; iii) light activations at 4 h, 6 h and 8 h and iv) light activations at 4 h, 6 h, 8 h and 10 h. After 3 days, expression of CD11b on U937 cell surface was measured by staining with a fluorescent (PE)-conjugated anti-CD11b mAb (BD Biosciences) using flow cytometry. All conditions were performed in triplicate.

NB4 differentiation assay. Myelocytic differentiation of NB4 cells was assessed by quantifying CD11b⁺, CD11b⁺CD45⁺CD13^{high} or CD11b⁺CD45⁺CD13^{low} populations using flow cytometry. NB4 cells (between 6.0×10^4 and 10×10^4 cells/condition) were plated in 24-well plates and cultured with soluble RA (3 µg/mL) or light-activatable RA⁺ NPs (10 µg/mL) for 3 days. The NPs were suspended in serum free medium and added to cells for 4 h. The cells were then washed by centrifugation (1300 rpm, 5 min) to remove non-internalized NPs, and half of the samples were exposed to UV light (365 nm, 100 Watts, 5 min). The cells were then cultured up to 3 days in RPMI-1640 medium supplemented with 10 % fetal bovine serum and 100 U/mL PenStrep with half medium changes every 3 days.

NB4 RARE cell line generation. The signal lenti RARE reporter kit (CLS-016L SABiosciences) was used for the establishment of a RA reporter NB4 cell line. For that purpose, retronectin solution (15 µg/cm², 30 µg, 500 µL on PBS, Takara) was plated in a 24-well plate 2 hours prior to cell seeding. The plate was kept at room temperature and was washed one time, immediately before seeding, with PBS. NB4 cells (1×10^5) were plated in 175 µL of RPMI-1640 medium (Gibco) supplemented with 0.5 % FBS and 100 U/mL PenStrep and to this condition 125 µL of signal lentiviral particles were added to a total experimental volume of 300 µL. After a gentle swirl of the plate the cells were incubated 20 hours at 37 °C in a humidified incubator with 5 % CO₂ atmosphere. In the following day, cells were washed and allowed to recover in the incubator for 24 hours cultured in 500 µL of fresh RPMI-1640 medium supplemented with 10 % FBS and 100 U/mL PenStrep. After that, 2 µg/mL of puromycin (Invitrogen) was added to the culture medium for selection of transduced cells. Evaluation of selection efficiency in puromycin-containing medium was performed every 3 days for a period of 5 weeks.

NB4 RARE luciferase assay. To assess the biological effect of RA in RAR-regulated signalling pathway activity, luciferase reporter assay was performed. NB4-RARE cells (2.5×10^4 cells/condition) were plated in v-shaped 96-well plates and cultured with soluble RA (10 µM) or light-activatable RA⁺ NPs (5 µg/mL). The NPs were suspended in serum free medium and added to cells for 1 h. The cells were then washed by centrifugation (1300 rpm, 5 min) to remove non-internalized NPs, and half of the samples were exposed to blue light (405 nm, 80 mW, 5 min). The cells were then cultured for 12/24 hours in RPMI-1640 medium supplemented with 10 % fetal bovine serum and 100 U/mL PenStrep. After these incubation times, the conditions were centrifuged (1500 rpm, 3 min), excess medium carefully aspirated and the cells washed with 100 µL of PBS. After a new centrifugation and removal of PBS, 60 µL of cell lysis buffer (8 mM of magnesium chloride; 1 mM DL-Dithiothreitol; 1 mM Ethylenediaminetetraacetic acid; 25 mM of 1 M Trizma Base with 1 M Sodium phosphate monobasic; 15 % Glycerol; and 1 % Triton X-100), was added to each condition. The plate was kept on ice, under

agitation for 15 min to allow complete lysis and then the plate was placed on -80°C for the amount of time necessary for the samples to freeze. After these steps, the plate was removed from the -80°C , put on ice and allowed to defrost at slow rate.

For the preparation of the luminescence reading, 40 μL of ATP (100 μM , Sigma) was added to 1960 μL of reading buffer solution (8 mM of magnesium chloride; 1 mM DL-Dithiothreitol; 1 mM Ethylenediaminetetraacetic acid; 25 mM of 1 M Trizma Base with 1 M Sodium phosphate monobasic; and 15 % Glycerol) to a final concentration of 2 μM ATP. On a second tube, 2 mL of D-Luciferin working solution (167 μM , Sigma) was prepared protected from light. The injection system of the luminometer was primed until ready. Following that step, the luminometer software was programmed to set the temperature to 37°C , and under stirring for the duration of the experiment accept 50 μL of sample per condition in a 96-white plate, inject 100 μL of ATP working solution 3 seconds after reading cycle begins; inject 100 μL of D-Luciferin working solution 4 seconds after reading cycle begins and read the luminescence 5 seconds after reading cycle begins. The luciferase luminescence was quantified in a microplate luminometer reader LumiStar Galaxy (BMG Labtech). All conditions were performed in triplicate.

NB4 RARE differentiation by cell conditioned medium obtained from NB4 cells exposed to RA or RA⁺NPs. NB4 cells ($3 \times 10^6/\text{mL}$) were grown in RPMI supplemented with 10% (v/v) FBS, penicillin and streptomycin. Cells were treated with RA⁺NPs (10 $\mu\text{g}/\text{mL}$) for 4 h, washed with PBS to remove the NPs that were not internalized, activated by a blue laser for 5 min, and then cultured for 18 h under hypoxia conditions (0.5% O_2) in exosome-depleted medium. A separate group of cells was treated with RA (3 $\mu\text{g}/\text{mL}$) for 22 h in hypoxia conditions (0.5% O_2) in exosome-depleted medium. Then, in both groups, cells were centrifuged at 10,000 g (4°C ; 30 min) and part of the supernatant (named in the plot as "Sup") added to NB4 RARE cells (100,000/mL; 1 mL of the Sup). Alternatively, in both groups, cells were centrifuged in multiple steps⁶⁴³ to remove exosomes (named in the plot as "exo") and added to NB4 RARE cells (100,000/mL; 5 $\mu\text{g}/\text{mL}$ de exosomes per mL of media) plated in a 24 well plate. After 24 h, the luciferase assay was performed according to instructions of the luciferase kit (briteliteTM).

U937 differentiation assay. Myelocytic differentiation of U937 cells was assessed by the quantification of CD11b expression by flow cytometry. U937-B412 cells (6.0×10^4 cells/condition) were cultured either with or without ZnSO_4 (0.1 mM). To induce the expression of promyelocytic leukaemia zinc finger/RAR α (PLZF/RAR α) in U937-B412 cells they were treated for 24 h with ZnSO_4 (0.1 mM). Then cells were treated with soluble RA or light-activatable RA⁺ NPs (transfection for 4 h followed by light activation for 5 min) for 3 days. After 1 and 3 days, expression of CD11b on U937 cell surface was measured by staining with a fluorescent (PE)-conjugated anti-CD11b mAb (BD Biosciences) using flow cytometry. All conditions were performed in triplicate.

AML differentiation assay. AML bone marrow mononuclear cells isolated by Ficoll-Histopaque (GE Healthcare) gradient centrifugation, enriched using the MACS CD34 isolation kit (Miltenyi Biotec) and cryopreserved were kindly provided by Dr. Rajeev Gupta (Department of Haematology, UCL Cancer Institute). The AML cells were isolated from an 85 years old man patient with AML

34+117+33+13+DR+ 35% blasts and a 70 years old woman with RAEB2/evolving AML 34+117+33+12% blasts. Both samples had formal karyotyping/extended FISH panels. Briefly, neither patients were PML-RARA: one was standard risk (normal karyotype with a small trisomy 8 subclone), and the other was high risk with complex karyotype. The isolated CD34⁺ AML cells were maintained in StemSpan SFEM medium (Stemcell Technologies) supplemented with a human cytokine cocktail containing SCF (50 ng/mL, Stemcell Technologies), TPO (15 ng/mL) and Flt-3L (50 ng/mL, PeproTech) plus PenStrep (10,000 U/mL, Lonza) and Fungizone (25 mg/mL, Sigma) up to 3 days. Prior to the colony-forming cell (CFC) and long-term culture-initiating cell (LTC-IC) assays, AML cells were incubated for 4 h in Ex-Vivo (Lonza) serum free medium, with and without blank NPs or RA⁺ NPs in a 24 well plate. After that time, the cells were washed to remove loosely bound NPs. For CFC assays (2.0 × 10⁵ cells/condition) AML cells were plated in triplicate in MethoCult H4230 medium (3 mL, StemCell Technologies) supplemented with SCF [50 ng/mL], IL-3 [10 ng/mL], and Flt-3L [50 ng/mL], all human, plus PenStrep (10,000 U/mL, Lonza) and Fungizone (25 mg/mL, Sigma) in 6-well plate. In some conditions, RA⁺ NPs accumulated within the cells were activated by a UV light (365 nm, 100 W, 5 min). Cultures were scored after 14 days for the presence of clusters and colonies containing >20 cells using an inverted microscope. LTC-IC assays were performed in triplicate in a 6-well plate gelatinized for 2 h prior to adding the feeders. The feeder layer was composed of a 1:1 mixture of irradiated (80 Gy) SL/SL (1.5 × 10⁴ cells/condition) and M210B4 mouse fibroblasts (1.5 × 10⁴ cells/condition), kindly provided by Dr. Rajeev Gupta (Department of Haematology, UCL Cancer Institute). AML cells (1 × 10⁶ cells/condition) were plated in Myelocult H5100 medium (StemCell Technologies), supplemented with Flt-3L [50 ng/mL], hydrocortisone [10⁻⁶ M] (StemCell Technologies) and PenStrep (10,000 U/mL, Lonza) and fungizone (25 mg/mL, Sigma). For some conditions UV light (365 nm, 100 Watts, 5 min) was used to trigger RA release. After the cells were inoculated, weekly half medium changes were performed (with Flt-3L [100 ng/mL]) for the duration of the culture. After 5 weeks, all cells were harvested and placed into methylcellulose based assay for the detection of AML-CFC as described above.

High-throughput gene expression assay. Gene expression was evaluated by real time PCR in NB4 cells and U937-B412 cells previously stimulated with ZnSO₄ (0.1 M), using a 96.96 microfluidic chip (Fluidigm Corporation). Cells were exposed to either soluble RA (1 and 10 μM) or light-activatable RA⁺NPs (0.1, 1 and 10 μg/mL) for 8 h, 24 h or 48 h. From each sample (*n*=3) a maximum of 0.45 × 10⁶ cells were collected for RNA extraction using RNeasy Micro Kit. Afterwards, samples were processed using Fluidigm standard protocols. Briefly, cDNA was obtained from 50 ng of RNA using Reverse Transcription Master Mix (Fluidigm Corporation). Then samples were pre-amplified for 12 cycles, to increase the number of copies of target DNA, with Fluidigm PreAmp Master Mix (Fluidigm Corporation) and a pool of all the primers tested in the chip. Prior to qPCR reactions the pre-amplification reaction was treated with Exonuclease I to eliminate the carryover of unincorporated primers. Finally, samples and genes pre-mix are prepared separately accordingly to manufactures instructions using SsoFast EvaGreen Supermix with Low ROX (Bio-Rad Laboratories) and loaded into the chip. A pneumatically operated desktop instrument (IFC Controller HX) was used to mix samples and genes pre-mix in the qPCR chamber reaction of the chip. After this procedure, the chip was analysed using Biomark HD (Fluidigm Corporation) for the thermal cycling and real time fluorescent readings. A melting curve was performed after 30 cycles, for quality control. DeltaCt was calculated using Real

Time PCR Analysis Software 4.1.3 (Fluidigm Corporation) and data was further analysed with Cluster 3.0 and Java Trew View to produced gene expression heatmaps and hierarchical clustering.

Generation of a THP-1- GFP cell line. Viral particles for GFP-expression were produced in 293T cells using a standard protocol. Briefly, 293T cells were transfected with GFP DNA construct (30 µg) and pCL-Eco (DNA:pCL-Eco; 15 µg) both solubilised in a DNA-CaCl₂ mixture (1 mL). Transfection efficiency was evaluated by fluorescence microscopy. After 72 hours viral particles were collected and THP-1 cells were infected (2 x 10⁵ cells/ml in a 6-well plate with 4µg/ml polybrene).

Quantitative reverse transcription-polymerase chain reaction (qRT-PCR) analysis. Total RNA was extracted and purified using RNeasy Micro Kit (Qiagen) and immediately stored at -80°C. Total RNA was quantified in a NanoDrop ND-1000 Spectrophotometer (NanoDrop Technologies, Inc., USA) by spectrophotometry at 260 nm. The cDNA was reverse transcribed from 0,5 µg of total RNA, using TaqMan Reverse Transcription Reagents kit (Invitrogen) according to the manufacturer's instructions. The cDNA obtained was stored at -20°C until further analysis by qRT-PCR using SYBR Green technology and qRT-PCR analyses were performed using the ABI PRISM 7500 Fast System (Applied Biosystems). Quantification of target genes was performed relative to GAPDH gene according to the equation: $2^{[-(Ct_{\text{sample}} - Ct_{\text{GAPDH}})]}$. The mean minimal cycle threshold values (Ct) were calculated from quadruplicate reactions. The list of the primers can be found in

***In vivo* study: subcutaneous implantation.** The animal work has been conducted according to relevant national and international guidelines and approved by the Bioethics Committee of University of Salamanca. On the day before injecting the cells, PDMS cylindrical constructs (∅_{internal} = 1.0 cm; ∅_{external} = 1.5 cm) were implanted subcutaneously on NOD/SCID mice (Jackson Laboratory) maintained in pathogen-free conditions with irradiated chow. For the *ex-vivo* activation studies in the day of the experiment, NB4 cells were suspended in serum free medium with (i) no NPs, (ii) with empty NPs (10 µg/mL) or RA⁺ NPs (10 µg/mL) for 4 h. At the end, cells were washed by centrifugation (1300 rpm, 5 min), and the ones treated with RA⁺ NPs were either activated or not with a blue laser (405 nm, 80 mW) for 5 min. NB4 cells (5 × 10⁶ cells per PDMS construct) were injected subcutaneously in the center of the PDMS construct embedded in Matrigel (200 µL, BD Biosciences). Five days after injection of the cells, animals were sacrificed by cervical dislocation and cells within the cylindrical construct were collected and characterized by flow cytometry. For the *in vivo* activation studies in the day of the experiment, NB4 cells were suspended in serum free medium with (i) no NPs, (ii) with RA⁺ NPs (10 µg/mL) for 4 h. At the end, cells were washed by centrifugation (1300 rpm, 5 min), and 5 × 10⁶ NB4 cells per PDMS construct were injected subcutaneously in the center of the PDMS construct embedded in Matrigel (200 µL). One day after injection, experimental groups were either activated or not with a blue optical fibre (405 nm, 80 mW) for 5 min. Three days after injection of the cells, animals were sacrificed by cervical dislocation and cells within the cylindrical construct were collected and characterized by flow cytometry.

***In vivo* study: bone marrow modulation.** NOD.CB17-Prkdcscid /J (NOD/SCID) female mice ($n=12$) aged 6-8 weeks were employed in this experiment. Before cell injection, mice received 1.5 Gy of total body irradiation from a ^{137}Cs source and were also treated with 200 μg of mouse anti-CD122 monoclonal antibody (NS122) by intraperitoneal injection. Human THP-1 cells were incubated with 20 $\mu\text{g}/\text{mL}$ of RA^+NPs in RPMI medium for 4 hours, followed by extensive wash with PBS to remove non-internalised NPs. The cells were then resuspended in RPMI medium with 10% FBS and left in the culture incubator overnight. On the following day, the cells loaded with RA^+NPs were collected and 1×10^7 cells /mouse in 200 μL PBS were injected into the NOD/SCID mice intravenously, through the tail vein. After 6 days, the mice were randomly divided into two groups: one of the groups was blue laser irradiated ($n=6$) and the other group was not irradiated ($n=6$). In the blue laser irradiated group, each mouse was anesthetized with 3.5% chloral hydrate in PBS and the craniums were exposed to a blue laser (405 nm, 80 mWatts) for 5 min. The mice in the non-irradiated group received the same treatment without blue laser activation. After 48 or 72 h, the mice were sacrificed, and the long bones/ craniums were collected. The long bones including the femurs, tibias and pelvis were crushed in PBS containing 1% bovine serum albumin (BSA, sigma) and 2 mM EDTA (Invitrogen). The samples were then filtered with 70 μm cell strainer and treated with ACK solution to lyse red blood cells. The resulting cells were stained using PE conjugated anti-human CD45 antibody (eBioscience). The results were measured by flow cytometry and the data were analysed with FlowJo software.

The mouse craniums were collected for the *ex vivo* staining examination followed by the traditional protocol. Briefly, the mouse craniums were cut into four pieces along the sutures producing one frontal, two parietals and one occipital bone. Only parietal bones were used in this experiment. Bone pieces were fixed in 4% paraformaldehyde for 30 min, washed twice with PBS, blocked with 2% BSA-0.01% Triton X-100 in PBS (BSA buffer) for 1 hr, and incubated with primary antibodies (diluted 1:100 in BSA buffer) overnight at 4°C. After washing with BSA buffer for 2 hr, bones were incubated with secondary antibodies (diluted 1:200 in BSA buffer) for 2 hr, washed with BSA buffer for 2 hr, and nuclei were stained using DAPI. The primary antibodies included mouse anti-human CD45 antibody (BD) and rabbit anti- human CD11b antibody (Abcam). The secondary antibodies included goat anti-mouse 555 (Invitrogen) and goat anti-rabbit 488 antibodies. The bone pieces were finally examined with a confocal microscope (Nikon Eclipse Ti) under FITC/TRITC/DIC signal channel. Images were analysed in ImageJ. Analyse Particles was used after thresholding to quantify positive signals and measure the total area occupied by these particles.

***In vivo* study: CRABP2 expression on mouse cranium.** NOD.CB17-Prkdcscid /J (NOD/SCID) female mice aged 6-8 weeks were employed in this experiment. The mouse craniums were collected from the last experiment. In this experiment, we also collected the mouse craniums without any treatment as the control. The *ex vivo* staining examination was followed by the traditional protocol. Briefly, the mouse craniums were cut into four pieces along the sutures producing one frontal, two parietals and one occipital bone. Only parietal bones were used in this experiment. Bone pieces were fixed in 4% paraformaldehyde for 30 min, washed twice with PBS, blocked with 2% BSA-0.01% Triton X-100 in PBS (BSA buffer) for 1 h, and incubated with primary antibodies (anti-CRABP2 antibody, ab74265, diluted 1:100 in BSA buffer) overnight at 4°C. After washing with BSA buffer, bones were incubated with secondary antibodies (goat anti-rabbit 488 antibodies, diluted 1:200 in BSA buffer) for

2 h and then washed with BSA buffer. Nuclei were stained using DAPI. The bone pieces were finally examined with a confocal microscope (Nikon Eclipse Ti) under DAPI/FITC/DIC signal channel. Images were analysed in ImageJ. Analyse Particles was used after thresholding to quantify positive signals and measure the total area occupied by these particles. Comparison between CD11b, CD45 and CRABP2 positive areas was used as a proxy of the release of RA by NPs and paracrine effect in the parietal bones of irradiated and non-irradiated mice.

Statistical analysis. Statistical analyses were performed with GraphPad Prism software. For multiple comparisons, a two-way ANOVA followed by a Holm-Sidak post-test was performed. Results were considered significant when $P < 0.05$. Data are shown as mean \pm s.e.m. unless other specification.

**CHAPTER 4 - Prospective studies on
nanoformulations that are able to modulate
healthy and leukemic niches**

4.1. Abstract

Great advances have been made in this century in the development of drug delivery systems for AML therapy, which improves the application of previously used drugs in clinical practice and also opens new venues for new biomolecules to be used in therapy. The use of stem cells as carriers in cell-mediated drug delivery strategies is an attractive emerging approach to overcome the current limitations of conventional medicines. Stem cells can act not only as “shields” for therapeutic agents, but also as specific targeting agents by themselves due to their natural tropism for specific tissues, organs and sites of injury^{594,455}, with the added advantage of being able to cross biological barriers, such as anatomical (e.g. blood brain barrier)⁵⁶³ or physiological barriers (e.g. tumour site heterogeneity). In this chapter we further investigate the functional effect of cell-mediated targeted delivery of photo-triggerable NPs to the BM niche on MLL-AF9 AML mouse model. We also explored different options regarding cell type used as carriers and type of molecule delivered by photo-triggerable NPs.

Our results indicate that RA can activate different differentiation pathways depending on whether it is delivered extra-cellularly, or intracellularly by activation of RA⁺NPs. RA⁺NPs can induce AML differentiation towards monocytic/macrophage lineage not only *in vitro* but also *in vivo*. Also, we have shown *in vitro* evidence that soluble RA and more significantly, activation of RA⁺NPs, stimulate antitumoral M1 macrophage activation. This macrophage induced differentiation *in vivo* seems to have “systemic” anti-leukemic effect within the BM leukemic niche, as we observed a significant reduction of leukemic cells in the BM of animals treated with RA⁺NPs when compared with animals treated with empty NPs (RA⁻NPs).

We also explored the potential use of this system using healthy HSCs as RA⁺NP carriers. Our results indicate that RA⁺NPs can be loaded in human UCB CD34⁺ cells as efficiently as observed in human AML CD34⁺ cell lines (4h internalization). Although, UCB CD34⁺ cells seem to be more sensitive to blue laser irradiation, shorter irradiation time (1 min) at lower laser power level (40mW) was still sufficient to trigger RA release from NPs and trigger the expression of CD38 in UCB CD34⁺ cells.

The drug delivery systems describe here, composed of carrier cells and RA⁺NPs offer a versatile a promising therapeutic strategy for targeting BM not only on hematopoietic malignancies, such as AML but also for regenerative medicine, such as HSCT.

4.2. Introduction

Several drug delivery strategies have been developed to increase the therapeutic efficiency of bioactive molecules. However, their clinical translation has been limited due to their poor specificity and efficient drug release at desired location. Furthermore, many therapeutic agents can be recognized and destroyed in their route to desired sites by host’s immune system, such as the mononuclear phagocytic system (MPS)⁴⁶³, thus decreasing their therapeutic potential.

The use of stem cells as carriers in cell-mediated drug delivery strategies is an attractive emerging approach to overcome the current limitations of conventional medicines. Stem cells can act not only as “shields” for therapeutic agents, but also as specific targeting agents by themselves due to their natural tropism for specific tissues, organs and sites of injury^{594,455}, with the added advantage of being able to

cross biological barriers, such as anatomical (e.g. blood brain barrier)⁵⁶³ or physiological barriers (e.g. tumor site heterogeneity). Moreover, stem cells themselves can be used as therapeutic agents as they can be modified to secrete trophic factors to promote the recovery of the damaged tissue and potentially differentiate to a wide variety of functional cells and consequently help in the repopulation of their target site.

MSCs and HSCs have high bioavailability and can be harvested readily from bone marrow of healthy unaffected individuals or isolated from UCB units⁵⁹⁹⁻⁶⁰⁴. MSCs have been used as NP carriers to target brain tumours^{568,605}, in regenerative medicine⁶⁰⁶ and cancer therapy^{604,607}. HSCs are also good candidates to target NPs to the HSC niche at the bone marrow in regenerative medicine (e.g. hematopoietic stem cell transplant – HSTC) and to treat haematological malignancies (e.g. leukemia). NPs can modulate HSC paracrine activity and their engraftment in the BM^{608,593}. NPs can also be used to target HSCs into the BM niche or to recruit other cells to the niche⁵⁴⁸.

LSC could also potentially be used as NP carriers, as they could serve as targeting agents to otherwise difficult access leukemic niches. This constitutes a special environment where LSCs responsible for relapses reside and traditional chemotherapy cannot reach. However, the use of LSCs should be made with caution as they could potentially have detrimental effects on the host. For example, systems using LSC could include the expression of self-destructive suicide genes after it reaches the target sites to prevent carrier-derived tumor formation or even go through rounds of genetic correction for leukemia mutations, using the recently described CRISPR/ Cas9 gene correction systems.

HSC transplantation with bone marrow and mobilized peripheral blood is an important therapeutic tool in the management of hematological malignancies and some inherited blood disorders¹³⁷. Unfortunately, repopulation of hematopoiesis can be adversely affected by the inability of HSCs to home to appropriate marrow niches or poor engrafting efficiency and self-renewal. In addition, individuals requiring an allogeneic HSC transplant may have problems to find a suitable matched donor^{260,261}. UCB may offer an important resource for such patients; however, individual units of cord blood (CB) contain too few HSCs to allow them to be transplanted into adults without a substantial delay in engraftment²⁶⁷. Therefore, methodologies to increase the number or engraftment efficiency of stem cells could provide substantial clinical benefit. Although strategies to accomplish this goal have been developed in the last years such as exogenous treatment of the HSCs with pro-survival/pro-engraftment factors^{644,645} and the stimulation of the adult HSC niche^{646, 623, 596}, they have shown limited success.

In the bone marrow, HSCs reside within the context of a complex microenvironment of different cell types and extracellular molecules that dictate stem cell self-renewal and differentiation⁶⁴⁷⁻⁶⁵⁰. The direct stimulation of the adult HSC niche might be a strategy to improve HSC engraftment. In mouse models, the pharmacologic use of PTH increases the number of HSCs mobilized into the peripheral blood for stem cell harvests, protects stem cells from repeated exposure to cytotoxic chemotherapy and expands stem cells in transplant recipients⁶⁴⁷. However, the effect is modest. An alternative to the direct manipulation of endogenous HSC niche is to enhance the engraftment of HSCs into the bone marrow niche. Several approaches have been described in the last few years to accelerate and improve the engraftment of HSCs including inhibition or deletion of CD26⁶⁴⁴, exposure to recombinant human NOV⁶⁴⁵, treatment with prostaglandin E2⁶⁵¹ or cholera toxin⁶⁵², but these approaches are at pre-clinical stage. All the methodologies described so far are based in the exogenous treatment of the stem cells with pro-

survival/pro-engraftment factors before their intravenous delivery. In most cases, although the stem cell treatments contribute for efficient mobilization of the HSC to the bone marrow niche their effect may not be enough to promote a successful and rapid engraftment.

An alternative to the 2 previous approaches is to potentiate both the expansion and engraftment of HSCs⁶⁵³. The transcription factor HOXB4 is a particularly attractive candidate for use in HSC expansion and engraftment. Studies have shown that HOXB4 mediates a significant expansion of HSCs and long-term repopulation potential either *in vitro* or *in vivo*^{654,655}. However, the expression of HOXB4 should be in a regulated manner to avoid potential unwanted effects. High expression levels of HOXB4 led to a statistically significant reduced engraftment of the transduced cells at the BM⁶⁵⁶, reduce the differentiation of stem cells into the erythroid cell lineage⁶⁵⁶, and increases the risk of leukemia⁶⁵⁷. Furthermore, the stability of HOXB4 protein in physiological conditions has proven to be an obstacle to its clinical application⁶⁵⁸.

To be used as drug carriers in cell-mediated delivery systems, NPs need to possess some specific characteristics. They must be biocompatible, without exerting cytotoxic effects to carrier cells, or without affecting their critical stem cell biological characteristics such as, self-renewal, proliferation and differentiation capacity as well as their migratory and homing capacity. Also, NPs components need to be biodegradable by the normal cell metabolism.

In this chapter our objective was to explore the potential use of NP-delivery systems not only to modulate the diseased HSC BM niche in AML but also healthy HSC BM niches. To achieve this, the murine AML disease model MLL-AF9 and intravital microscopy was used to find out how the remote release of RA within the BM niche affects the interaction between delivery cells and malignant cells. Next, we explored the possibility of using healthy HSCs (e.g UCB CD34⁺) as delivery cells. Finally, we explore the possibility of using NP systems to carry HoxB4 inside HSC during HSCT. We hypothesize that transiently increasing the levels of the transcription factor HOXB4 in bone marrow transplanted HSCs may increase HSC engraftment and proliferation.

4.3. Results and discussion

4.3.1 In vitro effect of RA+NPs in AML mouse model MLL-AF9

Although humanized murine AML models provide a better experimental setting towards a translational use of this NP formulation, it has some limitations when it comes to study fundamental biological interactions. Since our main goal was to study the paracrine effect of the release of RA from carrier cells and the interaction between carrier cells and BM niche components, we decided to use a murine AML disease model, which allows to apply a more straight experimental approach without affecting so much normal BM homeostasis, like the normally required procedure of myeloablation, which affects the homeostasis of the normal bone marrow (i.e. deterioration of sinusoids by irradiation⁶⁵⁹), and provides more reliable information about the complex niche interactions without the “noise” introduced by using cells coming from different species. For this purpose, we decided to use a murine AML model which encompasses the fusion oncogene MLL-AF9, similar to the human cell line THP-1, used in the previous chapter. In this model, most of the Leukaemia Stem Cells (LSCs) are downstream myeloid lineage cells, phenotypically similar to GMP cells⁶⁶⁰.

Like in the other cell types tested, most RA+NPs are internalized by MLL-AF9 blasts after just 4 h of treatment (data not shown), so for the *in vitro* tests we followed the same methodology as before (**Figure 4.A**), 4 hours internalization followed by wash and 5 minutes exposure for blue laser activation, after which the differentiation at 72h post treatment was evaluated by flow cytometry (**Figure 4.B**). Interestingly, in these cells, soluble RA and RA delivered by NP activation seem to promote distinct differentiation pathways (**Figure 4.C**). Although to a lesser extent than in other cell lines, soluble RA was able to induce differentiation of MLL-AF9 blasts towards granulocyte lineage, more specifically towards neutrophil-like cells (CD11b⁺Ly6G⁺) as previously reported⁶⁶¹. However, when RA was delivered intracellularly by photo-activation of RA+NPs, granulocyte differentiation was not significant, on the other hand, RA+NPs appear to prime monocyte/macrophage differentiation (CD11b⁺Ly6G⁻F4/80⁺) (**Figure 4.D**). Although previous studies have shown differentiation towards monocyte/macrophage lineage *in vitro* when AML cell lines were treated with vitamin D⁶⁶², which can be further enhanced by combining vitamin D treatment with RA, this was the first time to our knowledge that monocyte/macrophage differentiation was observed with RA treatment alone. Furthermore, activation of RA+NPs seems to promote the type 1 macrophage polarization (M1) (MHC II⁺CD206⁻) which has been shown to suppress tumour growth⁶⁶³, and not type 2 macrophages (M2), contrary to previous reports for the human AML cell lines HL-60 and THP-1 differentiation *in vitro* when combined RA+VitD treatments were used⁶⁶⁴. Of note, RA differentiation effect in APL was associated with restoration of normal PU.1 gene expression⁶⁶⁵, a transcription factor essential for macrophage differentiation and full neutrophil maturation⁶⁶⁶. Also, RA has been previously reported to negatively regulate neuropeptide Y gene expression⁶⁶⁷, a widely expressed neuroregulatory peptide, which suppresses macrophage activity⁶⁶⁸.

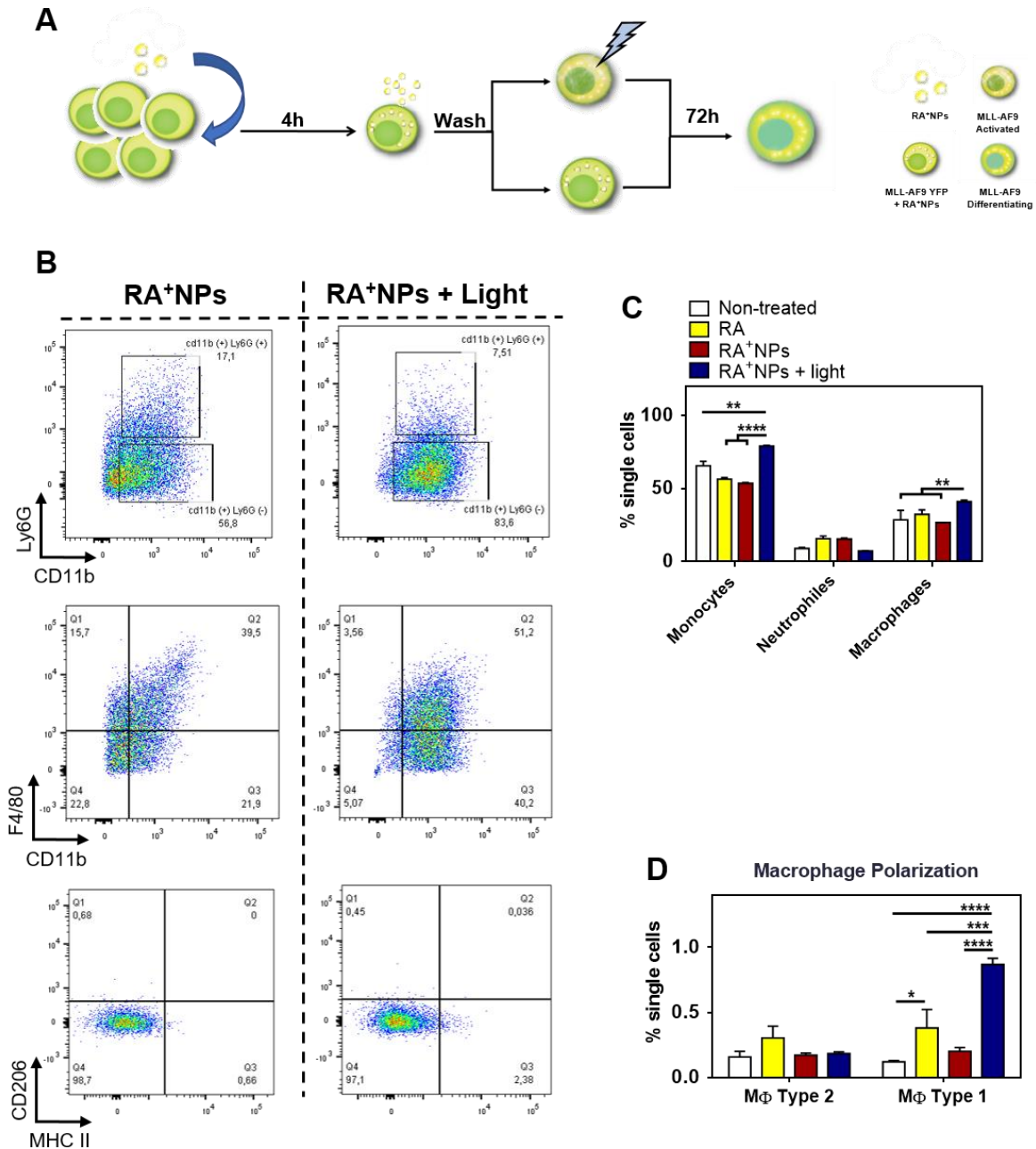


Figure 4.1 – *In vitro* Differentiation profile of MLL-AF9 YFP blast cells after treatment with soluble RA or RA+NPs. (A) Schematic representation of the experiment. MLL-AF9 YFP cells were incubated in serum-free RPMI-1640 with RA+NPs (10 μ g/mL) for 4 h. Then, cells were washed three times with PBS to remove NPs not internalized, activated or not by blue laser (405nm, 80mW) during 5 min, and cultured in complete medium for additional 3 days. Alternatively, MLL-AF9 YFP were cultured in complete medium for 3 days having soluble RA (3 μ g/mL). **(B)** Representative gating strategy for Lin⁻ MLL-AF9 YFP cells treated with RA+NPs. Dead cells excluded by DAPI staining. **(C-D)** Percentages of positive single cells were calculated based in the FMOs controls and are shown in each scatter plot. **(C)** Monocytes (Ly6G⁻CD11b⁺), Neutrophil (Ly6G⁺CD11b⁺) and Macrophage (Ly6G⁻CD11b⁺F4/80⁺) differentiation markers. **(D)** Percentage of macrophage activation markers for type 1 (MHC II⁺CD206⁻) and type 2 (MHC II⁻CD206⁺) polarization. In D and E results are expressed as mean \pm s.e.m. (n=3). Statistical analyses were performed by two-way ANOVA followed by a Holm-Sidak post-test. *P<0.05, **P<0.01, ***P<0.001 and ****P<0.0001.

4.3.2 Paracrine effect of RA+NPs in AML mouse model MLL-AF9 leukaemic niche

To better understand the therapeutic potential of RA+NPs it was important to confirm if the same type of differentiation could be observed *in vivo* and how this differentiation *in situ* - within the leukaemic BM microenvironment - could affect the progression of the disease. We also adopted a different methodology, closer to the normal disease progression, where we allowed LSC to invade and remodel the BM niche in steady state (initiation) before applying our treatment during the progression phase of the disease, which was followed by intravital microscopy⁷⁰. In short, first mTmG MLL-AF9 blasts were injected in healthy mice to induce disease infiltration. After 12-14 days YFP MLL-AF9 blasts previously loaded with RA+NPs or empty NPs were injected. One or two days later, after confirming by intravital microscopy the homing of YFP blasts to the same niche as mTmG blasts, the nanoparticles were activated by exposing the mouse calvaria to the blue laser for 10 minutes. This activation was repeated the following day. Three days after the last activation, the progression of the disease and MLL-AF9 activity were monitored inside the niche by time-lapse image acquisition (**Figure 4.2A**). In the end of the acquisitions, mice were sacrificed, and BM was collected from the calvaria and long bones and analysed by flow cytometry (**Figure 4.2B**).

The *in vivo* results allowed to confirm the observations made in chapter 3, where we have shown that NP loading of cells did not affect their homing capacity and RA release from NPs could be triggered remotely with the blue laser. More importantly, our results show that RA⁺NP were able to induce a reduction of both MLL-AF9 blasts population (YFP⁺ and mTmG⁺) in the BM of animal, particularly in the calvaria BM, the site of activation (**Figure 4.2C**). These results suggest that RA+NPs could help to decrease the disease burden of the resident mTmG⁺ MLL-AF9 AML mouse model. Furthermore, when looking at differentiation of YFP⁺ carrier cells (**Figure 4.2D**), we can observe a small increase in the neutrophil population in the calvaria BM of animals treated with RA⁺NPs. Although this increase is not statistically significant, this effect could only be observed at the calvaria BM and not in the long bones, suggesting this observation was due to activation of NPs at the calvaria BM. As for macrophage differentiation (**Figure 4.2E**), we did not observe significant differences between treatment groups at the whole BM, but by looking at the YFP⁺ cells differentiation we can observe a significant increase in the macrophage population, not only at the calvaria BM, but also at the long bones BM.

Although we did not explore the mechanisms behind the observed effect and more experiments would be necessary to fully understand these results in this experimental setting for AML disease model, at least three hypotheses should be considered: the effect of blue laser irradiation (405nm), the impact of NPs and their photo-activation by-products, and finally the effect of RA release by carrier cells within the leukemic niche.

Indeed, other studies have reported that blue light exposure can induce reactive oxygen species (ROS) generation^{669,670} and ROS have also been shown to promote macrophage differentiation and activation⁶⁷¹. Also, ROS have been shown to induce an increase in RAR α protein levels⁶⁷², the main RAR isotype involved in RA dependent differentiation in APL^{327,328}. Furthermore, although in a different biological scenario, UV irradiation in skin cells is known to promote the production of vitamin D⁶⁷³, a molecule also involved in the promotion of macrophage differentiation⁶⁶².

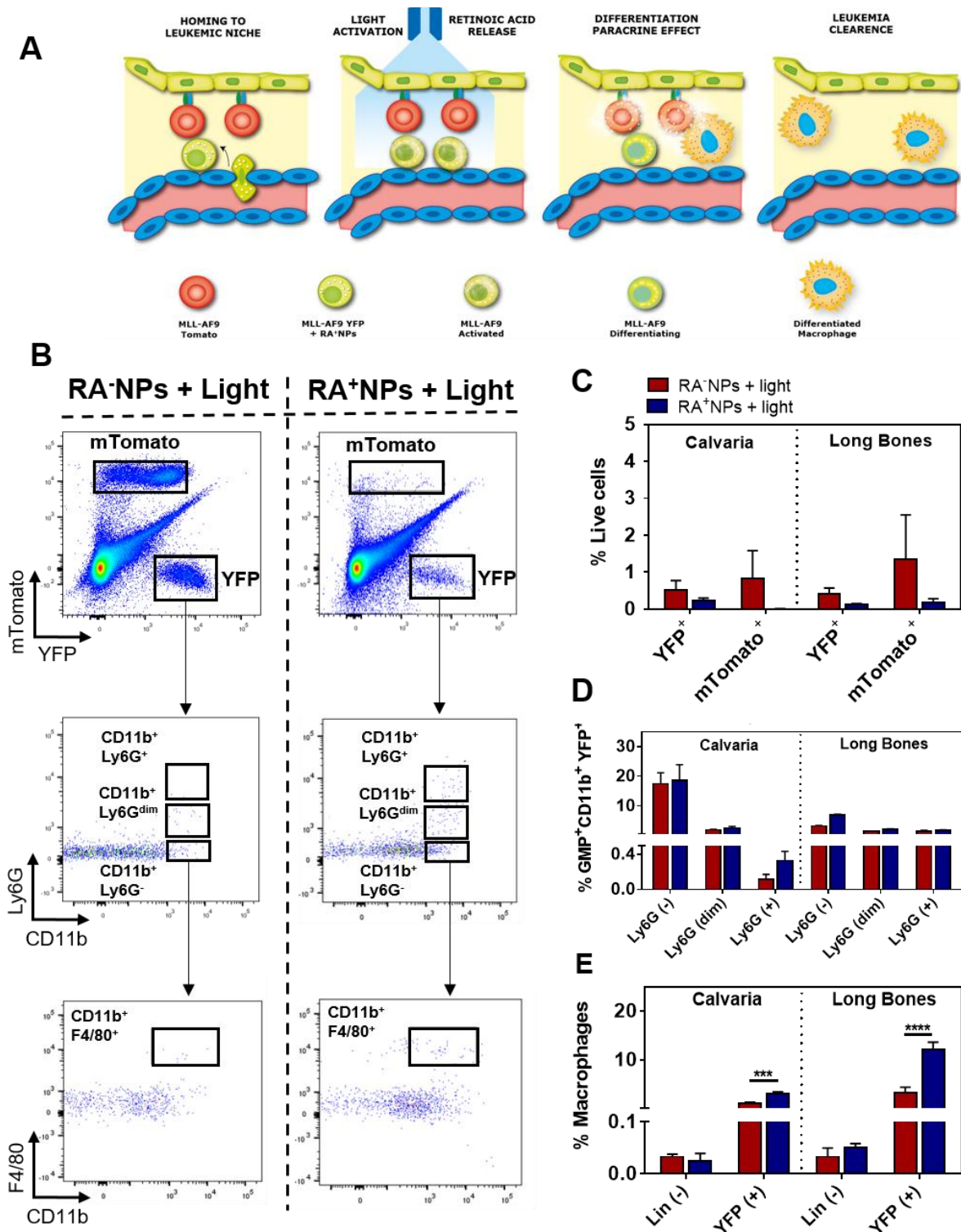


Figure 4.2 - In vivo activation of AML MLL-AF9 differentiation program by light at the bone marrow. (A) Schematic representation of the protocol for the generation murine MLL-AF9 mTmG AML disease model (12 days infiltration) and treatment with delivery cells MLL-AF9 YFP⁺ previously transfected with RA⁺NPs (n=3) or RA⁻NPs (n=3) by tail vein injection. After the homing (1 day) of delivery cells, the NPs were remotely activated by irradiating the mouse calvaria with a blue laser (5 min, 405 nm, 80mW) on the following two days. On the fifth day after MLL-AF9 YFP injection mouse were sacrificed and BM from the calvaria and long bones isolated for flow cytometry analysis. (B) Representative plots of flow cytometry gating strategy analysis for MLL-AF9 YFP⁺ and mTomato⁺ calvaria and long bone BM composition (C) and MLL-AF9 YFP⁺ differentiation in (D) neutrophils

or (E) macrophages. (C) Percentage of MLL-AF9 YFP⁺ or mTomato⁺ cells in BM of the calvaria and in the long bones. (D) Percentage of the neutrophil differentiation (CD11b⁺Ly6G⁺) at the calvaria and long bones quantified within the GMP population, identified by gating by Lin⁻Sca1⁻c-kit⁺ CD16/32^{high}CD34⁺ of MLL-AF9 YFP⁺ cell population. (E) Percentages of macrophage differentiation (CD11b⁺Ly6G⁺F4/80⁺) at the calvaria and long bones at the hole BM or MLL-AF9 YFP⁺ population. Dead cells excluded by DAPI staining and percentages of YFP and mTmG cells were calculated based on the total BM live cells. Percentages of positive single cells were calculated based in the FMOs controls. Results are expressed as mean±s.e.m. (n=3). Statistical analyses were performed by two-way ANOVA followed by a Holm-Sidak post-test. ***P<0.001 and ****P<0.0001.

Also, the mononuclear phagocytic system (MPS) has been shown to be determinant for the systemic recognition and clearance of NPs in the organism⁴⁶⁴. However, the exact mechanisms and the direct metabolic effects of NPs in macrophages are still under scrutiny. One of the mechanisms proposed is the recognition of polyanions (e.g. dextran sulphate) by folate receptors present in macrophages^{532,533}. Also, a recent study has shown that different NP systems can induce different metabolic reprogramming effects in macrophages, through: increased glycolytic activity, altered tricarboxylic acid cycle, and reduced ATP generation, which are consistent with a proinflammatory phenotype (M1) of macrophages⁶⁷⁴.

These effects that can be mediated by the radiation or directly by the NPs, may have some contribution for the results observed in this work. Nevertheless, it must be low because no significant effect was seen *in vivo* when mice were treated with RA-NPs loaded MLL-AF9 blasts and irradiated with the blue laser. This suggests that RA release from NPs is the main factor responsible for monocyte/macrophage differentiation.

4.3.3 Effect of RA+NPs in CD34+ cells

In a clinical setting, the use of LSC as NP carriers is not desirable for the obvious reasons, so we decided to investigate the possibility of using healthy hematopoietic cells as carriers and what would be the effect of the NPs and their light-activation in healthy hematopoietic cells. To do this we decided to test the NPs in UCB CD34⁺ cells, a common cell source used in hematopoietic stem cell transplant (HSCT), but as the availability of these cells is scarce, we did the initial tests in a CD34⁺ immortalized AML cell line, the KG1a.

Internalization and cytotoxicity of NP and laser exposure

The first step was to determine the CD34⁺ cells uptake of nanoparticles and the conditions of NP treatment and activation (laser exposure) which do not affect the viability. Our initial approach was the same conditions used during chapter 3. Briefly KG1a cells were treated with different concentrations of RA+NPs (0.1, 1 and 10ug/mL) for 4 hours in complete RPMI-1640 media with 1% FBS. After the incubation period cells were washed with PBS several times to remove non-internalized NPs and replated with complete RPMI-1640 with 10% FBS and irradiated or not with a blue laser (405nm, 5 minutes at 80mw). After 48h cells were collected and AnxV/PI (AnV/PI) flow cytometry protocol was used to assess the toxicity of the NPs (**Figure 4.3A**).

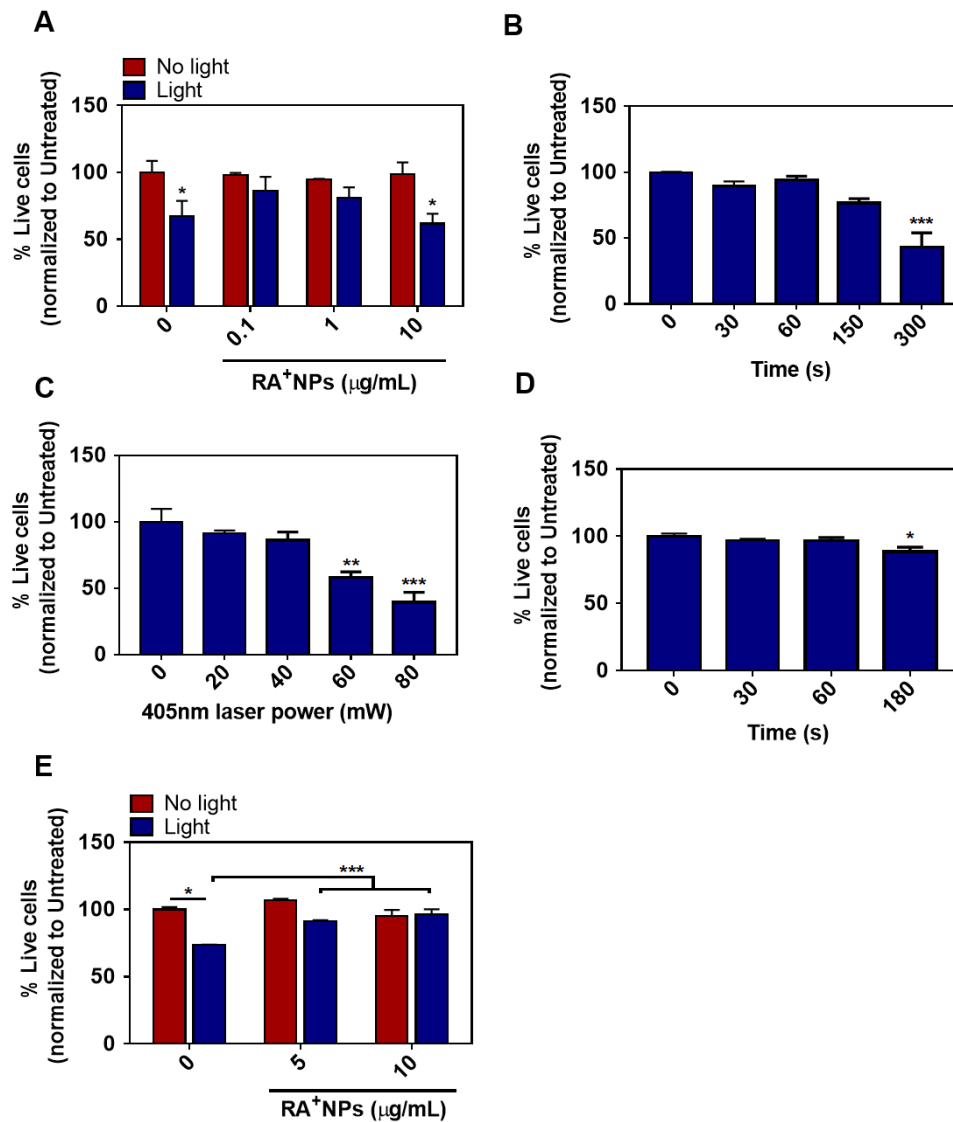


Figure 4.3 - Cytotoxicity of RA+NPs and light activation at human AML CD34+ cell line (KG1a) and UCB CD34+. Cytotoxicity of RA+NPs and laser exposure against human leukaemic cell line KG1a (A, B) and UCB CD34+ cells (C-E) and evaluated 48 h post-treatment by Annexin/PI staining followed by flow cytometry analysis. Live cells were negative for Annexin V and PI staining. (A) Cells were cultured in medium supplemented with different concentrations of RA+NPs for 4 h, washed and exposed or not to a blue laser (5 min, 405nm 80mW). (B) Cells were exposed to a blue laser at 80mW for different time periods. (C) Cells were exposed to a blue laser for 5 minutes at different laser powers. (D) Cells were exposed to a blue laser at 40mW for different time periods. (E) Cells were cultured in medium supplemented with different concentrations of RA+NPs for 4 h, washed and exposed or not to a blue laser (1 min, 405nm 40mW). All results are expressed as mean \pm s.e.m (n = 3). Statistical analyses were performed by one-way ANOVA (B-D) or two-way ANOVA (A, E) followed by a Holm-Sidak post-test. *P<0.05, **P<0.01, ***P<0.001.

According to these results, the NPs alone do not show any cytotoxicity in non-irradiated KG1a cells. However, we could observe <25% decrease in viability when comparing non-irradiated with irradiated pairs in cells without NP treatment and when treated with 10 $\mu\text{g/mL}$ NPs. Surprisingly, in cells treated with 0.1 and 1 $\mu\text{g/mL}$ of NP we couldn't observe any significant effect in their viability after being exposed to blue laser. These results suggest that RA⁺NPs could exert a protective effect against

irradiation, which could be due to irradiation absorption by the photo-responsive element of the NPs, DMNC. The next step was to find non-toxic conditions for the laser exposure. To do this, we tested different times of laser exposure while maintaining the laser power at 80mW and after 48h in culture the viability was assessed again using AnV/PI protocol (**Figure 4.3B**). These experiments confirm that 300 seconds (5 minutes) of laser exposure in KG1a cells already have a significant effect in their viability, but no toxic effect was observed up to 150 seconds of laser exposure at 80mW.

With the acquired knowledge regarding the toxicity of NPs and blue laser in KG1a cells, we could now start testing the cytotoxicity in UCB CD34+ cells. As the laser exposure seemed to have a higher impact in cell viability, we started to test different laser powers (**Figure 4.3C**) and we could observe that using laser powers higher than 20mW for 5 minutes had a significant effect in cell viability. Despite the fact that we could already observe a toxic effect using 40mW laser power, reducing the laser power would also reduce the amount of released cargo from the NPs, so we tried to find a compromise between laser power and exposure time and tested the toxicity of 40mW for different exposure times (**Figure 4.3D**). At 40mW laser power, we observed a decrease in viability for laser exposure over 60 seconds. Finally, we tested the combined effect of the laser exposure and NP treatment in UCB CD34+ cells (**Figure 4.3E**). Although the laser exposure still seems to have a negative effect in viability in cells without NP treatment, just like in KG1a, the toxicity effect is decreased with increased concentrations of NP treatment. In fact, no significant toxicity is observed in cells treated with 10 μ g/mL NPs with or without subsequent laser exposure for 60 seconds at 40mW laser power. This could be due to the anti-apoptotic properties of RA⁶⁷⁵ and/or due to the presence of the photo-sensible antenna (DMNC), which could diminish the irradiation effects on cells.

Next, we wanted to characterize the internalization kinetics and the dilution of internalized NPs during extended cell culture periods (**Figure 4.4A**).

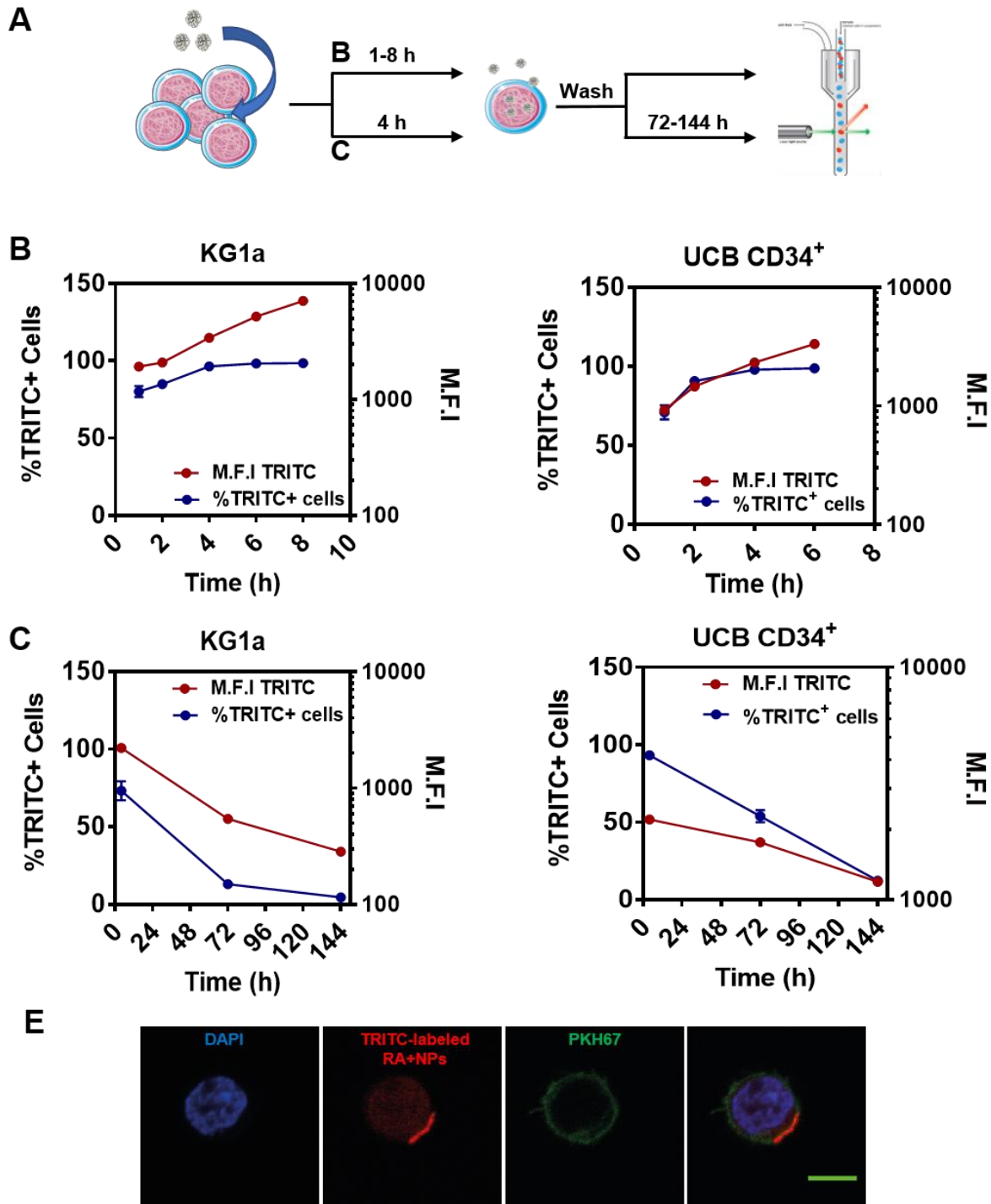


Figure 4.4 - Cellular uptake and dilution of RA+NPs in human AML CD34⁺ cell line (KG1a) and UCB CD34⁺ cells. (A, B) Uptake of TRITC-labelled RA+NPs (10 μg/mL) in human AML CD34⁺ cell line (KG1a) (A) and UCB CD34⁺ cells (B) as determined by FACS. Cells were cultured in medium supplemented with NPs for the time defined in the graph, washed and characterized by flow cytometry. The results are expressed as mean±s.e.m (n = 3). (C, D) Dilution of TRITC labelled RA+NPs with cell culture. KG1a (C) and UCB CD34⁺ cells (D), were transfected with RA+NPs in serum-free media for 4h, washed with PBS to remove non-internalized RA+NPs and cultured in complete media for additional 4h, 3 days and 6 days. After each incubation time cells were washed and NP dilution evaluated by flow cytometry. The results are expressed as mean±s.e.m (n=3) (E) Representative confocal imaging of 4 h internalization of TRITC-labeled RA+NPs (red) at UCB CD34⁺ cells stained with the membrane marker PKH67 green and nuclear staining DAPI (scale bar 5μm)

Similar to what has been done in chapter 3, cells were treated TRITC-labelled RA+NPs for different periods of time and after several washes with PBS, internalization levels were assessed by flow cytometry (**Figure 4.4B**). Both KG1a and UCB CD34⁺ cells show similar internalization kinetics to what was observed in other cell lines (chapter 3). Although it only takes 4 hours to have almost all the cells with NPs internalised (%TRITC), they seem to continue to accumulate NPs over this time, which is shown by the continuous increase in the mean fluorescence intensity (M.F.I) of TRITC in the cells. In the case of UCB CD34⁺ cells, we also observed by confocal microscopy the internalized NPs after 4h. Surprisingly, we did not observe a homogenous distribution of the NPs in the cell cytoplasm as we expected, instead in the case of UCB CD34⁺ cells, the internalization seems to be polarized. This could indicate that NP internalization in these cells is mainly by pinocytosis and not by receptor mediated endocytosis, as the observed cytoplasmic deformation only occurs during phagocytosis and micropinocytosis internalization, but HSC do not have phagocytic activity. (**Figure 4.4E**).

For the dilution experiments, cells were treated with TRITC-labelled RA+NPs for 4 hours after which they were extensively washed and replated and cultured for an additional 3 or 6 days. To have a baseline, the internalization level was measured after 4h of NP treatment. At the selected time points cells were collected and the percentage of NP-loaded cells was evaluated by flow cytometry (**Figure 4.4C**). In KG1a cells, after 3 days and 6 days only 15% and 5%, respectively, of the cells retained the NPs. When compared to percentage of internalization observed at 4 hours of internalization, these reductions represent approximately a 3-fold decrease for every 3 days in culture. In UCB CD34⁺ cells, similar to what we observed in KG1a, there was a 2-fold and 3-fold reduction of nanoparticles after 3 days and 6 days in culture, respectively.

Biological effect of RA-NPs in CD34⁺ cells

Next, we evaluated the differentiation capacity effect of RA+NP in CD34⁺ cells. We started to test the effect of RA+NPs in the differentiation of KG1a cells and also the differentiation potential of RA+NPs after 3 and 6 days in culture before activation. The RA+NPs were internalized for 4h hours and after being washed with PBS, divided into 3 groups, one where cells were irradiated with the blue laser right after wash (4 h activation), in the second and third group cell were cultured for additional 72 h or 144h, respectively, before laser activation. As a control condition, soluble RA was added to cells at the same time of laser activation of each group. In all groups the differentiation was evaluated 3 days after activation, by flow cytometry with CD11b/CD13 staining (**Figure 4.5A**). At 4 hours activation, all treatments seem to initiate the differentiation program of KG1a, observed by the decrease in CD13⁺CD11b⁻ population and increase of CD13^{dim}CD11b^{+/+} populations, however statistical significant terminal differentiation (CD13⁺CD11b⁺) can only be observed when cells are treated with RA+NPs and activated by blue laser (**Figure 4.5B**). As we observed previously, the percentage of cells that retain RA+NPs decreased with culture time (**Figure 4.4B**), so as expected the differentiation potential of the NPs was diminished when NPs were activated only after 72 or 144 h.

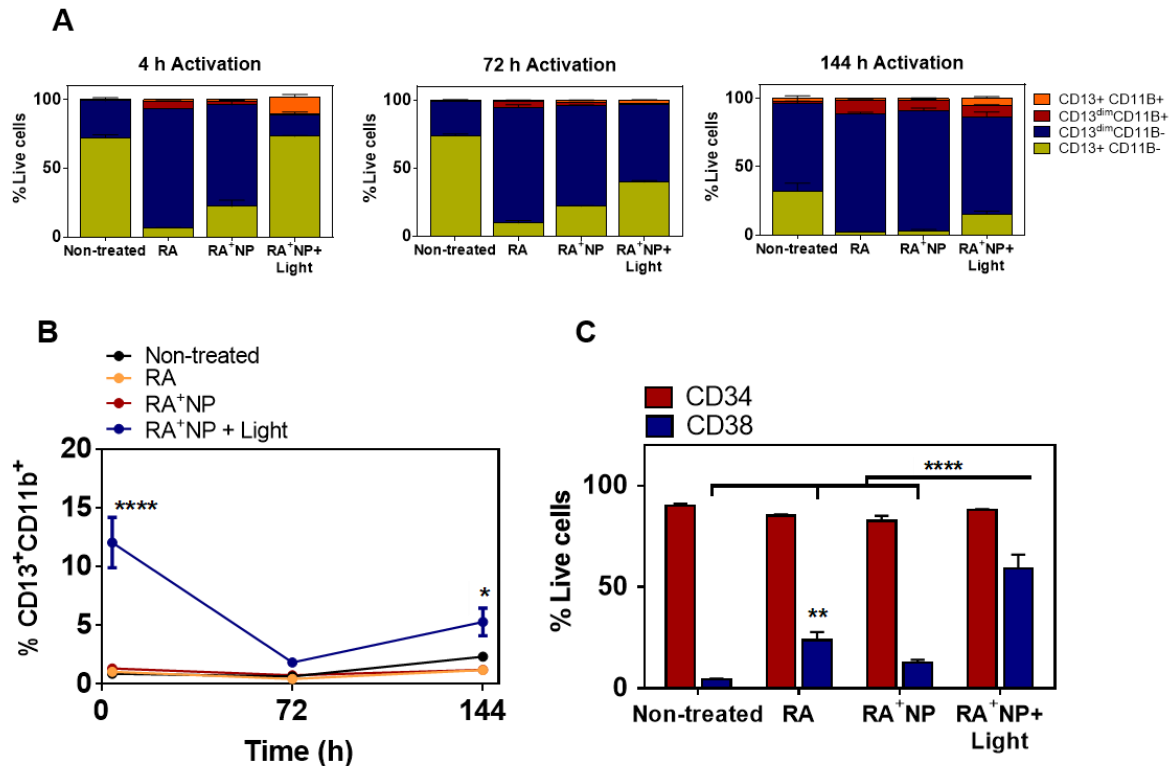


Figure 4.5 - Differentiation profile of in human AML CD34⁺ cell line (KG1a) and UCB CD34⁺ cells after treatment with soluble RA or RA+NPs. (A, B) KG1a cells were incubated in complete IMDM with 2% serum with soluble RA or 10 $\mu\text{g}/\text{mL}$ RA+NPs for 4 h. Then, cells were washed three times with PBS to remove NPs not internalized and replated in IMDM 20% serum. Cells were irradiated with a blue Laser (405 nm 80mW, 3 min) immediately or after 3 or 6 days and then cultured for 3 days after being irradiated. (A) Flow cytometry analysis of differentiated KG1a cells cultured for 3 days. Cells were initially gated in an FSC/SSC plot and gated analysed for CD13 and CD11b expression levels. Percentages of positive cells were calculated based in the isotype. (A) Percentages of CD13⁺CD11b⁻, CD13⁺ CD11b⁺, CD13^{dim}CD11b⁻ and CD13^{dim}CD11b⁺ in KG1a cells activated at 4h, 3 days and 6 days after RA+NP treatment and differentiated for 72 h. (B) KG1a CD13⁺ CD11b⁺ differentiation profile evolution at different times of activation. (C) UCB CD34⁺ cells were incubated in complete XVIVO15 media (supplemented with Flt3 and SCF), with soluble RA or 1 $\mu\text{g}/\text{mL}$ RA+NPs for 4 h. Then, cells were washed three times with PBS to remove NPs and irradiated with a blue Laser (405nm 40mW, 60 sec). After 3 days in culture, cells were stained for CD34 and CD38 markers and differentiation analysed by flow cytometry. The results are expressed as mean \pm s.e.m (n=3). Statistical analyses were performed by two-way ANOVA followed by a Holm-Sidak post-test. *P<0.05, **P<0.01 and ****P<0.0001.

Next, we tested the NPs effect on the differentiation of UCB CD34⁺ cells following a similar methodology as previously described, however we only tested activation right after 4 h of internalization, and 72h later cells were stained for CD34 and CD38 and differentiation evaluated by flow cytometry. Again, cells treated with RA⁺NPs and activated by light showed the most significant increase in CD38 staining when compared to all other conditions. Furthermore, none of the treatments had an effect in CD34 expression. These results are in line with previous observations, where soluble RA induced CD38 expression in normal hematopoietic progenitor cells and leukemic human cells. However, CD38 increased expression was only correlated with terminal differentiation in CD34⁻ progenitors and leukemic promyelocytic cell lines (e.g. HL-60). Conversely, in CD34⁺ leukemic cell lines (e.g. KG1a) and in primary human CD34⁺ cell cultures derived from AML patients, CD38 expression and terminal differentiation were not correlated⁶⁷⁶.

Since we have shown that polymeric photo-triggerable NPs could be efficiently loaded in human HSC and remotely activated without toxic effects while maintaining their functionality, we decided to further explore their potential use to modulate healthy HSC.

4.3.4 Production and characterization of functional TAT-HoxB4 recombinant protein

To have functional HoxB4 that could be used in this study, we produced a recombinant version of HoxB4 fusion protein, TAT-HoxB4. We have used a TAT-HoxB4 expression vector that has a C-terminal 6xHistag which allows us to purify the protein by affinity and a N-Terminal TAT sequence, which facilitates the internalization of the protein⁶⁷⁷. The protein was produced similarly to what has been done in the past^{655,658}. In short, recombinant HoxB4 was produced in *E.coli* expression system and purified by affinity under denaturing conditions (in the presence of Urea) and elution made with increasing concentrations of imidazole (**Figure 4.6A** panel I). Then the protein underwent a second purification step using an ionic-exchange chromatography (**Figure 4.6A** panel II) and finally eluted and shock-refolded in a single step by using high concentration of NaCl (**Figure 4.6A** panel III). Finally, the protein was eluted in PBS. As a result of the needed multiple purification, resulting protein concentration was very low to be used in our experiments, so we decided to concentrate it by using an Amicon 10 kDa. The purity and concentration of the TAT-HoxB4 and fusion protein were determined by sodium dodecyl sulfate-polyacrylamide gel electrophoresis (SDS-PAGE) and detected with Coomassie Blue staining. The purified TAT-HoxB4 run as ~37 kDa protein and the concentration was estimated by comparison with a BSA protein standard in the same gel.

To demonstrate that the purified protein had biological activity, we proceeded to an electrophoretic mobility shift assay (EMSA). Purified TAT-HoxB4 protein was incubated with an oligo containing the HoxB4 consensus sequence (5'-CGAATTGATTGATGCACTAATTGG AG-3'). The detection of the shift was done using a DNA/Protein double stain kit and although the shift is not very clear at the protein level, when looking at the DNA probe bands it was clear that the produced protein interacts with the probe, by the observed shift in the DNA band (**Figure 4.6B**). To confirm that this shift was not caused by unspecific interaction with contaminant proteins present in the TAT-HoxB4 solution, we also included a control in which we previously incubated the protein extract with an antibody for HoxB4. The increased shift observed in this condition confirms the specificity of the interaction and overall that the produced protein is functionally active and able to interact with its target, contrary to the commercial HoxB4.

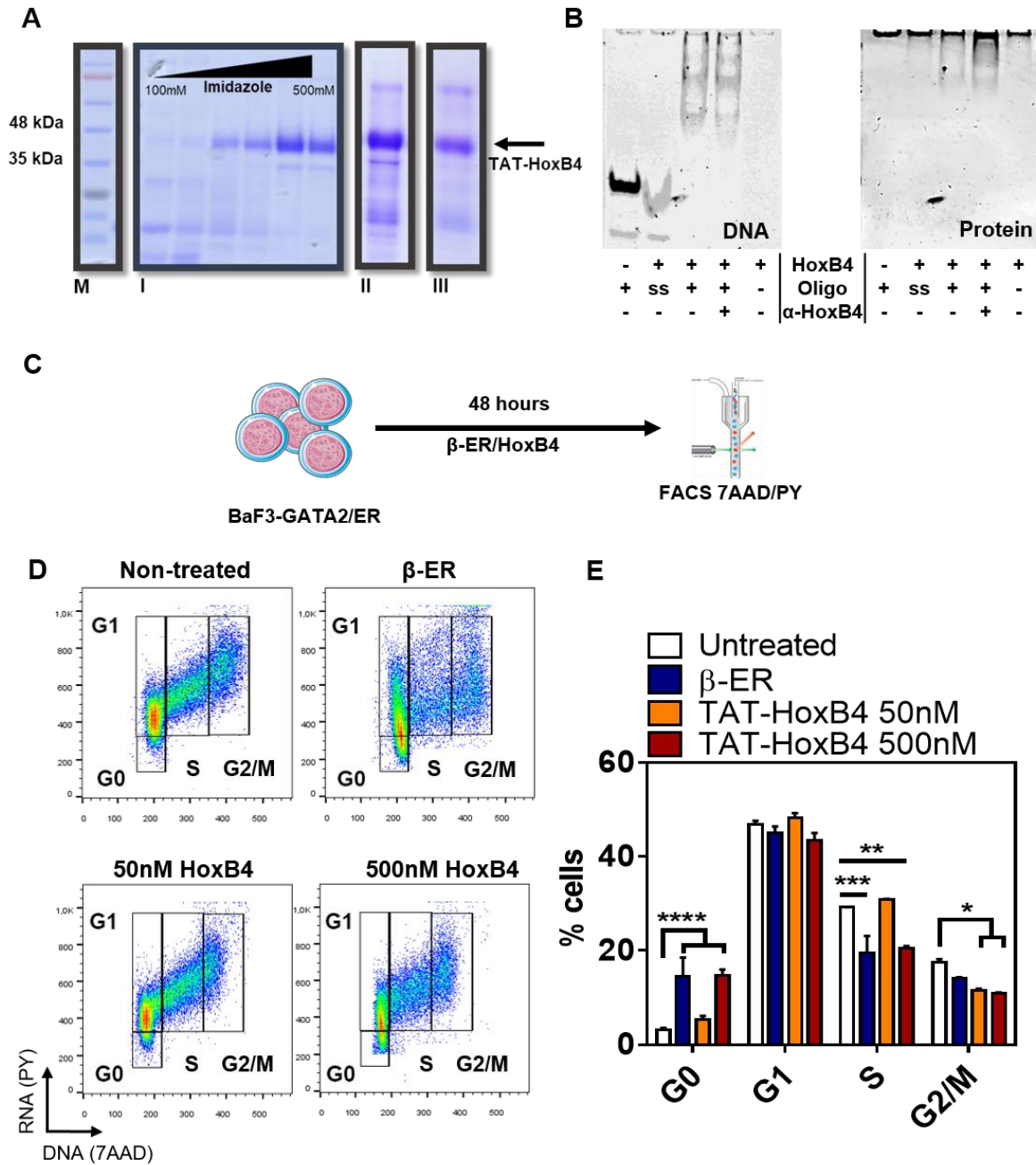


Figure 4.6 - Production and validation of biological activity of TAT-HoxB4. (A) Purification of recombinant TAT-HoxB4 (~37kDa) by (I) HisTrap affinity followed by (II) cationic exchange and a final step of shock-refolding by (III) fast desalting. (B) DNA-Binding competence of produced TAT-HoxB4 assessed by electrophoretic mobility shift assay using a probe for the consensus HoxB4-PBX1 binding site oligo sequence (5' CGA ATT GAT TGA TGC ACT AAT TGG 3'). Activity of Hoxb4 confirmed by the shift in the presence of double-stranded oligo and further specificity of the reaction confirmed by the supershift in the presence of an anti-HoxB4 antibody, observed in the increase of intensity of higher bands in both DNA(SYBR Green) and protein stain(SYPR Ruby). (C) Schematic representation of the methodology used for cell cycle and G0 determination experiments. (D) and (E) Flow cytometry results of the effect of TAT-Hoxb4 on the cell cycle of modified murine pro-B cells, BaF3-GATA2. (D) Gating strategy. (E) Percentages of the cell cycle phases determined after 48 h of a single treatment with β -ER or TAT-HoxB4 (50nM and 500nM). Statistical analyses were performed by two-way ANOVA followed by a Holm-Sidak post-test. * $P < 0.05$, ** $P < 0.01$ *** $P < 0.001$ and **** $P < 0.0001$.

4.3.5 Effect of TAT-HoxB4 in the cell cycle

Next, we wanted to evaluate if the produced protein was biologically active. Because the quiescence of HSCs is a key aspect for the homing and maintenance of stemness of the HSC⁶⁵⁴, we decided to evaluate the influence of TAT-HoxB4 in the cell cycle. Classical flow cytometry cell cycle assays allow to determine the different phases of the cycle (G1/0, S, G2/M) only by DNA levels, however it does not allow to distinguish between quiescent cells (G0) from active G1 cells as they will have similar DNA amounts. By using a RNA fluorescent probe, we can separate G0 and G1 phases, as the dormant G0 cells will have lower levels of RNA when compared to G1⁶⁷⁸.

To validate and optimize the G0 determination protocol we initially used the BaF3 murine cell line stably expressing a GATA2-Estrogen Receptor inducible construct (BaF3-GATA2/ER). This cell line was previously used to determine the role of GATA2 in the cell cycle of haematopoietic stem and progenitor cells, where the addition of β -estradiol (β -ER) to the culture media will activate the transcription of GATA2, increasing the quiescence of the cells⁴⁰⁶. Also, HoxB4 has been reported as a direct downstream target of the GATA2 in human CD34⁺ cells⁶⁷⁹.

For cell cycle assays and G0 determination (**Figure 4.6C**), BaF3-GATA2 were cultured with RPMI culture medium supplemented with murine IL-3 and treated with a single addition of TAT-HoxB4 (50 and 500 nM) or β -ER (1 μ m) as an internal control of G0 induction. After 48h in culture, cells were stained for DNA (7-AAD) and RNA (Pyronin) and analysed by flow cytometry (**Figure 4.6D**). Only at high concentrations of HoxB4 a similar level of G0 to the one observed in the control conditions (β -ER) could be achieved (**Figure 4.6E**). These results go along with previous observations that HoxB4 protein is very unstable in culture medium⁶⁵⁸, with a reported half -life of 2h and that continuous supplementation of fresh HoxB4 is needed to achieve a positive effect in the expansion of HSCs⁶⁸⁰.

To better understand the dose effect of TAT-HoxB4 in the cell cycle of HSCs we tested the influence of different HoxB4 dosages during cell culture. Although our final objective is to deliver HoxB4 to human UCB CD34⁺, the availability of this cells is scarce, so we decided to use as a model the KG1a⁶⁸¹ cell line, a differentiation-resistant human AML cell line containing a very primitive population of CD34⁺CD38⁻. For this purpose, we treated KG1a cells with TAT-HoxB4 for 48 h (**Figure 4.7A**), in one experimental group TAT-HoxB4 was renewed after 24h, in the other group was renewed every 8 h. After the treatments cells were collected and analysed for cell cycle (G0 arrest) (**Figure 4.7B**) and for gene expression (**Figure 4.8B**).

With cell cycle analysis we could observe that only two treatments of HoxB4 are already enough to induce quiescence in these cells, however only when multiple treatments are applied that we can see most of the cells acquiring a quiescence state (**Figure 4.7C**).

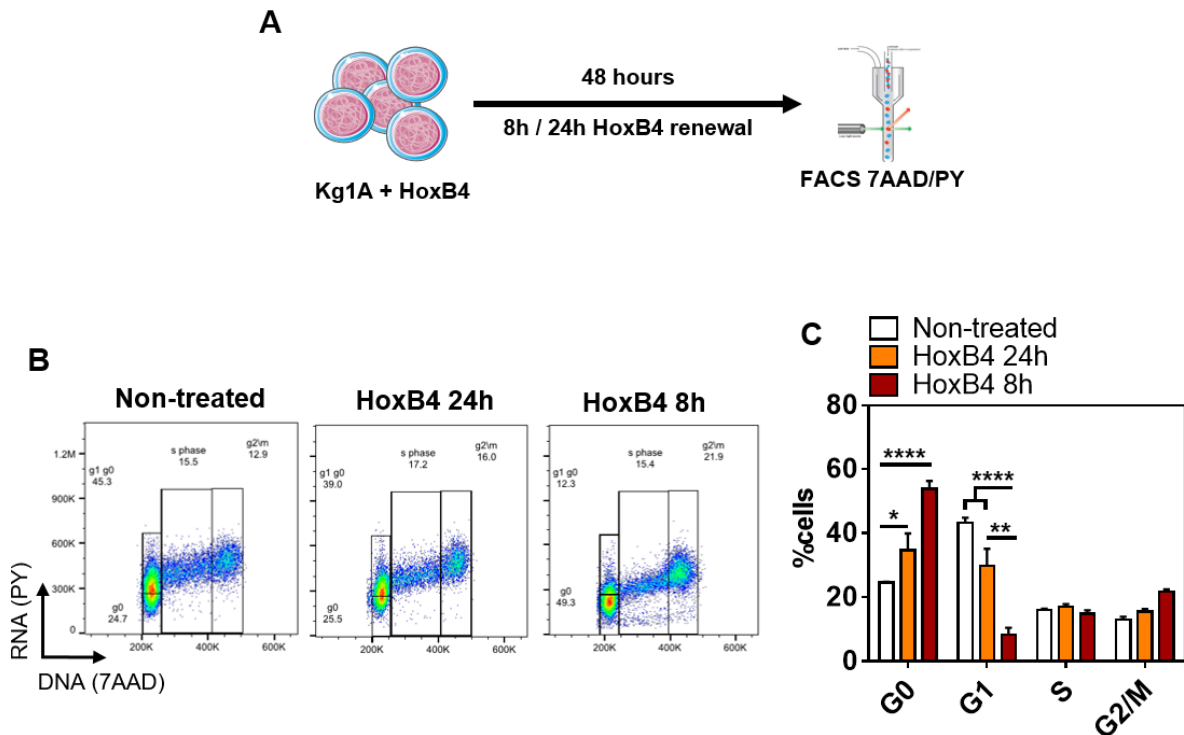


Figure 4.7 - TAT-HoxB4 Dosage effect in the cell cycle of human AML CD34+ cell line KG1a. KG1a cells were incubated in complete IMDM supplemented with HoxB4 (500nM). Every 8h or 24h cells were supplemented with fresh HoxB4. Cells were collected 48h after the first treatment and stained with 7AAD (DNA) and PyroninY (RNA) followed by flow cytometry analysis of the cell cycle and G0 determination. (A) Schematic representation of the methodology used. (B) Representative gating strategy for cell cycle analysis. (C) Percentages of the cell cycle phases determined after 48 hours of multiple treatments with TAT-HoxB4 (500nM), every 24h or every 8h. Results are expressed as mean±s.e.m (n=3). Statistical analyses were performed by two-way ANOVA followed by a Holm-Sidak post-test. *P<0.05, **P<0.01 ***P<0.001 and ****P<0.0001.

Next, we monitored the effects of the different TAT-HoxB4 treatments on the transcriptional regulation of key genes related with HoxB4 regulation cascade (HEMGN, GATA2, CUL4 and PBX1) and cell-cycle associated genes CDC20 and CDK2 (Figure 4.8). Consistent with the cell cycle data, the strongest upregulation of HoxB4 related genes was observed in the 8 hours treatments, with PBX1, a transcriptional co-factor of HoxB4, being the most upregulated; followed by the Hoxb4 direct targets HEMGN and GATA2. Also, not surprisingly, we could observe high levels of expression of CUL4, a ubiquitin ligase protein, previously associated with the high levels of cellular degradation of HoxB4⁶⁵⁸. As for CDC20 and CDK2, cell cycle regulators in cell division (M phase) and S phase entry, we could observe an increase with HoxB4, but no significant difference was observed with different HoxB4 treatments. This data supports the double role of HoxB4 in the maintenance of HSC stemness by promoting an accumulation in G0 without a full cell cycle arrest, allowing the expansion of HSCs.

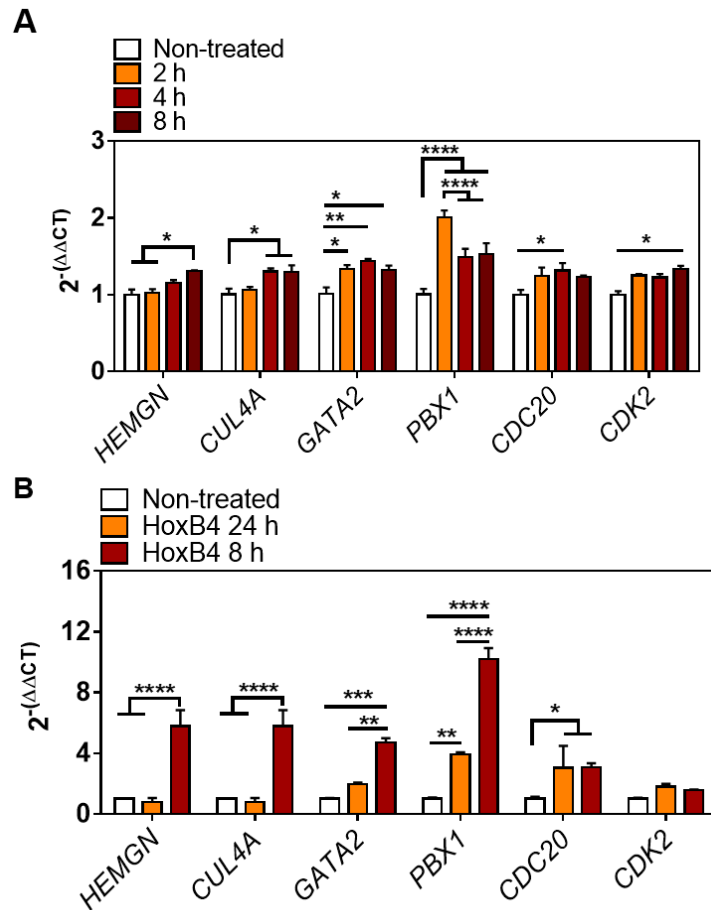


Figure 4.8 - Genes modulated by HoxB4 during G0 induction in KG1a cells as assessed by qRT-PCR analyses. (A) Gene expression profile of KG1a cells 2 h, 4 h and 8 h after treatment with 500nM HoxB4. (B) Gene expression of KG1a cells after 48 h of treatment with HoxB4 (500nM), with HoxB4 renewal every 24h or every 8h. In each run, the expression of each gene was normalized by GAPDH gene. Gene expression in each experimental group was normalized by the corresponding gene expression observed in nontreated KG1a cells. Results are expressed as mean \pm s.e.m (n=3). Statistical analyses were performed by two-way ANOVA followed by a Holm-Sidak post-test. *P<0.05, **P<0.01 ***P<0.001 and ****P<0.0001.

4.3.6 Immobilization of HoxB4 in NPs

Next, we hypothesized that if we could encapsulate or immobilize the TAT-HoxB4 in a nanoparticle system, we could improve not only the stability of the protein, but also take advantage of the light-activatable NP platforms developed in our group which would allow us to control with higher precision the time, location and dosage of the release. Our first approach was to try to encapsulate TAT-HoxB4 by replacing RA with the TAT-HoxB4 in PEI-DMNC:DS nanoparticles (**Figure 4.9A**). However, despite many attempts using different concentrations of HoxB4 we could not detect any protein associated with the NPs using Coomassie (**Figure 4.9B**). In fact, all the protein seems to be lost during the first centrifugation at 350g. In normal conditions, we can only achieve sedimentation of soluble proteins with >10000g forces, so this sedimentation of TAT-HoxB4 at 350g may indicate that the protein is losing solubility either by forming aggregates with itself and/or with dextran sulphate, the polyanion block of the nanoparticles.

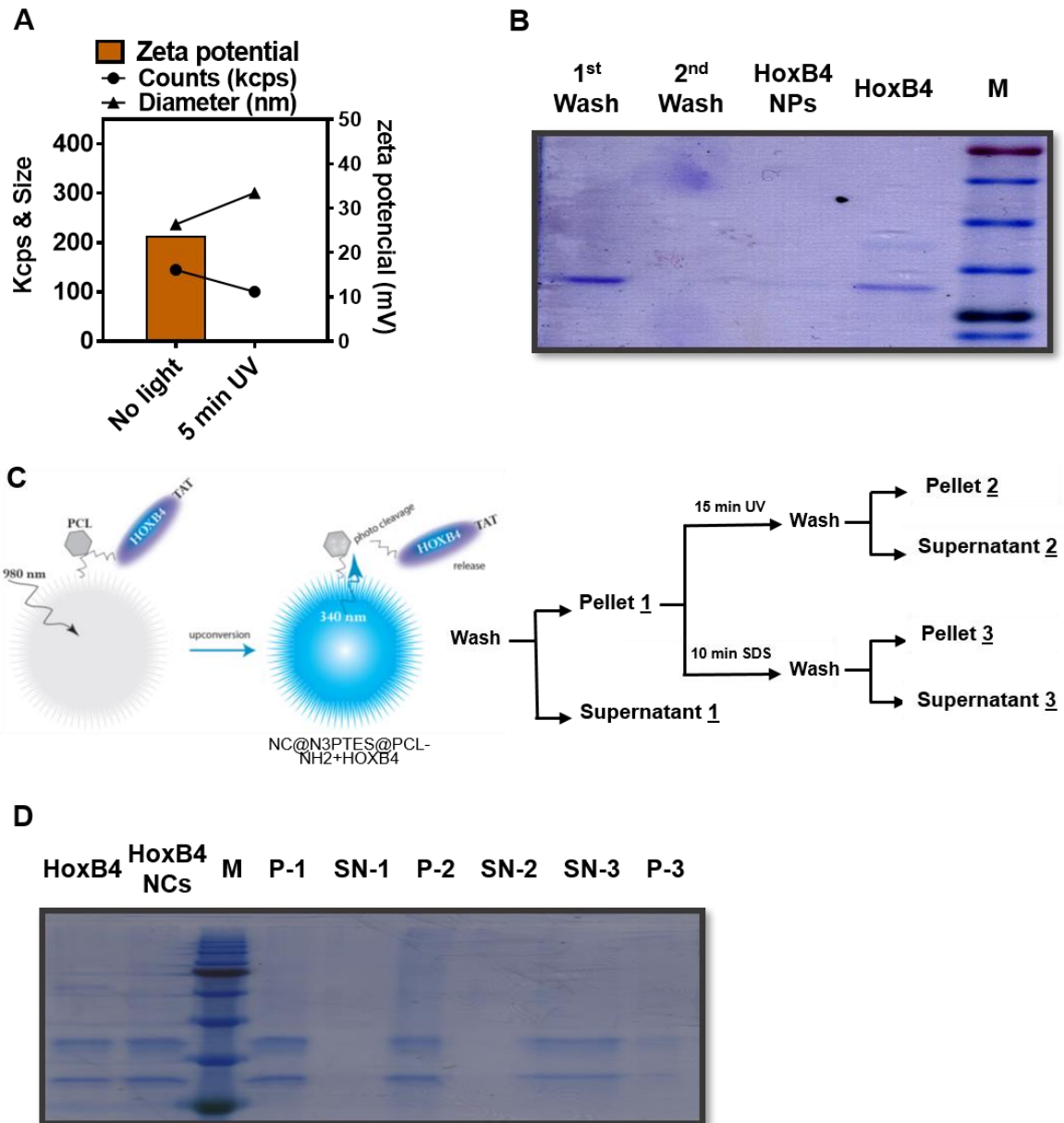


Figure 4.9 - HoxB4 ligation to light sensitive NP platforms. (A, B) Characterization of the encapsulation of TAT-HOXB4 in PEI-DMNC:DS NPs. Size, zeta potential and number of NPs (Kcps) of NPs in an aqueous suspension exposed or not to UV light (5min 100W). (B) Evaluation of encapsulation efficiency by SDS-PAGE. (C) Schematic representation of procedure to test the covalent ligation of TAT-HOXB4 (positively charged) to the PCL of up-conversion nanocrystals (negatively charged) SDS was used to eliminate electrostatic interactions. (D) SDS-PAGE evaluation of supernatants (SN) and pellets (P) from the different steps.

As the physical encapsulation did not seem to be feasible with the DS:PEI-DMNC NP system we decided to try a different approach. In this second approach we used an up-conversion nanocrystal (NC) system developed in our group, which can convert infrared irradiation to UV irradiation. These NCs were functionalized with a photocleavable linker (PCL), sensible to the UV, which allows to covalently bond proteins by their C-terminal; in the case of our recombinant HoxB4 this is especially relevant as the TAT-sequence is at the N-terminal. In this way, we could maintain the full functionality of TAT-HoxB4 and still use light stimulus to control the release. After confirming the functionalization of the

NCs with the PCL, the carboxylic group of TAT-HoxB4 was activated and the ligation made by click-chemistry. To confirm the ligation reaction (**Figure 4.9C**), we run both pellets and supernatants (**Figure 4.9D**, SN-1) of a 5000g centrifugation of TAT-HoxB4+NC suspension, before (**Figure 4.9D**, P-1 and SN-1) and after 10 minutes irradiation with UV (**Figure 4.9D**, P-2 and SN-2). Despite we could detect almost all the protein with the NCs pellet before irradiation, we were unable to detect protein in the supernatant after UV irradiation of the NC suspension. As the NCs are negatively charged and the TAT-HoxB4 has a positive isoelectric point (pI.~10), we hypothesized that TAT-HoxB4 could be interacting electrostatically with the NC surface instead of being covalently bound by the PCL. To test this, we incubated the TAT-HoxB4+NCs with a 10%SDS PBS solution for 10 minutes before proceeding to the centrifugation. By using a detergent, we expect to reduce the electrostatic interactions. In fact, by doing this most of the protein was detected in the supernatant of the solution (**Figure 4.9D**, SN-3) Although some protein could be detected in the pellet fraction (**Figure 4.9D**, P-3), this was likely to be still either some carryover from the protein in the SN or still protein electrostatically bound to the NC.

While we were able to produce biological active HoxB4 protein, which can regulate HSC self-renewal, conjugation of HoxB4 to a nanoplatform showed to be more challenging than expected and further work is need to overcome the obstacles found during the development of this work.

4.4. Conclusions

In this chapter we were able to demonstrate that at the feasibility in AML therapy of targeted spatio-temporal controlled drug release system, composed by LSCs and photo triggerable RA⁺NPs, can be successfully used in an AML disease model. Our results show that, instead of alternately to soluble RA treatments, RA⁺NPs can be used to induce AML differentiation towards monocytic/macrophage lineage not only *in vitro* but also *in vivo* in an MLL-AF9 mouse model of AML. Also, we have shown *in vitro* evidence that soluble RA and more significantly, activation of RA⁺NPs, stimulate antitumoral M1 macrophage activation. This macrophage induced differentiation *in vivo* seems to have “systemic” anti-leukemic effect within the BM leukemic niche, as we observed a significant reduction of leukemic cells in the BM of animals treated with RA⁺NPs when compared with animals treated with empty NPs (RA⁻ NPs).

We also explored the potential use of this system using healthy HSCs as RA⁺NP carriers. Our results indicate that RA⁺NPs can be loaded in human UCB CD34⁺ cells as efficiently as observed in human AML CD34⁺ cell lines (4h internalization). Although, UCB CD34⁺ cells seem to be more sensitive to blue laser irradiation, shorter irradiation time (1 min) at lower laser power level (40mW) was still sufficient to trigger RA release from NPs and trigger the expression of CD38 in UCB CD34⁺cells.

In the final part of this chapter, we were able to produce biologically functional HOXB4, which we were able to show it is capable to induce a quiescent state in human AML CD34⁺ cell lines. Unfortunately, HOXB4 loading or surface ligation in NP proved to be difficult, probably due to its intrinsic physico-chemical properties (e.g. size, charge, conformation).

4.5. Materials and Methods

Quantitative reverse transcription-polymerase chain reaction (qRT-PCR) analysis. Total RNA was extracted and purified using RNeasy Micro Kit (Qiagen) and immediately stored at -80°C. Total RNA was quantified in a NanoDrop ND-1000 Spectrophotometer (NanoDrop Technologies, Inc., USA) by spectrophotometry at 260 nm. The cDNA was reverse transcribed from 0.5 µg of total RNA, using TaqMan Reverse Transcription Reagents kit (Invitrogen) according to the manufacturer's instructions. The cDNA obtained was stored at -20°C until further analysis by qRT-PCR using SYBR Green technology and qRT-PCR analyses were performed using the ABI PRISM 7500 Fast System (Applied Biosystems). Quantification of target genes was performed relative to GAPDH gene according to the equation: $2^{-(Ct_{\text{sample}} - Ct_{\text{GAPDH}})}$. The mean minimal cycle threshold values (Ct) were calculated from quadruplicate reactions.

RA+NPs internalization by MLL-AF9 blasts and differentiation - MLL-AF9 YFP cells were incubated in serum-free RPMI-1640 with RA+NPs (10 µg/mL) for 4 h. Then, cells were washed three times with PBS to remove NPs not internalized, activated or not by blue laser (405nm, 80mW) during 5 min, and cultured in complete medium for additional 3 days. Alternatively, MLL-AF9 YFP were cultured in complete medium for 3 days having soluble RA (3µg/mL). The differentiation at 72h post treatment was evaluated by flow cytometry: GMPs (Ly6G⁺CD11b⁻), Neutrophil (Ly6G⁺CD11b⁺) and Macrophage (Ly6G⁻ CD11b⁺F4/80⁺) differentiation markers. Percentage of macrophage activation markers for type 1 (MHC II⁺CD206⁻) and type 2 (MHC II⁻CD206⁺) polarization. Percentage of myelocytic differentiation MLL-AF9 cells in neutrophils or macrophages and percentage of type 1 and type 2 macrophage polarization.

Intravital microscopy to monitor cell activity inside the calvaria BM niche. First mTmG MLL-AF9 blasts were injected in healthy mice to induce disease infiltration. After 12-14 days YFP MLL-AF9 blasts previously loaded with RA+NPs or empty NPs were injected. One or two days later, after confirming by intravital microscopy the homing of YFP blasts to the same niche as mTmG blasts, the nanoparticles were activated by exposing the mouse calvaria to the blue laser for 10 minutes. This activation was repeated the following day. Three days after the last activation, the progression of the disease and MLL-AF9 activity were monitored inside the niche by time-lapse image acquisition. In the end of the acquisitions, mice were sacrificed and BM was collected from the calvaria and long bones and analysed by flow cytometry.

Treatment with delivery cells MLL-AF9 YFP+ previously transfected with RA-NPs (n=3) or RA+NPs (n=3) by tail vein injection. After the homing (1 day) of delivery cells, the NPs were remotely activated by irradiating the mouse calvaria with a blue laser (5 min, 405 nm, 80mW) on the following two days. On the fifth day after MLL-AF9 YFP injection mouse were sacrificed and BM from the calvaria and long bones isolated for flow cytometry analysis.

NPs in UCB CD34⁺ cells Internalization and Cytotoxicity of RA+NPs and light activation at human AML CD34⁺ cell line (KG1a) and UCB CD34⁺ Briefly KG1a cells were treated with different concentrations of RA+NPs (0.1, 1 and 10 μ g/mL) for 4 hours in complete RPMI-1640 media with 1% FBS. After the incubation period cells were washed with PBS several times to remove non-internalized NPs and replated with complete RPMI-1640 with 10% FBS and irradiated or not with a blue laser (405nm, 5 minutes at 80mw). After 48h cells were collected and AnV/PI flow cytometry protocol was used to assess the toxicity of the NPs. To find non-toxic conditions for the laser exposure, cells were exposed to a blue laser at 80mW for different time periods.....

Cellular uptake and dilution of RA+NPs in human AML CD34⁺ cell line (KG1a) and UCB CD34⁺ cells. Uptake of TRITC-labelled RA+NPs (10 μ g/mL) in human AML CD34⁺ cell line (KG1a) and UCB CD34⁺ cells was determined by FACS. Cells were cultured in medium supplemented with NPs, washed and characterized by flow cytometry. Dilution of TRITC labelled RA+NPs with cell culture. KG1a and UCB CD34⁺ cells were transfected with RA+NPs in serum-free media for 4h, washed with PBS to remove non-internalized RA+NPs and cultured in complete media for additional 4h, 3 days and 6 days. After each incubation time cells were washed and NP dilution evaluated by flow cytometry.

Differentiation capacity of RA+NP in KG1a e UCB CD34⁺ cells. *The RA+NPs were* internalized for 4h hours and after being washed with PBS, divided into 3 groups, one where cells were irradiated with the blue laser right after wash (4 h activation), in the second and third group cell were cultured for additional 72 h or 144h, respectively, before laser activation. As a control condition, soluble RA was added to cells at the same time of laser activation of each group. In all groups the differentiation was evaluated 3 days after activation by flow cytometry by CD11b/CD13 staining

TAT-HoxB4 production. Recombinant HoxB4 was produced in E.coli expression system and purified by affinity using an HisTrap HP chromatography column (GE Healthcare) under denaturing conditions (in the presence of 8M Urea) and elution made with increasing concentrations of imidazole (Figure 4.6A panel I). Then the protein underwent a second purification step using an ionic-exchange chromatography (HiTrap SP HP, GE Healthcare) (Figure 4.6A panel II) and finally eluted and shock-refolded in a single step by using 20mM HEPES supplemented with 1M NaCl (Figure 4.6A panel III). At this point, the sample buffer was then exchanged to PBS, using an HiTrap desalting column and as the resulting eluted protein concentration was low, purified recombinant HoxB4 was concentrated using Amicon 10 kDa. The purity and concentration of the TAT-HoxB4 and fusion protein were determined by sodium dodecyl sulfate-polyacrylamide gel electrophoresis (SDS-PAGE) and detected with Coomassie Blue staining. The purified TAT-HoxB4 run as ~37 kDa protein and the concentration was estimated by comparison with a BSA protein standard in the same gel.

Validation of biological activity of TAT-HoxB4. An electrophoretic mobility shift assay (EMSA) was used. Purified TAT-HoxB4 protein was incubated with an oligo containing the HoxB4 consensus sequence (5'-CGAATTGATTGATGCACTAATTGG AG-3') for 1hour and then loaded in a 6% non-denaturing polyacrylamide gel. The detection of the shift was done using a DNA/Protein double stain kit

Effect of TAT-HoxB4 in cell cycle. Classical flow cytometry cell cycle assays allow to determine the different phases of the cycle (G1/0, S, G2/M) only by DNA levels, however it does not allow to distinguish between quiescent cells (G0) from active G1 cells as they will have similar DNA amounts. By using a RNA fluorescent probe, we can separate G0 and G1 phases, as the dormant G0 cells will have lower levels of RNA when compared to G1. BaF3 murine cell line stably expressing a GATA2-Estrogen Receptor inducible construct (BaF3-GATA2/ER). For cell cycle assays and G0 determination, BaF3-GATA2 were cultured with RPMI culture medium supplemented with murine IL-3 and treated with a single addition of TAT-HoxB4 (50 and 500 nM) or β -ER (1 μ m) as an internal control of G0 induction. After 48h in culture cells were stained for DNA (7-AAD) and RNA (Pyronein) and analysed by flow cytometry.

TAT-HoxB4 Dosage effect in the cell cycle of human AML CD34+ cell line KG1a. KG1a cells were incubated in complete IMDM supplemented with HoxB4 (500nM). Every 8h or 24h cells were supplemented with fresh HoxB4. Cells were collected 48h after the first treatment and stained with 7AAD (DNA) and PyroninY (RNA) followed by flow cytometry analysis of the cell cycle and G0 determination.

Immobilization or Encapsulation of HoxB4. Encapsulate TAT-HoxB4 by replacing RA with the TAT-HoxB4 in PEI-DMNC:DS nanoparticles. Detect protein associated with the NPs using Coomassie. Encapsulation efficiency by SDS-PAGE. Covalent ligation of TAT-HOXB4 (positively charged) to the PCL of up-conversion nanocrystals...

Statistical analysis. Statistical analyses were performed with GraphPad Prism software. For multiple comparisons, a two-way ANOVA followed by a Holm-Sidak post-test was performed. Results were considered significant when $P < 0.05$. Data are shown as mean \pm s.e.m. unless other specification.

CHAPTER 5 - General Conclusions and Future Work

General conclusions and Future work

In conclusion, with this work we were able to develop a naturally targeted drug delivery system for AML therapy, featuring a high degree of precision in the spatio-temporal control of drug release and delivery.

To achieve this, we developed a biocompatible photo-triggerable NP system to deliver RA intracellularly. Photo-triggerable RA⁺NPs can be quickly internalized and avoid cellular degradation by lysosomal escape, which allows a prolonged intracellular accumulation of functional NPs inside LSC⁴⁰⁰. Our nanoformulation, allowed us to explore the natural tropism of LSCs (as a targeting strategy) to deliver RA⁺NPs in leukaemic niches of the BM in a stealthy manner, as cell carriers avoid systemic immunological recognition and response. We would also expect this system to have less off-target accumulation and side effects, when compared with other targeted drug delivery systems. Although we did not evaluate the systemic distribution in the whole animal, we believe the great majority of RA⁺NP loaded cells would naturally accumulate at the BM. Furthermore, our photo-triggerable system allowed us to choose, with precision, the time and location (i.e. calvarium bone) of RA release from NPs by an external stimulus (i.e. blue laser irradiation – 405nm).

We also observed that RA⁺NPs can help to reduce leukaemia burden in MLL-AF9 AML mouse model and promote macrophage differentiation of carrier cells *in vitro* and *in vivo*. However, further investigation is necessary to clarify our observations. Although it was not possible to analyse before the submission of this thesis, we also used intravital microscopy imaging techniques⁷⁰ to acquire calvaria tilescans, and 3h time-lapses of calvarium BM before and after exposure to blue laser in animals treated with NP-loaded MLL-AF9 cells. Intravital imaging was performed in the same animals used in flow cytometry characterization of BM cell composition in animals treated with empty NP (RA⁻NPs) and RA⁺NPs. We are now conducting image analyses in order to better understand the mechanism. This kind of analysis would allow to observe biological events to support our results, such as: phagocytic events from carrier cells, apoptotic events from either carrier cells or resident leukaemic cells. We could also investigate the different migration patterns of both MLL-AF9 blasts used in this experiment. We would expect to find the majority of YFP⁺ to migrate preferentially to the vicinity of mTmG MLL-AF9 cells expanding in the BM of treated mice.

Preliminary data obtained by particle analysis, showed that we could potentially use two-photon laser to activate RA⁺NPs with high precision, which coupled with intravital imaging could allow us to study, in deeper detail, the interaction promoted by our system within the bone marrow niche. For example, we could activate carrier cells preferentially located at different niches (endosteal v.s. perivascular niche) and follow the promoted effects by intravital time-lapse imaging.

Our observations could be further improved towards a potential clinical application by:

1) doing a better characterization of BM cells, either by a better choice of antibody panel choice which could better identify macrophages and type of activation, or by better discrimination of different BM fractions (e.g. flushing central marrow diaphysis and trabecular-rich areas by crushing metaphysis area⁶⁸²;

2) testing the impact of RA⁺NPs related LSC clearance in the survival;

3) using in a combined therapy approach, with other therapeutic agents⁶⁸³; for example, RA⁺NPs could be used in combination anti-CD38-based therapeutic agent (Mol Cancer Ther. 2004 Mar;3(3):345-52).

RA is a signalling molecules with pleiotropic effects, serving as key modulator in different parts of the organism. in the modulation of haematopoiesis, while it induces LSC differentiation in APL or in HSPCs, it can also be involved in the regulation of HSC self-renewal and maintenance³⁸⁰. Making RA⁺NPs a good candidate to be tested in HSCT therapy used during remission therapy. Although we did not fully explore this option, our results indicate that HSC could be a good candidate to be the carrier cell on our drug delivery system, as we showed that RA⁺NPs can be loaded and activated efficiently in UCB CD34⁺. Also, a fast NP internalization protocol can decrease the exposure of HSC to normoxia atmospheric conditions, which compromises HSC recovery from the BM and cord blood²⁷⁴.

Besides AML, RA+NPs could potential be explored in other types of cancer therapy, such as brain tumours, or other hematopoietic malignancies specially in other leukaemia, bone metastasis and also in regenerative therapy. For example, we could take advantage of the small RA passive release (leakiness of the NPs) to help in maintaining HSC functionality during transplantation. This would probably potentiate a higher efficiency in terms of numbers of HSCs that reach the niche. On the other hand, due to the rarity and difficulty to isolate HSCs in high numbers for experimental purposes, maybe by using cells with higher availability as NP carriers would be more rewarding; such as: MSC, Macrophages/Monocytes, T cells, NK cells.

NP delivery systems are attractive for the delivery of protein and in particular transcription factors. They can help in stabilizing and protecting proteins from degradation and also because they can serve as an intracellular delivery system, important in transcription factors delivery as they often require post-translational modifications in order to become biologically active. In this work, the conjugation of functional HOXB4 with a NP-delivery system failed and we are actively looking for other alternatives. In the meantime, further NP improvements have been made in our group which would allow a higher diversity of applicability either by allowing for an easier conjugation/loading of proteins, small molecules or nucleic acids⁶⁸⁴⁻⁶⁸⁶, or by using light wavelengths which allow higher body penetration and less toxic effect than 405nm laser irradiation. In particular, Jimenez-Balsa A *et al* NP systems would be specially interesting as it could possibly allow for a double delivery system, by encapsulating a small molecule and conjugate any other type of biomolecule to the photo-cleavable linker.

CHAPTER 6 - References

References

1. Montesinos, P., *et al.* Differentiation syndrome in patients with acute promyelocytic leukemia treated with all-trans retinoic acid and anthracycline chemotherapy: characteristics, outcome, and prognostic factors. *Blood* **113**, 775-783 (2009).
2. Duan, C.W., *et al.* Leukemia propagating cells rebuild an evolving niche in response to therapy. *Cancer Cell* **25**, 778-793 (2014).
3. Haeckel, E.H.P.A. *The Riddle of the Universe at the Close of the Nineteenth Century*, (Harper, 1902).
4. Pappenheim, A. Ueber entwicklung und ausbildung der erythroblasten. *Archiv für pathologische Anatomie und Physiologie und für klinische Medizin* **145**, 587-643 (1896).
5. Till, J.E. & McCulloch, E.A. A direct measurement of the radiation sensitivity of normal mouse bone marrow cells. *Radiation research* **14**, 213-222 (1961).
6. Schofield, R. The relationship between the spleen colony-forming cell and the haemopoietic stem cell. *Blood cells* **4**, 7-25 (1978).
7. Kricun, M.E. Red-yellow marrow conversion: its effect on the location of some solitary bone lesions. *Skeletal radiology* **14**, 10-19 (1985).
8. Orkin, S.H. & Zon, L.I. Hematopoiesis: an evolving paradigm for stem cell biology. *Cell* **132**, 631-644 (2008).
9. Guenechea, G., Gan, O.I., Dorrell, C. & Dick, J.E. Distinct classes of human stem cells that differ in proliferative and self-renewal potential. *Nature immunology* **2**, 75 (2001).
10. Ema, H., *et al.* Quantification of self-renewal capacity in single hematopoietic stem cells from normal and Lnk-deficient mice. *Developmental cell* **8**, 907-914 (2005).
11. Osawa, M., Hanada, K.-i., Hamada, H. & Nakauchi, H. Long-term lymphohematopoietic reconstitution by a single CD34-low/negative hematopoietic stem cell. *Science* **273**, 242-245 (1996).
12. Morrison, S.J., Wandycz, A.M., Hemmati, H.D., Wright, D.E. & Weissman, I.L. Identification of a lineage of multipotent hematopoietic progenitors. *Development* **124**, 1929-1939 (1997).
13. Yang, L., *et al.* Identification of Lin⁻Sca1⁺ kit⁺ CD34⁺ Flt3⁻ short-term hematopoietic stem cells capable of rapidly reconstituting and rescuing myeloablated transplant recipients. *Blood* **105**, 2717-2723 (2005).
14. Muller-Sieburg, C.E., Sieburg, H.B., Bernitz, J.M. & Cattarossi, G. Stem cell heterogeneity: implications for aging and regenerative medicine. *Blood* **119**, 3900-3907 (2012).
15. Yamamoto, R., *et al.* Clonal analysis unveils self-renewing lineage-restricted progenitors generated directly from hematopoietic stem cells. *Cell* **154**, 1112-1126 (2013).
16. Purton, L.E. & Scadden, D.T. Limiting factors in murine hematopoietic stem cell assays. *Cell stem cell* **1**, 263-270 (2007).
17. Kiel, M.J., *et al.* SLAM family receptors distinguish hematopoietic stem and progenitor cells and reveal endothelial niches for stem cells. *cell* **121**, 1109-1121 (2005).
18. Kent, D.G., *et al.* Prospective isolation and molecular characterization of hematopoietic stem cells with durable self-renewal potential. *Blood* **113**, 6342-6350 (2009).
19. Benveniste, P., *et al.* Intermediate-term hematopoietic stem cells with extended but time-limited reconstitution potential. *Cell stem cell* **6**, 48-58 (2010).
20. Muller-Sieburg, C.E., Cho, R.H., Karlsson, L., Huang, J.-F. & Sieburg, H.B. Myeloid-biased hematopoietic stem cells have extensive self-renewal capacity but generate diminished lymphoid progeny with impaired IL-7 responsiveness. *Blood* **103**, 4111-4118 (2004).
21. Dykstra, B., *et al.* Long-term propagation of distinct hematopoietic differentiation programs in vivo. *Cell stem cell* **1**, 218-229 (2007).
22. Benz, C., *et al.* Hematopoietic stem cell subtypes expand differentially during development and display distinct lymphopoietic programs. *Cell stem cell* **10**, 273-283 (2012).
23. Galan-Diez, M., Cuesta-Dominguez, A. & Kousteni, S. The Bone Marrow Microenvironment in Health and Myeloid Malignancy. *Cold Spring Harb Perspect Med* (2017).
24. Ellis, R. The distribution of active bone marrow in the adult. *Physics in Medicine & Biology* **5**, 255 (1961).
25. Hayman, J.A., *et al.* Distribution of proliferating bone marrow in adult cancer patients determined using FLT-PET imaging. *International Journal of Radiation Oncology•Biology•Physics* **79**, 847-852 (2011).
26. Boulais, P.E. & Frenette, P.S. Making sense of hematopoietic stem cell niches. *Blood* **125**, 2621-2629 (2015).
27. Goncalves, K.A., *et al.* Angiogenin promotes hematopoietic regeneration by dichotomously regulating quiescence of stem and progenitor cells. *Cell* **166**, 894-906 (2016).

28. Zhou, B.O., Ding, L. & Morrison, S.J. Hematopoietic stem and progenitor cells regulate the regeneration of their niche by secreting Angiopoietin-1. *Elife* **4**, e05521 (2015).
29. Zheng, J., Huynh, H., Umikawa, M., Silvano, R. & Zhang, C.C. Angiopoietin-like protein 3 supports the activity of hematopoietic stem cells in the bone marrow niche. *Blood*, blood-2010-2006-291716 (2010).
30. Crisan, M., *et al.* BMP signalling differentially regulates distinct haematopoietic stem cell types. *Nature communications* **6**, 8040 (2015).
31. Goldman, D.C., *et al.* BMP4 regulates the hematopoietic stem cell niche. *Blood* **114**, 4393-4401 (2009).
32. Singbrant, S., *et al.* Canonical BMP signaling is dispensable for hematopoietic stem cell function in both adult and fetal liver hematopoiesis, but essential to preserve colon architecture. *Blood*, blood-2009-2005-220988 (2010).
33. Bruns, I., *et al.* Megakaryocytes regulate hematopoietic stem cell quiescence through CXCL4 secretion. *Nature medicine* **20**, 1315 (2014).
34. Greenbaum, A., *et al.* CXCL12 in early mesenchymal progenitors is required for haematopoietic stem-cell maintenance. *Nature* **495**, 227 (2013).
35. Omatsu, Y., *et al.* The essential functions of adipo-osteogenic progenitors as the hematopoietic stem and progenitor cell niche. *Immunity* **33**, 387-399 (2010).
36. Zhao, M., *et al.* Megakaryocytes maintain homeostatic quiescence and promote post-injury regeneration of hematopoietic stem cells. *Nature medicine* **20**, 1321 (2014).
37. Zhao, M., *et al.* FGF signaling facilitates postinjury recovery of mouse hematopoietic system. *Blood* **120**, 1831-1842 (2012).
38. Itkin, T., *et al.* FGF-2 expands murine hematopoietic stem and progenitor cells via proliferation of stromal cells, c-Kit activation and CXCL12 downregulation. *Blood*, blood-2011-2011-394692 (2012).
39. Johns, J. & Borjesson, D. Downregulation of CXCL12 signaling and altered hematopoietic stem and progenitor cell trafficking in a murine model of acute Anaplasma phagocytophilum infection. *Innate immunity* **18**, 418-428 (2012).
40. Christopher, M.J., Rao, M., Liu, F., Woloszynek, J.R. & Link, D.C. Expression of the G-CSF receptor in monocytic cells is sufficient to mediate hematopoietic progenitor mobilization by G-CSF in mice. *Journal of Experimental Medicine*, jem. 20101700 (2011).
41. Demetri, G.D. & Griffin, J.D. Granulocyte colony-stimulating factor and its receptor. *Blood* **78**, 2791-2808 (1991).
42. Bernad, A., *et al.* Interleukin-6 is required in vivo for the regulation of stem cells and committed progenitors of the hematopoietic system. *Immunity* **1**, 725-731 (1994).
43. Cheng, C.-W., *et al.* Prolonged fasting reduces IGF-1/PKA to promote hematopoietic-stem-cell-based regeneration and reverse immunosuppression. *Cell stem cell* **14**, 810-823 (2014).
44. Vionnie, W., *et al.* Distinctive mesenchymal-parenchymal cell pairings govern B cell differentiation in the bone marrow. *Stem cell reports* **7**, 220-235 (2016).
45. Yue, R., Zhou, B.O., Shimada, I.S., Zhao, Z. & Morrison, S.J. Leptin receptor promotes adipogenesis and reduces osteogenesis by regulating mesenchymal stromal cells in adult bone marrow. *Cell stem cell* **18**, 782-796 (2016).
46. Zhou, B.O., Yue, R., Murphy, M.M., Peyer, J.G. & Morrison, S.J. Leptin-receptor-expressing mesenchymal stromal cells represent the main source of bone formed by adult bone marrow. *Cell stem cell* **15**, 154-168 (2014).
47. Butler, J.M., *et al.* Endothelial cells are essential for the self-renewal and repopulation of Notch-dependent hematopoietic stem cells. *Cell stem cell* **6**, 251-264 (2010).
48. Varnum-Finney, B., *et al.* Notch2 governs the rate of generation of mouse long- and short-term repopulating stem cells. *The Journal of clinical investigation* **121**, 1207-1216 (2011).
49. Stier, S., *et al.* Osteopontin is a hematopoietic stem cell niche component that negatively regulates stem cell pool size. *Journal of Experimental Medicine* **201**, 1781-1791 (2005).
50. Nakada, D., *et al.* Oestrogen increases haematopoietic stem-cell self-renewal in females and during pregnancy. *Nature* **505**, 555 (2014).
51. Himgburg, H.A., *et al.* Pleiotrophin mediates hematopoietic regeneration via activation of RAS. *The Journal of clinical investigation* **124**, 4753-4758 (2014).
52. Ding, L., Saunders, T.L., Enikolopov, G. & Morrison, S.J. Endothelial and perivascular cells maintain haematopoietic stem cells. *Nature* **481**, 457 (2012).
53. Calvi, L., *et al.* Osteoblastic cells regulate the haematopoietic stem cell niche. *Nature* **425**, 841 (2003).
54. Smith-Berdan, S., *et al.* Robo4 cooperates with CXCR4 to specify hematopoietic stem cell localization to bone marrow niches. *Cell stem cell* **8**, 72-83 (2011).
55. Smith-Berdan, S., Nguyen, A., Hong, M.A. & Forsberg, E.C. ROBO4-mediated vascular integrity regulates the directionality of hematopoietic stem cell trafficking. *Stem cell reports* **4**, 255-268 (2015).

56. Waterstrat, A., Rector, K., Geiger, H. & Liang, Y. Quantitative trait gene *Slit2* positively regulates murine hematopoietic stem cell numbers. *Scientific reports* **6**, 31412 (2016).
57. Yamazaki, S., *et al.* Nonmyelinating Schwann cells maintain hematopoietic stem cell hibernation in the bone marrow niche. *Cell* **147**, 1146-1158 (2011).
58. Kimura, S., Roberts, A.W., Metcalf, D. & Alexander, W.S. Hematopoietic stem cell deficiencies in mice lacking c-Mpl, the receptor for thrombopoietin. *Proceedings of the National Academy of Sciences* **95**, 1195-1200 (1998).
59. Qian, H., *et al.* Critical role of thrombopoietin in maintaining adult quiescent hematopoietic stem cells. *Cell stem cell* **1**, 671-684 (2007).
60. Yoshihara, H., *et al.* Thrombopoietin/MPL signaling regulates hematopoietic stem cell quiescence and interaction with the osteoblastic niche. *Cell stem cell* **1**, 685-697 (2007).
61. Sungaran, R., Markovic, B. & Chong, B. Localization and regulation of thrombopoietin mRNA expression in human kidney, liver, bone marrow, and spleen using in situ hybridization. *Blood* **89**, 101-107 (1997).
62. Sitnicka, E., *et al.* The effect of thrombopoietin on the proliferation and differentiation of murine hematopoietic stem cells. *Blood* **87**, 4998-5005 (1996).
63. Kaushansky, K., *et al.* Promotion of megakaryocyte progenitor expansion and differentiation by the c-Mpl ligand thrombopoietin. *Nature* **369**, 568 (1994).
64. Kaushansky, K., *et al.* Thrombopoietin, the Mpl ligand, is essential for full megakaryocyte development. *Proceedings of the National Academy of Sciences* **92**, 3234-3238 (1995).
65. De Sauvage, F.J., *et al.* Stimulation of megakaryocytopoiesis and thrombopoiesis by the c-Mpl ligand. *Nature* **369**, 533 (1994).
66. Cobas, M., *et al.* β -catenin is dispensable for hematopoiesis and lymphopoiesis. *Journal of Experimental Medicine* **199**, 221-229 (2004).
67. Koch, U., *et al.* Simultaneous loss of β - and γ -catenin does not perturb hematopoiesis or lymphopoiesis. *Blood* **111**, 160-164 (2008).
68. Sugimura, R., *et al.* Noncanonical Wnt signaling maintains hematopoietic stem cells in the niche. *Cell* **150**, 351-365 (2012).
69. Nilsson, S.K., Johnston, H.M. & Coverdale, J.A. Spatial localization of transplanted hemopoietic stem cells: inferences for the localization of stem cell niches. *Blood* **97**, 2293-2299 (2001).
70. Lo Celso, C., *et al.* Live-animal tracking of individual haematopoietic stem/progenitor cells in their niche. *Nature* **457**, 92-96 (2009).
71. Xie, Y., *et al.* Detection of functional haematopoietic stem cell niche using real-time imaging. *Nature* **457**, 97-101 (2009).
72. Kim, S., Lin, L., Brown, G.A., Hosaka, K. & Scott, E.W. Extended time-lapse in vivo imaging of tibia bone marrow to visualize dynamic hematopoietic stem cell engraftment. *Leukemia* **31**, 1582 (2017).
73. Haylock, D.N., *et al.* Hemopoietic stem cells with higher hemopoietic potential reside at the bone marrow endosteum. *Stem cells* **25**, 1062-1069 (2007).
74. Grassinger, J., Haylock, D.N., Williams, B., Olsen, G.H. & Nilsson, S.K. Phenotypically identical hemopoietic stem cells isolated from different regions of bone marrow have different biologic potential. *Blood* **116**, 3185-3196 (2010).
75. Lord, B.I., Testa, N.G. & Hendry, J.H. The relative spatial distributions of CFUs and CFUc in the normal mouse femur. *Blood* **46**, 65-72 (1975).
76. Gong, J.K. Endosteal marrow: a rich source of hematopoietic stem cells. *Science* **199**, 1443-1445 (1978).
77. Taichman, R.S. & Emerson, S.G. Human osteoblasts support hematopoiesis through the production of granulocyte colony-stimulating factor. *Journal of Experimental Medicine* **179**, 1677-1682 (1994).
78. Taichman, R.S., Reilly, M.J. & Emerson, S.G. Human osteoblasts support human hematopoietic progenitor cells in vitro bone marrow cultures. *Blood* **87**, 518-524 (1996).
79. El-Badri, N., Wang, B. & Good, R. Osteoblasts promote engraftment of allogeneic hematopoietic stem cells. *Experimental hematology* **26**, 110-116 (1998).
80. Zhang, J., *et al.* Identification of the haematopoietic stem cell niche and control of the niche size. *Nature* **425**, 836 (2003).
81. Ponomaryov, T., *et al.* Induction of the chemokine stromal-derived factor-1 following DNA damage improves human stem cell function. *The Journal of clinical investigation* **106**, 1331-1339 (2000).
82. Nilsson, S.K., *et al.* Osteopontin, a key component of the hematopoietic stem cell niche and regulator of primitive hematopoietic progenitor cells. *Blood* **106**, 1232-1239 (2005).
83. Grassinger, J., *et al.* Thrombin-cleaved osteopontin regulates hemopoietic stem and progenitor cell functions through interactions with $\alpha 9\beta 1$ and $\alpha 4\beta 1$ integrins. *Blood* **114**, 49-59 (2009).

84. Morad, V., *et al.* The myelopoietic supportive capacity of mesenchymal stromal cells is uncoupled from multipotency and is influenced by lineage determination and interference with glycosylation. *Stem cells* **26**, 2275-2286 (2008).
85. Jung, Y., *et al.* Annexin II expressed by osteoblasts and endothelial cells regulates stem cell adhesion, homing, and engraftment following transplantation. *Blood* **110**, 82-90 (2007).
86. Puri, M.C. & Bernstein, A. Requirement for the TIE family of receptor tyrosine kinases in adult but not fetal hematopoiesis. *Proceedings of the National Academy of Sciences* **100**, 12753-12758 (2003).
87. Arai, F., *et al.* Tie2/angiopoietin-1 signaling regulates hematopoietic stem cell quiescence in the bone marrow niche. *Cell* **118**, 149-161 (2004).
88. Ding, L. & Morrison, S.J. Haematopoietic stem cells and early lymphoid progenitors occupy distinct bone marrow niches. *Nature* **495**, 231 (2013).
89. Milner, L.A. & Bigas, A. Notch as a mediator of cell fate determination in hematopoiesis: evidence and speculation. *Blood* **93**, 2431-2448 (1999).
90. Karanu, F.N., *et al.* The notch ligand jagged-1 represents a novel growth factor of human hematopoietic stem cells. *Journal of Experimental Medicine* **192**, 1365-1372 (2000).
91. Kode, A., *et al.* FoxO1-dependent induction of acute myeloid leukemia by osteoblasts in mice. *Leukemia* **30**, 1 (2016).
92. Maillard, I., *et al.* Canonical notch signaling is dispensable for the maintenance of adult hematopoietic stem cells. *Cell stem cell* **2**, 356-366 (2008).
93. Kunisaki, Y., *et al.* Arteriolar niches maintain haematopoietic stem cell quiescence. *Nature* **502**, 637 (2013).
94. Nombela-Arrieta, C., *et al.* Quantitative imaging of haematopoietic stem and progenitor cell localization and hypoxic status in the bone marrow microenvironment. *Nature cell biology* **15**, 533 (2013).
95. Bowers, M., *et al.* Osteoblast ablation reduces normal long-term hematopoietic stem cell self-renewal but accelerates leukemia development. *Blood* **125**, 2678-2688 (2015).
96. Krevvata, M., *et al.* Inhibition of leukemia cell engraftment and disease progression in mice by osteoblasts. *Blood* **124**, 2834-2846 (2014).
97. Itkin, T., *et al.* Distinct bone marrow blood vessels differentially regulate haematopoiesis. *Nature* **532**, 323 (2016).
98. Acar, M., *et al.* Deep imaging of bone marrow shows non-dividing stem cells are mainly perisinusoidal. *Nature* **526**, 126 (2015).
99. Chen, J.Y., *et al.* Hoxb5 marks long-term haematopoietic stem cells and reveals a homogenous perivascular niche. *Nature* **530**, 223 (2016).
100. Koechlein, C.S., *et al.* High-resolution imaging and computational analysis of haematopoietic cell dynamics in vivo. *Nature communications* **7**, 12169 (2016).
101. Méndez-Ferrer, S., *et al.* Mesenchymal and haematopoietic stem cells form a unique bone marrow niche. *nature* **466**, 829 (2010).
102. Sacchetti, B., *et al.* Self-renewing osteoprogenitors in bone marrow sinusoids can organize a hematopoietic microenvironment. *Cell* **131**, 324-336 (2007).
103. Kobayashi, H., *et al.* Angiocrine factors from Akt-activated endothelial cells balance self-renewal and differentiation of haematopoietic stem cells. *Nature cell biology* **12**, 1046 (2010).
104. Poulos, M.G., *et al.* Endothelial Jagged-1 is necessary for homeostatic and regenerative hematopoiesis. *Cell reports* **4**, 1022-1034 (2013).
105. Rafii, S., Butler, J.M. & Ding, B.-S. Angiocrine functions of organ-specific endothelial cells. *Nature* **529**, 316 (2016).
106. Rafii, S., *et al.* Human bone marrow microvascular endothelial cells support long-term proliferation and differentiation of myeloid and megakaryocytic progenitors. *Blood* **86**, 3353-3363 (1995).
107. Winkler, I.G., *et al.* Vascular niche E-selectin regulates hematopoietic stem cell dormancy, self renewal and chemoresistance. *Nature medicine* **18**, 1651 (2012).
108. Sugiyama, T., Kohara, H., Noda, M. & Nagasawa, T. Maintenance of the hematopoietic stem cell pool by CXCL12-CXCR4 chemokine signaling in bone marrow stromal cell niches. *Immunity* **25**, 977-988 (2006).
109. Asada, N., *et al.* Differential cytokine contributions of perivascular haematopoietic stem cell niches. *Nature cell biology* **19**, 214 (2017).
110. Kusumbe, A.P., *et al.* Age-dependent modulation of vascular niches for haematopoietic stem cells. *Nature* **532**, 380 (2016).
111. Spencer, J.A., *et al.* Direct measurement of local oxygen concentration in the bone marrow of live animals. *Nature* **508**, 269 (2014).
112. Takubo, K., *et al.* Regulation of the HIF-1 α level is essential for hematopoietic stem cells. *Cell stem cell* **7**, 391-402 (2010).

113. Katayama, Y., *et al.* Signals from the sympathetic nervous system regulate hematopoietic stem cell egress from bone marrow. *Cell* **124**, 407-421 (2006).
114. Yamazaki, K. & Allen, T.D. Ultrastructural morphometric study of efferent nerve terminals on murine bone marrow stromal cells, and the recognition of a novel anatomical unit: The “neuro-reticular complex”. *Developmental Dynamics* **187**, 261-276 (1990).
115. Kalinkovich, A., *et al.* Blood-forming stem cells are nervous: direct and indirect regulation of immature human CD34+ cells by the nervous system. *Brain, behavior, and immunity* **23**, 1059-1065 (2009).
116. Méndez-Ferrer, S., Lucas, D., Battista, M. & Frenette, P.S. Haematopoietic stem cell release is regulated by circadian oscillations. *Nature* **452**, 442 (2008).
117. Asada, N., *et al.* Matrix-embedded osteocytes regulate mobilization of hematopoietic stem/progenitor cells. *Cell stem cell* **12**, 737-747 (2013).
118. Asada, N. & Katayama, Y. Regulation of hematopoiesis in endosteal microenvironments. *International journal of hematology* **99**, 679-684 (2014).
119. Yamazaki, S., *et al.* TGF- β as a candidate bone marrow niche signal to induce hematopoietic stem cell hibernation. *Blood* **113**, 1250-1256 (2009).
120. Tavassoli, M. & Aoki, M. Localization of megakaryocytes in the bone marrow. *Blood cells* **15**, 3-14 (1989).
121. Nakamura-Ishizu, A., Takubo, K., Fujioka, M. & Suda, T. Megakaryocytes are essential for HSC quiescence through the production of thrombopoietin. *Biochemical and biophysical research communications* **454**, 353-357 (2014).
122. Söderberg, S.S., Karlsson, G. & Karlsson, S. Complex and Context Dependent Regulation of Hematopoiesis by TGF- β Superfamily Signaling. *Annals of the New York Academy of Sciences* **1176**, 55-69 (2009).
123. Brun, A.C.M., Fan, X., Björnsson, J.M., Humphries, R.K. & Karlsson, S. Enforced adenoviral vector-mediated expression of HOXB4 in human umbilical cord blood cd34+ cells promotes myeloid differentiation but not proliferation. *Molecular Therapy* **8**, 618-628 (2003).
124. Olson, T.S., *et al.* Megakaryocytes promote murine osteoblastic HSC niche expansion and stem cell engraftment after radioablative conditioning. *Blood* **121**, 5238-5249 (2013).
125. Alexander, K.A., *et al.* Osteal macrophages promote in vivo intramembranous bone healing in a mouse tibial injury model. *Journal of bone and mineral research* **26**, 1517-1532 (2011).
126. Chang, M.K., *et al.* Osteal tissue macrophages are intercalated throughout human and mouse bone lining tissues and regulate osteoblast function in vitro and in vivo. *The Journal of Immunology* **181**, 1232-1244 (2008).
127. Pettit, A.R., Chang, M.K., Hume, D.A. & Raggatt, L.-J. Osteal macrophages: a new twist on coupling during bone dynamics. *Bone* **43**, 976-982 (2008).
128. Winkler, I.G., *et al.* Bone marrow macrophages maintain hematopoietic stem cell (HSC) niches and their depletion mobilizes HSCs. *Blood* **116**, 4815-4828 (2010).
129. Chow, A., *et al.* Bone marrow CD169+ macrophages promote the retention of hematopoietic stem and progenitor cells in the mesenchymal stem cell niche. *Journal of Experimental Medicine*, jem. 20101688 (2011).
130. Albiero, M., *et al.* Bone marrow macrophages contribute to diabetic stem cell mobilopathy by producing oncostatin M. *Diabetes*, db141473 (2015).
131. Williams, D.A., Rios, M., Stephens, C. & Patel, V.P. Fibronectin and VLA-4 in haematopoietic stem cell–microenvironment interactions. *Nature* **352**, 438 (1991).
132. Scott, L.M., Priestley, G.V. & Papayannopoulou, T. Deletion of $\alpha 4$ integrins from adult hematopoietic cells reveals roles in homeostasis, regeneration, and homing. *Molecular and cellular biology* **23**, 9349-9360 (2003).
133. Dutta, P., *et al.* Myocardial infarction accelerates atherosclerosis. *Nature* **487**, 325 (2012).
134. Dutta, P., *et al.* Macrophages retain hematopoietic stem cells in the spleen via VCAM-1. *Journal of Experimental Medicine* **212**, 497-512 (2015).
135. Casanova-Acebes, M., *et al.* Rhythmic modulation of the hematopoietic niche through neutrophil clearance. *Cell* **153**, 1025-1035 (2013).
136. Ludin, A., *et al.* Monocytes-macrophages that express α -smooth muscle actin preserve primitive hematopoietic cells in the bone marrow. *Nature immunology* **13**, 1072 (2012).
137. Hoggatt, J., Singh, P., Sampath, J. & Pelus, L.M. Prostaglandin E2 enhances hematopoietic stem cell homing, survival, and proliferation. *Blood* **113**, 5444-5455 (2009).
138. Chow, A., *et al.* CD169+ macrophages provide a niche promoting erythropoiesis under homeostasis and stress. *Nature medicine* **19**, 429 (2013).
139. Ramos, P., *et al.* Macrophages support pathological erythropoiesis in polycythemia vera and β -thalassemia. *Nature medicine* **19**, 437 (2013).

140. Wheway, J., *et al.* A fundamental bimodal role for neuropeptide Y1 receptor in the immune system. *Journal of Experimental Medicine* **202**, 1527-1538 (2005).
141. Kuo, L.E., *et al.* Neuropeptide Y acts directly in the periphery on fat tissue and mediates stress-induced obesity and metabolic syndrome. *Nature medicine* **13**, 803 (2007).
142. Lee, N.J. & Herzog, H. NPY regulation of bone remodelling. *Neuropeptides* **43**, 457-463 (2009).
143. Park, M.H., *et al.* Neuropeptide Y regulates the hematopoietic stem cell microenvironment and prevents nerve injury in the bone marrow. *The EMBO journal* **34**, 1648-1660 (2015).
144. Summers, C., *et al.* Neutrophil kinetics in health and disease. *Trends in immunology* **31**, 318-324 (2010).
145. Liu, F., Wu, H.Y., Wesselschmidt, R., Kornaga, T. & Link, D.C. Impaired production and increased apoptosis of neutrophils in granulocyte colony-stimulating factor receptor-deficient mice. *Immunity* **5**, 491-501 (1996).
146. Singh, P., Hu, P., Hoggatt, J., Moh, A. & Pelus, L.M. Expansion of bone marrow neutrophils following G-CSF administration in mice results in osteolineage cell apoptosis and mobilization of hematopoietic stem and progenitor cells. *Leukemia* **26**, 2375 (2012).
147. Petit, I., *et al.* G-CSF induces stem cell mobilization by decreasing bone marrow SDF-1 and up-regulating CXCR4. *Nature immunology* **3**, 687 (2002).
148. Valenzuela-Fernández, A.n., *et al.* Leukocyte elastase negatively regulates stromal cell-derived factor-1 (SDF-1)/CXCR4 binding and functions by amino-terminal processing of SDF-1 and CXCR4. *Journal of Biological Chemistry* **277**, 15677-15689 (2002).
149. Lévesque, J.-P., Takamatsu, Y., Nilsson, S.K., Haylock, D.N. & Simmons, P.J. Vascular cell adhesion molecule-1 (CD106) is cleaved by neutrophil proteases in the bone marrow following hematopoietic progenitor cell mobilization by granulocyte colony-stimulating factor. *Blood* **98**, 1289-1297 (2001).
150. Lévesque, J.-P., Hendy, J., Winkler, I.G., Takamatsu, Y. & Simmons, P.J. Granulocyte colony-stimulating factor induces the release in the bone marrow of proteases that cleave c-KIT receptor (CD117) from the surface of hematopoietic progenitor cells. *Experimental hematology* **31**, 109-117 (2003).
151. Heissig, B., *et al.* Recruitment of stem and progenitor cells from the bone marrow niche requires MMP-9 mediated release of kit-ligand. *Cell* **109**, 625-637 (2002).
152. Levesque, J.-P., *et al.* Characterization of hematopoietic progenitor mobilization in protease-deficient mice. *Blood* **104**, 65-72 (2004).
153. Wilson, A., *et al.* Hematopoietic stem cells reversibly switch from dormancy to self-renewal during homeostasis and repair. *Cell* **135**, 1118-1129 (2008).
154. Kreso, A. & Dick, J.E. Evolution of the cancer stem cell model. *Cell stem cell* **14**, 275-291 (2014).
155. Walkley, C.R., *et al.* A microenvironment-induced myeloproliferative syndrome caused by retinoic acid receptor γ deficiency. *Cell* **129**, 1097-1110 (2007).
156. Walkley, C.R., Shea, J.M., Sims, N.A., Purton, L.E. & Orkin, S.H. Rb regulates interactions between hematopoietic stem cells and their bone marrow microenvironment. *Cell* **129**, 1081-1095 (2007).
157. Schepers, K., Campbell, T.B. & Passegué, E. Normal and leukemic stem cell niches: insights and therapeutic opportunities. *Cell stem cell* **16**, 254-267 (2015).
158. Wiseman, D.H. Donor cell leukemia: a review. *Biology of Blood and Marrow Transplantation* **17**, 771-789 (2011).
159. Kode, A., *et al.* Leukaemogenesis induced by an activating β -catenin mutation in osteoblasts. *Nature* **506**, 240 (2014).
160. Dong, L., *et al.* Leukaemogenic effects of Ptpn11 activating mutations in the stem cell microenvironment. *Nature* **539**, 304 (2016).
161. Geyh, S., *et al.* Insufficient stromal support in MDS results from molecular and functional deficits of mesenchymal stromal cells. *Leukemia* **27**, 1841 (2013).
162. Raaijmakers, M.H., *et al.* Bone progenitor dysfunction induces myelodysplasia and secondary leukaemia. *Nature* **464**, 852 (2010).
163. Bruns, I., *et al.* Multiple myeloma-related deregulation of bone marrow-derived CD34+ hematopoietic stem and progenitor cells. *Blood* **120**, 2620-2630 (2012).
164. Asada, N., Takeishi, S. & Frenette, P.S. Complexity of bone marrow hematopoietic stem cell niche. *Int J Hematol* **106**, 45-54 (2017).
165. Kim, Y.-W., *et al.* Defective Notch activation in microenvironment leads to myeloproliferative disease. *Blood* **112**, 4628-4638 (2008).
166. Zambetti, N.A., *et al.* Mesenchymal inflammation drives genotoxic stress in hematopoietic stem cells and predicts disease evolution in human pre-leukemia. *Cell Stem Cell* **19**, 613-627 (2016).
167. Medyouf, H., *et al.* Myelodysplastic cells in patients reprogram mesenchymal stromal cells to establish a transplantable stem cell niche disease unit. *Cell stem cell* **14**, 824-837 (2014).
168. Zhang, B., *et al.* Inhibition of interleukin-1 signaling enhances elimination of tyrosine kinase inhibitor-treated CML stem cells. *Blood* **128**, 2671-2682 (2016).

169. Kim, J.-A., *et al.* Microenvironmental remodeling as a parameter and prognostic factor of heterogeneous leukemogenesis in acute myelogenous leukemia. *Cancer research* **75**, 2222-2231 (2015).
170. Ge, J., Hou, R., Liu, Q., Zhu, R. & Liu, K. Stromal-derived factor-1 deficiency in the bone marrow of acute myeloid leukemia. *International journal of hematology* **93**, 750 (2011).
171. Crofton, P., *et al.* Effects of intensive chemotherapy on bone and collagen turnover and the growth hormone axis in children with acute lymphoblastic leukemia. *The Journal of Clinical Endocrinology & Metabolism* **83**, 3121-3129 (1998).
172. Fitter, S., *et al.* Long-term imatinib therapy promotes bone formation in CML patients. *Blood* **111**, 2538-2547 (2008).
173. El-Ziny, M.A., *et al.* Low turnover bone disease in Egyptian children with acute leukemia. *Hematology* **10**, 327-333 (2005).
174. Frisch, B.J., *et al.* Functional inhibition of osteoblastic cells in an in vivo mouse model of myeloid leukemia. *Blood* **119**, 540-550 (2012).
175. Hanoun, M., *et al.* Acute myelogenous leukemia-induced sympathetic neuropathy promotes malignancy in an altered hematopoietic stem cell niche. *Cell Stem Cell* **15**, 365-375 (2014).
176. Wang, W., *et al.* Aberrant Notch signaling in the bone marrow microenvironment of acute lymphoid leukemia suppresses osteoblast-mediated support of hematopoietic niche function. *Cancer research, canres.* 2092.2015 (2016).
177. Reinisch, A., *et al.* A humanized bone marrow ossicle xenotransplantation model enables improved engraftment of healthy and leukemic human hematopoietic cells. *Nature medicine* **22**, 812 (2016).
178. Berk, L.C., *et al.* Disturbed CXCR4/CXCL12 axis in paediatric precursor B-cell acute lymphoblastic leukaemia. *British journal of haematology* **166**, 240-249 (2014).
179. Lim, M., *et al.* Altered mesenchymal niche cells impede generation of normal hematopoietic progenitor cells in leukemic bone marrow. *Leukemia* **30**, 154 (2016).
180. Colmone, A., *et al.* Leukemic cells create bone marrow niches that disrupt the behavior of normal hematopoietic progenitor cells. *Science* **322**, 1861-1865 (2008).
181. Schepers, K., *et al.* Myeloproliferative neoplasia remodels the endosteal bone marrow niche into a self-reinforcing leukemic niche. *Cell stem cell* **13**, 285-299 (2013).
182. Zhang, B., *et al.* Altered microenvironmental regulation of leukemic and normal stem cells in chronic myelogenous leukemia. *Cancer cell* **21**, 577-592 (2012).
183. Veiga, J.P., Costa, L.F., Sallan, S.E., Nadler, L.M. & Cardoso, A.A. Leukemia-stimulated bone marrow endothelium promotes leukemia cell survival. *Experimental hematology* **34**, 610-621 (2006).
184. Hatfield, K., *et al.* Primary human acute myeloid leukaemia cells increase the proliferation of microvascular endothelial cells through the release of soluble mediators. *British journal of haematology* **144**, 53-68 (2009).
185. Pizzo, R.J., *et al.* Phenotypic, genotypic, and functional characterization of normal and acute myeloid leukemia-derived marrow endothelial cells. *Experimental hematology* **44**, 378-389 (2016).
186. Cogle, C.R., *et al.* Functional integration of acute myeloid leukemia into the vascular niche. *Leukemia* **28**, 1978 (2014).
187. Bosse, R.C., *et al.* Chemosensitizing AML cells by targeting bone marrow endothelial cells. *Experimental hematology* **44**, 363-377. e365 (2016).
188. Arranz, L., *et al.* Neuropathy of haematopoietic stem cell niche is essential for myeloproliferative neoplasms. *Nature* **512**, 78 (2014).
189. Perez-Atayde, A.R., *et al.* Spectrum of tumor angiogenesis in the bone marrow of children with acute lymphoblastic leukemia. *The American journal of pathology* **150**, 815 (1997).
190. Aguayo, A., *et al.* Angiogenesis in acute and chronic leukemias and myelodysplastic syndromes. *Blood* **96**, 2240-2245 (2000).
191. Huan, J., *et al.* RNA trafficking by acute myelogenous leukemia exosomes. *Cancer research* **73**, 918-929 (2013).
192. Huang, J., *et al.* Mesenchymal stromal cells derived from acute myeloid leukemia bone marrow exhibit aberrant cytogenetics and cytokine elaboration. *Blood Cancer Journal* **5**, e302 (2015).
193. Corrado, C., *et al.* Chronic myelogenous leukaemia exosomes modulate bone marrow microenvironment through activation of epidermal growth factor receptor. *Journal of cellular and molecular medicine* **20**, 1829-1839 (2016).
194. Taverna, S., *et al.* Exosomal shuttling of miR-126 in endothelial cells modulates adhesive and migratory abilities of chronic myelogenous leukemia cells. *Molecular cancer* **13**, 169 (2014).
195. Paggetti, J., *et al.* Exosomes released by chronic lymphocytic leukemia cells induce the transition of stromal cells into cancer-associated fibroblasts. *Blood* **126**, 1106-1117 (2015).
196. Muntión, S., *et al.* Microvesicles from mesenchymal stromal cells are involved in HPC-microenvironment crosstalk in myelodysplastic patients. *PloS one* **11**, e0146722 (2016).

197. Yamamoto, J.F. & Goodman, M.T. Patterns of leukemia incidence in the United States by subtype and demographic characteristics, 1997–2002. *Cancer Causes & Control* **19**, 379-390 (2008).
198. Derolf, Å.R., *et al.* Improved patient survival for acute myeloid leukemia: a population-based study of 9729 patients diagnosed in Sweden between 1973 and 2005. *Blood* **113**, 3666-3672 (2009).
199. Juliusson, G., *et al.* Age and acute myeloid leukemia: real world data on decision to treat and outcomes from the Swedish Acute Leukemia Registry. *Blood* **113**, 4179-4187 (2009).
200. Shah, A., Andersson, T.M.L., Racht, B., Björkholm, M. & Lambert, P.C. Survival and cure of acute myeloid leukaemia in England, 1971-2006: a population-based study. *British journal of haematology* **162**, 509-516 (2013).
201. Meyers, J., Yu, Y., Kaye, J.A. & Davis, K.L. Medicare fee-for-service enrollees with primary acute myeloid leukemia: an analysis of treatment patterns, survival, and healthcare resource utilization and costs. *Applied health economics and health policy* **11**, 275-286 (2013).
202. Döhner, H., *et al.* Diagnosis and management of acute myeloid leukemia in adults: recommendations from an international expert panel, on behalf of the European LeukemiaNet. *Blood* **115**, 453-474 (2010).
203. Sant, M., *et al.* Survival for haematological malignancies in Europe between 1997 and 2008 by region and age: results of EURO CARE-5, a population-based study. *The Lancet Oncology* **15**, 931-942 (2014).
204. Sill, H., Olipitz, W., Zebisch, A., Schulz, E. & Wölfler, A. Therapy-related myeloid neoplasms: pathobiology and clinical characteristics. *British journal of pharmacology* **162**, 792-805 (2011).
205. Shimizu, Y., Schull, W.J. & Kato, H. Cancer risk among atomic bomb survivors: the RERF Life Span Study. *JAMA* **264**, 601-604 (1990).
206. Goldin, L.R., *et al.* Familial aggregation of acute myeloid leukemia and myelodysplastic syndromes. *Journal of clinical oncology* **30**, 179 (2012).
207. Seif, A.E. Pediatric leukemia predisposition syndromes: clues to understanding leukemogenesis. *Cancer genetics* **204**, 227-244 (2011).
208. Mrózek, K., *et al.* Prognostic significance of the European LeukemiaNet standardized system for reporting cytogenetic and molecular alterations in adults with acute myeloid leukemia. *Journal of clinical oncology* **30**, 4515 (2012).
209. Grimwade, D. & Mrózek, K. Diagnostic and prognostic value of cytogenetics in acute myeloid leukemia. *Hematology/Oncology Clinics* **25**, 1135-1161 (2011).
210. Grimwade, D., *et al.* Refinement of cytogenetic classification in acute myeloid leukemia: determination of prognostic significance of rare recurring chromosomal abnormalities amongst 5,876 younger adult patients treated in the UK Medical Research Council trials. *Blood*, blood-2009-2011-254441 (2010).
211. Network, C.G.A.R. Genomic and epigenomic landscapes of adult de novo acute myeloid leukemia. *New England Journal of Medicine* **368**, 2059-2074 (2013).
212. Patel, J.P., *et al.* Prognostic relevance of integrated genetic profiling in acute myeloid leukemia. *New England Journal of Medicine* **366**, 1079-1089 (2012).
213. Arber, D.A., *et al.* The 2016 revision to the World Health Organization (WHO) classification of myeloid neoplasms and acute leukemia. *Blood*, blood-2016-2003-643544 (2016).
214. Lindsley, R.C., *et al.* Acute myeloid leukemia ontogeny is defined by distinct somatic mutations. *Blood* **125**, 1367-1376 (2015).
215. Khwaja, A., *et al.* Acute myeloid leukaemia. *Nature reviews Disease primers* **2**, 16010 (2016).
216. Grisolan, J.L., O'Neal, J., Cain, J. & Tomasson, M.H. An activated receptor tyrosine kinase, TEL/PDGFB β R, cooperates with AML1/ETO to induce acute myeloid leukemia in mice. *Proceedings of the National Academy of Sciences* **100**, 9506-9511 (2003).
217. Schessl, C., *et al.* The AML1-ETO fusion gene and the FLT3 length mutation collaborate in inducing acute leukemia in mice. *The Journal of clinical investigation* **115**, 2159-2168 (2005).
218. Gilliland, D.G. & Griffin, J.D. The roles of FLT3 in hematopoiesis and leukemia. *Blood* **100**, 1532-1542 (2002).
219. Takahashi, S. Current findings for recurring mutations in acute myeloid leukemia. *Journal of hematology & oncology* **4**, 36 (2011).
220. Kihara, R., *et al.* Comprehensive analysis of genetic alterations and their prognostic impacts in adult acute myeloid leukemia patients. *Leukemia* **28**, 1586 (2014).
221. Greif, P.A., *et al.* GATA2 zinc finger 1 mutations associated with biallelic CEBPA mutations define a unique genetic entity of acute myeloid leukemia. *Blood* **120**, 395-403 (2012).
222. Corces-Zimmerman, M.R., Hong, W.-J., Weissman, I.L., Medeiros, B.C. & Majeti, R. Preleukemic mutations in human acute myeloid leukemia affect epigenetic regulators and persist in remission. *Proceedings of the National Academy of Sciences* **111**, 2548-2553 (2014).
223. Shlush, L.I., *et al.* Identification of pre-leukaemic haematopoietic stem cells in acute leukaemia. *Nature* **506**, 328 (2014).

224. Krönke, J., *et al.* Clonal evolution in relapsed NPM1-mutated acute myeloid leukemia. *Blood* **122**, 100-108 (2013).
225. Genovese, G., *et al.* Clonal hematopoiesis and blood-cancer risk inferred from blood DNA sequence. *New England Journal of Medicine* **371**, 2477-2487 (2014).
226. Jaiswal, S., *et al.* Age-related clonal hematopoiesis associated with adverse outcomes. *New England Journal of Medicine* **371**, 2488-2498 (2014).
227. Busque, L., *et al.* Recurrent somatic TET2 mutations in normal elderly individuals with clonal hematopoiesis. *Nature genetics* **44**, 1179 (2012).
228. Papaemmanuil, E., *et al.* Genomic classification and prognosis in acute myeloid leukemia. *New England Journal of Medicine* **374**, 2209-2221 (2016).
229. Döhner, H., Weisdorf, D.J. & Bloomfield, C.D. Acute myeloid leukemia. *New England Journal of Medicine* **373**, 1136-1152 (2015).
230. Estey, E.H. Acute myeloid leukemia: 2014 Update on risk-stratification and management. *American journal of hematology* **89**, 1063-1081 (2014).
231. Löwenberg, B. Sense and nonsense of high-dose cytarabine for acute myeloid leukemia. *Blood* **121**, 26-28 (2013).
232. Löwenberg, B., *et al.* Cytarabine dose for acute myeloid leukemia. *New England Journal of Medicine* **364**, 1027-1036 (2011).
233. Gong, Q., *et al.* High doses of daunorubicin during induction therapy of newly diagnosed acute myeloid leukemia: a systematic review and meta-analysis of prospective clinical trials. *PLoS one* **10**, e0125612 (2015).
234. Li, X., Xu, S., Tan, Y. & Chen, J. The effects of idarubicin versus other anthracyclines for induction therapy of patients with newly diagnosed leukaemia. *The Cochrane Library* (2015).
235. De Lima, M., *et al.* Implications of potential cure in acute myelogenous leukemia: development of subsequent cancer and return to work. *Blood* **90**, 4719-4724 (1997).
236. Fernandez, H.F., *et al.* Anthracycline dose intensification in acute myeloid leukemia. *New England Journal of Medicine* **361**, 1249-1259 (2009).
237. Burnett, A.K., *et al.* Optimization of chemotherapy for younger patients with acute myeloid leukemia: results of the medical research council AML15 trial. *Journal of clinical oncology* **31**, 3360-3368 (2013).
238. Carella, A.M., *et al.* Treatment of "poor risk" acute myeloid leukemia with fludarabine, cytarabine and G-CSF (flag regimen): a single center study. *Leukemia & lymphoma* **40**, 295-303 (2001).
239. Herzig, R.H., Lazarus, H.M., Wolff, S.N., Phillips, G.L. & Herzig, G.P. High-dose cytosine arabinoside therapy with and without anthracycline antibiotics for remission reinduction of acute nonlymphoblastic leukemia. *Journal of Clinical Oncology* **3**, 992-997 (1985).
240. Dombret, H., *et al.* International phase 3 study of azacitidine vs conventional care regimens in older patients with newly diagnosed AML with > 30% blasts. *Blood* **126**, 291-299 (2015).
241. Hills, R.K., *et al.* Addition of gemtuzumab ozogamicin to induction chemotherapy in adult patients with acute myeloid leukaemia: a meta-analysis of individual patient data from randomised controlled trials. *The lancet oncology* **15**, 986-996 (2014).
242. Amadori, S., *et al.* Gemtuzumab ozogamicin versus best supportive care in older patients with newly diagnosed acute myeloid leukemia unsuitable for intensive chemotherapy: results of the randomized phase III EORTC-GIMEMA AML-19 trial. *Journal of Clinical Oncology* (2016).
243. Stone, R.M., *et al.* The multi-kinase inhibitor midostaurin (M) prolongs survival compared with placebo (P) in combination with daunorubicin (D)/cytarabine (C) induction (ind), high-dose C consolidation (consol), and as maintenance (maint) therapy in newly diagnosed acute myeloid leukemia (AML) patients (pts) age 18-60 with FLT3 mutations (mut): an international prospective randomized (rand) P-controlled double-blind trial (CALGB 10603/RATIFY [Alliance]). (Am Soc Hematology, 2015).
244. Armand, P., *et al.* Validation and refinement of the disease risk index for allogeneic stem cell transplantation: a study from the CIBMTR. *Blood*, blood-2014-2001-552984 (2014).
245. Gupta, V., Tallman, M.S. & Weisdorf, D.J. Allogeneic hematopoietic cell transplantation for adults with acute myeloid leukemia: myths, controversies, and unknowns. *Blood* **117**, 2307-2318 (2011).
246. Sorror, M.L., *et al.* Comorbidity-age index: a clinical measure of biologic age before allogeneic hematopoietic cell transplantation. *Journal of Clinical Oncology* **32**, 3249 (2014).
247. Koreth, J., *et al.* Allogeneic stem cell transplantation for acute myeloid leukemia in first complete remission: systematic review and meta-analysis of prospective clinical trials. *Jama* **301**, 2349-2361 (2009).
248. Yanada, M., Matsuo, K., Emi, N. & Naoe, T. Efficacy of allogeneic hematopoietic stem cell transplantation depends on cytogenetic risk for acute myeloid leukemia in first disease remission. *Cancer* **103**, 1652-1658 (2005).

249. Weick, J.K., *et al.* A randomized investigation of high-dose versus standard-dose cytosine arabinoside with daunorubicin in patients with previously untreated acute myeloid leukemia: a Southwest Oncology Group study. *Blood* **88**, 2841-2851 (1996).
250. Popat, U., *et al.* Long-term outcome of reduced-intensity allogeneic hematopoietic SCT in patients with AML in CR. *Bone marrow transplantation* **47**, 212 (2012).
251. Sorrow, M.L., *et al.* Hematopoietic cell transplantation (HCT)-specific comorbidity index: a new tool for risk assessment before allogeneic HCT. *Blood* **106**, 2912-2919 (2005).
252. Appelbaum, F.R. The current status of hematopoietic cell transplantation. *Annual review of medicine* **54**, 491-512 (2003).
253. Vellenga, E., *et al.* Autologous peripheral blood stem cell transplantation for acute myeloid leukemia. *Blood*, blood-2011-2007-370247 (2011).
254. Demirer, T., *et al.* Transplantation of allogeneic hematopoietic stem cells: an emerging treatment modality for solid tumors. *Nature Reviews Clinical Oncology* **5**, 256 (2008).
255. Gupta, V., *et al.* Comparable survival after HLA-well-matched unrelated or matched sibling donor transplantation for acute myeloid leukemia in first remission with unfavorable cytogenetics at diagnosis. *Blood*, blood-2010-2004-278317 (2010).
256. Litzow, M.R., *et al.* Allogeneic transplantation for therapy-related myelodysplastic syndrome and acute myeloid leukemia. *Blood* **115**, 1850-1857 (2010).
257. McClune, B.L., *et al.* Effect of age on outcome of reduced-intensity hematopoietic cell transplantation for older patients with acute myeloid leukemia in first complete remission or with myelodysplastic syndrome. *Journal of Clinical Oncology* **28**, 1878 (2010).
258. Farag, S.S., *et al.* Comparison of reduced-intensity hematopoietic cell transplantation with chemotherapy in patients age 60-70 years with acute myelogenous leukemia in first remission. *Biology of Blood and Marrow Transplantation* **17**, 1796-1803 (2011).
259. Cornelissen, J.J., *et al.* The European LeukemiaNet AML Working Party consensus statement on allogeneic HSCT for patients with AML in remission: an integrated-risk adapted approach. *Nature reviews Clinical oncology* **9**, 579 (2012).
260. Nivison-Smith, I., *et al.* Relative survival of long-term hematopoietic cell transplant recipients approaches general population rates. *Biology of Blood and Marrow Transplantation* **15**, 1323-1330 (2009).
261. Thomas, E.D. Bone marrow transplantation: a review. in *Seminars in hematology*, Vol. 36 95-103 (1999).
262. Gragert, L., *et al.* HLA match likelihoods for hematopoietic stem-cell grafts in the US registry. *New England Journal of Medicine* **371**, 339-348 (2014).
263. Anasetti, C., *et al.* Peripheral-blood stem cells versus bone marrow from unrelated donors. *New England Journal of Medicine* **367**, 1487-1496 (2012).
264. Pasquini, M.C., *et al.* Comparative outcomes of donor graft CD34+ selection and immune suppressive therapy as graft-versus-host disease prophylaxis for patients with acute myeloid leukemia in complete remission undergoing HLA-matched sibling allogeneic hematopoietic cell transplantation. *Journal of Clinical Oncology* **30**, 3194 (2012).
265. Delaney, C., Gutman, J.A. & Appelbaum, F.R. Cord blood transplantation for haematological malignancies: conditioning regimens, double cord transplant and infectious complications. *British journal of haematology* **147**, 207-216 (2009).
266. Munoz, J., *et al.* Concise review: umbilical cord blood transplantation: past, present, and future. *Stem cells translational medicine* **3**, 1435-1443 (2014).
267. Barker, J.N. Umbilical cord blood (UCB) transplantation: an alternative to the use of unrelated volunteer donors? *ASH Education Program Book* **2007**, 55-61 (2007).
268. Wagner, J.E., *et al.* Transplantation of unrelated donor umbilical cord blood in 102 patients with malignant and nonmalignant diseases: influence of CD34 cell dose and HLA disparity on treatment-related mortality and survival. *Blood* **100**, 1611-1618 (2002).
269. Brunstein, C.G., *et al.* Allogeneic hematopoietic cell transplantation for hematological malignancy: relative risks and benefits of double umbilical cord blood. *Blood*, blood-2010-2005-285304 (2010).
270. Danby, R. & Rocha, V. Improving engraftment and immune reconstitution in umbilical cord blood transplantation. *Frontiers in immunology* **5**, 68 (2014).
271. Barker, J.N., *et al.* Searching for unrelated donor hematopoietic stem cells: availability and speed of umbilical cord blood versus bone marrow. *Biology of Blood and Marrow Transplantation* **8**, 257-260 (2002).
272. Akel, S., Regan, D., Wall, D., Petz, L. & McCullough, J. Current thawing and infusion practice of cryopreserved cord blood: the impact on graft quality, recipient safety, and transplantation outcomes. *Transfusion* **54**, 2997-3009 (2014).

273. Dahi, P.B., *et al.* “No wash” albumin-dextran dilution for double-unit cord blood transplantation is safe with high rates of sustained donor engraftment. *Biology of Blood and Marrow Transplantation* **20**, 490-494 (2014).
274. Mantel, C.R., *et al.* Enhancing hematopoietic stem cell transplantation efficacy by mitigating oxygen shock. *Cell* **161**, 1553-1565 (2015).
275. Li, P., *et al.* Epoxyeicosatrienoic acids enhance embryonic haematopoiesis and adult marrow engraftment. *Nature* **523**, 468 (2015).
276. Levine, M. & Hoey, T. Homeobox proteins as sequence-specific transcription factors. *Cell* **55**, 537-540 (1988).
277. Sauvageau, G., Iscove, N.N. & Humphries, R.K. In vitro and in vivo expansion of hematopoietic stem cells. *Oncogene* **23**, 7223 (2004).
278. Antonchuk, J., Sauvageau, G. & Humphries, R.K. HOXB4-induced expansion of adult hematopoietic stem cells ex vivo. *Cell* **109**, 39-45 (2002).
279. Sauvageau, G., *et al.* Overexpression of HOXB4 in hematopoietic cells causes the selective expansion of more primitive populations in vitro and in vivo. *Genes & development* **9**, 1753-1765 (1995).
280. Krosl, J., *et al.* In vitro expansion of hematopoietic stem cells by recombinant TAT-HOXB4 protein. *Nature medicine* **9**, 1428 (2003).
281. Fischbach, N.A., *et al.* HOXB6 overexpression in murine bone marrow immortalizes a myelomonocytic precursor in vitro and causes hematopoietic stem cell expansion and acute myeloid leukemia in vivo. *Blood* **105**, 1456-1466 (2005).
282. Fournier, M., Lebert-Ghali, C.-É., Krosl, G. & Bijl, J.J. HOXA4 induces expansion of hematopoietic stem cells in vitro and confers enhancement of pro-B-cells in vivo. *Stem cells and development* **21**, 133-142 (2011).
283. Lawrence, H.J., *et al.* Loss of expression of the Hoxa-9 homeobox gene impairs the proliferation and repopulating ability of hematopoietic stem cells. *Blood* **106**, 3988-3994 (2005).
284. Thorsteinsdottir, U., *et al.* Overexpression of the myeloid leukemia-associated Hoxa9 gene in bone marrow cells induces stem cell expansion. *Blood* **99**, 121-129 (2002).
285. de Pater, E., *et al.* Gata2 is required for HSC generation and survival. *Journal of Experimental Medicine* **210**, 2843-2850 (2013).
286. Hock, H., *et al.* Gfi-1 restricts proliferation and preserves functional integrity of haematopoietic stem cells. *Nature* **431**, 1002 (2004).
287. Iwama, A., *et al.* Enhanced self-renewal of hematopoietic stem cells mediated by the polycomb gene product Bmi-1. *Immunity* **21**, 843-851 (2004).
288. Kamminga, L.M., *et al.* The Polycomb group gene Ezh2 prevents hematopoietic stem cell exhaustion. *Blood* **107**, 2170-2179 (2006).
289. Rizo, A., Dontje, B., Vellenga, E., de Haan, G. & Schuringa, J.J. Long-term maintenance of human hematopoietic stem/progenitor cells by expression of BMI1. *Blood* **111**, 2621-2630 (2008).
290. Zhang, X.-B., *et al.* High incidence of leukemia in large animals after stem cell gene therapy with a HOXB4-expressing retroviral vector. *The Journal of clinical investigation* **118**, 1502-1510 (2008).
291. Bhatia, M., *et al.* Quantitative analysis reveals expansion of human hematopoietic repopulating cells after short-term ex vivo culture. *Journal of Experimental Medicine* **186**, 619-624 (1997).
292. Conneally, E., Cashman, J., Petzer, A. & Eaves, C. Expansion in vitro of transplantable human cord blood stem cells demonstrated using a quantitative assay of their lympho-myeloid repopulating activity in nonobese diabetic–scid/scid mice. *Proceedings of the National Academy of Sciences* **94**, 9836-9841 (1997).
293. Metcalf, D. Hematopoietic cytokines. *Blood* **111**, 485-491 (2008).
294. Ogawa, M. Differentiation and proliferation of hematopoietic stem cells. *Blood* **81**, 2844-2853 (1993).
295. Li, W., Jiang, K. & Ding, S. Concise review: A chemical approach to control cell fate and function. *Stem cells* **30**, 61-68 (2012).
296. Audet, J., Miller, C.L., Eaves, C.J. & Piret, J.M. Common and distinct features of cytokine effects on hematopoietic stem and progenitor cells revealed by dose–response surface analysis. *Biotechnology and bioengineering* **80**, 393-404 (2002).
297. Miller, C.L. & Eaves, C.J. Expansion in vitro of adult murine hematopoietic stem cells with transplantable lympho-myeloid reconstituting ability. *Proceedings of the National Academy of Sciences* **94**, 13648-13653 (1997).
298. Zhang, C.C., *et al.* Angiopoietin-like proteins stimulate ex vivo expansion of hematopoietic stem cells. *Nature medicine* **12**, 240 (2006).
299. Himgurg, H.A., *et al.* Pleiotrophin regulates the expansion and regeneration of hematopoietic stem cells. *Nature medicine* **16**, 475 (2010).

300. Amsellem, S., *et al.* Ex vivo expansion of human hematopoietic stem cells by direct delivery of the HOXB4 homeoprotein. *Nature medicine* **9**, 1423 (2003).
301. Iriuchishima, H., *et al.* Ex vivo maintenance of hematopoietic stem cells by quiescence induction through Fbxw7a overexpression. *Blood*, blood-2010-2007-294801 (2010).
302. Miharada, K., Sigurdsson, V. & Karlsson, S. Dppa5 improves hematopoietic stem cell activity by reducing endoplasmic reticulum stress. *Cell reports* **7**, 1381-1392 (2014).
303. Takubo, K., *et al.* Regulation of glycolysis by Pdk functions as a metabolic checkpoint for cell cycle quiescence in hematopoietic stem cells. *Cell stem cell* **12**, 49-61 (2013).
304. Liu, X., *et al.* Maintenance of mouse hematopoietic stem cells ex vivo by reprogramming cellular metabolism. *Blood*, blood-2014-2004-568949 (2015).
305. Perry, J.M., *et al.* Cooperation between both Wnt/ β -catenin and PTEN/PI3K/Akt signaling promotes primitive hematopoietic stem cell self-renewal and expansion. *Genes & development* (2011).
306. Huang, J., Nguyen-McCarty, M., Hexner, E.O., Danet-Desnoyers, G. & Klein, P.S. Maintenance of hematopoietic stem cells through regulation of Wnt and mTOR pathways. *Nature medicine* **18**, 1778 (2012).
307. Boitano, A.E., *et al.* Aryl hydrocarbon receptor antagonists promote the expansion of human hematopoietic stem cells. *Science* **329**, 1345-1348 (2010).
308. Fares, I., *et al.* Pyrimidoindole derivatives are agonists of human hematopoietic stem cell self-renewal. *Science* **345**, 1509-1512 (2014).
309. Luis, T.C., *et al.* Canonical wnt signaling regulates hematopoiesis in a dosage-dependent fashion. *Cell stem cell* **9**, 345-356 (2011).
310. Varnum-Finney, B., *et al.* The Notch ligand, Jagged-1, influences the development of primitive hematopoietic precursor cells. *Blood* **91**, 4084-4091 (1998).
311. Bhardwaj, G., *et al.* Sonic hedgehog induces the proliferation of primitive human hematopoietic cells via BMP regulation. *Nature immunology* **2**, 172 (2001).
312. Yeoh, J.S., *et al.* Fibroblast Growth Factor-1 and-2 Preserve Long-Term Repopulating Ability of Hematopoietic Stem Cells in Serum-Free Cultures. *Stem cells* **24**, 1564-1572 (2006).
313. Zhang, C.C. & Lodish, H.F. Insulin-like growth factor 2 expressed in a novel fetal liver cell population is a growth factor for hematopoietic stem cells. *Blood* **103**, 2513-2521 (2004).
314. Xu, Y., Shi, Y. & Ding, S. A chemical approach to stem-cell biology and regenerative medicine. *Nature* **453**, 338 (2008).
315. Schugar, R., Robbins, P. & Deasy, B. Small molecules in stem cell self-renewal and differentiation. *Gene therapy* **15**, 126 (2008).
316. Li, W. & Ding, S. Small molecules that modulate embryonic stem cell fate and somatic cell reprogramming. *Trends in pharmacological sciences* **31**, 36-45 (2010).
317. De Lima, M., *et al.* Transplantation of ex vivo expanded cord blood cells using the copper chelator tetraethylenepentamine: a phase I/II clinical trial. *Bone marrow transplantation* **41**, 771 (2008).
318. Delaney, C., *et al.* Notch-mediated expansion of human cord blood progenitor cells capable of rapid myeloid reconstitution. *Nature medicine* **16**, 232 (2010).
319. De Lima, M., *et al.* Cord-blood engraftment with ex vivo mesenchymal-cell coculture. *New England Journal of Medicine* **367**, 2305-2315 (2012).
320. Cutler, C., *et al.* Prostaglandin-modulated umbilical cord blood hematopoietic stem cell transplantation. *Blood*, blood-2013-2005-503177 (2013).
321. Horwitz, M.E., *et al.* Umbilical cord blood expansion with nicotinamide provides long-term multilineage engraftment. *The Journal of clinical investigation* **124**, 3121-3128 (2014).
322. Papat, U., *et al.* Enforced fucosylation of cord blood hematopoietic cells accelerates neutrophil and platelet engraftment after transplantation. *Blood*, blood-2015-2001-607366 (2015).
323. Wagner Jr, J.E., *et al.* Phase I/II trial of StemRegenin-1 expanded umbilical cord blood hematopoietic stem cells supports testing as a stand-alone graft. *Cell Stem Cell* **18**, 144-155 (2016).
324. Wang, Z.-Y. & Chen, Z. Acute promyelocytic leukemia: from highly fatal to highly curable. *Blood* **111**, 2505-2515 (2008).
325. Lallemand-Breitenbach, V., *et al.* Retinoic acid and arsenic synergize to eradicate leukemic cells in a mouse model of acute promyelocytic leukemia. *Journal of Experimental Medicine* **189**, 1043-1052 (1999).
326. GHITIS, J. Brief Note: Acute Promyelocytic Leukemia? *Blood* **21**, 237-240 (1963).
327. Chen, Z. Acute promyelocytic leukaemia: novel insights into the mechanisms of cure. *Nature Reviews Cancer* **10**, 775 (2010).
328. Nasr, R., *et al.* Eradication of acute promyelocytic leukemia-initiating cells through PML-RARA degradation. *Nature medicine* **14**, 1333 (2008).

329. Labrecque, J., *et al.* Impaired granulocytic differentiation in vitro in hematopoietic cells lacking retinoic acid receptors $\alpha 1$ and γ . *Blood* **92**, 607-615 (1998).
330. Niu, C., *et al.* Studies on treatment of acute promyelocytic leukemia with arsenic trioxide: remission induction, follow-up, and molecular monitoring in 11 newly diagnosed and 47 relapsed acute promyelocytic leukemia patients. *Blood* **94**, 3315-3324 (1999).
331. Chen, S.-J., Zhou, G.-B., Zhang, X.-W., Mao, J.-H. & Chen, Z. From an old remedy to a magic bullet: molecular mechanisms underlying the therapeutic effects of arsenic in fighting leukemia. *Blood* **117**, 6425-6437 (2011).
332. Lo-Coco, F., *et al.* Retinoic acid and arsenic trioxide for acute promyelocytic leukemia. *New England Journal of Medicine* **369**, 111-121 (2013).
333. Ng, C.-H. & Chng, W.-J. Recent advances in acute promyelocytic leukaemia. *F1000Research* **6**(2017).
334. Sanz, M.A., *et al.* Management of acute promyelocytic leukemia: recommendations from an expert panel on behalf of the European LeukemiaNet. *Blood* **113**, 1875-1891 (2009).
335. Mi, J., Li, J., Shen, Z., Chen, S. & Chen, Z. How to manage acute promyelocytic leukemia. *Leukemia* **26**, 1743 (2012).
336. Burnett, A.K., *et al.* Arsenic trioxide and all-trans retinoic acid treatment for acute promyelocytic leukaemia in all risk groups (AML17): results of a randomised, controlled, phase 3 trial. *The lancet oncology* **16**, 1295-1305 (2015).
337. Ma, H.S., *et al.* All-trans retinoic acid synergizes with FLT3 inhibition to eliminate FLT3/ITD+ leukemia stem cells in vitro and in vivo. *Blood* **127**, 2867-2878 (2016).
338. Martelli, M.P., *et al.* Arsenic trioxide and all-trans retinoic acid target NPM1 mutant oncoprotein levels and induce apoptosis in NPM1-mutated AML cells. *Blood* **125**, 3455-3465 (2015).
339. El Hajj, H., *et al.* Retinoic acid and arsenic trioxide trigger degradation of mutated NPM1, resulting in apoptosis of AML cells. *Blood* **125**, 3447-3454 (2015).
340. Schlenk, R.F., *et al.* All-trans retinoic acid as adjunct to intensive treatment in younger adult patients with acute myeloid leukemia: results of the randomized AMLSG 07-04 study. *Annals of hematology* **95**, 1931-1942 (2016).
341. Boutzen, H., *et al.* Isocitrate dehydrogenase 1 mutations prime the all-trans retinoic acid myeloid differentiation pathway in acute myeloid leukemia. *Journal of Experimental Medicine*, jem. 20150736 (2016).
342. Verhagen, H.J., *et al.* Primary acute myeloid leukemia cells with overexpression of EVI-1 are sensitive to all-trans retinoic acid. *Blood* **127**, 458-463 (2016).
343. Iijima, K., Honma, Y. & Niitsu, N. Granulocytic differentiation of leukemic cells with t(9; 11)(p22; q23) induced by all-trans-retinoic acid. *Leukemia & lymphoma* **45**, 1017-1024 (2004).
344. Fujiki, A., *et al.* All-trans retinoic acid combined with 5-Aza-2'-deoxycytidine induces C/EBP α expression and growth inhibition in MLL-AF9-positive leukemic cells. *Biochemical and biophysical research communications* **428**, 216-223 (2012).
345. Gutierrez-Mazariegos, J., Theodosiou, M., Campo-Paysaa, F. & Schubert, M. Vitamin A: a multifunctional tool for development. in *Seminars in cell & developmental biology*, Vol. 22 603-610 (Elsevier, 2011).
346. Ross, S.A., McCaffery, P.J., Drager, U.C. & De Luca, L.M. Retinoids in embryonal development. *Physiological reviews* **80**, 1021-1054 (2000).
347. Sakashita, A., *et al.* 9-cis-retinoic acid: effects on normal and leukemic hematopoiesis in vitro. *Blood* **81**, 1009-1016 (1993).
348. McKenna, N.J. EMBO Retinoids 2011: Mechanisms, biology and pathology of signaling by retinoic acid and retinoic acid receptors. *Nuclear receptor signaling* **10**(2012).
349. Liu, Y., *et al.* All-trans retinoic acid arrests cell cycle in leukemic bone marrow stromal cells by increasing intercellular communication through connexin 43-mediated gap junction. *Journal of hematology & oncology* **8**, 110 (2015).
350. Brown, C.C. & Noelle, R.J. Seeing through the dark: new insights into the immune regulatory functions of vitamin A. *European journal of immunology* **45**, 1287-1295 (2015).
351. Duester, G. Families of retinoid dehydrogenases regulating vitamin A function. *The FEBS Journal* **267**, 4315-4324 (2000).
352. Budhu, A., Gillilan, R. & Noy, N. Localization of the RAR interaction domain of cellular retinoic acid binding protein-III1. *Journal of molecular biology* **305**, 939-949 (2001).
353. Dong, D., Ruuska, S.E., Levinthal, D.J. & Noy, N. Distinct roles for cellular retinoic acid-binding proteins I and II in regulating signaling by retinoic acid. *Journal of Biological Chemistry* **274**, 23695-23698 (1999).
354. Topletz, A.R., *et al.* Comparison of the function and expression of CYP26A1 and CYP26B1, the two retinoic acid hydroxylases. *Biochemical pharmacology* **83**, 149-163 (2012).

355. Ghiaur, G., *et al.* Regulation of human hematopoietic stem cell self-renewal by the microenvironment's control of retinoic acid signaling. *Proceedings of the National Academy of Sciences* **110**, 16121-16126 (2013).
356. Pemrick, S.M., Lucas, D. & Grippo, J. The retinoid receptors. *Leukemia* **8**, S1-10 (1994).
357. Evans, R.M. The steroid and thyroid hormone receptor superfamily. *Science* **240**, 889-895 (1988).
358. Kastner, P., *et al.* Murine isoforms of retinoic acid receptor gamma with specific patterns of expression. *Proceedings of the National Academy of Sciences* **87**, 2700-2704 (1990).
359. Zelent, A., *et al.* Differentially expressed isoforms of the mouse retinoic acid receptor beta generated by usage of two promoters and alternative splicing. *The EMBO Journal* **10**, 71-81 (1991).
360. Kastner, P., *et al.* Genetic evidence that the retinoid signal is transduced by heterodimeric RXR/RAR functional units during mouse development. *Development* **124**, 313-326 (1997).
361. Nagy, L., *et al.* Mechanism of corepressor binding and release from nuclear hormone receptors. *Genes & development* **13**, 3209-3216 (1999).
362. Mangelsdorf, D.J. & Evans, R.M. The RXR heterodimers and orphan receptors. *Cell* **83**, 841-850 (1995).
363. Glass, C.K. & Rosenfeld, M.G. The coregulator exchange in transcriptional functions of nuclear receptors. *Genes & development* **14**, 121-141 (2000).
364. Mendoza-Parra, M.-A. & Gronemeyer, H. Genome-wide studies of nuclear receptors in cell fate decisions. in *Seminars in cell & developmental biology*, Vol. 24 706-715 (Elsevier, 2013).
365. Chanda, B., Ditadi, A., Iscove, N.N. & Keller, G. Retinoic acid signaling is essential for embryonic hematopoietic stem cell development. *Cell* **155**, 215-227 (2013).
366. Collins, S.J. Retinoic acid receptors, hematopoiesis and leukemogenesis. *Current opinion in hematology* **15**, 346-351 (2008).
367. Douer, D. & Koeffler, H.P. Retinoic acid enhances colony-stimulating factor-induced clonal growth of normal human myeloid progenitor cells in vitro. *Experimental cell research* **138**, 193-198 (1982).
368. Douer, D. & Koeffler, H. Retinoic acid enhances growth of human early erythroid progenitor cells in vitro. *The Journal of clinical investigation* **69**, 1039-1041 (1982).
369. Aglietta, M., Piacibello, W., Sanavio, F., Visconti, A. & Gavosto, F. Retinoic acid enhances the growth of only one subpopulation of granulomonocyte precursors. *Acta haematologica* **71**, 97-99 (1984).
370. Van Bockstaele, D., *et al.* Direct effects of 13-cis and all-trans retinoic acid on normal bone marrow (BM) progenitors: Comparative study on BM mononuclear cells and on isolated CD 34+ BM cells. *Annals of hematology* **66**, 61-66 (1993).
371. Jacobsen, S., *et al.* All-trans-and 9-cis-retinoic acid: potent direct inhibitors of primitive murine hematopoietic progenitors in vitro. *Journal of Experimental Medicine* **179**, 1665-1670 (1994).
372. Smeland, E.B., *et al.* All-trans retinoic acid directly inhibits granulocyte colony-stimulating factor-induced proliferation of CD34+ human hematopoietic progenitor cells. *Blood* **84**, 2940-2945 (1994).
373. Fahlman, C., *et al.* All-trans-and 9-cis-retinoic acid inhibit growth of normal human and murine B cell precursors. *The Journal of Immunology* **155**, 58-65 (1995).
374. Rusten, L.S., *et al.* The RAR-RXR as well as the RXR-RXR pathway is involved in signaling growth inhibition of human CD34+ erythroid progenitor cells. *Blood* **87**, 1728-1736 (1996).
375. Purton, L.E., Bernstein, I.D. & Collins, S.J. All-trans retinoic acid enhances the long-term repopulating activity of cultured hematopoietic stem cells. *Blood* **95**, 470-477 (2000).
376. Tsai, S., Bartelmez, S., Sitnicka, E. & Collins, S. Lymphohematopoietic progenitors immortalized by a retroviral vector harboring a dominant-negative retinoic acid receptor can recapitulate lymphoid, myeloid, and erythroid development. *Genes & development* **8**, 2831-2841 (1994).
377. Purton, L.E., Bernstein, I.D. & Collins, S.J. All-trans retinoic acid delays the differentiation of primitive hematopoietic precursors (lin⁻ c-kit⁺ Sca-1⁺) while enhancing the terminal maturation of committed granulocyte/monocyte progenitors. *Blood* **94**, 483-495 (1999).
378. Purton, L.E., *et al.* RAR γ is critical for maintaining a balance between hematopoietic stem cell self-renewal and differentiation. *Journal of Experimental Medicine* **203**, 1283-1293 (2006).
379. Brown, G., Marchwicka, A., Cunningham, A., Toellner, K.-M. & Marcinkowska, E. Antagonizing retinoic acid receptors increases myeloid cell production by cultured human hematopoietic stem cells. *Archivum immunologiae et therapeuticae experimentalis* **65**, 69-81 (2017).
380. Cabezas-Wallscheid, N., *et al.* Vitamin A-retinoic acid signaling regulates hematopoietic stem cell dormancy. *Cell* **169**, 807-823. e819 (2017).
381. Ronn, R.E., *et al.* Retinoic acid regulates hematopoietic development from human pluripotent stem cells. *Stem Cell Reports* **4**, 269-281 (2015).
382. Kuwata, T., *et al.* Vitamin A deficiency in mice causes a systemic expansion of myeloid cells. *Blood* **95**, 3349-3356 (2000).
383. Walkley, C., Yuan, Y., Chandraratna, R. & McArthur, G. Retinoic acid receptor antagonism in vivo expands the numbers of precursor cells during granulopoiesis. *Leukemia* **16**, 1763 (2002).

384. Purton, L.E., *et al.* RARgamma is critical for maintaining a balance between hematopoietic stem cell self-renewal and differentiation. *J Exp Med* **203**, 1283-1293 (2006).
385. Zelent, A., Guidez, F., Melnick, A., Waxman, S. & Licht, J.D. Translocations of the RAR α gene in acute promyelocytic leukemia. *Oncogene* **20**, 7186 (2001).
386. Breitman, T., Selonick, S.E. & Collins, S.J. Induction of differentiation of the human promyelocytic leukemia cell line (HL-60) by retinoic acid. *Proceedings of the National Academy of Sciences* **77**, 2936-2940 (1980).
387. Ricote, M., *et al.* Normal hematopoiesis after conditional targeting of RXR α in murine hematopoietic stem/progenitor cells. *Journal of leukocyte biology* **80**, 850 (2006).
388. Kastner, P., *et al.* Positive and negative regulation of granulopoiesis by endogenous RAR α . *Blood* **97**, 1314-1320 (2001).
389. Dewamitta, S.R., Joseph, C., Purton, L.E. & Walkley, C.R. Erythroid-extrinsic regulation of normal erythropoiesis by retinoic acid receptors. *British journal of haematology* **164**, 280-285 (2014).
390. Mongan, N.P. & Gudas, L.J. Diverse actions of retinoid receptors in cancer prevention and treatment. *Differentiation* **75**, 853-870 (2007).
391. Petros, R.A. & DeSimone, J.M. Strategies in the design of nanoparticles for therapeutic applications. *Nature reviews Drug discovery* **9**, 615 (2010).
392. Wicki, A., Witzigmann, D., Balasubramanian, V. & Huwyler, J. Nanomedicine in cancer therapy: challenges, opportunities, and clinical applications. *Journal of controlled release* **200**, 138-157 (2015).
393. Smith, A. Big moment for nanotech: oncology therapeutics poised for a leap. *OncLive* <http://www.onclive.com/publications/Oncology-live/2013/June-2013/Big-Moment-for-Nanotech-Oncology-Therapeutics-Poised-for-a-Leap> **4**, 2-25 (2013).
394. Ferrari, M. Cancer nanotechnology: opportunities and challenges. *Nature Reviews Cancer* **5**, 161 (2005).
395. Swartz, M.A., Hirose, S. & Hubbell, J.A. Engineering approaches to immunotherapy. *Science translational medicine* **4**, 148rv149-148rv149 (2012).
396. Kearney, C.J. & Mooney, D.J. Macroscale delivery systems for molecular and cellular payloads. *Nature materials* **12**, 1004 (2013).
397. Peer, D., *et al.* Nanocarriers as an emerging platform for cancer therapy. *Nature nanotechnology* **2**, 751 (2007).
398. Shi, J., Votruba, A.R., Farokhzad, O.C. & Langer, R. Nanotechnology in drug delivery and tissue engineering: from discovery to applications. *Nano letters* **10**, 3223-3230 (2010).
399. Sinha, R., Kim, G.J., Nie, S. & Shin, D.M. Nanotechnology in cancer therapeutics: bioconjugated nanoparticles for drug delivery. *Molecular cancer therapeutics* **5**, 1909-1917 (2006).
400. Boto, C., *et al.* Prolonged intracellular accumulation of light-inducible nanoparticles in leukemia cells allows their remote activation. *Nature communications* **8**, 15204 (2017).
401. Inman, S. FDA approves second-line MM-398 regimen for metastatic pancreatic cancer. *OncLive*. Vol. 2018.
402. Ipsen. Study of Irinotecan Liposome Injection (ONIVYDE®) in Patients With Small Cell Lung Cancer. (<https://ClinicalTrials.gov/show/NCT03088813>, 2018).
403. Ipsen. Study of Nanoliposomal Irinotecan (Nal-IRI)-Containing Regimens in Patients With Previously Untreated, Metastatic Pancreatic Adenocarcinoma. (<https://ClinicalTrials.gov/show/NCT02551991>, 2015).
404. Consortium, S.P.O. Phase 1 Study of MM-398 Plus Cyclophosphamide in Pediatric Solid Tumors. (<https://ClinicalTrials.gov/show/NCT02013336>, 2013).
405. Miele, E., Spinelli, G.P., Miele, E., Tomao, F. & Tomao, S. Albumin-bound formulation of paclitaxel (Abraxane® ABI-007) in the treatment of breast cancer. *International journal of nanomedicine* **4**, 99 (2009).
406. Tipping, A.J., *et al.* High GATA-2 expression inhibits human hematopoietic stem and progenitor cell function by effects on cell cycle. *Blood* **113**, 2661-2672 (2009).
407. Corporation, S.B. Study of Weekly Genexol®-PM Plus Gemcitabine in Subjects With Recurrent and Metastatic Adenocarcinoma of the Pancreas. (<https://ClinicalTrials.gov/show/NCT02739633>, 2016).
408. Gachon University Gil Medical, C. A Phase II Study of Weekly Genexol-PM in Patients With Hepatocellular Carcinoma After Failure of Sorafenib. (2020).
409. Stathopoulos, G.P., *et al.* Liposomal cisplatin combined with paclitaxel versus cisplatin and paclitaxel in non-small-cell lung cancer: a randomized phase III multicenter trial. *Ann Oncol* **21**, 2227-2232 (2010).
410. Nippon Kayaku Co, L. A Phase III Study of NK105 in Patients With Breast Cancer. (2016).
411. MediGene. EndoTAG-1 Gemcitabine Combination Therapy to Treat Locally Advanced and/or Metastatic Adenocarcinoma of the Pancreas. (<https://ClinicalTrials.gov/show/NCT00377936>, 2005).
412. MediGene. A Trial Evaluating the Pharmacokinetics and Mode of Action of EndoTAG®-1 in Tumor Patients With Hepatic Metastases. (<https://ClinicalTrials.gov/show/NCT00542048>, 2007).

413. Institute, J.B. Trial of Neoadjuvant EndoTAG-1 in Combination With Paclitaxel in HER2-negative Breast Cancer. (<https://ClinicalTrials.gov/show/NCT01537536>, 2011).
414. MediGene. EndoTAG-1 in Triple Receptor Negative Breast Cancer Patients. (2010).
415. Aadi, L.L.C. A Phase 2 Study of ABI-009 in Patients With Advanced Malignant PEComa. (2018).
416. Mayo, C. & National Cancer, I. Nanoparticle Albumin-Bound Rapamycin in Treating Patients With Advanced Cancer With mTOR Mutations. (2017).
417. National Cancer, I. & National Institutes of Health Clinical, C. Trial of CRLX101, a Nanoparticle Camptothecin With Olaparib in People With Relapsed/Refractory Small Cell Lung Cancer. (2018).
418. Young, C., Schluep, T., Hwang, J. & Eliasof, S. CRLX101 (formerly IT-101)-A Novel Nanopharmaceutical of Camptothecin in Clinical Development. *Curr Bioact Compd* 7, 8-14 (2011).
419. NewLink Genetics, C. CRLX101 in Combination With Bevacizumab for Metastatic Renal Cell Carcinoma (mRCC) Versus Standard of Care (SOC). (2016).
420. Merrimack, P. MM-302 Plus Trastuzumab vs. Chemotherapy of Physician's Choice Plus Trastuzumab in HER2-Positive Locally Advanced/Metastatic Breast Cancer Patients. (2016).
421. Therapeutics, B. A Phase 2 Study to Determine the Safety and Efficacy of BIND-014 (Docetaxel Nanoparticles for Injectable Suspension), Administered to Patients With Metastatic Castration-Resistant Prostate Cancer. (2016).
422. Therapeutics, B. A Phase 2 Study to Determine the Safety and Efficacy of BIND-014 (Docetaxel Nanoparticles for Injectable Suspension), Administered to Patients With Metastatic Castration-Resistant Prostate Cancer. (<https://ClinicalTrials.gov/show/NCT01812746>, 2013).
423. Mebiopharm Co, L. Study of MBP-426 in Patients With Second Line Gastric, Gastroesophageal, or Esophageal Adenocarcinoma. (2012).
424. University Hospital, B., Switzerland. Anti-EGFR Immunoliposomes in Solid Tumors. (<https://ClinicalTrials.gov/show/NCT01702129>, 2007).
425. Swiss Group for Clinical Cancer, R. Anti-EGFR-immunoliposomes Loaded With Doxorubicin in Patients With Advanced Triple Negative EGFR Positive Breast Cancer. (2019).
426. Celision. Study of ThermoDox With Standardized Radiofrequency Ablation (RFA) for Treatment of Hepatocellular Carcinoma (HCC). (<https://ClinicalTrials.gov/show/NCT02112656>, 2014).
427. Jazz, P., The, L. & Lymphoma, S. Phase III Study of CPX-351 Versus 7+3 in Patients 60-75 Years Old With Untreated High Risk (Secondary) Acute Myeloid Leukemia. (2016).
428. Pharmaceuticals, J. Multicenter Study Of CPX-1 (Irinotecan HCl: Floxuridine) Liposome Injection In Patients With Advanced Colorectal Cancer. (<https://ClinicalTrials.gov/show/NCT00361842>, 2006).
429. Nanospectra Biosciences, I. Efficacy Study of AuroLase Therapy in Subjects With Primary and/or Metastatic Lung Tumors. (<https://ClinicalTrials.gov/show/NCT01679470>, 2012).
430. Nanospectra Biosciences, I. MRI/US Fusion Imaging and Biopsy in Combination With Nanoparticle Directed Focal Therapy for Ablation of Prostate Tissue. (<https://ClinicalTrials.gov/show/NCT02680535>, 2016).
431. Nanobiotix & PharmaEngine. NBTXR3 Crystalline Nanoparticles and Radiation Therapy in Treating and Randomized Patients in Two Arms With Soft Tissue Sarcoma of the Extremity and Trunk Wall. (2018).
432. SynerGene Therapeutics, I. Phase II Study of Combined Temozolomide and SGT-53 for Treatment of Recurrent Glioblastoma. (2018).
433. SynerGene Therapeutics, I. Phase II Study of Combined Temozolomide and SGT-53 for Treatment of Recurrent Glioblastoma. (<https://ClinicalTrials.gov/show/NCT02340156>, 2014).
434. Sierra Oncology, I. Study of PNT2258 for Treatment of Relapsed or Refractory Non-Hodgkin's Lymphoma. (<https://ClinicalTrials.gov/show/NCT01733238>, 2012).
435. Senesco Technologies, I. Safety and Tolerability Study of SNS01-T in Relapsed or Refractory B Cell Malignancies (Multiple Myeloma, B Cell Lymphoma, or Plasma Cell Leukemia (PCL)). (<https://ClinicalTrials.gov/show/NCT01435720>, 2011).
436. Silence Therapeutics Gmb, H., Granzer Regulatory, C., Services & GmbH, F.G.K.C.R. Atu027 Plus Gemcitabine in Advanced or Metastatic Pancreatic Cancer (Atu027-I-02). (2015).
437. Corporation, A.B. Safety, Pharmacokinetics and Preliminary Anti-Tumor Activity of Intravenous TKM-080301 in Subjects With Advanced Hepatocellular Carcinoma. (<https://ClinicalTrials.gov/show/NCT02191878>, 2014).
438. Dicerna Pharmaceuticals, I. Phase Ib/2, Multicenter, Dose Escalation Study of DCR-MYC in Patients With Hepatocellular Carcinoma. (<https://ClinicalTrials.gov/show/NCT02314052>, 2014).
439. Mirna Therapeutics, I. & Texas, C.P.R.I.o. A Multicenter Phase I Study of MRX34, MicroRNA miR-RX34 Liposomal Injection. (<https://ClinicalTrials.gov/show/NCT01829971>, 2013).
440. Pharmaceuticals, C. Safety Study of CALAA-01 to Treat Solid Tumor Cancers. (<https://ClinicalTrials.gov/show/NCT00689065>, 2008).

441. Pharmaceuticals, A. Dose Escalation Trial to Evaluate the Safety, Tolerability, Pharmacokinetics and Pharmacodynamics of Intravenous ALN-VSP02 In Patients With Advanced Solid Tumors With Liver Involvement. (<https://ClinicalTrials.gov/show/NCT00882180>, 2009).
442. Pharmaceuticals, A. Multi-center, Open Label, Extension Study of ALN-VSP02 in Cancer Patients Who Have Responded to ALN-VSP02 Treatment. (<https://ClinicalTrials.gov/show/NCT01158079>, 2010).
443. Center, M.D.A.C. & Cancer Prevention Research Institute of, T. EphA2 Gene Targeting Using Neutral Liposomal Small Interfering RNA Delivery. (2020).
444. Gradalis, I. Phase I Intratumoral Pbi-shRNA STMN1 LP in Advanced and/or Metastatic Cancer. (<https://ClinicalTrials.gov/show/NCT01505153>, 2012).
445. Serono, E.M.D. & Merck, K. Cancer Vaccine Study for Unresectable Stage III Non-small Cell Lung Cancer (START). (2012).
446. Michael Morse, M.D., GlaxoSmithKline & Duke, U. Study to Assess dHER2+AS15 Cancer Vaccine Given in Combination With Lapatinib to Patients With Metastatic Breast Cancer. (2011).
447. ImmunoVaccine Technologies, I. A Phase I Safety Study of a Cancer Vaccine to Treat HLA-A2 Positive Advanced Stage Ovarian, Breast and Prostate Cancer. (<https://ClinicalTrials.gov/show/NCT01095848>, 2010).
448. Ltd, L.P., Hospital, R.A. & Ltd, T.C.R.P. Safety Study of a Liposomal Vaccine to Treat Malignant Melanoma. (<https://ClinicalTrials.gov/show/NCT01052142>, 2009).
449. Milton, S.H.M.C. JVRS-100 for the Treatment of Patients With Relapsed or Refractory Leukemia. (2014).
450. Center, N.I.o.H.C. & Institute, N.C. TNF-Bound Colloidal Gold in Treating Patients With Advanced Solid Tumors. (<https://ClinicalTrials.gov/show/NCT00356980>, 2006).
451. Bregoli, L., *et al.* Nanomedicine applied to translational oncology: a future perspective on cancer treatment. *Nanomedicine: Nanotechnology, Biology and Medicine* **12**, 81-103 (2016).
452. Truong, N.P., Whittaker, M.R., Mak, C.W. & Davis, T.P. The importance of nanoparticle shape in cancer drug delivery. *Expert opinion on drug delivery* **12**, 129-142 (2015).
453. Stylianopoulos, T., *et al.* Diffusion of particles in the extracellular matrix: the effect of repulsive electrostatic interactions. *Biophysical journal* **99**, 1342-1349 (2010).
454. Nel, A.E., *et al.* Understanding biophysicochemical interactions at the nano-bio interface. *Nature Materials* **8**, 543 (2009).
455. Bhatia, S. Nanoparticles types, classification, characterization, fabrication methods and drug delivery applications. in *Natural Polymer Drug Delivery Systems* 33-93 (Springer, 2016).
456. Dawidczyk, C.M., Russell, L.M. & Searson, P.C. Nanomedicines for cancer therapy: state-of-the-art and limitations to pre-clinical studies that hinder future developments. *Frontiers in chemistry* **2**, 69 (2014).
457. Mendes, R., Carreira, B., Baptista, P.V. & Fernandes, A.R. Non-small cell lung cancer biomarkers and targeted therapy-two faces of the same coin fostered by nanotechnology. *Expert Review of Precision Medicine and Drug Development* **1**, 155-168 (2016).
458. Ju, S., *et al.* Grape exosome-like nanoparticles induce intestinal stem cells and protect mice from DSS-induced colitis. *Molecular Therapy* **21**, 1345-1357 (2013).
459. Tang, L. & Cheng, J. Nonporous silica nanoparticles for nanomedicine application. *Nano today* **8**, 290-312 (2013).
460. Albanese, A., Tang, P.S. & Chan, W.C. The effect of nanoparticle size, shape, and surface chemistry on biological systems. *Annual review of biomedical engineering* **14**, 1-16 (2012).
461. Gu, Z., Biswas, A., Zhao, M. & Tang, Y. Tailoring nanocarriers for intracellular protein delivery. *Chemical Society Reviews* **40**, 3638-3655 (2011).
462. Locatelli, E. & Franchini, M.C. Biodegradable PLGA-b-PEG polymeric nanoparticles: synthesis, properties, and nanomedical applications as drug delivery system. *Journal of Nanoparticle Research* **14**, 1316 (2012).
463. Danhier, F., *et al.* PLGA-based nanoparticles: an overview of biomedical applications. *Journal of controlled release* **161**, 505-522 (2012).
464. von Roemeling, C., Jiang, W., Chan, C.K., Weissman, I.L. & Kim, B.Y. Breaking down the barriers to precision cancer nanomedicine. *Trends in biotechnology* **35**, 159-171 (2017).
465. Lu, Y., Aimetti, A.A., Langer, R. & Gu, Z. Bioresponsive materials. *Nature Reviews Materials* **2**, 16075 (2017).
466. Danhier, F. To exploit the tumor microenvironment: since the EPR effect fails in the clinic, what is the future of nanomedicine? *Journal of Controlled Release* **244**, 108-121 (2016).
467. Arrieta, O., *et al.* High liposomal doxorubicin tumour tissue distribution, as determined by radiopharmaceutical labelling with ^{99m}Tc-LD, is associated with the response and survival of patients with unresectable pleural mesothelioma treated with a combination of liposomal doxorubicin and cisplatin. *Cancer chemotherapy and pharmacology* **74**, 211-215 (2014).

468. Koukourakis, M., *et al.* Liposomal doxorubicin and conventionally fractionated radiotherapy in the treatment of locally advanced non-small-cell lung cancer and head and neck cancer. *Journal of clinical oncology* **17**, 3512-3521 (1999).
469. Ramanathan, R.K., *et al.* Abstract CT224: Pilot study in patients with advanced solid tumors to evaluate feasibility of ferumoxytol (FMX) as tumor imaging agent prior to MM-398, a nanoliposomal irinotecan (nal-IRI). (AACR, 2014).
470. Cho, K., Wang, X., Nie, S. & Shin, D.M. Therapeutic nanoparticles for drug delivery in cancer. *Clinical cancer research* **14**, 1310-1316 (2008).
471. Tran, S., DeGiovanni, P.-J., Piel, B. & Rai, P. Cancer nanomedicine: a review of recent success in drug delivery. *Clinical and translational medicine* **6**, 44 (2017).
472. Fodor, L., Elman, M. & Ullmann, Y. *Aesthetic applications of intense pulsed light*, (Springer Science & Business Media, 2010).
473. Iani, V., Moan, J. & Ma, L.W. Measurements of light penetration into human tissues in vivo. in *Photochemotherapy: Photodynamic Therapy and Other Modalities*, Vol. 2625 378-384 (International Society for Optics and Photonics, 1996).
474. Gohy, J.-F. & Zhao, Y. Photo-responsive block copolymer micelles: design and behavior. *Chemical Society Reviews* **42**, 7117-7129 (2013).
475. Clara, B., Falk, R., Alexander, G., Günter, M. & Alexander, H. Light-Controlled Tools. *Angewandte Chemie International Edition* **51**, 8446-8476 (2012).
476. Lin, Q., *et al.* Anticancer drug release from a mesoporous silica based nanophotocage regulated by either a one- or two-photon process. *Journal of the American Chemical Society* **132**, 10645-10647 (2010).
477. Tong, R., Chiang, H.H. & Kohane, D.S. Photoswitchable nanoparticles for in vivo cancer chemotherapy. *Proceedings of the National Academy of Sciences* **110**, 19048-19053 (2013).
478. Wang, W., *et al.* Efficient triplet-triplet annihilation-based upconversion for nanoparticle phototargeting. *Nano letters* **15**, 6332-6338 (2015).
479. Rwei, A.Y., *et al.* Repeatable and adjustable on-demand sciatic nerve block with phototriggerable liposomes. *Proceedings of the National Academy of Sciences* **112**, 15719-15724 (2015).
480. Zhan, C., *et al.* Phototriggered local anesthesia. *Nano letters* **16**, 177-181 (2015).
481. Yavuz, M.S., *et al.* Gold nanocages covered by smart polymers for controlled release with near-infrared light. *Nature materials* **8**, 935 (2009).
482. Hoare, T., *et al.* A magnetically triggered composite membrane for on-demand drug delivery. *Nano letters* **9**, 3651-3657 (2009).
483. Campbell, S., Maitland, D. & Hoare, T. Enhanced pulsatile drug release from injectable magnetic hydrogels with embedded thermosensitive microgels. *ACS Macro Letters* **4**, 312-316 (2015).
484. Peiris, P.M., *et al.* Enhanced delivery of chemotherapy to tumors using a multicomponent nanochain with radio-frequency-tunable drug release. *ACS nano* **6**, 4157-4168 (2012).
485. Schleich, N., *et al.* Comparison of active, passive and magnetic targeting to tumors of multifunctional paclitaxel/SPIO-loaded nanoparticles for tumor imaging and therapy. *Journal of Controlled Release* **194**, 82-91 (2014).
486. Yan, F., *et al.* Paclitaxel-liposome-microbubble complexes as ultrasound-triggered therapeutic drug delivery carriers. *Journal of controlled release* **166**, 246-255 (2013).
487. Krasovitski, B., Frenkel, V., Shoham, S. & Kimmel, E. Intramembrane cavitation as a unifying mechanism for ultrasound-induced bioeffects. *Proceedings of the National Academy of Sciences*, 201015771 (2011).
488. Wang, C.-H., *et al.* Aptamer-conjugated and drug-loaded acoustic droplets for ultrasound theranosis. *Biomaterials* **33**, 1939-1947 (2012).
489. Dromi, S., *et al.* Pulsed-high intensity focused ultrasound and low temperature-sensitive liposomes for enhanced targeted drug delivery and antitumor effect. *Clinical Cancer Research* **13**, 2722-2727 (2007).
490. Kagatani, S., *et al.* Electroresponsive pulsatile depot delivery of insulin from poly(dimethylaminopropylacrylamide) gel in rats. *Journal of pharmaceutical sciences* **86**, 1273-1277 (1997).
491. George, P.M., *et al.* Electrically controlled drug delivery from biotin-doped conductive polypyrrole. *Advanced Materials* **18**, 577-581 (2006).
492. Ge, J., Neofytou, E., Cahill III, T.J., Beygui, R.E. & Zare, R.N. Drug release from electric-field-responsive nanoparticles. *ACS nano* **6**, 227-233 (2011).
493. Murakami, Y. & Maeda, M. DNA-responsive hydrogels that can shrink or swell. *Biomacromolecules* **6**, 2927-2929 (2005).
494. Battig, M.R., Soontornworajit, B. & Wang, Y. Programmable release of multiple protein drugs from aptamer-functionalized hydrogels via nucleic acid hybridization. *Journal of the American Chemical Society* **134**, 12410-12413 (2012).

495. Gubeli, R.J., *et al.* Pharmacologically triggered hydrogel for scheduling hepatitis B vaccine administration. *Scientific reports* **3**, 2610 (2013).
496. Versteegen, R.M., Rossin, R., ten Hoeve, W., Janssen, H.M. & Robillard, M.S. Click to release: instantaneous doxorubicin elimination upon tetrazine ligation. *Angewandte Chemie* **125**, 14362-14366 (2013).
497. Tong, R. & Kohane, D.S. Shedding light on nanomedicine. *Wiley Interdisciplinary Reviews: Nanomedicine and Nanobiotechnology* **4**, 638-662 (2012).
498. Weissleder, R. A clearer vision for in vivo imaging. (Nature Publishing Group, 2001).
499. Sordillo, L.A., Pu, Y., Pratavieira, S., Budansky, Y. & Alfano, R.R. Deep optical imaging of tissue using the second and third near-infrared spectral windows. *Journal of biomedical optics* **19**, 056004 (2014).
500. Karu, T.I. *The science of low-power laser therapy*, (Gordon & Breach Science Publishers, 1998).
501. Desmet, K.D., *et al.* Clinical and experimental applications of NIR-LED photobiomodulation. *Photomedicine and Laser Therapy* **24**, 121-128 (2006).
502. Rastogi, R.P., Kumar, A., Tyagi, M.B. & Sinha, R.P. Molecular mechanisms of ultraviolet radiation-induced DNA damage and repair. *Journal of nucleic acids* **2010**(2010).
503. Kramer, G.F. & Ames, B.N. Oxidative mechanisms of toxicity of low-intensity near-UV light in *Salmonella typhimurium*. *Journal of bacteriology* **169**, 2259-2266 (1987).
504. Avci, P., *et al.* Low-level laser (light) therapy (LLLT) in skin: stimulating, healing, restoring. in *Seminars in cutaneous medicine and surgery*, Vol. 32 41-52 (Frontline Medical Communications, 2013).
505. Flusberg, B.A., *et al.* Fiber-optic fluorescence imaging. *Nature methods* **2**, 941 (2005).
506. Yelin, D., *et al.* Three-dimensional miniature endoscopy. *Nature* **443**, 765 (2006).
507. Klan, P., *et al.* Photoremovable Protecting Groups in Chemistry and Biology: Reaction Mechanisms and Efficacy. *Chemical Reviews* **113**, 119-191 (2013).
508. Jiang, J., Tong, X., Morris, D. & Zhao, Y. Toward photocontrolled release using light-dissociable block copolymer micelles. *Macromolecules* **39**, 4633-4640 (2006).
509. Lin, Q., *et al.* Highly discriminating photorelease of anticancer drugs based on hypoxia activatable phototrigger conjugated chitosan nanoparticles. *Advanced materials* **25**, 1981-1986 (2013).
510. Dvir, T., Banghart, M.R., Timko, B.P., Langer, R. & Kohane, D.S. Photo-targeted nanoparticles. *Nano letters* **10**, 250-254 (2009).
511. Brieke, C., Rohrbach, F., Gottschalk, A., Mayer, G. & Heckel, A. Light-controlled tools. *Angewandte Chemie International Edition* **51**, 8446-8476 (2012).
512. Liu, Q., Wang, W., Zhan, C., Yang, T. & Kohane, D.S. Enhanced precision of nanoparticle phototargeting in vivo at a safe irradiance. *Nano letters* **16**, 4516-4520 (2016).
513. Jain, P.K., Lee, K.S., El-Sayed, I.H. & El-Sayed, M.A. Calculated absorption and scattering properties of gold nanoparticles of different size, shape, and composition: applications in biological imaging and biomedicine. *The journal of physical chemistry B* **110**, 7238-7248 (2006).
514. Link, S. & El-Sayed, M.A. Shape and size dependence of radiative, non-radiative and photothermal properties of gold nanocrystals. *International reviews in physical chemistry* **19**, 409-453 (2000).
515. Timko, B.P., Dvir, T. & Kohane, D.S. Remotely triggerable drug delivery systems. *Advanced materials* **22**, 4925-4943 (2010).
516. Huschka, R., *et al.* Gene silencing by gold nanoshell-mediated delivery and laser-triggered release of antisense oligonucleotide and siRNA. *ACS nano* **6**, 7681-7691 (2012).
517. Wang, Q., Zhao, Y., Yang, Y., Xu, H. & Yang, X. Thermosensitive phase behavior and drug release of in situ gelable poly (N-isopropylacrylamide-co-acrylamide) microgels. *Colloid and Polymer Science* **285**, 515-521 (2007).
518. Timko, B.P., *et al.* Near-infrared-actuated devices for remotely controlled drug delivery. *Proceedings of the National Academy of Sciences* **111**, 1349-1354 (2014).
519. Leung, S.J. & Romanowski, M. NIR-activated content release from plasmon resonant liposomes for probing single-cell responses. *ACS nano* **6**, 9383-9391 (2012).
520. Jiang, T., *et al.* Poly aspartic acid peptide-linked PLGA based nanoscale particles: potential for bone-targeting drug delivery applications. *International journal of pharmaceutics* **475**, 547-557 (2014).
521. Sou, K., Goins, B., Oyajobi, B.O., Travi, B.L. & Phillips, W.T. Bone marrow-targeted liposomal carriers. *Expert opinion on drug delivery* **8**, 317-328 (2011).
522. Moghimi, S.M. Exploiting bone marrow microvascular structure for drug delivery and future therapies. *Advanced Drug Delivery Reviews* **17**, 61-73 (1995).
523. Beloqui, A., *et al.* Biodistribution of nanostructured lipid carriers (NLCs) after intravenous administration to rats: influence of technological factors. *European Journal of Pharmaceutics and Biopharmaceutics* **84**, 309-314 (2013).
524. Hussain, M.M., *et al.* Chylomicron-chylomicron remnant clearance by liver and bone marrow in rabbits. Factors that modify tissue-specific uptake. *The Journal of biological chemistry* **264**, 9571-9582 (1989).

525. Qiu, L.B., Dickson, H., Hajibagheri, N. & Crocker, P.R. Extruded erythroblast nuclei are bound and phagocytosed by a novel macrophage receptor. *Blood* **85**, 1630-1639 (1995).
526. Rankin, S.M. The bone marrow: a site of neutrophil clearance. *J Leukoc Biol* **88**, 241-251 (2010).
527. Boerman, O.C., *et al.* Optimization of technetium-99m-labeled PEG liposomes to image focal infection: effects of particle size and circulation time. (1997).
528. Allen, T., Austin, G., Chonn, A., Lin, L. & Lee, K. Uptake of liposomes by cultured mouse bone marrow macrophages: influence of liposome composition and size. *Biochimica et Biophysica Acta (BBA)- Biomembranes* **1061**, 56-64 (1991).
529. Awasthi, V., Garcia, D., Klipper, R., Goins, B. & Phillips, W. Neutral and anionic liposome-encapsulated hemoglobin: effect of postinserted poly (ethylene glycol)-distearoylphosphatidylethanolamine on distribution and circulation kinetics. *Journal of Pharmacology and Experimental Therapeutics* **309**, 241-248 (2004).
530. Schettini, D.A., *et al.* Improved targeting of antimony to the bone marrow of dogs using liposomes of reduced size. *International journal of pharmaceutics* **315**, 140-147 (2006).
531. Sou, K., Goins, B., Takeoka, S., Tsuchida, E. & Phillips, W.T. Selective uptake of surface-modified phospholipid vesicles by bone marrow macrophages in vivo. *Biomaterials* **28**, 2655-2666 (2007).
532. Xia, W., *et al.* A functional folate receptor is induced during macrophage activation and can be used to target drugs to activated macrophages. *Blood* **113**, 438-446 (2009).
533. Zhao, X., Li, H. & Lee, R.J. Targeted drug delivery via folate receptors. *Expert opinion on drug delivery* **5**, 309-319 (2008).
534. R Jansen, D., C Krijger, G., I Kolar, Z., A Zonnenberg, B. & Rijn Zeevaart, J. Targeted radiotherapy of bone malignancies. *Current drug discovery technologies* **7**, 233-246 (2010).
535. Krishnan, V., *et al.* CD19-Targeted nanodelivery of doxorubicin enhances therapeutic efficacy in B-cell acute lymphoblastic leukemia. *Molecular pharmaceutics* **12**, 2101-2111 (2015).
536. Zong, H., *et al.* In vivo targeting of leukemia stem cells by directing parthenolide-loaded nanoparticles to the bone marrow niche. *Leukemia* **30**, 1582 (2016).
537. Estelrich, J., Sánchez-Martín, M.J. & Busquets, M.A. Nanoparticles in magnetic resonance imaging: from simple to dual contrast agents. *International journal of nanomedicine* **10**, 1727 (2015).
538. Gobbo, O.L., Sjaastad, K., Radomski, M.W., Volkov, Y. & Prina-Mello, A. Magnetic nanoparticles in cancer theranostics. *Theranostics* **5**, 1249 (2015).
539. Song, S., Hao, Y., Yang, X., Patra, P. & Chen, J. Using gold nanoparticles as delivery vehicles for targeted delivery of chemotherapy drug fludarabine phosphate to treat hematological cancers. *Journal of nanoscience and nanotechnology* **16**, 2582-2586 (2016).
540. Suk, J.S., Xu, Q., Kim, N., Hanes, J. & Ensign, L.M. PEGylation as a strategy for improving nanoparticle-based drug and gene delivery. *Advanced drug delivery reviews* **99**, 28-51 (2016).
541. Tardi, P., *et al.* In vivo maintenance of synergistic cytarabine: daunorubicin ratios greatly enhances therapeutic efficacy. *Leukemia research* **33**, 129-139 (2009).
542. Tardi, P., Wan, C.P.L. & Mayer, L. Passive and semi-active targeting of bone marrow and leukemia cells using anionic low cholesterol liposomes. *Journal of drug targeting* **24**, 797-804 (2016).
543. Pan, X.Q., *et al.* Strategy for the treatment of acute myelogenous leukemia based on folate receptor β -targeted liposomal doxorubicin combined with receptor induction using all-trans retinoic acid. *Blood* **100**, 594-602 (2002).
544. Silva, E.L., *et al.* Improved in vitro antileukemic activity of all-trans retinoic acid loaded in cholesteryl butyrate solid lipid nanoparticles. *Journal of nanoscience and nanotechnology* **16**, 1291-1300 (2016).
545. Knapp, C.M., He, J., Lister, J. & Whitehead, K.A. Lipidoid nanoparticle mediated silencing of Mcl-1 induces apoptosis in mantle cell lymphoma. *Experimental Biology and Medicine* **241**, 1007-1013 (2016).
546. Dorrance, A.M., *et al.* Targeting leukemia stem cells in vivo with antagomiR-126 nanoparticles in acute myeloid leukemia. *Leukemia* **29**, 2143 (2015).
547. Zhou, S., *et al.* Intracellular pH-responsive and rituximab-conjugated mesoporous silica nanoparticles for targeted drug delivery to lymphoma B cells. *Journal of Experimental & Clinical Cancer Research* **36**, 24 (2017).
548. Swami, A., *et al.* Engineered nanomedicine for myeloma and bone microenvironment targeting. *Proceedings of the National Academy of Sciences* **111**, 10287-10292 (2014).
549. Mu, C.-F., Xiong, Y., Bai, X., Sheng, Y.-J. & Cui, J. Codelivery of Ponatinib and SAR302503 by Active Bone-Targeted Polymeric Micelles for the Treatment of Therapy-Resistant Chronic Myeloid Leukemia. *Molecular pharmaceutics* **14**, 274-283 (2016).
550. Zong, H., *et al.* In vivo targeting of leukemia stem cells by directing parthenolide-loaded nanoparticles to the bone marrow niche. *Leukemia* **30**, 1582-1586 (2016).
551. Shi, Y., *et al.* Multistep targeted nano drug delivery system aiming at leukemic stem cells and minimal residual disease. *Molecular pharmaceutics* **10**, 2479-2489 (2013).

552. Huang, B., *et al.* Apoptosis induction and imaging of cadmium-telluride quantum dots with wogonin in multidrug-resistant leukemia K562/A02 cell. *Journal of nanoscience and nanotechnology* **16**, 2499-2503 (2016).
553. Peng, M.-X., *et al.* Apoptotic mechanism of human leukemia K562/A02 cells induced by magnetic ferroferric oxide nanoparticles loaded with wogonin. *Chinese medical journal* **129**, 2958 (2016).
554. Shahabadi, N., Falsafi, M. & Mansouri, K. Improving antiproliferative effect of the anticancer drug cytarabine on human promyelocytic leukemia cells by coating on Fe₃O₄@ SiO₂ nanoparticles. *Colloids and Surfaces B: Biointerfaces* **141**, 213-222 (2016).
555. Gossai, N.P., *et al.* Drug conjugated nanoparticles activated by cancer cell specific mRNA. *Oncotarget* **7**, 38243 (2016).
556. Petrushev, B., *et al.* Gold nanoparticles enhance the effect of tyrosine kinase inhibitors in acute myeloid leukemia therapy. *International journal of nanomedicine* **11**, 641 (2016).
557. Simon, T., *et al.* Design of FLT3 inhibitor-gold nanoparticle conjugates as potential therapeutic agents for the treatment of acute myeloid leukemia. *Nanoscale research letters* **10**, 466 (2015).
558. Vinhas, R., Fernandes, A.R. & Baptista, P.V. Gold nanoparticles for BCR-ABL1 gene silencing: improving tyrosine kinase inhibitor efficacy in chronic myeloid leukemia. *Molecular Therapy-Nucleic Acids* **7**, 408-416 (2017).
559. Yao, Q., Cao, F., Feng, C., Zhao, Y. & Wang, X. SERS detection and targeted ablation of lymphoma cells using functionalized Ag nanoparticles. in *Plasmonics in Biology and Medicine XIII*, Vol. 9724 972407 (International Society for Optics and Photonics, 2016).
560. Martucci, N.M., *et al.* Nanoparticle-based strategy for personalized B-cell lymphoma therapy. *International journal of nanomedicine* **11**, 6089 (2016).
561. Nevala, W.K., Butterfield, J.T., Sutor, S.L., Knauer, D.J. & Markovic, S.N. Antibody-targeted paclitaxel loaded nanoparticles for the treatment of CD20+ B-cell lymphoma. *Scientific Reports* **7**, 45682 (2017).
562. Ihler, G.M., Glew, R.H. & Schnure, F.W. Enzyme loading of erythrocytes. *Proceedings of the National Academy of Sciences* **70**, 2663-2666 (1973).
563. Brynskikh, A.M., *et al.* Macrophage delivery of therapeutic nanozymes in a murine model of Parkinson's disease. *Nanomedicine* **5**, 379-396 (2010).
564. Behfar, A., Crespo-Diaz, R., Terzic, A. & Gersh, B.J. Cell therapy for cardiac repair—lessons from clinical trials. *Nature Reviews Cardiology* **11**, 232 (2014).
565. Firor, A.E., Jares, A. & Ma, Y. From humble beginnings to success in the clinic: chimeric antigen receptor-modified T-cells and implications for immunotherapy. *Experimental biology and medicine* **240**, 1087-1098 (2015).
566. Ikeda, H. & Shiku, H. Adoptive immunotherapy of cancer utilizing genetically engineered lymphocytes. *Cancer Immunology, Immunotherapy* **64**, 903-909 (2015).
567. Sharma, R.R., Pollock, K., Hubel, A. & McKenna, D. Mesenchymal stem or stromal cells: a review of clinical applications and manufacturing practices. *Transfusion* **54**, 1418-1437 (2014).
568. Roger, M., *et al.* Mesenchymal stem cells as cellular vehicles for delivery of nanoparticles to brain tumors. *Biomaterials* **31**, 8393-8401 (2010).
569. Huang, W.-C., *et al.* Tumortropic adipose-derived stem cells carrying smart nanotherapeutics for targeted delivery and dual-modality therapy of orthotopic glioblastoma. *Journal of Controlled Release* **254**, 119-130 (2017).
570. Cao, B., Yang, M., Zhu, Y., Qu, X. & Mao, C. Stem cells loaded with nanoparticles as a drug carrier for in vivo breast cancer therapy. *Advanced Materials* **26**, 4627-4631 (2014).
571. Paris, J.L., *et al.* Decidua-derived mesenchymal stem cells as carriers of mesoporous silica nanoparticles. In vitro and in vivo evaluation on mammary tumors. *Acta biomaterialia* **33**, 275-282 (2016).
572. Mooney, R., *et al.* Conjugation of pH-responsive nanoparticles to neural stem cells improves intratumoral therapy. *Journal of Controlled Release* **191**, 82-89 (2014).
573. Paris, J.L., *et al.* Vectorization of ultrasound-responsive nanoparticles in placental mesenchymal stem cells for cancer therapy. *Nanoscale* **9**, 5528-5537 (2017).
574. Zhao, Y., *et al.* Targeted delivery of doxorubicin by nano-loaded mesenchymal stem cells for lung melanoma metastases therapy. *Scientific reports* **7**, 44758 (2017).
575. Yang, M., *et al.* Mitomycin C-treated human-induced pluripotent stem cells as a safe delivery system of gold nanorods for targeted photothermal therapy of gastric cancer. *Nanoscale* **9**, 334-340 (2017).
576. Bhatia, M., Rachumallu, R., Singh, R. & Bhatta, R.S. Erythrocytes-based synthetic delivery systems: transition from conventional to novel engineering strategies. *Expert opinion on drug delivery* **11**, 1219-1236 (2014).
577. Ahn, S., Jung, S.Y., Seo, E. & Lee, S.J. Gold nanoparticle-incorporated human red blood cells (RBCs) for X-ray dynamic imaging. *Biomaterials* **32**, 7191-7199 (2011).

578. Millán, C.G., Castañeda, A.Z., Marinero, M.L.S. & Lanao, J.M. Factors associated with the performance of carrier erythrocytes obtained by hypotonic dialysis. *Blood Cells, Molecules, and Diseases* **33**, 132-140 (2004).
579. Briones, E., Colino, C.I., Millán, C.G. & Lanao, J.M. Increasing the selectivity of amikacin in rat peritoneal macrophages using carrier erythrocytes. *European Journal of Pharmaceutical Sciences* **38**, 320-324 (2009).
580. Hamidi, M., Zarei, N., Zarrin, A. & Mohammadi-Samani, S. Preparation and in vitro characterization of carrier erythrocytes for vaccine delivery. *International journal of pharmaceutics* **338**, 70-78 (2007).
581. He, H., *et al.* Cell-penetrating peptides mediated encapsulation of protein therapeutics into intact red blood cells and its application. *Journal of Controlled Release* **176**, 123-132 (2014).
582. Kwon, Y.M., *et al.* L-Asparaginase encapsulated intact erythrocytes for treatment of acute lymphoblastic leukemia (ALL). *Journal of Controlled Release* **139**, 182-189 (2009).
583. Grivennikov, S.I., Greten, F.R. & Karin, M. Immunity, inflammation, and cancer. *Cell* **140**, 883-899 (2010).
584. Lee, S. Monocytes: a novel drug delivery system targeting atherosclerosis. *Journal of drug targeting* **22**, 138-145 (2014).
585. Penberthy, T.W., Jiang, Y. & Graves, D.T. Leukocyte adhesion molecules. *Critical Reviews in Oral Biology & Medicine* **8**, 380-388 (1997).
586. Wong, D., Prameya, R. & Dorovini-Zis, K. Adhesion and migration of polymorphonuclear leukocytes across human brain microvessel endothelial cells are differentially regulated by endothelial cell adhesion molecules and modulate monolayer permeability. *Journal of neuroimmunology* **184**, 136-148 (2007).
587. Eniola, A.O. & Hammer, D.A. Artificial polymeric cells for targeted drug delivery. *Journal of controlled release* **87**, 15-22 (2003).
588. Eniola, A.O. & Hammer, D.A. In vitro characterization of leukocyte mimetic for targeting therapeutics to the endothelium using two receptors. *Biomaterials* **26**, 7136-7144 (2005).
589. Eniola, A.O., Rodgers, S.D. & Hammer, D.A. Characterization of biodegradable drug delivery vehicles with the adhesive properties of leukocytes. *Biomaterials* **23**, 2167-2177 (2002).
590. Coussens, L.M. & Werb, Z. Inflammation and cancer. *Nature* **420**, 860 (2002).
591. Choi, M.-R., *et al.* A cellular Trojan Horse for delivery of therapeutic nanoparticles into tumors. *Nano letters* **7**, 3759-3765 (2007).
592. Steinfeld, U., Pauli, C., Kaltz, N., Bergemann, C. & Lee, H.-H. T lymphocytes as potential therapeutic drug carrier for cancer treatment. *International journal of pharmaceutics* **311**, 229-236 (2006).
593. Stephan, M.T., Moon, J.J., Um, S.H., Bershteyn, A. & Irvine, D.J. Therapeutic cell engineering with surface-conjugated synthetic nanoparticles. *Nature medicine* **16**, 1035 (2010).
594. Huang, W.-C., *et al.* Tumortropic monocyte-mediated delivery of echogenic polymer bubbles and therapeutic vesicles for chemotherapy of tumor hypoxia. *Biomaterials* **71**, 71-83 (2015).
595. Bexell, D., Svensson, A. & Bengzon, J. Stem cell-based therapy for malignant glioma. *Cancer treatment reviews* **39**, 358-365 (2013).
596. Hu, Y.-L., Fu, Y.-H., Tabata, Y. & Gao, J.-Q. Mesenchymal stem cells: a promising targeted-delivery vehicle in cancer gene therapy. *Journal of Controlled Release* **147**, 154-162 (2010).
597. Müller, F.-J., Snyder, E.Y. & Loring, J.F. Gene therapy: can neural stem cells deliver? *Nature Reviews Neuroscience* **7**, 75 (2006).
598. Porada, C.D. & Almeida-Porada, G. Mesenchymal stem cells as therapeutics and vehicles for gene and drug delivery. *Advanced drug delivery reviews* **62**, 1156-1166 (2010).
599. Derubeis, A.R. & Cancedda, R. Bone marrow stromal cells (BMSCs) in bone engineering: limitations and recent advances. *Annals of biomedical engineering* **32**, 160-165 (2004).
600. Pontikoglou, C., Deschaseaux, F., Sensebé, L. & Papadaki, H.A. Bone marrow mesenchymal stem cells: biological properties and their role in hematopoiesis and hematopoietic stem cell transplantation. *Stem Cell Reviews and Reports* **7**, 569-589 (2011).
601. Rehman, F.U., *et al.* Synergy and translation of allogenic bone marrow stem cells after photodynamic treatment of rheumatoid arthritis with tetra sulfonatophenyl porphyrin and TiO₂ nanowhiskers. *Nano Research* **9**, 3305-3321 (2016).
602. Wang, D., Miller, S.C., Kopečková, P. & Kopeček, J. Bone-targeting macromolecular therapeutics. *Advanced drug delivery reviews* **57**, 1049-1076 (2005).
603. Xie, H., *et al.* Mesenchymal Stem Cell-Derived Microvesicles Support Ex Vivo Expansion of Cord Blood-Derived CD34. *Stem cells international* **2016**(2016).
604. Yang, F., Leung, V.Y., Luk, K.D., Chan, D. & Cheung, K.M. Mesenchymal stem cells arrest intervertebral disc degeneration through chondrocytic differentiation and stimulation of endogenous cells. *Molecular Therapy* **17**, 1959-1966 (2009).

605. Roger, M., *et al.* The potential of combinations of drug-loaded nanoparticle systems and adult stem cells for glioma therapy. *Biomaterials* **32**, 2106-2116 (2011).
606. Yang, F., *et al.* Genetic engineering of human stem cells for enhanced angiogenesis using biodegradable polymeric nanoparticles. *Proceedings of the National Academy of Sciences* **107**, 3317-3322 (2010).
607. Sekiya, I., Larson, B.L., Vuoristo, J.T., Cui, J.G. & Prockop, D.J. Adipogenic differentiation of human adult stem cells from bone marrow stroma (MSCs). *Journal of Bone and Mineral Research* **19**, 256-264 (2004).
608. Aday, S., *et al.* Inflammatory modulation of stem cells by Magnetic Resonance Imaging (MRI)-detectable nanoparticles. *Rsc Advances* **4**, 31706-31709 (2014).
609. Huang, Y.-C. & Liu, T.-J. Mobilization of mesenchymal stem cells by stromal cell-derived factor-1 released from chitosan/tripolyphosphate/fucoidan nanoparticles. *Acta biomaterialia* **8**, 1048-1056 (2012).
610. De Botton, S., *et al.* Incidence, clinical features, and outcome of all trans-retinoic acid syndrome in 413 cases of newly diagnosed acute promyelocytic leukemia. The European APL Group. *Blood* **92**, 2712-2718 (1998).
611. Warrell, R.P., Jr., *et al.* Differentiation therapy of acute promyelocytic leukemia with tretinoin (all-trans-retinoic acid). *N Engl J Med* **324**, 1385-1393 (1991).
612. Russo, D., *et al.* All-trans retinoic acid (ATRA) in patients with chronic myeloid leukemia in the chronic phase. *Leukemia* **12**, 449-454 (1998).
613. Si, J., Mueller, L. & Collins, S.J. CaMKII regulates retinoic acid receptor transcriptional activity and the differentiation of myeloid leukemia cells. *J Clin Invest* **117**, 1412-1421 (2007).
614. Timko, B.P., Dvir, T. & Kohane, D.S. Remotely triggerable drug delivery systems. *Advanced materials* **22**, 4925-4943 (2010).
615. Rwei, A.Y., Wang, W. & Kohane, D.S. Photoresponsive nanoparticles for drug delivery. *Nano Today* **10**, 451-467 (2015).
616. Bansal, A. & Zhang, Y. Photocontrolled nanoparticle delivery systems for biomedical applications. *Acc Chem Res* **47**, 3052-3060 (2014).
617. Spring, B.Q., *et al.* A photoactivable multi-inhibitor nanoliposome for tumour control and simultaneous inhibition of treatment escape pathways. *Nat Nanotechnol* (2016).
618. Boussif, O., *et al.* A versatile vector for gene and oligonucleotide transfer into cells in culture and in vivo: polyethylenimine. *Proc Natl Acad Sci U S A* **92**, 7297-7301 (1995).
619. Maia, J., *et al.* Controlling the neuronal differentiation of stem cells by the intracellular delivery of retinoic acid-loaded nanoparticles. *ACS Nano* **5**, 97-106 (2011).
620. Dvir, T., Banghart, M.R., Timko, B.P., Langer, R. & Kohane, D.S. Photo-targeted nanoparticles. *Nano Lett* **10**, 250-254 (2010).
621. Tiyaboonchai, W., Woiszwilllo, J. & Middaugh, C.R. Formulation and characterization of amphotericin B-polyethylenimine-dextran sulfate nanoparticles. *J Pharm Sci* **90**, 902-914 (2001).
622. Guidez, F., *et al.* Poor response to all-trans retinoic acid therapy in a t(11;17) PLZF/RAR alpha patient. *Leukemia* **8**, 312-317 (1994).
623. Licht, J.D., *et al.* Clinical and molecular characterization of a rare syndrome of acute promyelocytic leukemia associated with translocation (11;17). *Blood* **85**, 1083-1094 (1995).
624. Ruthardt, M., *et al.* Opposite effects of the acute promyelocytic leukemia PML-retinoic acid receptor alpha (RAR alpha) and PLZF-RAR alpha fusion proteins on retinoic acid signalling. *Mol Cell Biol* **17**, 4859-4869 (1997).
625. Spicuglia, S., *et al.* Characterisation of genome-wide PLZF/RARA target genes. *PLoS One* **6**, e24176 (2011).
626. Bewersdorf, J., Bennett, B.T. & Knight, K.L. H2AX chromatin structures and their response to DNA damage revealed by 4Pi microscopy. *Proc Natl Acad Sci U S A* **103**, 18137-18142 (2006).
627. Leith, C.P., *et al.* Acute myeloid leukemia in the elderly: assessment of multidrug resistance (MDR1) and cytogenetics distinguishes biologic subgroups with remarkably distinct responses to standard chemotherapy. A Southwest Oncology Group study. *Blood* **89**, 3323-3329 (1997).
628. Meng, H., *et al.* Engineered design of mesoporous silica nanoparticles to deliver doxorubicin and P-glycoprotein siRNA to overcome drug resistance in a cancer cell line. *ACS Nano* **4**, 4539-4550 (2010).
629. Drach, J., Lopez-Berestein, G., McQueen, T., Andreeff, M. & Mehta, K. Induction of differentiation in myeloid leukemia cell lines and acute promyelocytic leukemia cells by liposomal all-trans-retinoic acid. *Cancer Res* **53**, 2100-2104 (1993).
630. Tiwari, M.D., Mehra, S., Jadhav, S. & Bellare, J.R. All-trans retinoic acid loaded block copolymer nanoparticles efficiently induce cellular differentiation in HL-60 cells. *Eur J Pharm Sci* **44**, 643-652 (2011).
631. Szuts, E.Z. & Harosi, F.I. Solubility of retinoids in water. *Arch Biochem Biophys* **287**, 297-304 (1991).

632. Huang, P.X., Chandra, V. & Rastinejad, F. Retinoic Acid Actions through Mammalian Nuclear Receptors. *Chemical Reviews* **114**, 233-254 (2014).
633. Douer, D. & Koeffler, H.P. Retinoic acid. Inhibition of the clonal growth of human myeloid leukemia cells. *J Clin Invest* **69**, 277-283 (1982).
634. Liu, T.X., *et al.* Gene expression networks underlying retinoic acid-induced differentiation of acute promyelocytic leukemia cells. *Blood* **96**, 1496-1504 (2000).
635. Pitha-Rowe, I., Petty, W.J., Kitareewan, S. & Dmitrovsky, E. Retinoid target genes in acute promyelocytic leukemia. *Leukemia* **17**, 1723-1730 (2003).
636. Mao, M., *et al.* RIG-E, a human homolog of the murine Ly-6 family, is induced by retinoic acid during the differentiation of acute promyelocytic leukemia cell. *Proc Natl Acad Sci U S A* **93**, 5910-5914 (1996).
637. Gilleron, J., *et al.* Image-based analysis of lipid nanoparticle-mediated siRNA delivery, intracellular trafficking and endosomal escape. *Nat Biotechnol* **31**, 638-646 (2013).
638. Sahay, G., *et al.* Efficiency of siRNA delivery by lipid nanoparticles is limited by endocytic recycling. *Nat Biotechnol* **31**, 653-658 (2013).
639. Lee, T.T., *et al.* Light-triggered in vivo activation of adhesive peptides regulates cell adhesion, inflammation and vascularization of biomaterials. *Nat Mater* **14**, 352-360 (2015).
640. Dudani, J.S., Jain, P.K., Kwong, G.A., Stevens, K.R. & Bhatia, S.N. Photoactivated Spatiotemporally-Responsive Nanosensors of in Vivo Protease Activity. *ACS Nano* **9**, 11708-11717 (2015).
641. Shanmugam, V., Selvakumar, S. & Yeh, C.S. Near-infrared light-responsive nanomaterials in cancer therapeutics. *Chem Soc Rev* **43**, 6254-6287 (2014).
642. Wang, F., *et al.* Simultaneous phase and size control of upconversion nanocrystals through lanthanide doping. *Nature* **463**, 1061-1065 (2010).
643. Thery, C., Amigorena, S., Raposo, G. & Clayton, A. Isolation and characterization of exosomes from cell culture supernatants and biological fluids. *Curr Protoc Cell Biol* **Chapter 3**, Unit 3 22 (2006).
644. Christopherson, K.W., 2nd, Hangoc, G., Mantel, C.R. & Broxmeyer, H.E. Modulation of hematopoietic stem cell homing and engraftment by CD26. *Science* **305**, 1000-1003 (2004).
645. Gupta, R., Hong, D., Iborra, F., Sarno, S. & Enver, T. NOV (CCN3) functions as a regulator of human hematopoietic stem or progenitor cells. *Science* **316**, 590-593 (2007).
646. Adams, G.B., *et al.* Therapeutic targeting of a stem cell niche. *Nature biotechnology* **25**, 238 (2007).
647. Adams, G.B., *et al.* Therapeutic targeting of a stem cell niche. *Nat Biotechnol* **25**, 238-243 (2007).
648. Calvi, L.M., *et al.* Osteoblastic cells regulate the haematopoietic stem cell niche. *Nature* **425**, 841-846 (2003).
649. Hooper, A.T., *et al.* Engraftment and reconstitution of hematopoiesis is dependent on VEGFR2-mediated regeneration of sinusoidal endothelial cells. *Cell Stem Cell* **4**, 263-274 (2009).
650. Mendez-Ferrer, S., *et al.* Mesenchymal and haematopoietic stem cells form a unique bone marrow niche. *Nature* **466**, 829-834 (2010).
651. Hoggatt, J., Singh, P., Sampath, J. & Pelus, L.M. Prostaglandin E2 enhances hematopoietic stem cell homing, survival, and proliferation. *Blood* **113**, 5444-5455 (2009).
652. Adams, G.B., *et al.* Haematopoietic stem cells depend on Galpha(s)-mediated signalling to engraft bone marrow. *Nature* **459**, 103-107 (2009).
653. Boitano, A.E., *et al.* Aryl hydrocarbon receptor antagonists promote the expansion of human hematopoietic stem cells. *Science* **329**, 1345-1348 (2010).
654. Amsellem, S., *et al.* Ex vivo expansion of human hematopoietic stem cells by direct delivery of the HOXB4 homeoprotein. *Nat Med* **9**, 1423-1427 (2003).
655. Krosl, J., *et al.* In vitro expansion of hematopoietic stem cells by recombinant TAT-HOXB4 protein. *Nat Med* **9**, 1428-1432 (2003).
656. Pilat, S., *et al.* HOXB4 enforces equivalent fates of ES-cell-derived and adult hematopoietic cells. *Proc Natl Acad Sci U S A* **102**, 12101-12106 (2005).
657. Zhang, X.B., *et al.* High incidence of leukemia in large animals after stem cell gene therapy with a HOXB4-expressing retroviral vector. *J Clin Invest* **118**, 1502-1510 (2008).
658. Lee, J., *et al.* Improved ex vivo expansion of adult hematopoietic stem cells by overcoming CUL4-mediated degradation of HOXB4. *Blood* **121**, 4082-4089 (2013).
659. Hooper, A.T., *et al.* Engraftment and reconstitution of hematopoiesis is dependent on VEGFR2-mediated regeneration of sinusoidal endothelial cells. *Cell stem cell* **4**, 263-274 (2009).
660. Somervaille, T.C. & Cleary, M.L. Identification and characterization of leukemia stem cells in murine MLL-AF9 acute myeloid leukemia. *Cancer Cell* **10**, 257-268 (2006).
661. Sakamoto, K., *et al.* Sensitivity of MLL-rearranged AML cells to all-trans retinoic acid is associated with the level of H3K4me2 in the RAR α promoter region. *Blood Cancer Journal* **4**, e205 (2014).

662. Mangelsdorf, D.J., Koeffler, H.P., Donaldson, C.A., Pike, J.W. & Haussler, M.R. 1, 25-Dihydroxyvitamin D₃-induced differentiation in a human promyelocytic leukemia cell line (HL-60): receptor-mediated maturation to macrophage-like cells. *The Journal of cell biology* **98**, 391-398 (1984).
663. Sinha, P., Clements, V.K. & Ostrand-Rosenberg, S. Reduction of Myeloid-Derived Suppressor Cells and Induction of M1 Macrophages Facilitate the Rejection of Established Metastatic Disease. *The Journal of Immunology* **174**, 636-645 (2005).
664. Takahashi, H., *et al.* Induced differentiation of human myeloid leukemia cells into M2 macrophages by combined treatment with retinoic acid and 1 α , 25-dihydroxyvitamin D₃. *PLoS one* **9**, e113722 (2014).
665. Mueller, B.U., *et al.* Heterozygous PU. 1 mutations are associated with acute myeloid leukemia. *Blood* **100**, 998-1007 (2002).
666. Anderson, K.L., *et al.* PU. 1 and the granulocyte-and macrophage colony-stimulating factor receptors play distinct roles in late-stage myeloid cell differentiation. *Blood* **94**, 2310-2318 (1999).
667. Magni, P., Beretta, E., Scaccianoce, E. & Motta, M. Retinoic acid negatively regulates neuropeptide Y expression in human neuroblastoma cells. *Neuropharmacology* **39**, 1628-1636 (2000).
668. Phan, T.A. & Taylor, A.W. The neuropeptides α -MSH and NPY modulate phagocytosis and phagolysosome activation in RAW 264.7 cells. *Journal of neuroimmunology* **260**, 9-16 (2013).
669. De Jager, T., Cockrell, A. & Du Plessis, S. Ultraviolet Light Induced Generation of Reactive Oxygen Species. in *Ultraviolet Light in Human Health, Diseases and Environment* 15-23 (Springer, 2017).
670. Santos, T., *et al.* Blue light potentiates neurogenesis induced by retinoic acid-loaded responsive nanoparticles. *Acta biomaterialia* **59**, 293-302 (2017).
671. Covarrubias, A., Byles, V. & Horng, T. ROS sets the stage for macrophage differentiation. *Cell research* **23**, 984 (2013).
672. Cao, Y., *et al.* Oridonin stabilizes retinoic acid receptor alpha through ROS-activated NF- κ B signaling. *BMC cancer* **15**, 248 (2015).
673. Engelsen, O. The relationship between ultraviolet radiation exposure and vitamin D status. *Nutrients* **2**, 482-495 (2010).
674. Saborano, R., *et al.* Metabolic Reprogramming of Macrophages Exposed to Silk, Poly (lactic-co-glycolic acid), and Silica Nanoparticles. *Advanced healthcare materials* **6**, 1601240 (2017).
675. Sorg, O., *et al.* Spectral properties of topical retinoids prevent DNA damage and apoptosis after acute UV-B exposure in hairless mice. *Photochem Photobiol* **81**, 830-836 (2005).
676. Prus, E. & Fibach, E. Retinoic acid induction of CD38 antigen expression on normal and leukemic human myeloid cells: relationship with cell differentiation. *Leukemia & lymphoma* **44**, 691-698 (2003).
677. Nagahara, H., *et al.* Transduction of full-length TAT fusion proteins into mammalian cells: TAT-p27Kip1 induces cell migration. *Nat Med* **4**, 1449-1452 (1998).
678. Schmid, I., Cole, S.W., Korin, Y.D., Zack, J.A. & Giorgi, J.V. Detection of cell cycle subcompartments by flow cytometric estimation of DNA-RNA content in combination with dual-color immunofluorescence. *Cytometry* **39**, 108-116 (2000).
679. Fujiwara, T., *et al.* Gene expression profiling identifies HOXB4 as a direct downstream target of GATA-2 in human CD34⁺ hematopoietic cells. *PLoS One* **7**, e40959 (2012).
680. Cszaszar, E., *et al.* An automated system for delivery of an unstable transcription factor to hematopoietic stem cell cultures. *Biotechnol Bioeng* **103**, 402-412 (2009).
681. Koeffler, H.P., Billing, R., Lusic, A.J., Sparkes, R. & Golde, D.W. An undifferentiated variant derived from the human acute myelogenous leukemia cell line (KG-1). *Blood* **56**, 265-273 (1980).
682. Duarte, D., *et al.* Inhibition of endosteal vascular niche remodeling rescues hematopoietic stem cell loss in AML. *Cell stem cell* **22**, 64-77. e66 (2018).
683. Young Yhee, J., Son, S., Lee, H. & Kim, K. Nanoparticle-based combination therapy for cancer treatment. *Current pharmaceutical design* **21**, 3158-3166 (2015).
684. Lino, M.M., *et al.* Modulation of Angiogenic Activity by Light-Activatable miRNA-Loaded Nanocarriers. *ACS nano* (2018).
685. Jiménez-Balsa, A.n., *et al.* Nanoparticles Conjugated with Photocleavable Linkers for the Intracellular Delivery of Biomolecules. *Bioconjugate chemistry* **29**, 1485-1489 (2018).
686. Lino, M.M., Simões, S., Pinho, S. & Ferreira, L. Intracellular delivery of more than one protein with spatio-temporal control. *Nanoscale* **9**, 18668-18680 (2017).